



Politechnika Wroclawska

FIELD OF SCIENCE: Natural sciences

DISCIPLINE OF SCIENCE: Chemical Sciences (Nauki Chemiczne)

DOCTORAL DISSERTATION

**Metallic nanoclusters as fluorescent probes
for multiphoton microscopy**

**Metaliczne nanoklastry jako fluorescencyjne
znaczniki w mikroskopii wielofotonowej**

Anna Pniakowska, Msc Eng.

Supervisor:

Dr hab. Joanna Olesiak-Bańska, prof. uczelni

Keywords: nanoclusters, nonlinear optics, gold, silver, fluorescence, chirality

WROCLAW 2024

This work was supported by Sonata Bis 9 project (2019/34/E/ST5/00276),
financed by National Science Centre in Poland.

ACKNOWLEDGEMENTS

First and foremost, I would like to express my sincere gratitude to my supervisor Professor Joanna Olesiak-Bańska, for the guidance, support and believing in me since the very beginning of my scientific career. For over 9 years she brings the motivation, provide helpful ideas, inspired fruitful discussions and encourage to think out of the box. It was a pleasure to be continuously inspired by her success and passion to science. She is being truly an excellent mentor. This thesis wouldn't appear without her involvement.

My sincere thanks goes to Professor Rodolphe Antoine, who provided me an opportunity to join his team as an intern. Our fruitful collaboration extended to our joint project, giving me an excellent chance to expand my knowledge and skills. I am thankful for this experience.

Further I would like to thank professor Marek Samoć for your precious time spent on our joint projects, for your wisdom and experience. I am grateful for the discussions, for your patience and continuous support.

I have a special thanks to Dominika Benkowska, Patryk Obstarczyk, Maciej Lipok, Manuela Grelich-Mucha and Agata Hajda for all your friendship, celebration of the best times and support in most difficult ones. I am thankful for all of the discussions, for inspirations and creation of a friendly place, where I felt like a part of the team. Thank you for your presence thought my PhD journey.

Last but certainly not least, I would like to express my deepest gratitude to my husband Tomek and our daughter Zosia for all the love, patience, understanding and support through all challenging time. I am grateful for believing in my capabilities, supporting my decisions and for encouragement since the very beginning of my scientific career. You both are the reason I make it through – I dedicate this dissertation to you.

TABLE OF CONTENTS

List of abbreviations	6
Abstract	7
Abstract in Polish (streszczenie pracy)	9
1 Purpose and hypothesis of the work	12
2 Introduction	13
2.1 Noble metal Nanoclusters – synthesis and characterization	13
2.1.1 Fundamental knowledge of noble metal nanoclusters	13
2.1.2 Synthesis of nanoclusters	16
2.2 One-photon optical properties of nanoclusters	17
2.2.1 Fluorescence of nanoclusters	18
2.2.2 Chirality of nanoclusters	24
2.3 Nonlinear optical properties of nanoclusters	30
2.3.1 General introduction	30
2.3.2 Two-photon excited luminescence	31
2.3.3 Two-photon absorption	33
3 Published work	37
3.1 ARTICLE 1: Plasmonic enhancement of two-photon excited luminescence of gold nanoclusters	37
3.1.1 Short description of research work and results	37
3.1.2 Research contribution of PhD candidate	42
3.1.3 Contribution statements of co-authors	43
3.1.4 Article and Supplementary Material	43
3.2 ARTICLE 2: Gold-Doping Effect on Two-Photon Absorption and Luminescence of Atomically Precise Silver Ligated Nanoclusters	61
3.2.1 Short description of research work and results	61
3.2.2 Research contribution of PhD candidate	67
3.2.3 Contribution statements of co-authors	68
3.2.4 Article and Supplementary Materials	74
3.3 ARTICLE 3: Strong fluorescence-detected two-photon circular dichroism of chiral gold nanoclusters	96
3.3.1 Short descriptions of research work and results	96
3.3.2 Research contribution of PhD candidate	101
3.3.3 Contribution statements of co-authors	102

3.3.4	Article and Supplementary Materials	103
4	Summary and perspectives.....	116
5	Published works	118
6	Bibliography	119

LIST OF ABBREVIATIONS

- 1PL- one-photon luminescence
- 2PL – two-photon luminescence
- AFM - Atomic Force Microscope
- AuNCs – gold nanoclusters
- AuNRs – gold nanorods
- CD - circular dichroism
- CPL - circularly polarized luminescence
- FDCD – fluorescence detected circular dichroism
- GM –Göppert Mayer (unit)
- LSPR – localized surface plasmon resonance
- NIR – near infrared
- NLO – nonlinear optics
- PAGE – polyacrylamide gel electrophoresis
- PL – photoluminescence
- QY – quantum yield
- TCSPC – time-correlated single photon counting
- TPCD – two-photon circular dichroism
- TEM – transmission electron microscopy
- TPEL – two-photon excited luminescence
- VCD - vibrational circular dichroism

ABSTRACT

The dissertation discusses the linear and nonlinear optical properties of noble metal nanoclusters (NCs), as probes with unique optical properties. These very small nanostructures (with diameters below 2 nm) have attracted strong interest among researchers in recent years due to their attractive optical properties: strong Vis-NIR photoluminescence, improved photostability, distinctive chirality and others properties, such as catalytic or magnetic. This thesis focuses on optical properties of nanoclusters.

The dissertation is sectioned into two main parts: literature overview and experimental section. The introduction addresses the research motivation and main goals of this study, which are: synthesis of atomically precise gold nanoclusters, characterization of their linear optical properties: luminescent and chiroptical ones and then nonlinear optical properties (absorption, fluorescent and chirality), determined exclusively through fluorescence of nanoclusters. Each subsection present current state of knowledge and recall examples solely from recent reports.

The second part of this thesis consists of three articles, supplemented with short description of research work which I performed in terms of these manuscripts. Here I present a short introduction, which highlights the aim of the study, address current research problems and propose modern solutions. Then, I demonstrate methodology applied to proposed solution and major results, which I obtained through the study. Then, I shortly discuss obtained results. The detailed description of my research work is presented in followed articles and supplementary materials.

Studies presented in Chapter 3 demonstrate strategies to enhance one- and two-photon properties of nanoclusters via luminescent techniques: gold doping of silver nanoclusters, rigidification of an outer layer of nanoclusters and plasmonic enhancement in the vicinity of plasmonic nanoparticles. The aim of this dissertation is to develop functional nanomaterials with unique and strong optical properties that can potentially be used in the imaging and detection of biological materials, with the particular emphasis on applications in multiphoton microscopy. For this purpose atomically precise gold and silver nanoclusters have been proposed, presenting relevant stability and improved optical properties. Thesis provide the detailed description of synthesis methods, including the purification and separation of mixtures of nanoclusters. Due to the unique, fluorescent and chiral optical properties of nanoclusters, main part of the thesis research is devoted to a detailed analysis of one- and two-photon chiral optical response established on the basis of fluorescence techniques.

Chapter 3.1 of the experimental study includes Article 1, which describe the plasmon-enhanced luminescence of single fluorophores, atomically precise gold nanoclusters, Au₁₈, detected in the close proximity of gold nanorods. This study presents how low quantities of nanoclusters can be detected, down to individual particles. In this work I synthesized nanoclusters and performed detailed characterization of nanoclusters and nanorods: size-purity of nanoclusters and optical properties of both materials. I have verified optimal

conditions of detection of single nanoclusters through plasmonic nanoparticles, including choice of medium of detection, separation of gold nanorods, choice of concentration of nanoclusters and selection of particular excitation parameters. I have observed 25-times enhanced near-infrared emission of nanoclusters.

Article 2 presented in the chapter 3.2 discuss how optical properties of nanoclusters are strongly dependent on the structure of atomically precise nanoclusters. Here systematic study on changes of optical properties of nanoclusters were verified on the level of single-atom doping: by doping of one gold atom to the structure of Ag_{25} NCs, obtaining $\text{Ag}_{24}\text{Au}_1$ NCs, or by doping of several atoms, obtaining $\text{Ag}_{25-x}\text{Au}_x$ NCs. I have analyzed the continuous changes in absorption and luminescence, quantum yield and luminescence lifetime, and finally the nonlinear optical properties of nanoclusters: two-photon absorption and two-photon brightness. I have observed that incorporation of heteroatom into Ag_{25} nanoclusters stabilizes the structure and results in strongly enhanced quantum yield (10-times), elongated luminescence lifetime (from 1.1 to 1.8 μs) and increased two-photon brightness (from 1.5 to 20 GM) compared to undoped nanoclusters. Further doping of gold atoms deteriorate optical properties due to changed geometry and electron charge localization. Here, the nonlinear optical properties of nanoclusters are established on a wide range of wavelengths, including off-resonance region of excitation.

Article 3 included in the chapter 3.3. consider luminescence as a tool to establish two-photon circular dichroism of nanoclusters. In this work, I have synthesized arginine stabilized AuNCs in two enantiomeric forms and analyzed their chiroptical properties in linear and nonlinear range. I have determined their two-photon properties in a wide range of wavelengths, obtaining high values of two-photon absorption (1743 GM) and two-photon brightness (1102 GM). Due to remarkable fluorescent and chiral properties of these NCs I obtained strong, 245-fold enhanced two-photon circular dichroism with respect to the one-photon dissymmetry factor. Due to over two-magnitude stronger two-photon chiroptical properties, comparable with literature findings of other works on nanoclusters, I raised a question about the general rule of boosting the chiroptical properties under nonlinear excitation.

In conclusion, this thesis presents silver and gold nanoclusters as interesting probes due to their one- and two-photon properties. These properties can be significantly improved by applying a range of techniques, which influence the structure of nanoclusters. The major studies of this work show the utility of analyzed fluorescence as a mean to determine another properties of nanoclusters, such as absorption cross sections and chirality in the one- and two-photon regime. Proposed techniques: two-photon excited luminescence and two-photon fluorescence-detected circular dichroism offer a wide range of possibilities to describe the nonlinear optical properties: two-photon absorption, two-photon brightness, two-photon circular dichroism, simultaneously opening new paths of applications of NCs in the biological materials investigations, e.g. in chiral multiphoton microscopy.

ABSTRACT IN POLISH (STRESZCZENIE PRACY)

Przedmiotem rozprawy jest analiza liniowych i nieliniowych właściwości optycznych nanoklastrów, jako fluorescencyjnych markerów. Te małe nanostruktury (o średnicach poniżej 2 nm) wzbudzają ostatnimi latami ogromne zainteresowanie badaczy ze względu na ich atrakcyjne właściwości optyczne: silną fotoluminescencję w zakresie spektralnym Vis-NIR, wzmocnioną fotostabilność, wyjątkową chiralność, a także inne unikalne właściwości, jak np. katalityczne lub magnetyczne. Niniejsza rozprawa skupia się na właściwościach optycznych nanoklastrów.

Rozprawa jest podzielona na dwie główne części: przegląd literaturowy i część eksperymentalną. We wstępie została ujęta motywacja badań i główne cele pracy, którymi są: synteza atomowo precyzyjnych nanoklastrów złota, charakterystyka ich liniowych właściwości optycznych: luminescencyjnych i chiralnych, a następnie nieliniowych właściwości optycznych (absorpcja, fluorescencja i chiralność), wyznaczonych z wykorzystaniem fluorescencji nanoklastrów. Każdy podrozdział przedstawia aktualny stan wiedzy i odwołuje się do najnowszych badań opublikowanych na przestrzeni ostatnich lat.

Druga część tej rozprawy składa się z trzech artykułów, uzupełnionych krótkim opisem badań, które samodzielnie wykonałem w ramach tych prac. W każdym podrozdziale zawarłem krótkie wprowadzenie, które podkreśla cel badania, porusza bieżące problemy badawcze i proponuje nowoczesne rozwiązania. Następnie zarysowałem metodologię, zastosowaną do proponowanego rozwiązania i przedstawiłem główne wyniki, które uzyskałem w wyniku badań. Następnie przeprowadziłem krótką polemikę nad uzyskanymi wynikami. Szczegółowy opis mojej pracy badawczej przedstawiłem w załączonych artykułach i materiałach uzupełniających.

Badania przedstawione w rozdziale 3 omawiają strategie wzmocnienia jedno- i dwufotonowych właściwości nanoklastrów za pomocą technik luminescencyjnych: domieszkowania złotem nanoklastrów srebra, usztywnienia struktury nanoklastrów i wzmocnienia plazmonowego w pobliżu nanocząstek złota. Celem tej rozprawy jest opracowanie funkcjonalnych nanomateriałów o wyjątkowych, silnych właściwościach optycznych, które potencjalnie mogą być wykorzystane w obrazowaniu i wykrywaniu materiałów biologicznych, ze szczególnym uwzględnieniem zastosowań w mikroskopii wielofotonowej. W tym celu zaproponowano atomowo precyzyjne nanoklastry złota i srebra, prezentujące wysoką stabilność i wyjątkowe właściwości optyczne. Praca doktorska zawiera szczegółowy opis metod syntezy, w tym oczyszczania i rozdzielania mieszanin nanoklastrów. Ze względu na unikalne, fluorescencyjne i chiralne właściwości optyczne nanoklastrów, znacząca część badań pracy poświęcona jest szczegółowej analizie jedno- i dwufotonowej chiralnej odpowiedzi optycznej.

Artykuł 1 zawarty w rozdziale 3.1 przedstawia wzmocnioną plazmonowo luminescencję pojedynczych fluoroforów, atomowo precyzyjnych nanoklastrów złota Au_{18} , rejestrowanych w pobliżu nanoprętów złota. W pracy przedstawiono, że nanoklastry złota są wykrywalne na poziomie pojedynczych cząsteczek. W ramach powyższych badań zsyntetyzowałem nanoklastry i przeprowadziłem szczegółową charakterystykę nanoklastrów i nanoprętów złota: analizę rozmiaru nanoklastrów i właściwości optycznych obu nanomateriałów. Określiłam optymalne warunki detekcji pojedynczych nanoklastrów za pomocą plazmonicznych nanocząstek, m. in. procedurę separacji nanoprętów złota, wybór ośrodka detekcji, stężenia nanoklastrów i poszczególnych parametrów wzbudzenia. Zaobserwowałam 25-krotnie wzmocnioną emisję nanoklastrów złota w bliskiej podczerwieni.

Artykuł 2 przedstawiony w rozdziale 3.2 opisuje ścisłą zależność właściwości optycznych nanoklastrów złota od struktury atomowo precyzyjnych nanoklastrów. Systematyczne badania zmian właściwości optycznych nanoklastrów zostało zweryfikowane poprzez wymianę pojedynczych atomów na skutek: domieszkowania pojedynczym atomem złota struktury nanoklastrów Ag_{25} , uzyskując $Ag_{24}Au_1$, lub domieszkowania wieloma atomami złota, uzyskując $Ag_{25-x}Au_x$. Dokonałam analizy systematycznych zmian absorpcji i luminescencji, wydajności kwantowej i czasu życia luminescencji, a także nieliniowych właściwości optycznych nanoklastrów: absorpcji dwufotonowej i efektywnego przekroju czynnego na absorpcję dwufotonową. Zaobserwowałam, że wprowadzenie heteroatomu do nanoklastrów Ag_{25} stabilizuje strukturę i skutkuje silnie wzmocnioną wydajnością kwantową (10-krotnie), wydłużonym czasem życia luminescencji (od 1,1 do 1,8 μs) i zwiększonym efektywnym przekrojem czynnym na absorpcję dwufotonową (od 1,5 do 20 GM) w porównaniu z niedomieszkowanymi nanoklastrami. Dalsze domieszkowanie atomami złota zuboża właściwości optyczne ze względu na zmienioną geometrię i lokalizację ładunku elektronowego. Nieliniowe właściwości optyczne nanoklastrów zostały zbadane w szerokim zakresie długości fal, również poza rezonansowym obszarem wzbudzenia.

Artykuł 3 zawarty w rozdziale 3.3. porusza zagadnienie luminescencji jako narzędzia do wyznaczenia dwufotonowego dichroizmu kołowego nanoklastrów. W tej pracy zsyntetyzowałam stabilizowane arginina nanoklastry złota w dwóch formach enancjomerycznych i przeanalizowałam ich właściwości chiralno-optyczne w zakresie liniowego i nieliniowego wzbudzenia. Wyznaczyłam dwu-fotonowe właściwości optyczne na szerokim zakresie długości fal wzbudzenia, uzyskując wysokie wartości absorpcji dwufotonowej (1743 GM) i efektywnego przekroju czynnego na absorpcję dwufotonową (1102 GM). Ze względu na niezwykle właściwości fluorescencyjne i chiralne tych nanoklastrów uzyskałam silny, 245-krotnie wzmocniony dwufotonowy dichroizm kołowy w odniesieniu do jednofotonowego odpowiednika współczynnika dysymetrii. Ze względu na dwa rzędy wielkości silniejsze dwufotonowe właściwości chiralno-optyczne, porównywalne z wynikami dwufotonowego dichroizmu kołowego nanoklastrów, opublikowanymi w innych pracach, zasugerowałam możliwość obecności ogólnej zasady wzmacniania właściwości chiralno-optycznych przy dwu-fotonowym wzbudzeniu.

Podsumowując, niniejsza rozprawa przedstawia nanoklastry srebra i złota jako interesujące znaczniki ze względu na ich jedno- i dwufotonowe właściwości. Właściwości te można dodatkowo wzmocnić, stosując szereg technik, które wpływają na strukturę nanoklastrów. Znacząca część badań pracy doktorskiej wskazuje na użyteczność fluorescencji jako narzędzia do określania innych właściwości nanoklastrów, takich jak przekroje czynne na absorpcję i chiralność w zakresie wzbudzenia jedno- i dwufotonowego. Zaproponowane techniki: dwufotonowo wzbudzona luminescencja i dwufotonowy fluorescencyjny dichroizm kołowy oferują szeroki zakres możliwości opisu nieliniowych właściwości optycznych: dwufotonowej absorpcji, dwufotonowego efektywnego przekroju czynnego na absorpcję dwufotonową, dwufotonowego dichroizmu kołowego, jednocześnie otwierając zupełnie nowe możliwości zastosowań nanoklastrów w badaniach materiałów biologicznych, np. w chiralnej mikroskopii wielofotonowej.

CHAPTER 1 |

1 PURPOSE AND HYPOTHESIS OF THE WORK

The aim of this dissertation is to verify whether noble metal nanoclusters can be considered as an efficient fluorophores for multiphoton microscopy, demonstrating relevant optical properties, e.g. high quantum yield or/and long luminescence lifetime, or additional attractive properties, e.g. chirality. On the route to the answer I addressed the following hypothesis:

Hypothesis 1: Photoluminescence (PL) of nanoclusters and their detection can be significantly improved by specifically adapted chemical and physical techniques: alloy NCs formation, NCs functionalization, as well as modulation of NCs PL by surface plasmon resonance of plasmonic nanoparticles. Individual gold nanoclusters can be detected at single-particle level. Adapted strategies of luminescence enhancements are applicable in one- and two-photon regime of excitation.

Hypothesis 2: Luminescence can be used as a tool to determine two-photon circular dichroism of nanoclusters. Circular dichroism of nanoclusters is stronger under multiphoton excitation vs one-photon one.

Hypothesis 3: Gold-atom doping influence one- and two-photon optical properties of silver nanoclusters. Number of gold-atom dopants affects strongly the multiphoton optical response on NCs.

All formulated hypotheses were confirmed in three articles presented in this thesis. The first hypothesis is referring to different strategies of enhancing luminescent properties, which is presented in all three articles. The article 1 discusses plasmonic assisted luminescence enhancement of two-photon optical properties of single nanoclusters. Article 2 refers to gold-doping strategy of enhancement of quantum yield and photoluminescence lifetime of silver nanoclusters. Enhancement of those luminescent parameters influence strongly nonlinear optical properties, e.g. two-photon brightness. Article 3 presents the functionalization strategy for strong improvement of luminescent properties of nanoclusters stabilized with two ligands. It also discuss the effect of fluorescence mediated enhancement of two-photon chiroptical properties. Simultaneously, these works confirm the second hypothesis. Third hypothesis regarding the influence of single atom doping of nanoclusters on one- and two-photon properties of nanoclusters is discussed in details in article 2.

CHAPTER 2 |

2 INTRODUCTION

2.1 NOBLE METAL NANOCCLUSERS – SYNTHESIS AND CHARACTERIZATION

2.1.1 Fundamental knowledge of noble metal nanoclusters

Despite of significant progress done in terms of investigation of nanoscale materials, the exact boundary between nanomaterials and bulk matter is not yet fully understood.¹ Therefore the aim of current study is characterization of nanomaterials, their structure in relation to properties. Noble metal nanoclusters are commonly defined as <2nm sized particles containing from several to hundreds of metal atoms. Noble metal nanoparticles with sizes larger than the wavelength of the light present plasmonic properties and can be quantitatively described by Mie theory. When nanoparticle decreases in size to the diameter of electron free path (~50 nm) optical phenomena are explained on the basis of modified Mie theory.² The optical properties of nanoparticles are ruled by surface plasmon resonance effect, while optical properties of nanoclusters, with sizes <2nm, are dictated by the quantum size effect (Figure 1). In ultrasmall size regime, where every atom counts, the optical processes result from breaking the continuous density of states into discrete energy levels. In this circumstance, plasmonic properties disappear, and nanoparticles display molecular like behavior.³ It is seen in the shared common properties, very unique for specific groups of nanoclusters, built from known number of metallic atoms and stabilizing ligands, e.g. optical properties: circular dichroism, absorption, luminescence, and other related with them.

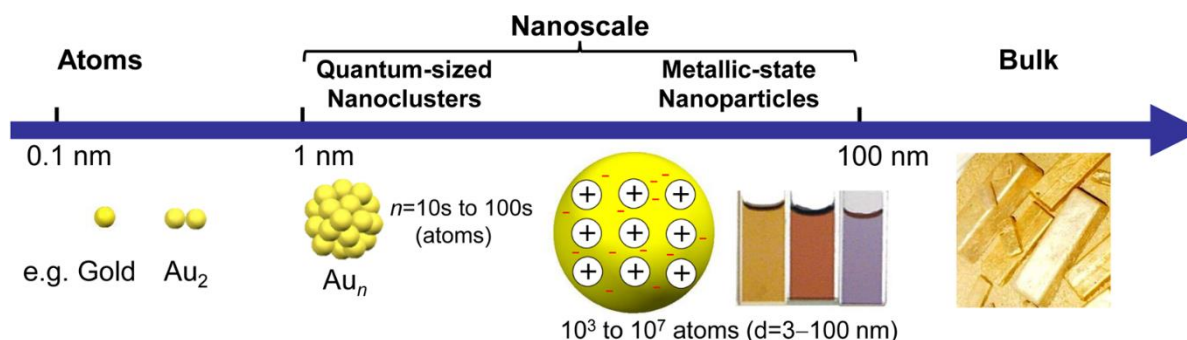


Figure 1. The nanoscale materials categorized on the size scale between atoms and bulk materials on two distinct types of

materials: quantum sized nanoclusters (1-3nm) and regular metallic-state nanoparticles (3-100nm). Adapted with permission from Ref. ¹

With down scaling the diameter of material to 2-3 nm, the local-field effect is no longer concerned. Here the other processes, such as particle size effect, surface ligand effect and valence state effect are considered. The effects are uniform and accurate specifically for ‘magic-sized’ clusters with well-defined number of building atoms. The terms ‘magic-sized’ and ‘atomically precise’ nanoclusters appeared to differentiate nanoclusters with well-known exact composition from the inhomogeneous mixtures of different-sized nanoclusters. Since nanoclusters can be assigned more accurately by formulas rather than the size range it is rational to refer to nanoclusters as ‘compounds’, recalling the exact number of metallic atoms and stabilizing ligands: e.g. $Au_n(SR)_m$, $Ag_n(SR)_m$ etc, where SR denote to thiolate ligands.³

In more detailed description of their composition metallic clusters are commonly referred to metal core surrounded by external “staple” motifs $SR[Au(SR)]_x$ ($x=0,1,2,3,\dots$).⁴ As an example, $Au_{25}(SR)_{18}$ nanoclusters, discussed within this thesis display an icosahedral Au_{13} kernel, protected by six dimeric staple motifs. Gold nanoclusters (AuNCs) are generally found as extremely stable nanostructures, however they tend to undergo oxidation reaction in presence of air or by chemical treatment, changing the charge state from -1 to 0 or +1, e.g. from $[Au_{25}(SR)_{18}]^{-1}$ to $[Au_{25}(SR)_{18}]^0$ and $[Au_{25}(SR)_{18}]^{+1}$. Oxidation of nanoclusters notably influences their optical properties, as evidenced in Figure 2.⁵

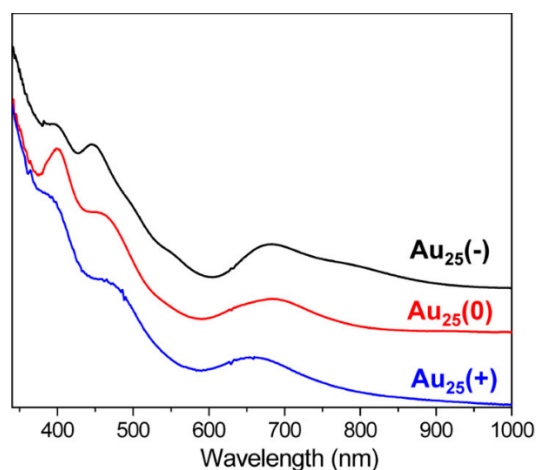


Figure 2. UV-vis spectra of $[Au_{25}(SC_2H_4Ph)_{18}]^q$ ($q = -1, 0, +1$). Reproduced with permission from ref⁵.

The discussion on the precise structure of nanoclusters is important in terms of understanding of nanoclusters properties. Quantization adjust the materials properties and leads to appearance of new properties, strongly related with the size of nanomaterials. Many changes in electronic structure arise from atom packing structure, very unique for certain ultra-small particles, which can be face centered cubic (fcc), similarly as reported for bigger nanostructures, but also very exotic, such as body-centered cubic (bcc) and hexagonal close-packed (hcp), not present in bulk gold or plasmonic nanoparticles.³ Apart from single-crystalline structure (fcc, bcc and hcp) bigger nanoclusters present multiple-twinned structure (icosahedron, dodecahedron), as shown in Figure 3a. Similarly as kernel structure, the surface is equally valuable for ligand-stabilized nanoclusters properties. Due to high surface-to-

volume ratio of nanoclusters, ligands formation can strongly influence the stability, chemical reactivity and induce particular properties of nanoclusters. Surface of nanoclusters are mainly

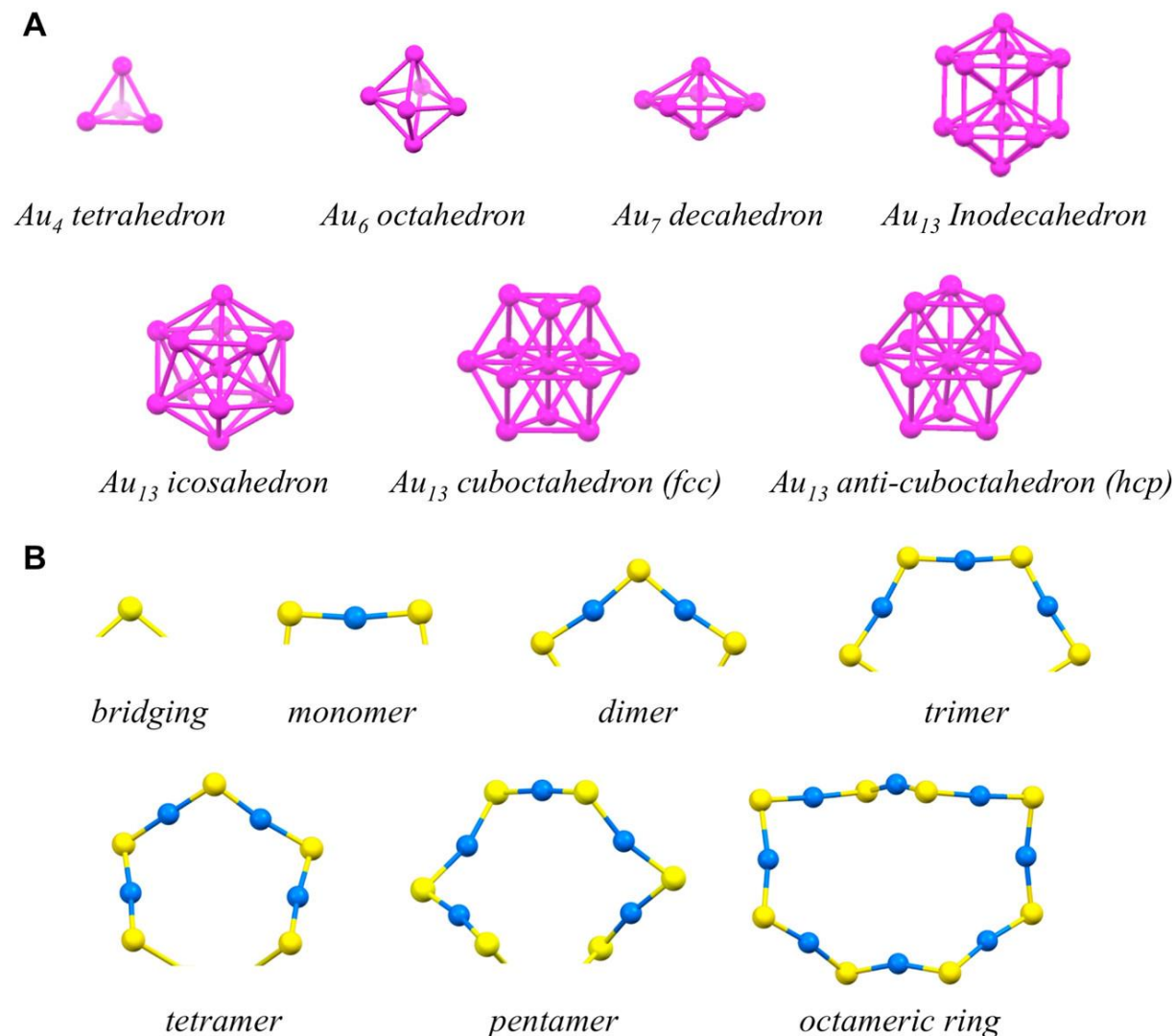


Figure 3. The collection of (a) basic kernel structures (pink represent Au atoms) and (b) staple motifs of $Au_n(SR)_m$ nanoclusters (blue represent Au atoms, yellow S atoms, R- groups are omitted for clarity). Adapted with permission from ref.³. Copyright © 2016, American Chemical Society

protected by oligomeric staple motifs (see Figure 3b), e.g. dimeric staple motifs of $Au_{25}(SR)_{18}$ ⁶ and tetrameric staples in $Au_{18}(SR)_{14}$ ⁷.

Considering staple motifs in gold nanoclusters, gold atoms can be bonded with two SR groups in the linear fashion, e. g. S-Au-S with 180° angle between them, while sulfur atom of the terminal SR group is bonded to staple Au and kernel Au atom, e.g. Au-S-Au with the 100° angle between them. Smaller nanoclusters, due to more curved surface usually require the arrangement of longer staple motifs, while larger nanoclusters, with lower curvature of the surface can be better covered by shorter staple motifs. As an example, bigger Au_{130} or Au_{133}

nanoclusters are protected by monomeric staple motifs, while smaller ones, Au₂₅ have dimeric and Au₂₀ ring-like staple motifs.³

Determination of the total structure of nanoclusters, with the exact atom positions is usually performed via single-crystal X-ray diffraction.³ In order to obtain crystalline structure there is a strong urge to provide chemically pure and homogeneous in size atomically precise clusters, prone to crystallization. Despite the challenging crystallization, understanding of optical properties without the crystal structure is severely difficult and complexed.

Since nanoclusters are extremely sensitive to the particle size, at the level of single atoms, the atomic control over the synthesis is highly required. The motivations beyond the investigation of methods to obtain atomically precise nanoclusters lie in the aim to determine the total structure, the comprehension of interactions between metal core and ligand interface and final understanding of the relation between structure and its properties. Even though control of the colloidal nanoparticles with atomic accuracy is not trivial, the tremendous work is already done in this field, especially in terms of gold and silver nanoclusters and nanocluster's alloys.^{8,9}

2.1.2 Synthesis of nanoclusters

WET CHEMICAL SYNTHESSES

The first method of synthesis was developed in 1994 by Brust and Schiffrin.¹⁰ Brust-Schiffrin syntheses consist of two steps: (1) The metal precursor (gold) provided in gold salt is dissolved in water solution and then transferred to organic phase in presence of phase-transfer agents (usually tetraoctylammonium bromide). (2) Then thiolate capping agent and reducing agent (usually sodium borohydride) are added sequentially to organic phase, forming thiolate-protected nanoclusters. Decades of further improvements of the method evolved to one-phase and two-phase syntheses, based on water and toluene.⁹ Currently, in the best scenario atomically precise nanoclusters are formed in 'one pot synthesis' specifically formulated for 'one size compound'. Aqueous medium of synthesis of nanoclusters is so far more complicated for best size-control than syntheses conducted in organic phase. Often water-soluble clusters are not able to crystallize to determine their crystal structure.³ However, aqueous medium of nanoclusters is highly desired for biomedical applications. Already number of water-soluble nanoclusters found application in bioimaging, biosensing and biotherapy¹¹ due to low toxicity,¹² good biocompatibility¹³ and photostability.¹⁴ Functional ligands of water-soluble nanoclusters have a strong potential to be drug delivery carriers.^{11,13}

Growth of noble metallic particles is usually hindered at the early stage via bonding of stabilizers to metallic cores.¹⁵ The protecting ligands of nanoclusters play a key role to avoid aggregations and provide unique properties. Therefore, variety of ligands have already been applied as ligands in water-soluble nanoclusters: thiolate ligands, DNA, polymers, peptides or proteins, depending on their further usability.¹⁶ Yet, among many types of nanoparticles the gold-thiolate nanoclusters, with the common formula Au_x(SR)_y are used as a model system,

owing to their significant robustness. Thiols can covalently bind to gold nanoclusters through strong gold-sulfur bonds. Common water-soluble thiolate ligands found in protocols of gold nanocluster synthesis are: glutathione, captopril, cysteine, mercaptobenzoic acid.

The one pot synthesis of thiolate nanoclusters is typically based on the strict kinetic control over the mixture through several parameters, such as: selective choice of solvent, ligand and reducing agent, and their exact reactant ratio, temperature and mixing conditions. Even a subtle change in the syntheses procedure can lead to the formation of different size or most probably - a mixture of different sized nanoclusters. However, size-focusing method of synthesis can provide an effective control over the structure of nanoclusters with satisfying homogeneity and stability of obtained materials.³

LIGAND EXCHANGE

Another method to obtain nanoclusters with desired properties is phase transfer of nanoclusters from medium of one polarity to another. Synthesis of organic nanoclusters is still most widely discovered. Therefore, phase transfer of nanoclusters from hydrophobic medium to hydrophilic one is so far better explored in the literature. In this approach, phase transfer strategy hydrophilic ligands form molecular layer on existing nanoclusters, changing their surface properties. Chosen new ligands, soluble in the target solvent, have to display good affinity with metal core and ability to maintain the original core structure of nanoclusters. Some of ligands exchange strategies are dictated by the aim to induce specific properties, e.g. catalytic¹⁷ and luminescent.¹⁸ In other cases ligand exchange is utilized as a strategy of a phase transfer to more favored medium.¹⁹

GALVANIC REACTION

One of interesting strategy to obtain nanoclusters is a redox reaction, in which noble metal ion is reduced by other less noble metal in solution as a result of electrochemical potential. The most well-known example of galvanic reaction is Ag(0) oxidation by Au(III) ions in the reaction of $3\text{Ag}(0) + \text{Au}(\text{III}) \rightarrow \text{Au}(0) + 3\text{Ag}(\text{I})$. Galvanic reaction was also proposed as a method for single atom doping of nanoclusters by Bootharaju et al.²⁰ Galvanic strategy of single gold atom doping of atomically precise Ag₂₅ clusters is described in the article 2 of this thesis.

2.2 ONE-PHOTON OPTICAL PROPERTIES OF NANOCLUSTERS

The uniformity and purity of nanoclusters, as well as the presence of well-established structure of nanoclusters results in predefined optical properties, such as discrete absorption bands in UV-Visible and near infrared range. Atomically-precise nanoclusters can be specifically designed to express additional properties – fluorescent, chiral, amphiphilic, magnetic, catalytic and many others.^{21, 22} The majority of studied noble metal nanoclusters, gold and silver ones have already quite well-defined structure and properties, vastly different from those of larger sized nanoparticles, built from thousands of atoms. Moreover, AuNCs and

AgNCs are most representative group of noble metal nanoclusters, which stands out with an excellent physico-chemical properties. Gold and silver are chemically less reactive than alkali metals, and AuNCs and AgNCs exhibit an extraordinary stability when metal atoms are bonded in form of icosahedral, decahedral or other highly symmetric core structure. They exhibit also great electrical conductivity, due to unpaired electron in conduction bands from s-orbital.

2.2.1 Fluorescence of nanoclusters

Bulk gold display very weak luminescence (PL QY = 10^{-10}) due to the majority of nonradiative decay and the lack of energy gap.^{2, 16} Through the years of investigation of nanomaterials luminescence of a thin metallic films and nanoparticles reached photoluminescence quantum yield (QY) about 10^{-5} . In 2000, Mohamed et al. observed first strong luminescence of plasmonic nanoparticles, with QY in the order of 10^{-4} - 10^{-3} , over million times stronger than for bulky metal.²³ At this time appeared also first reports on luminescence of gold nanoclusters that reached QY of 10^{-3} . With size focusing to single nanometer scale, gold materials showed discrete energy levels and increased luminescence, therefore further reported nanoclusters reached even several percent of QY.

Luminescence is an attractive property of nanoclusters which finds abundant usability, therefore inspire scientists to investigate its origin, mechanisms, strategies of enhancement and applications. Nowadays, number of nanoclusters can quite easily reach luminescent properties comparable to those of organic dyes and quantum dots. Moreover, apart from increased quantum yield, nanoclusters posses unique photostability, biocompatibility and tunability of emission.¹⁶

Luminescence of nanoclusters usually involves the electronic transitions of an occupied d bands and states above the Fermi level or transitions between the lowest unoccupied orbital and the highest occupied orbital – HOMO - LUMO.⁶ In other words, emission of nanoclusters arise then from both, sp-sp intraband and sp-d interband transitions (see Figure 4). The other description of luminescence of nanoclusters considers charge transfer due to the interaction between functional ligands and metal core, represent by ligand-to-metal charge transfer (LMCT)²⁴ or ligand-to-metal-metal charge transfer (LMMCT).²⁵

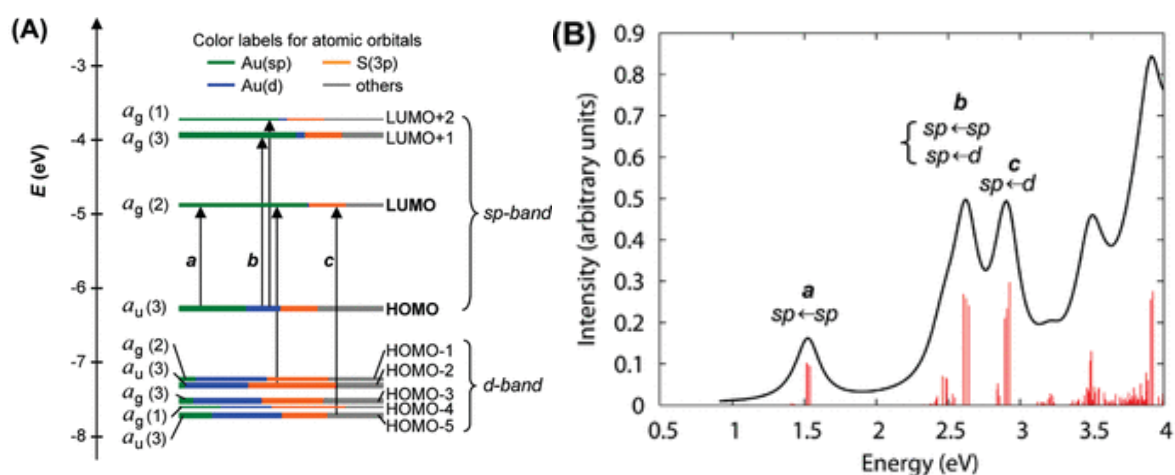


Figure 4. (A) Kohn–Sham orbital level diagram and (B) theoretical UV–vis absorption spectrum of $[Au_{25}(SH)_{18}]^-$ nanoclusters. Adapted with permission from ref 6.

In 2004 Dickson et al. have found that characteristic features of nanoclusters, such as emission is systematically shifted from UV to visible region in the manner of increased number of gold atoms, from 5 to 31, meaning the properties of nanoclusters are size tunable, since energy of HOMO – LUMO transitions change with number of atoms in nanoclusters.²⁶ However, further study of nanoclusters revealed higher complexity of the structure-properties relation, since many of the properties of nanoclusters are not simply scalable with size. The article 2 confirm the non-scalable, unique properties of certain nanoclusters with luminescent properties explained on the ground of single atom positions within the nanocluster's structure.

Chemical perspective on optical properties of nanoclusters shows strong influence of chemical and structural composition, or even geometry and symmetry of nanoclusters on their optical response. Dense packing of atoms in kernel of nanoclusters can provide rigid structure, which determine cluster stability and optical properties.³ The influence of ligands and the environment of nanoclusters luminescence was described in details by the group of Rongchao Jin.²⁷ They showed that PL intensity can be increased with raised number of electron-rich groups in ligands, which serve as a donor of electrons. Luminescence increases for such nanoclusters in following order: $Au_{25}(SC_6H_{13})_{18} < Au_{25}(SC_{12}H_{25})_{18} < Au_{25}(SC_2H_4Ph)_{18}$. Here, general structure of Au_{25} is preserved, as well as the '-1' charge state of nanoclusters. Interesting ligand influence on luminescence was observed through ligand exchange. The outer ligand shell can be partially or fully replaced with preserved kernel structure. As an example, group of Manzhou Zhu performed ligand exchange of Au_{25} nanoclusters stabilized by 2-(naphthalen-2-yl)ethanethiolate (NAPS) to several times more fluorescent $[Au_{25}(SCH_2CH_2Ph)_{18}]^{1-}$.²⁸

ENHANCEMENT OF LUMINESCENCE PROPERTIES

Through numerous studies of nanoclusters, an attractive luminescent properties have been widely developed. Emission of nanoclusters is found on a broad spectral range, from UV-visible range to near infrared (NIR), while long lifetimes nanoclusters hold promise of spectacular applications. The most well-controlled method to form fluorescent nanoclusters is a careful design of nanoclusters stabilized with electron donor-rich capping agent. Protecting nanoclusters with thiolate ligands commonly results in fluorescent nanoclusters with quantum yield (QY) equal several percents.²⁹ Although QY is far stronger than reported for bulk materials, compared to organic molecules or quantum dots QY of nanoclusters is relatively low.³⁰ The as-synthesized nanoclusters usually require some additional procedures of luminescence enhancements, to supplement other unique properties of nanoclusters for imaging or sensing purposes. Throughout the study of luminescent nanoclusters there have been proposed multiple strategies to enhance luminescence (Figure 5). The most common ones are discussed in more detail below as follows: rigidification of structure with additional ligand, controlled aggregation, self-assembly of nanoclusters, metal atom-doping and plasmon-assisted enhancement.

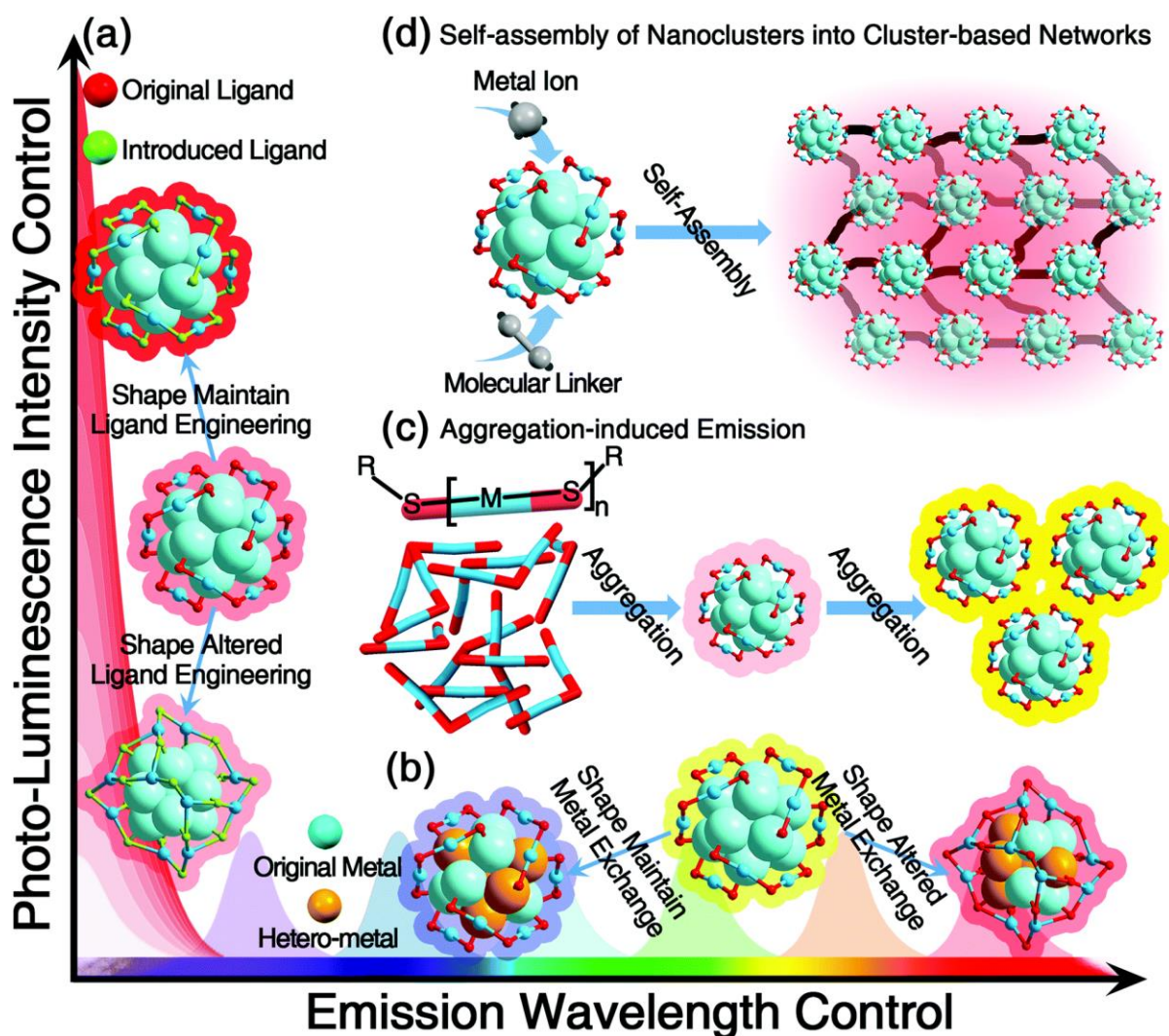


Figure 5. Schematic representation of methods for controlled tuning the emission wavelength and enhancement of luminescent properties. Selected strategies include (a) engineering of the ligand, (b) control over the metallic kernel, (c) aggregation-induced-emission and (d) self-assembly of nanoclusters. Reproduced from Ref.³⁰ with permission from the Royal Society of Chemistry.

RIGIDIFICATION OF NANOCUSTER'S STRUCTURE

Rigidification is one of the most powerful strategies to enhance luminescence of nanoclusters. The idea beyond rigidification induced luminescence enhancement is to create dense structure, which facilitate mobility of electrons and electronic transitions. Formation of dense, rigidified structure is therefore designed on the level of synthesis of nanoclusters and further surface functionalization. Often poor luminescence of nanoclusters is strongly boosted after functionalization with additional ligands. Some examples shows several times improved quantum yields caused by rigidification of structure with additional ligand via supramolecular host-guest interactions³¹ or electrostatic interactions.³² Another way to enhance luminescent properties involve ligand modification and surface motif reconstruction, e.g. exchange of ligands. Group of Crudden exchanged flexible phosphine ligands of gold nanoclusters with

rigid ligands - NHCs, which restricted vibrational dissipation of energy and enhanced PL emission.³³ Zhu and coworkers studied the relation between rigidity and peripheral thiol ligands in terms of luminescent enhancement. Applying highly rigid ligands (S-Adm, 1-adamantanethiol) result in stronger QY (11.7% for $\text{Au}_2\text{Cu}_6(\text{S-Adm})_6(\text{PPh}_3)_2$) compared to less rigid TBM (tert-butyl-mercaptan) (8.0% for $\text{Au}_2\text{Cu}_6(\text{TBM})_6(\text{PPh}_3)_2$).³⁴ Similarly as in previous example rigidity of nanoclusters is a result of steric hindrance of ligands which restrict the intramolecular rotations and promote photoluminescence enhancement. Rigidification induced enhancement of luminescence properties is described in more detail in the article 3 of this thesis.

CONTROLLED AGGREGATION OF NANOCLUSTERS

Aggregation-induced emission (AIE) is proposed as another strategy to enhance luminescent properties of nanoclusters. This approach considers restriction of intramolecular vibration and rotation of the ligands on the surface of nanoclusters to suppress the nonradiative excited state relaxation and facilitate the radiative energy transfer. AIE is commonly applied as cation- and solvent-induced aggregation.³⁵ As an example non-luminescent Au(I)-thiolate nanoclusters can generate gradually increased luminescence with progressed degree of solvent-induced aggregation, reaching even 15% of quantum yield.³⁵ The use of weakly polar solvent, 95% ethanol destabilize the Au(I)-thiolate complexes in water, neutralize the charge of nanoclusters and promote intra- and inter-complex Au(I)-Au(I) interactions. On the other hand, cation-induced aggregation creates electrostatic and coordination interactions between certain cations (e. g. Cd^{2+}) and carboxylic anions (e.g. glutathione). Except of neutralizing the negative charge of nanoclusters, the interactions facilitate formation of aurophilic bonds. Stronger inter- and intra-complex interactions restrains the vibrations and rotations of the complexes and reduce the nonradiative processes, enhancing the luminescent ones. Proposed mechanism of AIE luminescence enhancement was further analyzed with other materials, e.g. AuCu bimetallic NCs³⁶ or CuNCs³⁷

SELF ASSEMBLY OF NANOCLUSTERS

Discussed above AIE approach often suffers with structural inhomogeneity, which lead to instability of AIE structures, therefore possibly meet with difficulties for potential applications. Self-assembly is better organized form of bigger structures compared to AIE materials. The idea was already proposed for plasmonic nanoparticles, however in terms of nanoclusters the assembly process commonly result in unstable formation and further recrystallization or formation of nanoparticles. Interactions between nanoclusters surface are commonly rather weak, therefore the key for strengthening the interactions between nanoclusters require proper choice of molecules for capping ligands to direct spontaneous organization of nanoclusters via covalent and noncovalent bonds.³⁸ Gold nanoclusters have been most widely investigated among different metallic nanoclusters as a fundamental blocks for spontaneous assembly into highly luminescent structures.³⁹ X. Zhang found that pH-sensitive AIE can also lead to encapsulation of gold nanoclusters with Au(I)-thiolate complexes into high-ordered

networks.⁴⁰ Here pH-controllable supramolecular assemblies have certain degree of crystallization due to Au(I) thiolate shell formation on the surface of AuNCs, which result in significantly strong emission. Another interesting example of self-organized nanoclusters with improved luminescence was proposed by Munsier.⁴¹ Here shortwave infrared (SWIR) luminescence of gold nanoclusters stabilized with mercaptohexanoic acid - AuMHA was improved by incorporation of dithiol ligand of hexa(ethylene glycol) (HDT). Photoluminescence quantum yield, improved from 0.9% to 6.1% is explained by changes in the surface charge of AuNCs after addition of HDT ligand. Provided surface modifications affects energy transfer processes of surface electronic states which may create new discrete energy levels. The strongest PL intensity was recorded when HDT concentration was saturated causing dendritic network of self-assembled nanoclusters. Interestingly, self-assembled nanoclusters exhibit NIR-shifted luminescence, strongly desired for bioimaging purposes.

ALLOYING AND DOPING OF NANOCCLUSERS

In metallurgy, the overall mechanical properties of a single metal, such as hardness, corrosion resistance, plasticity, conductivity and many others, can be significantly enhanced by mixing with other metals to form alloys. Taking the inspiration from materials in bigger scale, this approach was adapted to nanoclusters to improve their properties. Introducing a new metal atoms affects optical and electronic states, overall reactivity and catalytic activity of metal alloys.⁴² Since doping of nanoclusters is performed in a small scale at the level of introducing single atoms, the effect is sensitive to the number and the nature of metal dopants.²⁰ Multi-metallic clusters are generally classified in the literature into two categories: replaced single or multiple atoms on existing nanoclusters is called a 'doped' cluster, while an 'alloy' name is used for a cluster that contain two or more different metal atoms in which presence of a parent cluster is not mandatory. As an example – single exchange of gold atom to platinum result in $\text{Pd}_1\text{Au}_{24}$,⁴³ which has a parent Au_{25} nanocluster, while an alloy cluster of $[\text{Ag}_{28}\text{Cu}_{12}(2,4\text{-DCBT})_{24}]^4$ is created even though $\text{Ag}_{40}(2,4\text{-DCBT})_{24}$ is unknown.⁴⁴

Doping of nanoclusters have already gained a lot of interest as a powerful method to enhance luminescence of nanoclusters. The literature is constantly growing in a possible variants of metallic atoms used for doping of noble-metal atom nanoclusters, e.g. Pd, Pt, Hg, Cd, Ag for doping of gold nanoclusters⁴⁵⁻⁴⁷ or Cu, Pt, Pd, Au^{44, 48} used for doping of silver nanoclusters. Strictly controlled doping or alloying can result in enhanced stability, luminescence and catalytic properties. Among them, luminescent properties are most generously described. As an example – quantum yield of nanoclusters can be effectively enhanced, even ~200 times, as reported for gold-silver alloys: $\text{Au}_{25-x}\text{Ag}_x$.⁴⁹ However, the alloys of Ag_{29} serves as an evidence of strong dependence of number of metal atoms doping on luminescence intensity. Here luminescent properties were raised with the increased amount of gold atoms.⁵⁰ Even 26-fold enhanced quantum yield (from QY = 0.9% to 24%) was reported for 40% Au doped Ag_{29} NCs (Figure 6). The stability and improved luminescent properties are explained by the structural changes upon exchanged Ag central core position of Ag_{29} and four phosphine-binding sites with gold atoms. Although continuous gold doping of Ag_{29} result in gradually improved luminescent properties, the article 2 in this thesis prove that referred example do not present

a general rule for luminescence enhancement, since Au doping to Ag_{25} may enhance or decrease the luminescence depending on the number of gold atom dopants.

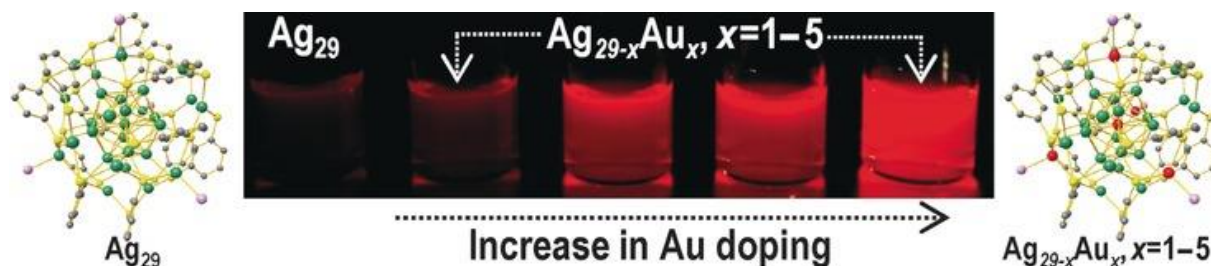


Figure 6. Enhanced luminescent properties as a result of Ag_{29} NCs gold doping. Most probable locations of Au atoms in $\text{Ag}_{29-x}\text{Au}_x$ ($x=1-5$) are illustrated in the x-ray crystal structures. Copyright(2016) Wiley. Used with permission from ⁵⁰.

NANOPHOTONIC PHOTOLUMINESCENCE ENHANCEMENT

Unique type of plasmonic PL enhancement is performed on the single-particle scale. Nanophotonic method of single-molecule luminescence enhancement is studied already from 1990s, showing promising results obtained on various materials, such as thin films, nanoparticles, nanoapertures. The biggest advantage of this method is to monitor individual events, eliminating the ensemble averaging of properties. For this purpose, pico- or nanomolar concentration of fluorophores are required. It is relevant in terms of observations of biological processes, which usually occur at the micromolar concentrations.⁵¹ Single-molecule spectroscopy which rely on fluorescence can provide fast, high-contrast and low-background detection.⁵²

In the literature there have been proposed different matrices for luminescence enhancement, e.g. zero-mode waveguides (ZMW) or plasmonic nanoparticles. ZMW consist of subwavelength holes in a metal film, which allow to illuminate molecules through the aperture without the diffraction limits. ZMW already provided strong fluorescence enhancement of organic fluorescent dyes^{53, 54} and single nanoclusters.⁵⁵ The usability of plasmon resonance phenomena to enhance luminescence of fluorophores is better known, and already verified under one- and two-photon excitation. Significant enhancement of luminescent properties were found for dyes,^{56, 57} fluorescent proteins⁵⁸ and quantum dots,⁵⁹ when excited in the vicinity of plasmonic nanoparticles. However, the method has never been used before for nanoclusters. Therefore, in this work I proposed plasmonic nanorod resonant enhancement of two-photon luminescence of gold nanoclusters $\text{Au}_{18}(\text{SG})_{14}$, as described in details in the article 1 of this thesis.

Described above strategies for fluorescence enhancement clearly shows the interest to fulfil strong needs of highly emissive materials designed specifically for versatile fluorescent-related applications. Fluorescent nanoclusters in majority are desired for imaging and sensing. For example, noble metal nanoclusters with enhanced luminescence have been used as markers to monitor kinetics of nanofibers growth.³⁹ Due to small sizes, bright-near infrared luminescence, good stability and biocompatibility they have been also used as agents for live-

cell imaging.⁶⁰ Part of fluorescent nanoclusters found application in theranostics and diagnostics, e.g. Hu and co-workers designed targeted drug delivery system of DHTP-AuNCs with A54 peptide and hyaluronic acid, which release the encapsulated drug under NIR radiation and delay the tumor growth by 125%.⁶¹ Another nanoclusters utilized luminescence for sterilization and disinfection. Fluorescent AuNCs stabilized with cysteine were successfully applied for bacterial detection and inhibition, since cysteine provide antibacterial effect while analysis of lowered luminescence controlled the death of bacteria *E. coli*.⁶² On the other hand, nanocluster can be even applied in luminescent solar concentrators (LSCs) due to strong quantum yield (QY = 53%), low reabsorption losses and high internal quantum efficiency (34-36%). Reported results are already competitive to those reported for LSCs based on colloidal dots and organic luminophores, particularly when prevent involvement of toxic heavy metals and hazardous organic solvents.⁶³

For some of more complexed applications nanoclusters requires more complexed systems. In some cases, fluorescent properties are not satisfactory enough, requiring additional beneficial properties, e.g. catalytic or antibacterial ones, with improved chemical stability, photostability or chirality.

2.2.2 Chirality of nanoclusters

ORIGIN OF CHIRALITY

Chirality is a universal phenomenon in nature, observed for materials, which structure and its mirror image cannot be superimposed. While the structure has an inversion center or symmetry plane it is considered achiral. Chirality of nanoclusters was first observed by Schaaff and Whetten⁶⁴ in 2000 and since then nanoclusters have been extensively studied to determine mechanisms of their chirality and to differentiate optical activity of nanoclusters from better known chiroptical response of nanoparticles and nanocrystals. Highly advanced development of chemical syntheses of nanoclusters ensures occurrence of optical activity directly at the level of synthesis,⁶⁵ ligand exchange⁶⁶ or enantioseparation from racemic mixtures⁶⁷. The most current knowledge of chirality of nanoclusters propose several possible origins of chirality, that are strictly related with structure of nanoclusters (Figure 7).⁶⁸ Therefore we distinguish chirality of nanoclusters induced by:

- I. Chiral ligands, e. g. surface adsorbates, which chirality causes new chiroptical effects in NCs, different from those obtained from ligands itself. Ligands can induce chirality independently from a chiral core of nanoclusters.
- II. Chiral interface, e. g. helical arrangement of organic-inorganic staple motifs of nanoclusters.
- III. Chiral kernel, which is typically associated with asymmetric metal core.
- IV. Chiral arrangement of ligands, e. g. ligands that forms 'swirl pattern'.
- V. Hierarchical chirality, which appears when several of described first four mechanisms of chirality are correlated with each other in a combined source of chirality.⁶⁸

In other sources, hierarchical chirality is also acknowledged when chiral organization in smaller scale, atomic- or nano-scale create chiral geometry in a bigger scale. As an

example, protein α -helices present hierarchical chirality from whole superstructure arrangement instead of individual chiral amino acids, which form this structure.⁶⁹

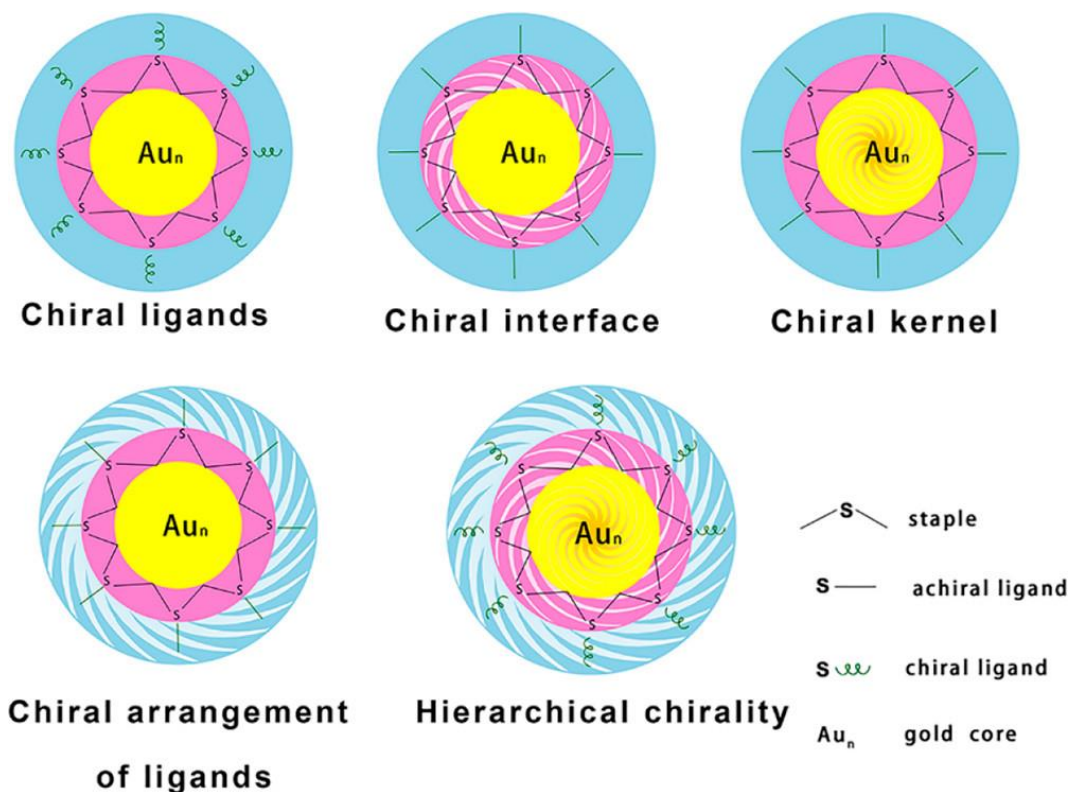


Figure 7. Different possibilities of origin of chirality of nanoclusters illustrated on Au-thiolate NCs, where metal kernel is marked in yellow, Au-SR staple in pink and ligand in blue. Helical motifs represent the chiral part in each case. Reprinted with permission from ⁶⁸. Copyright 2021 American Chemical Society.

The most investigated type of chirality of nanoclusters is related with ligand-induced chirality. Chiral thiol ligands, such as captopril⁶⁵, penicillamine⁷⁰, glutathione⁷¹, cysteine and their analogues⁷² induce strong chirality of atomically precise nanoclusters. However, it is worth to mention that achiral molecules, such as 2-phenylethanethiolate (2-PET)⁷³ or p-mercaptobenzoic acid⁷⁴ can also induce chiroptical response.¹⁵

Number of experimental works confirms the existence of proposed mechanisms of chirality and therefore stimulates the researchers to design nanoclusters of predefined, desired chirality. Then, potential of chiral nanostructures have been widely explored and utilized in the area of biosensing, enantiospecific separation, catalysis, chiral memory and chiroptical devices.¹⁵ As an example chiral nanoclusters have been already explored for enantioselective inhibition of amyloids aggregation.⁷⁵ Besides of chiral recognition of amyloid beta peptides, A β 42, nanoclusters can cross the blood-brain barrier without noticeable toxicity.

COMMON CHIROPTICAL METHODS OF DETECTION OF NANOCCLUSERS

Remarkable progress of synthesis of chiral nanoclusters forced further developments of characterization methods of their optical activity. Nowadays chiral properties of nanoclusters are widely analyzed via spectroscopic techniques: circular dichroism (CD), vibrational circular dichroism (VCD) and circularly polarized luminescence (CPL). Provided techniques of chiroptical analysis are often supported by single-crystal diffraction, nuclear magnetic resonance (NMR) and theoretical calculations. Among them single-crystal diffraction is undoubtedly underestimated technique in terms of determination of chirality, since unlike other techniques it can characterize optical activity of racemic mixtures.⁷⁶ NMR is the most accurate technique for determination of origin of the chirality, however the requirement of formation of single-crystal material at best quality may be a substantial limitation.⁷⁷

Growing number of experimental studies of chirality of nanoclusters inspire to perform theoretical simulations. Although theoretical study of this matter is firmly challenging so far since require precise knowledge of the structure and geometry of nanoparticle, and the environment of nanoparticle.⁷⁷

Nowadays the majority of chiroptical investigations of nanoclusters are performed through CD, VCD and CPL techniques. In principle, these techniques reveal the occurrence of electronic transitions sensitive to chiral geometry of materials. Electronic circular dichroism appears as a differential absorption of left and right-handed circularly polarized light evidenced for intrinsically chiral chromophore or chromophore in chiral environment. Changes in the extent of the absorption differences through applied frequency (wavelength range) appear in positive or negative CD bands, recorded in degrees scale (θ [deg]).⁶⁹ Known magnitude of CD can be easily transferred to absorptive dissymmetry factor (g_{abs}), often referred to as g-factor, which is the difference of molar extinction coefficients for left and right-handed circularly polarized light (molar circular dichroism) divided by molar extinction coefficient:⁷⁸

$$g_{abs} = \frac{\Delta\varepsilon}{\varepsilon} = \frac{\varepsilon_L - \varepsilon_R}{\varepsilon} = \frac{\Delta A}{A} = \frac{\theta}{32980 \cdot A} \quad (1)$$

Commonly, CD bands are observed in the part of spectrum of nanoclusters absorption. Positive and negative sign of CD bands is associated with inter- or intra-band transitions strictly related with ligands/stabilizers, metallic core and perturbations of ligands on nanocluster's core.¹⁵ CD bands of nanoclusters recorded in the region of >400nm are usually associated with chiral geometry of metal core, therefore asymmetry of a kernel or staple motifs. CD signals in the shorter wavelengths range, commonly the strongest in the CD spectrum, are related with ligands chirality.⁷¹ Therefore, chiroptical activity on a broader range of UV/VIS is considered as of combined chirality origin.

VCD and CPL techniques, similarly as CD, measure the difference of left and right-handed circularly polarized light. However, instead of electronic absorption, they consider the difference in vibrational transitions and luminescence intensity, respectively. Strong advantage of VCD spectroscopy is the ability to determine chirality in both, solid and solution states. CPL of nanoclusters is yet poorly described, since require presence of both, chirality and photoluminescence. On the other hand, the technique is particularly interesting for

understanding the relationship between chirality and excited states of nanoclusters perspective applications, such as diagnostics, imaging, medical treatment, electronics.

CIRCULAR DICHROISM OF FLUORESCENT NANOSTRUCTURES

Major part of this thesis is devoted to fluorescent based technique of determination of circular dichroism. FDCD method measure the difference of emission from sample excited with left- and right-handed circularly polarized light. Fluorescence detected circular dichroism (FDCD) is found as a perfect supplementation of CD study, providing highly sensitive and selective chiroptical information. Although technique will not supplement all CD studies since it requires the presence of fluorescent properties, it is considered as much more specific than CD, when sample contains multiple fluorescent and non-fluorescent moieties, easily distinguished by FDCD.^{79 80}

Common one-photon FDCD can be easily measured, even simultaneously with electronic CD (ECD), while CPL is usually more difficult in terms of set-up construction (Figure 8). The basic FDCD set-up consist of component, which create circularly polarized light, placed before sample, and detector, placed orthogonally to the excitation. Generation of circular excitation is usually performed by photoelastic modulator (PEM), quarter wave-plate, pulse replica generator (PRG), Babinet-Soleil compensator or others. In principle chiral samples emit with different intensities upon left- and right-handed circularly polarized excitation, F_L and F_R respectively, therefore CD signal can be calculated from the differences between them as follows:

$$\Delta A = 2 \frac{F_L - F_R}{F_L + F_R} \quad (2)$$

Despite many advantages of FDCD technique, it is important to consider possible artifacts that can appear in FDCD signal. Firstly, the principle of FDCD measurements already assume that the amount of absorbed light is fully transformed to emission, without any nonradiative energy dissipation, which unnecessary reflects the processes occurred in the samples. In addition, artifacts can be generated from the instrument/optical components, when circularly polarized excitation is affected by any linearly polarized contribution. Currently developed FDCD instruments can eliminate photoselection artifacts,⁷⁹ while home-built set-ups can minimize anisotropic part by placing the emission detector along the 54.7° , at so-called 'magic angle' direction or placing the linear polarizer right before the detector, with polarization set at the 'magic angle' (Figure 8).

FDCD is often incorrectly mistaken with CPL (circular polarized luminescence). Although both techniques rely on fluorescence, they measure different properties. FDCD is a fluorescent analogue of common ECD, since similarly measures the difference of absorption of left- and right-handed circularly polarized light. In other words, classic CD is a direct absorption based method, while FDCD is indirect, fluorescence-based technique, which determine absorption parameter of CD through analysis of differences in the excitation spectrum upon irradiation

of circularly polarized light and measurement of luminescence.⁸¹ On the contrary, CPL determines the difference in intensity of left- and right-handed circularly polarized components of luminescence emitted from chiral molecules.⁸²

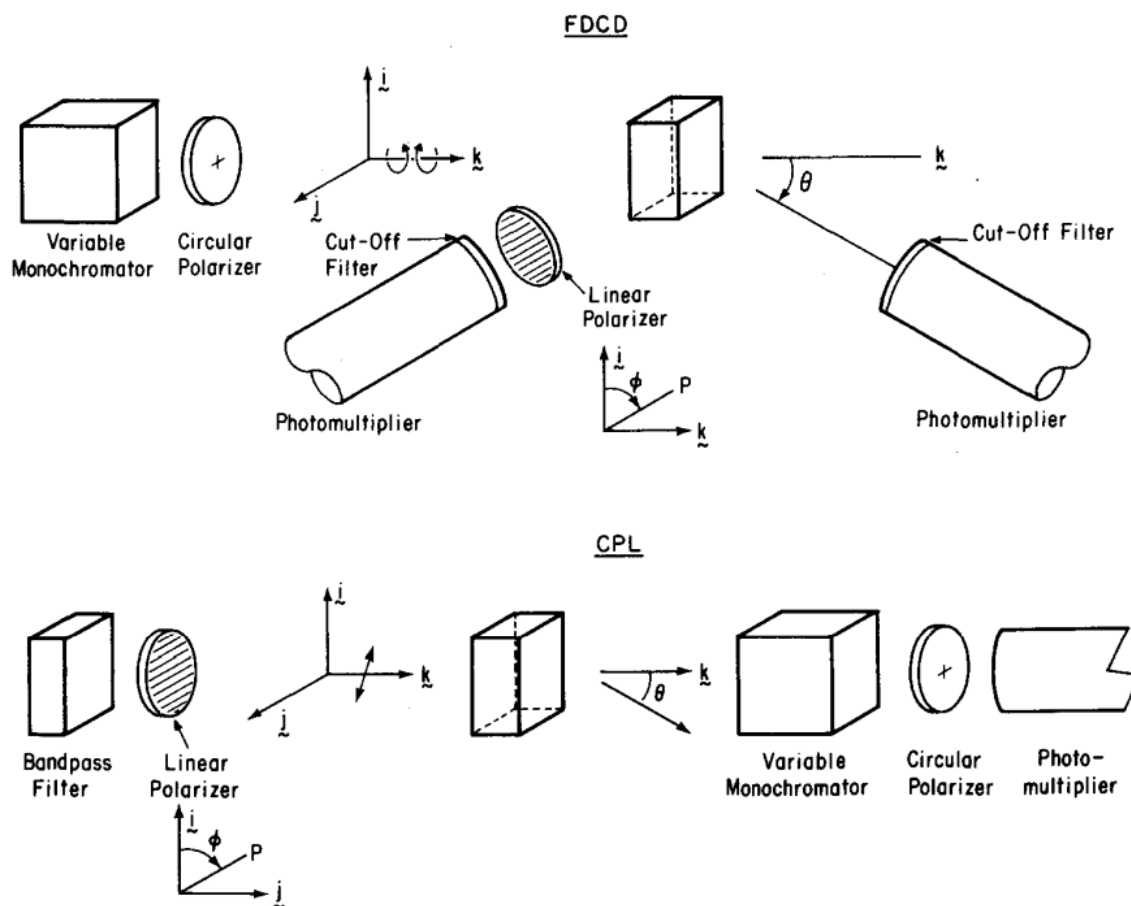


Figure 8. Comparison of FDCD and CPL set up. In FDCD circularly polarized light excites the sample, while the difference in fluorescence intensity is measured for left- and right-handed circular polarization of excitation. In CPL an unpolarized or linearly polarized light excite the sample, and the degree of circular polarization of emitted light is measured. Reprinted from ⁸³ with the permission of AIP Publishing.

Although the first reports on FDCD are dated early, from 1974 in work of Turner, Tinoco and Mestre on chiral tryptophan,⁸⁰ until now there are less than hundred studies referring to FDCD. It is worth to highlight that both, CPL and FDCD are valuable tools in various scientific disciplines for understanding the chirality and structural properties of molecules. Current study on FDCD, found in the literature present different motivations for applying proposed techniques: (I) to distinguish presence of multiple chromophores in a sample ⁸⁴ (II) aiming to provide greater sensitivity than ECD⁸⁵ and (III) when luminescent properties are used for investigation of excited states of chiral molecules. ⁸⁶

Applicability of FDCD was proven on supramolecular host-guest systems, ensuring nanomolar sensitivity, which is an order of magnitude higher sensitivity than in CD.⁸¹ Such spectacular sensitivity is promising for real biological samples with nanomolar concentrations regime. Electronic circular dichroism supplemented by FDCD can distinguish chiral analytes from each

other.⁸¹ FDCD enable to follow the process of chiral formation of nanostructures, such as of DNA formation in two different chromophore assemblies.⁸⁷

Although FDCD is yet poorly described in terms of chiral nanostructures, the literature offers a few examples of FDCD tested already on optically active fluorescent nanoparticles, such as CdS and CdSe quantum dots.⁸⁸ FDCD was theoretically applied to nanoantennas demonstrating two order of magnitude improved sensitivity.⁸⁹ FDCD was also applied in nonlinear regime as an imaging tool for single plasmonic gold nanoparticles, reaching several times elevated CD signal compared to detection by SHG and one-photon luminescence.⁹⁰

However, narrowing discussed group of nanomaterials to nanoclusters - first and the only experimental report on multiphoton circular dichroism of nanoclusters appeared in a recent work of Waszkielewicz et al.⁹¹ In this work two-photon circular dichroism of Au₂₅(Capt)₁₈ nanoclusters was analyzed through z-scan technique. The article 3 provide first two-photon investigations of circular dichroism of gold nanoclusters performed through fluorescent technique – FDCD.

2.3 NONLINEAR OPTICAL PROPERTIES OF NANOCCLUSERS

The aim of this thesis is to discuss the linear and nonlinear optical properties of thiolate nanoclusters and verify their abilities for multiphoton microscopy. Here a comprehensive characterization of nonlinear optical (NLO) responses, e.g. two-photon absorption, two-photon excited fluorescence and two-photon brightness will be considered. Deeper understanding of structure-properties relation can assure target-oriented design of nanoclusters which demonstrate desired optical properties, such as strong NLO response, for multiphoton purposes.

2.3.1 General introduction

Materials upon interaction of light provide a response represented by susceptibility χ of the medium to the applied electric field E , giving rise to an induced polarization P :

$$P_i = \varepsilon_0 \chi E \quad (3)$$

where ε_0 is electric permittivity of free space;

Linear optical properties arise from linear dependence of the material polarization P of medium on the electric field E . In the regime, where polarization of the material is no longer linearly dependent on the electric field, the material response in the electric dipole approximation of light-matter interaction can be described by nonlinear relation of induced polarization, as presented:

$$P_i = \chi_{ij}^{(1)} E_j + \chi_{ijk}^{(2)} E_j E_k + \chi_{ijkl}^{(3)} E_j E_k E_l + \dots \quad (4)$$

Where $\chi^{(n)}$ is n-th order susceptibility and E is electric field.

The first term of the Taylor series $\chi_{ij}^{(1)}$ corresponds to the linear phenomena, while the second and third ones to nonlinear optical (NLO) processes of the second and third order.⁹² Second-order nonlinear phenomena require a non-centrosymmetric medium⁹³ and consist of second harmonic generation (SHG), difference frequency generation, sum frequency mixing, optical rectification and Pockels effect. Third-order nonlinear processes are allowed in all media and represents third harmonic generation (THG), four-wave-mixing, Kerr effect, coherent and anti-Stokes Raman spectroscopy and two-photon absorption (TPA).⁹⁴ In this work, the third-order NLO properties of nanoclusters are described, with particular emphasis on two-photon absorption.

Nonlinear response of natural materials is rather weak and occur at sufficiently strong applied electric fields. However, since significant amount of energy can be confined in ultra-small volume of nanoparticle or even parts of nanoparticles, so called hot spots, the required source

power can be scaled down with higher order nonlinear processes, where field strength is raised to the second, third and subsequent powers.⁹⁵

The first nonlinear optical effect, two-photon absorption, was theoretically predicted by Maria Göppert Mayer in 1931, however it remained unexplored experimentally until the discovery of lasers in 1960. Since then number of techniques and set-ups have been developed to facilitate non-linear optical measurements and differentiate the components from NLO phenomena. The thesis discusses absorption and luminescent nonlinear optical properties of nanoclusters, therefore the paragraphs below are devoted to two-photon excited luminescence (TPEL) technique and measurements of two-photon absorption and two-photon brightness.

2.3.2 Two-photon excited luminescence

Two-photon excited fluorescence (TPEL) is a radiative nonlinear process that occur as a result of simultaneous absorption of two-photons by a molecule.⁹³ If single light source is used, absorbed photons provide the same energy, which sum corresponds to the energy gap between ground and excited state of a molecule. Since TPEL requires high photon flux to create conditions of simultaneous absorption of two photons, the only suitable source of excitation is provided by pulsed lasers. The excitation probability is proportional to the square of the laser intensity, therefore two-photon excitation occurs mostly in the focal plane and is strongly limited to the femtoliter size focal volume (Figure 9). Localized excitation assures improvement of the axial depth discrimination and greater contrast and resolution, compared to one-photon microscopy. Reduced area of photoexcitation decreases potential photobleaching (see bottom images of Figure 9). Two-photon excitation usually occur at near-infrared region, at so-called first ($\lambda_{exc} = 700 - 950$ nm) and second biological window ($\lambda_{exc} = 1000 - 1700$ nm), the region of reduced scattering, absorption and endogenous fluorescence (autofluorescence) of tissues.⁹⁶ Therefore, one of the major advantages of TPEL is ability to perform imaging of thick biological materials, assuring deeper penetration without the photodamage of sensitive samples.⁹⁷

The majority of nanoclusters possess wide excitation spectrum, which enable nanoclusters to excite with two-photon on a broad range of wavelengths.⁹⁸ Bright TPEL of nanoclusters appear primarily in visible wavelengths, however recently emerging NIR-emitting nanoclusters are found promising for multiphoton study on a broader scale.^{99, 100}

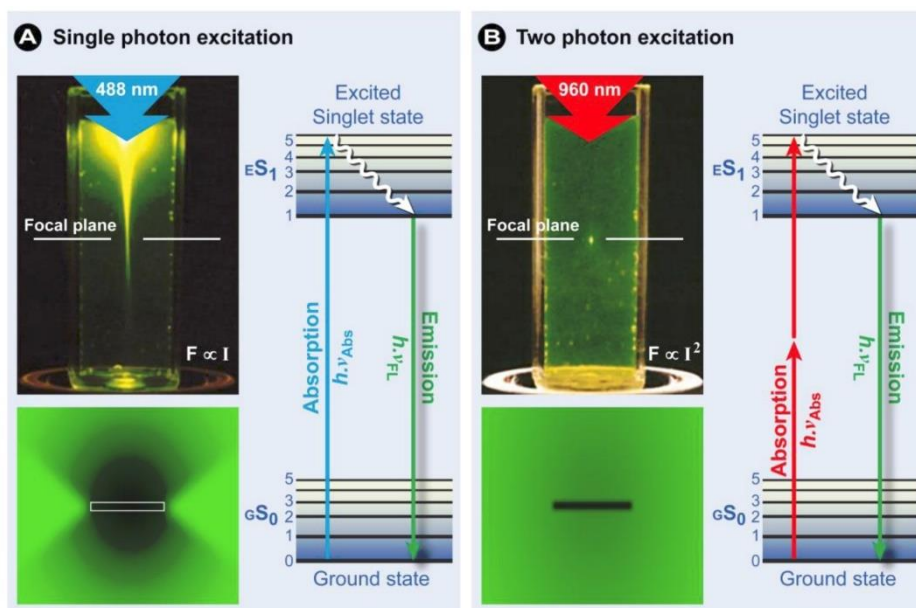


Figure 9. Comparison of (a) one-photon excitation and (b) two-photon excitation profiles on cuvettes with fluorophore, excited with laser beam at 488 and 960 nm, respectively. Two-photon excitation, conversely to one-photon one is focused in a spot in the focal plane. Bottom figures represent photobleaching effect on fluorescein-stained formvar film from one- and two-photon excitation. The Jablonski diagrams present the differences in photon absorption in both systems. Partially reproduced from ¹⁰¹ and ¹⁰² with permission from Macmillan Publishers Ltd: Nature Biotechnology © 2002.

Silver and gold nanoclusters are commonly demonstrated as remarkable absorbers, however rather poor emitters.¹⁰³ Paragraph 2.2.1. presents the discussion on strategies for luminescence enhancements of nanoclusters. Methods described there are also applicable on the ground of multiphoton excitation. Strong TPEL is crucial for confocal imaging or sensing under multiphoton microscopy, therefore a lot of efforts are put to explore nanoclusters as promising emitters with enhanced two-photon luminescence.

The literature already offers some examples of efficiently enhanced two-photon excited luminescence. Group of R. Antoine have recently reported 30-fold enhanced TPEL as a result of introduction of bulky counterions attached to gold clusters.¹⁰⁴ Large impact on TPEL enhancement of Au₁₅(SG)₁₃ and Au₁₈(SG)₁₄ was found there with appropriate choice of solvents and bulky counterions, tetrabutylammonium (TBA) and tetraoctylammonium (TOA).

Another strategy of improved two-photon excited luminescence by functionalization of nanoclusters was present in our group, which presents 7-fold enhanced TPEL of silver-gold nanoclusters after additional polymer stabilization of the structure (included in the published work, chapter 5).¹⁰⁵

Besides of strong enhancement of TPEL of nanoclusters, they often remains stable even at prolonged illumination under two-photon excitation.¹⁰⁶ Strong two-photon luminescence and stability provide an opportunity for multiphoton deep tissue imaging. L. Polavarapu et al. showed that water soluble and biocompatible nanoclusters with proved low toxicity can appear as an imaging agent of SH-SY5Y neuroblastoma cells. Here ultrasmall size of nanoclusters overcome limitations of bigger, metal nanoparticles and easily mark biological samples for two-photon live cell imaging.¹⁰⁶ Going a step further, the utility of water-soluble nanoclusters was already demonstrated in multiphoton studies *in vitro* and *in vivo*.¹⁰⁷ Group

of F. Wang first verified potential of ATT-Au/AgNCs in 4T1 cells *in vitro* under prolonged two-photon illumination. Nanoclusters provided strong red luminescence and maintained excellent photostability, therefore ATT-Au/AgNCs have been introduced to the living mice body and imaged under two-photon confocal microscope. First promising reports on two-photon studies of gold nanoclusters give hope of future common utility of nanoclusters in multiphoton bioimaging.

2.3.3 Two-photon absorption

In principle, two-photon absorption (TPA) is a simultaneous absorption of two photons in order to excite a molecule from ground state to the higher energy electronic state. Two-photon absorption cross-section (σ_2) determines quantitatively the probability of the two-photon process of simultaneous absorption of photons. The unit of σ_2 is Göppert Mayer (GM) (1 GM=10⁻⁵⁰ cm⁴ s per photon), named in honor to the contribution of Maria Göppert Mayer to the description of this process.

There are several approaches for investigation of TPA properties of materials, either direct or indirect ones.¹⁰⁸ Direct methods of TPA are related with monitoring the decrease of light transmittance after passing through a sample, and simultaneous recording of the incident intensity changes. An example of direct method of determination of TPA cross-section is z-scan technique.¹⁰⁹ Indirect methods involve comparison of measurement with another materials of well-established two-photon absorption cross-sections. An example of indirect method is two-photon excited luminescence (TPEL). TPA cross section, can be determined on the basis of known TPA cross-section and QY of a reference fluorophore and the comparison of TPEL and quantum yield of both samples, investigated and known one, at given concentration:

$$\sigma_{2,s} = \frac{F_{2,s(\lambda_{exc})} C_r \varphi_r(\lambda_{exc})}{F_{2,r(\lambda_{exc})} C_s \varphi_s(\lambda_{exc})} \sigma_{2,r} \quad (5)$$

where $F_{2(\lambda_{exc})}$ is integrated TPEL intensity at particular excitation wavelength, C is concentration, $\varphi(\lambda_{exc})$ is quantum yield, while 's' and 'r' indices denote to sample and reference, respectively. The fluorophore chosen as a reference has to meet the requirement of overlapping emission spectrum with characterized sample. Although TPA measurements based on TPEL are fast and simple, for some cases the requirements of detectable luminescence and the presence of reference sample in similar spectral range might be challenging. Therefore, direct methods are required, especially for standard fluorophores, used as a reference in indirect methods. In direct, z-scan technique TPA is determined through transmittance changes regarding the distance to focal plane. One of the main advantages of direct measurements is the applicability for both, fluorescent and nonfluorescent materials. However, direct methods can contain cumulative absorption and scattering effects. Time consuming measurements, strong requirements on accuracy and quality of a beam profile, and limitations of the technique, such as strong absorbance of the solvent in the desired detection range, makes TPEL technique more convenient.¹⁰⁸ TPEL method is independent of

Table 1. The summary of NLO properties of AuNCs, AgNCs and Ag@Au alloy nanoclusters.

Sample	σ_2 , [GM]	$\sigma_{2, \text{eff}}$ [GM]	λ [nm]	Technique	source
Au ₃₈ (PET) ₂₄ Au ₂₅ (Capt) ₁₈ Au ₂₅ (PET) ₁₈ Au ₂₅ (SG) ₁₈ Au ₁₈ (CyHT) ₁₈ Au ₁₈ (SG) ₁₈ Au ₁₈ (Capt) ₁₈	39 300 GM 668 GM 624 GM 164 GM 507 GM 13 GM 92 GM		1028nm (off resonance)	fsTAS (femtosecond pump/probe transient absorption spectroscopy)	G. Yousefalizadeh ¹¹⁰
Au ₂₅ (H ₁₃ C ₆ S) ₁₈	2 700 GM (in hexane)		1290nm (off-resonance)	TPEL	G. Ramakrishna ⁹⁹
Au ₂₅ (H ₁₃ C ₆ S) ₁₈ Au ₃₀₉ (H ₁₃ C ₆ S) ₁₈	427 000 GM (in hexane) 1 476 000 GM (in hexane)		800nm (in-resonance)	TPEL	G. Ramakrishna ⁹⁹
Ag ₂₉ (DHDLA) ₁₂	12 930 GM/ 873 GM/ N/A	0.48 GM 0.065 GM 0.031 GM	790 nm/ 860 nm/ 950 nm (in resonance)	TPEL	I. Russier-Antoine ¹¹¹
Ag ₃₁ (SG) ₁₉ Ag ₁₅ (SG) ₁₁	668GM 60 000 GM		(2.62 eV) (off resonance) (1.85 eV) (in resonance)	TD-DFT calculation	P. N. Day ¹¹²
Ag ₁₁ (SG) ₇ , Ag ₁₅ (SG) ₁₁ Ag ₃₁ (SG) ₁₉	6.6 GM 63.5 GM 950 GM	0.00033 GM 0.00169 GM 0.066 GM	800nm (in resonance)	TPEL	. Russier-Antoine ¹¹³
Ag ₂₅ (DMBT) ₁₈	1300 GM		1028nm (off resonance)	fsTAS (femtosecond pump/probe transient absorption spectroscopy)	G. Yousefalizadeh ¹¹⁰
Au ₁₅ @Ag Au ₁₈ @Ag Au ₂₅ @Ag	1900 GM 3900 GM 888 000 GM		800 nm (in resonance)	TPEL	T. Goodson ¹¹⁴
50:50 Ag: Au alloy	2260 GM		1028nm (off resonance)	fsTAS (femtosecond pump/probe transient absorption spectroscopy)	G. Yousefalizadeh ¹¹⁰

pulse duration and do not require complex optics. For relatively brightly luminescent samples, with QY above tens of percent, TPEL allows for measurements of low, micro- and nanomolar concentrations of a sample, reducing any possible aggregation and related effects of self-quenching, and reduce background noise related with scattering. Due to advantages and drawbacks of all techniques, the type of measurements should be specifically chosen for analyzed samples.

Recent studies have revealed an intriguing two-photon properties of gold and silver nanoclusters, presenting their potential for diverse applications in photonics and biomedicine.⁹⁸ Promising applications arise from strong two-photon absorption cross sections, with reported values in the range of hundreds to thousands of GMs.

The TPA of gold nanoclusters are getting the highest values among metallic nanoclusters, reaching even several hundred thousand GM units.^{106, 115-117} Although nonlinear properties of atomically precise gold nanoclusters, especially Au₂₅, have been most extensively studied, recently explored silver nanoclusters present values of thousands to hundred thousand GM.¹¹¹⁻¹¹³ The exact values of TPA in GM units are detailed in Table 1. Current work in the area of nonlinearity of nanoparticles is first focused on the strict control over atomical precision of nanocluster's composition, functionalization or doping.^{110, 111} Hence, one of the articles presented in this thesis considers gold doping influence on the magnitude of TPA of silver nanoclusters. Furthermore, rigidification of nanoclusters, introduction of additional ligands or compositional and structural modifications strongly influence optical properties.³⁷ Currently many efforts are directed on the enhancement of absorption and luminescent properties of nanoclusters, one- and two-photon one. There is observed a tendency of numerous enhanced two-photon properties even upon considerably slightly enhanced one-photon luminescent properties.¹⁰⁵ Unambiguously, TPA of nanoclusters reach enormous values at the resonance conditions, when excitation is well correlated at twice the one-photon absorption band.¹¹⁰ Reported in the literature giant two-photon absorption cross-sections are strictly related with presence of the 'double resonance effect', when electronic transitions energetically fit the real or virtual state of two-photon absorption. Scheme 1 illustrates how conditions of excitation play a crucial role for determination of two-photon absorption properties. Choice of specific two-photon excitation, which energy matches the particular energy levels of atomically precise nanoclusters results in large two-photon absorption, like observed for Au₂₅(SR)₁₈ at $\lambda_{exc} = 800$ nm, or Au₃₈(SR)₂₄ at $\lambda_{exc} = 800$ nm or 1028nm (Figure 10).

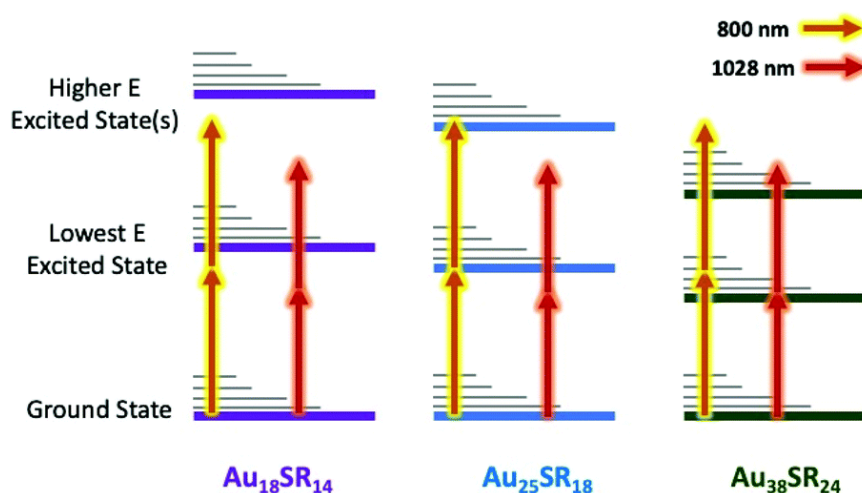


Figure 10. Scheme of the double resonance mechanism responsible for giant 2PA with 800 nm laser light for Au₂₅SR₁₈, strong 2PA for Au₃₈SR₂₄ under both, 800 nm and 1028 nm laser light and rather small 2PA for Au₁₈SR₁₄ with any of the excitations (800 nm and 1028 nm). Reproduced from Ref. ¹¹⁰ with permission from the Royal Society of Chemistry.

Off-resonance conditions of excitation of nanoclusters can still results in high TPA cross-sections. Discussed values of TPA of nanoclusters surpass those of conventional organic fluorophores, indicating superiority of nanoclusters among fluorescent probes and markers.

Such findings promise advancements in nonlinear optical imaging techniques and phototherapy, where high two-photon absorption cross-sections are crucial for achieving deep tissue penetration and high resolution.⁹⁸ Nowadays, even water soluble nanoclusters achieve significant multiphoton properties, therefore with ultrasmall sizes, tunability of optical properties and specificity due to variety of ligands, nanoclusters are successfully used for multiphoton applications. As an example remarkable two-photon properties of AgAu nanoclusters found application is DNA imaging in a liquid crystalline matrix under multiphoton microscope.¹¹⁸ TPA of nanoclusters stabilized with glutathione reached enormous values of 189 740 GM, which assured well staining of SH-SY5Y neuroblastoma cells.¹⁰⁶ Penicillamine stabilized nanoclusters effectively marked human cancer HeLa cells using confocal microscopy with two-photon excitation.¹¹⁹

CHAPTER 3 |

3 PUBLISHED WORK

3.1 ARTICLE 1: PLASMONIC ENHANCEMENT OF TWO-PHOTON EXCITED LUMINESCENCE OF GOLD NANOCCLUSERS

3.1.1 Short description of research work and results

INTRODUCTION

The first publication presents one of powerful methods to enhance detection of gold nanoclusters' luminescence using interaction with plasmonic nanoparticles. Remarkable optical properties of plasmonic nanoparticles are assigned to collective oscillation of valence band electrons, known as surface plasmon resonance (SPR). Plasmonic nanoparticles, e.g. gold nanorods (AuNRs) are already identified as a universal material for versatile applications, which unique properties were used for imaging,¹²⁰ biosensing,¹²¹ diagnostics,¹²² fabrication of superstructures¹²³, and many others extraordinary applications. Here we discuss the utility of plasmonic properties of nanorods for detection of single-particle fluorescent nanoclusters. Gold nanorods are well-known from narrow size distribution and well-established structure, presenting uniform optical properties, essential for systematic investigation of single-molecule and single-nanoparticle interaction. Due to chemically inert properties and biocompatibility of gold nanorods, they are particularly interesting for complexed systems with other materials. Additionally, tunable surface plasmon resonance of nanorods assures simple adjustability for desired conditions of study.¹²⁴ Owing to the shape of anisotropic gold nanorods, their sharp tips induce strong local electric field, which may be significantly intensified due to plasmon resonance.⁵⁶ In the following approach, luminescence of weakly emitting nanoclusters is strongly enhanced once the floating particles are found in close proximity of the plasmonic nanorod's tips.

Gold nanoclusters (AuNCs), besides plenty of advantages display relatively low luminescence. The early study on nanoclusters reported nanoclusters as emitters with QY not exceeding 1%, bringing strong limitation in application of AuNCs for fluorescence microscopy.⁹⁸ Further one-pot synthesis development result in improved luminescence of atomically precise AuNCs, however PL QY of those clusters is still limited up to ~5%.¹²⁵ In the following work, I have synthesized glutathione stabilized gold nanoclusters, Au₁₈(SG)₁₄, brightly luminescent in concentrated solution, however challenging for single-molecule imaging with standard detection techniques. Therefore, in this study I aimed to enhance single particle luminescence

signal of nanoclusters in the vicinity of plasmonic gold nanorods upon two-photon excitation. The idea of plasmon assisted enhanced luminescence was already investigated for quantum dots,¹²⁶ fluorescent dyes^{56, 127} and fluorescent proteins^{128, 129}. Here, for the first time described method was adapted to enhance luminescence of nanoclusters on a single-particle level. Although recent findings provide various single-molecule studies of detection of fluorophores under one-photon excitation, the multiphoton study is still poorly investigated in this field.⁵⁹ We took the advantage of higher order processes of multiphoton microscopy to monitor stronger interactions than possibly obtained in one-photon study, considering the quadratic dependence of intensity of two-photon induced emission on the excitation input.

Single-particle measurements hold a promise of deeper understanding of the nature of the plasmon–emitter interactions that is usually hidden beyond the bulk studies in a whole media, which contain also nanoparticle inhomogeneities and local environment changes.

METHODOLOGY

Single molecule luminescence enhancement can be performed through several methods, e.g. using zero-mode waveguide (ZMW) nanoapertures and nanogaps, plasmonic nanoparticles, metallic films or conjugating with quantum dots or dyes. Plasmon resonance strategy to enhance luminescence of single molecules was already studied on various plasmonic materials and various fluorescent chromophores, as explained in paragraph 2.2.1. Nanoclusters have never been applied in this approach as single molecules, therefore specific conditions for plasmonic investigation of a new material required careful optimization. Additionally, rarely explored two-photon study of plasmon luminescence enhancement needed examination of certain measurement conditions for efficient imaging of both – nanorods and nanoclusters.

First, gold nanorods require separation of individual nanoparticles and immobilization to glass sample surface. Gold nanorods, stabilized with surfactant, typically CTAB or CTAC prevent from aggregation and facilitate suspension. However, for a solid immobilization to the surface the CTAB agent require removal of its double layer. For this purpose, nanorods were numerously centrifuged and dissolved in water. Samples required careful optimization of the procedure of sample preparation through selection of accurate volume and concentration, time and speed of rotation, to remove double layer and simultaneously keep nanoparticles not only in non-aggregated form, yet still well separated from each other. Gold nanorods were further deposited on the glass surface by simple drop casting, removal of excess of sample and drying. Separation of single gold nanorods was estimated with the use of Atomic Force Microscope (AFM) and optical microscope in dark-field imaging. Narrow size distribution and proper separation of single plasmonic nanoparticles were determined with AFM before and CTAB double layer removal (Figure 11a).

Second issue of sample preparation involve appropriate concentration of nanoclusters and choice of medium for investigation of single nanorod-nanocluster luminescence events. Gold nanoclusters discussed in this work are water soluble, however pure water assure high mobility of nanoclusters, difficult for monitoring of single interaction events. To slow down the mobility of nanoclusters the different water:glycerine solvent conditions were tested.

Finally, I have determined luminescence enhancements of gold nanoclusters with two-photon fluorescence microscope. The home-made set-up consists of tuneable, mode-locked Ti:Sapphire laser, Nikon microscope body, Spectrograph Andor and APD detectors. Sample, placed on XYZ piezo-electric scanning stage is excited through high numerical aperture Nikon Plan Apo oil immersion objective. Two-photon excited emission from single nanorods is collected in epifluorescence mode on APD detectors, just after separation of signal from the incident laser beam on a dichroic mirror and shortpass filter (see Figure 11b). The major issue of two-photon measurements is addressed to appropriate conditions of measurements, often affected by Stoke shift of samples, but also technical parameters, such as determination of excitation power, strong enough for detection and yet not harmful for both of nanostructures, nanoclusters and nanorods. I have used multiphoton microscope to scan surface of glass sample with immobilized single plasmonic nanoparticles and then I collect luminescence time-traces of gold nanorods signal.

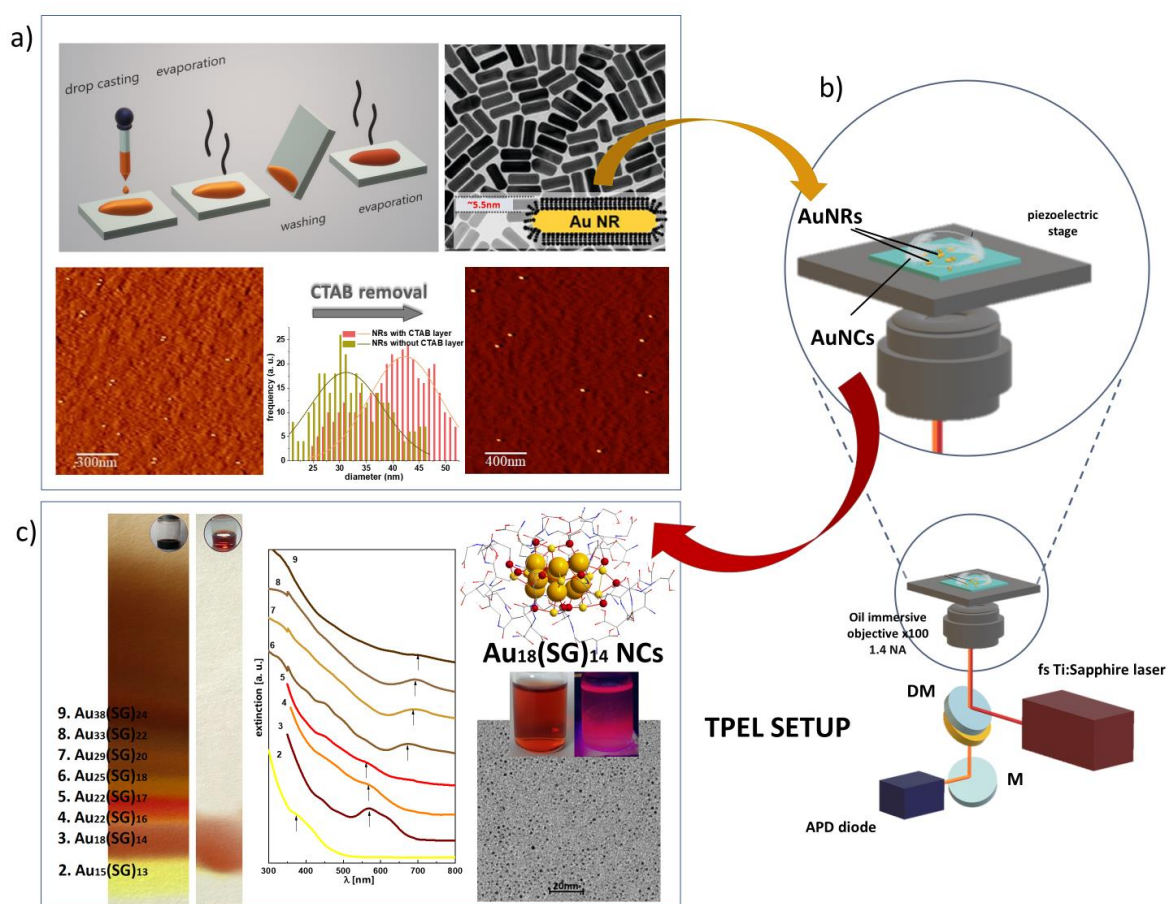


Figure 11. Illustration of general approach of gold nanorod assisted luminescence enhancement of single gold nanoclusters. A) The TEM and AFM image represent size of gold nanorods and dispersion of drop-casted nanoparticles on glass surface, before and after CTAB layer removal. B) Two-photon excited luminescence set-up (DM- dichroic mirror, M- mirror). C) gold nanoclusters solution, TEM image and identity proof provided by PAGE gel electrophoresis.

RESULTS AND DISCUSSION

The aim of this study was to monitor photoluminescence enhancement of single nanoclusters diffused in the close proximity of plasmonic nanoparticles. For this purpose, first general physico-chemical and optical properties of both materials, nanoclusters and gold nanoparticles were investigated.

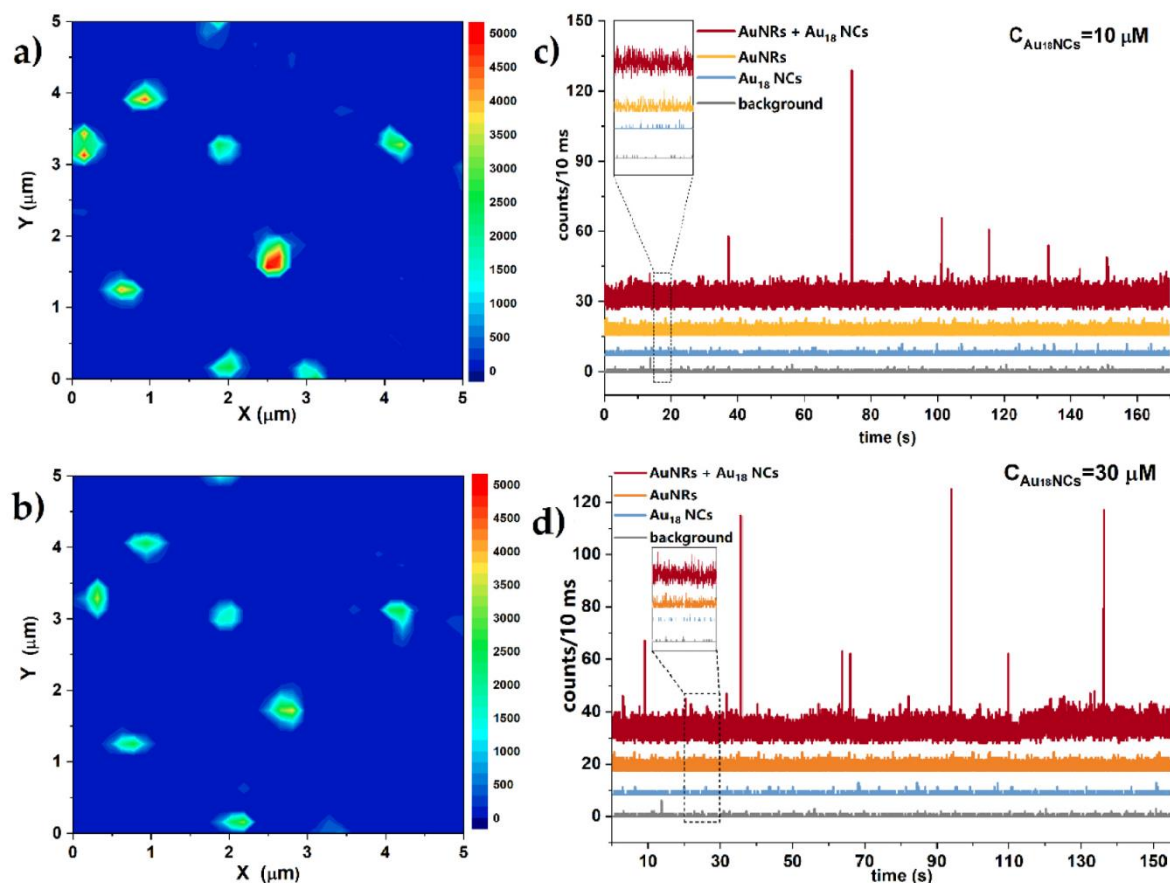


Figure 12. A) TPEL intensity map with bright luminescence from separated single AuNRs. B) Concentration dependent time-traces of luminescence of AuNCs on single plasmonic AuNRs. Over ~ 25 fold enhanced luminescence was recorded under two-photon excitation.

In this study I have synthesized and purified $\text{Au}_{18}(\text{SG})_{14}$ nanoclusters, which identity I have verified with PAGE gel electrophoresis (Figure 11c). Size determination with transmission electron microscopy (TEM) supplemented the spectroscopic analysis of their properties. Once I determined the major one-photon properties of nanoclusters further I have performed TPEL analysis of AuNCs through plasmonic nanoparticles. First, I have confirmed well-separation of single gold nanorods recording individual spots at TPEL intensity map (Figure 12a). Then I have monitored changes in luminescence intensity of drop-casted gold nanoclusters on single nanoparticles. Due to steady luminescence of gold nanorods under continuous low power irradiation, local bursts of luminescence were visibly monitored, referring to single nanoclusters floating nearby plasmonic nanoparticles. I have analyzed the two-photon excited luminescence enhancement of AuNCs at concentrations: $C = 10 - 30 \mu\text{M}$, and in different water:glycerine content. The strongest and most frequent enhancement events I have obtained for $30 \mu\text{M}$ AuNCs diluted in 1:1 solution of water and glycerine (Figure 12b), obtaining even ~ 25 -fold enhancement of luminescence from strongly diluted solution of gold nanoclusters in the vicinity of plasmonic nanoparticles. I have performed the experiment on

bare gold plasmonic nanoparticles and stabilized with CTAB layer. The more frequent and intense luminescence was recorded with shortest possible distance between nanoclusters and nanorods, therefore removal of any layers from bare gold nanoparticle facilitate single AuNCs detection. In this work, I have verified stability of nanoparticles under prolonged fs laser illumination, choosing 70 μW laser power, which did not affect nanoparticles structure, while assuring the reproducibility of obtained results.

In this work strong fluorescence enhancement was assured after meeting the requirements of overlapped surface plasmon resonance and emission of detected molecules. One of the other major impacts on two-photon luminescence enhancements is related with structural factors for both of materials: fluorophore (nanoclusters) and medium of detection (plasmonic nanoparticle). It is assumed that strongest enhancement of luminescence should appear at the sharp ends of plasmonic nanoparticle, at the strongest local electromagnetic field.⁵² Moreover, the nanoclusters structure impact on luminescence events have to be considered, since $\text{Au}_{18}(\text{SG})_{14}$ is not geometrically full symmetric and can create different level of emission enhancement depending on current orientation of AuNs.

Gold nanoclusters appeared here as a stable, homogeneous fluorophore, which fluorescent properties in NIR proved to have a strong potential in multiphoton microscopy. This preliminary study of interactions between single nanocluster and single plasmonic nanoparticle brings new possibilities for single nanoclusters sensing and imaging. This study opens nanoclusters on new category of strongly sensitive applications on the basis of single-molecule detection, even under two-photon excitation. In terms of this thesis, the applied strategy of plasmon mediated enhanced two-photon luminescence is a part of bigger picture on understanding the nonlinear optical properties of atomically precise clusters.

3.1.2 Research contribution of PhD candidate

Anna Pniakowska
Institute of Advanced Materials
Wroclaw University of Science and Technology

ul. Gdańska 7/9
50-344 Wroclaw

Autor contribution statement

I, Anna Pniakowska hereby declare that in the article: *A. Pniakowska, J. Olesiak-Bańska "Plasmonic Enhancement of Two-Photon Excited Luminescence of Gold Nanoclusters" Molecules, 2022, 27, 807*, I was responsible for:

- Methodology
- Investigation:
 - synthesis and purification of AuNCs,
 - PAGE gel electrophoresis of AuNCs,
 - determination of conditions for preparations of both samples, gold nanoclusters and gold nanorods;
 - analysis of morphology of AuNCs and AuNRs via TEM and AFM measurements;
 - one photon measurements: absorption and emission
 - dark-field scattering of AuNRs
 - two-photon measurements:
 - two-photon excited luminescence (TPEL),
 - TPEL time traces,
 - power dependent luminescence measurements,
- Visualization
- Data analysis
- Writing – original draft,



3.1.3 Contribution statements of co-authors

Joanna Olesiak-Bańska
Institute of Advanced Materials
Wroclaw University of Science and Technology

ul. Gdańska 7/9
50-344 Wroclaw

Author contribution statement

I, Joanna Olesiak-Bańska hereby declare that in the article: *A. Pniakowska, J. Olesiak-Bańska "Plasmonic Enhancement of Two-Photon Excited Luminescence of Gold Nanoclusters" Molecules, 2022, 27, 807*, I was responsible for:

- Conceptualization
- Writing : review and editing
- Supervision
- Funding acquisition


(signature)

3.1.4 Article and Supplementary Material

Article

Plasmonic Enhancement of Two-Photon Excited Luminescence of Gold Nanoclusters

Anna Pniakowska  and Joanna Olesiak-Banska * 

Advanced Materials Engineering and Modelling Group, Wrocław University of Science and Technology, Wybrzeże Wyspiańskiego 27, 50-370 Wrocław, Poland

* Correspondence: joanna.olesiak-banska@pwr.edu.pl

Abstract: Plasmonic-enhanced luminescence of single molecules enables imaging and detection of low quantities of fluorophores, down to individual molecules. In this work, we present two-photon excited luminescence of single gold nanoclusters, Au₁₈(SG)₁₄, in close proximity to bare gold nanorods (AuNRs). We observed 25-times enhanced emission of gold nanoclusters (AuNCs) in near infrared region, which was mainly attributed to the resonant excitation of localized surface plasmon resonance (LSPR) of AuNRs and spectral overlap of LSPR band with photoluminescence of AuNCs. This work is an initial step in application of combined nanoparticles: gold nanorods and ultrasmall nanoclusters in a wide range of multiphoton imaging and biosensing applications.

Keywords: gold nanorods; gold nanoclusters; two-photon excited luminescence; single molecule detection; plasmonic enhancement



Citation: Pniakowska, A.; Olesiak-Banska, J. Plasmonic Enhancement of Two-Photon Excited Luminescence of Gold Nanoclusters. *Molecules* **2022**, *27*, 807. <https://doi.org/10.3390/molecules27030807>

Academic Editor: Franck Rabilloud

Received: 30 December 2021

Accepted: 23 January 2022

Published: 26 January 2022

Publisher's Note: MDPI stays neutral with regard to jurisdictional claims in published maps and institutional affiliations.



Copyright: © 2022 by the authors. Licensee MDPI, Basel, Switzerland. This article is an open access article distributed under the terms and conditions of the Creative Commons Attribution (CC BY) license (<https://creativecommons.org/licenses/by/4.0/>).

1. Introduction

Unique optical properties of gold nanorods arise from collective oscillation of valence band electrons of metal nanoparticles, called surface plasmon resonance (SPR) [1]. Remarkable linear and nonlinear optical properties of gold nanostructures bring a wide range of application in surface-enhanced Raman spectroscopy [2], metal-enhanced fluorescence [3,4], and two-photon imaging [5]. Plasmonic nanostructures are one of the most commonly used materials as a platform of efficient optical detection for wide range of luminescent species [6–9]. Compared to other nanostructures, gold nanorods present narrow size distribution and well-established structure that lead to uniform optical properties, crucial for reliable investigation of single molecule and single-nanoparticle interaction [4,10]. Utility of gold nanorods is firmly motivated by tuneable surface plasmon resonance that can be tailored for the desired range of wavelengths above 600 nm. Besides, the tips of anisotropic plasmonic nanoparticles induce strong local electric field, easily accessible for interaction with chromophores floating nearby the nanoparticle. In this approach, amplification of electric field at the tips of nanorods led to enhanced luminescence of weakly emitting molecules. Careful selection of nanorods for interaction with specific fluorophores plays a key role in luminescence enhancement, since the mechanism of this process is strongly dependent on the spectral overlap of SPR band and emission spectrum of analysed fluorophores [6,11,12]. The distance between the nanoparticle and fluorophore is the second crucial factor governing emission enhancement [8,13]. Average highest enhancement has been observed in 5–20 nm distance from plasmonic surface [8,13,14].

Recent single-molecule findings provide detailed insights into processes that would be ordinarily averaged in bulk experiments. Although single-molecule studies of plasmon-enhanced luminescence detection are full of remarkable results discovered under one-photon excitation, studies of enhancement of multiphoton processes are still at the preliminary level. Compared to one-photon excitation, two-photon excitation is known for deeper penetration into (biological) samples, higher axial resolution, and better signal to noise

ratio, therefore, it is preferred in bioimaging applications. Two-photon excited photoluminescence and other multiphoton processes can also benefit from plasmonic enhancement. In theory, with higher order of multiphoton processes, proportionally stronger enhanced responses may appear. However, enhancement on single gold nanoparticle requires strictly controlled femtosecond (fs) laser power to avoid photoinduced reshaping of nanoparticles [15,16]. Nonlinear investigation of plasmon enhanced luminescence of chromophores is a relatively new method, which was examined only with quantum dots [10,17], fluorescent dyes [12,18], or fluorescent proteins [19]. Nanorod-assisted two-photon processes were usually enhanced several times, e.g., 11-times for T790 dyes [12] and 4-times for PVP dyes [18], while single-molecule study presented extremely strong enhancement, e.g., 1000-times for eqFP670 protein [19] and 10,000-times for CdSe/ZnS QDs [10].

Gold nanoclusters (AuNCs) with overall particle dimensions below 2 nm were categorized as a new class of nanomaterials, which attracted remarkable attention in recent years. Their photophysical and optical properties, tailored by atomically precise structure, arise from discrete electronic structure and molecule-like behaviour [5]. Nanoclusters possess unique emission. Depending on the nanoclusters size and structure, it can be located from blue to near infrared (NIR), the most attractive region in terms of bioimaging applications. Recent studies on toxicity and biodistribution of Au₁₈(SG)₁₄ in in vivo systems show promising results and are the first step to utilizing nanoclusters for bioimaging and biosensing applications [20–22]. Nanoclusters are well-characterised under one-photon excitation, but also present excellent nonlinear optical properties, which can be utilized in two-photon imaging [23–25]. Gold nanoclusters were found to be remarkable two-photon absorbers with high 2PA cross-sections (several hundred GM to several hundred thousand GM) [26,27]. However, photoluminescence quantum yield of nanoclusters is usually very low. Therefore, many techniques are examined to enhance the luminescence of nanoclusters.

Due to relatively low quantum yield of approximately 1–4%, it is challenging to image single nanoclusters using standard imaging techniques. To achieve single molecule sensitivity of detection, we used gold nanorod-assisted technique of luminescence enhancement of Au₁₈(SG)₁₄ (where SG stands for glutathione) on the basis of AuNCs diffusion in the vicinity of plasmonic nanoparticles. To determine most reproducible signal, we performed measurements on structurally consistent and equally sized nanorods and homogeneous nanoclusters build-up from the same number of gold atoms. In this manner, we synthesized and characterized one-photon optical properties of Au₁₈ NCs, which were further investigated in nonlinear regime. We performed systematic study of optical signal of AuNRs-AuNCs system under two-photon microscope, imaging individual nanorods. We demonstrate 25-fold enhancement of two-photon luminescence of nanoclusters as a result of resonant excitation of plasmonic nanorods.

2. Results

2.1. Synthesis and Characterisation of Gold Nanoclusters

The glutathione-protected gold nanoclusters, Au₁₈(SG)₁₄, were synthesized on the basis of Ghosh protocol with minor modifications [28,29]. Sodium cyanoborohydride used here as a milder reducing agent than NaBH₄ enabled the slowing down of the reduction of Au(I) and to favour size-selective growth of Au₁₈(SG)₁₄. The second factor influencing a slower reduction of gold is a dropwise addition of the reducer [29].

The extinction spectra of Au₁₈(SG)₁₄ obtained after synthesis revealed characteristic bands at 465, 515, and 590 nm (Figure 1a) and emission spectra at 750 nm (Figure 1b) following absorption and emission spectra reported previously [28,30]. The morphology of synthesized gold nanoclusters was determined under TEM (Figure 1a) revealing average size distribution equal to 1.75 ± 0.03 nm (Figure S1).

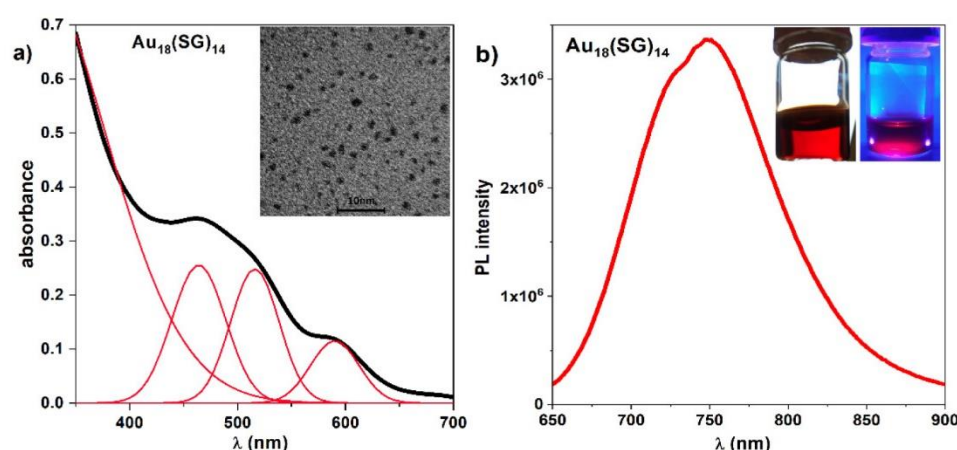


Figure 1. (a) Extinction spectra of $\text{Au}_{18}(\text{SG})_{14}$ with marked bands at 465, 515, and 590 nm. Upper right corner presents TEM image of NCs. (b) $\text{Au}_{18}(\text{SG})_{14}$ emission spectra with maximum peak position at 750 nm. Photographs in the inset present $\text{Au}_{18}(\text{SG})_{14}$ cluster solution in visible (left) and UV light (right).

In order to determine purity and homogeneity of synthesized nanoclusters, polyacrylamide gel electrophoresis was applied along with parallel separation of Au:SG nanoclusters mixture, synthesized according to the protocol described in the materials and methods. Final product of both glutathione nanoclusters, atomically-precise $\text{Au}_{18}(\text{SG})_{14}$ and Au:SG mixture, were maintained in a powder to provide better stability in time. In all experiments, the nanocluster powder was freshly dispersed in distilled water. Figure S2a shows well-distinguished fractions of Au:SG NCs marked 2–9, which correspond to nanoclusters with a precisely-defined number of building atoms: (2) $\text{Au}_{15}(\text{SG})_{13}$, (3) $\text{Au}_{18}(\text{SG})_{14}$, (4) $\text{Au}_{22}(\text{SG})_{16}$, (5) $\text{Au}_{22}(\text{SG})_{17}$, (6) $\text{Au}_{25}(\text{SG})_{18}$, (7) $\text{Au}_{29}(\text{SG})_{20}$, (8) $\text{Au}_{33}(\text{SG})_{22}$, and (9) $\text{Au}_{39}(\text{SG})_{24}$ [31]. The first fraction, $\text{Au}_{10}(\text{SG})_{10}$, visible only under UV light, was omitted here. As-synthesized $\text{Au}_{18}(\text{SG})_{14}$ NCs (right side of PAGE gel, Supplementary Materials, Figure S2a) shows only one band, indicating high purity of the synthesis. The same mobility of $\text{Au}_{18}(\text{SG})_{14}$ NCs and third fraction of Au:SG mixture confirms identification of synthesized product. Visible discontinuity of the linear alignment of the PAGE fractions were explained by nonuniform polymerization of separating gel or local polymer overheating. Regardless, it does not deteriorate the highest precision of gel electrophoresis separation since each AuNCs fraction presents unique UV/VIS spectra, characteristic for particular types of atomically-precise nanocluster (Supplementary Materials, Figure S2b) that resemble these reported previously [31].

2.2. Single Nanorods Sample Preparation for Multiphoton Study

Plasmonic enhancement of two-photon-excited luminescence was carried out on carefully prepared substrate of well dispersed nanoparticles acting as resonant platform for floating fluorophores. Gold nanorods used in this work present narrow size distribution within the sample, with average size of $42.2 \pm 7.6 \text{ nm} \times 17.4 \pm 3.8 \text{ nm}$, as determined by AFM microscope. AFM images of both samples, with 0.84 ug/mL concentrated AuNRs with CTAB, and with lowered concentration of CTAB, show relevant separation of nanoparticles, essential for further multiphoton study (Figure 2a,b). We determined $\approx 11 \text{ nm}$ length difference between covered and bare gold nanoparticles, implying $\approx 5.5 \text{ nm}$ thick CTAB bi-layer (Supplementary Materials, Figure S3), which is in good agreement with the literature [32,33]. Dark-field images and single molecule scattering spectra of individual AuNRs present overlapping LSPR peak position as overall solution of AuNRs, indicating high homogeneity of plasmonic nanoparticles (Supplementary Materials, Figure S4).

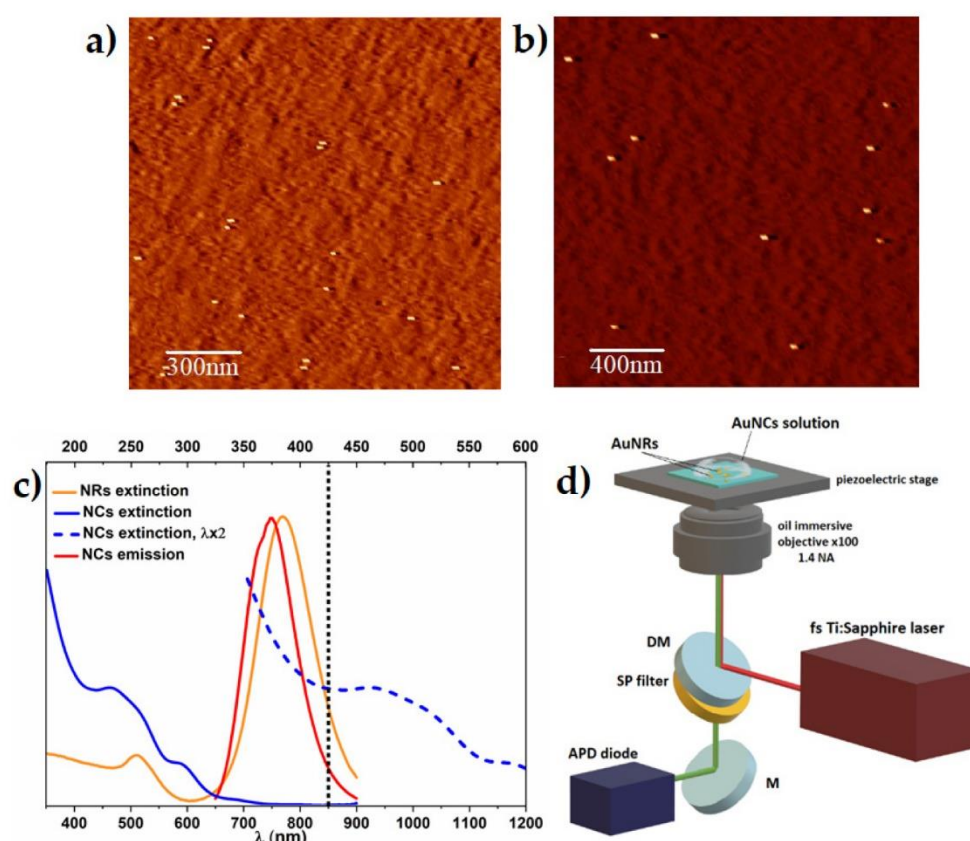


Figure 2. AFM images of (a) CTAB-coated and (b) bare gold nanorods. (c) Spectral overlap of longitudinal surface plasmon resonance band of nanorods (orange) and emission band of Au₁₈ nanoclusters emission (red). One-photon absorption of nanoclusters (blue solid line) with expected two-photon absorption spectrum (blue dotted line), plotted as one-photon absorption at the double wavelength. Vertical black dotted line represents the laser wavelength used in two-photon excitation ($\lambda_{\text{exc}} = 850$ nm). (d) A scheme of the experimental setup (NA = numerical aperture, APD = avalanche photodiode, DM = dichroic mirror, and M = mirror). Above the objective and on the top of the piezoelectric stage, glass sample is placed with immobilised gold nanorods and a droplet of nanoclusters diffusing in a glycerol solution.

2.3. Multiphoton Study of Single Nanoclusters Luminescence Enhancement on Single Nanorods

To verify wavelength dependence of two-photon absorption of AuNCs, we examined two-photon excited luminescence (TPEL) at several wavelengths and confirmed the origin of photoluminescence in simultaneous absorption of two photons for $\lambda > 820$ nm (see a log-log plot of TPEL intensity as a function of the incident laser average power in Supplementary Materials, Figure S5). Multiple reports [6,8,11] established that the strongest plasmonic enhancement of fluorophore emission was observed when excitation wavelength match the maximum of LSPR wavelength. To efficiently excite both the longitudinal surface plasmon resonance of AuNRs ($\lambda_{\text{LSPR}} = 770$ nm) and AuNCs in their range of two-photon absorption, we moved excitation wavelength to the NIR region to 850 nm (Figure 2c). The two-photon luminescence enhancement experiments were performed as shown in Figure 2d, with optical set-up described in detail in materials and methods.

Figure 3a shows multiphoton luminescence intensity images obtained by scanning the sample of gold nanorods immobilized on a glass surface. Individual bright spots correspond to strong emission intensity of well-dispersed single AuNRs. Stable photoluminescence from a single plasmonic emitter was recorded under prolonged laser power of 70 μW at the beam focus, as presented on the emission time trace graph (Figure 3c,d). Single gold nanorod maintained constant emission intensity for at least 3 min, which indicated preserved original shape of a nanorod (Figure 3c,d yellow lines). Chosen laser power was

sustained through all measurements as it was not harmful for nanorods, yet strong enough to detect single nanoparticle luminescence. The photon count window (bin time) was set to 10 ms to register clear on/off states of enhanced luminescence, not disturbed by signal to noise ratio.

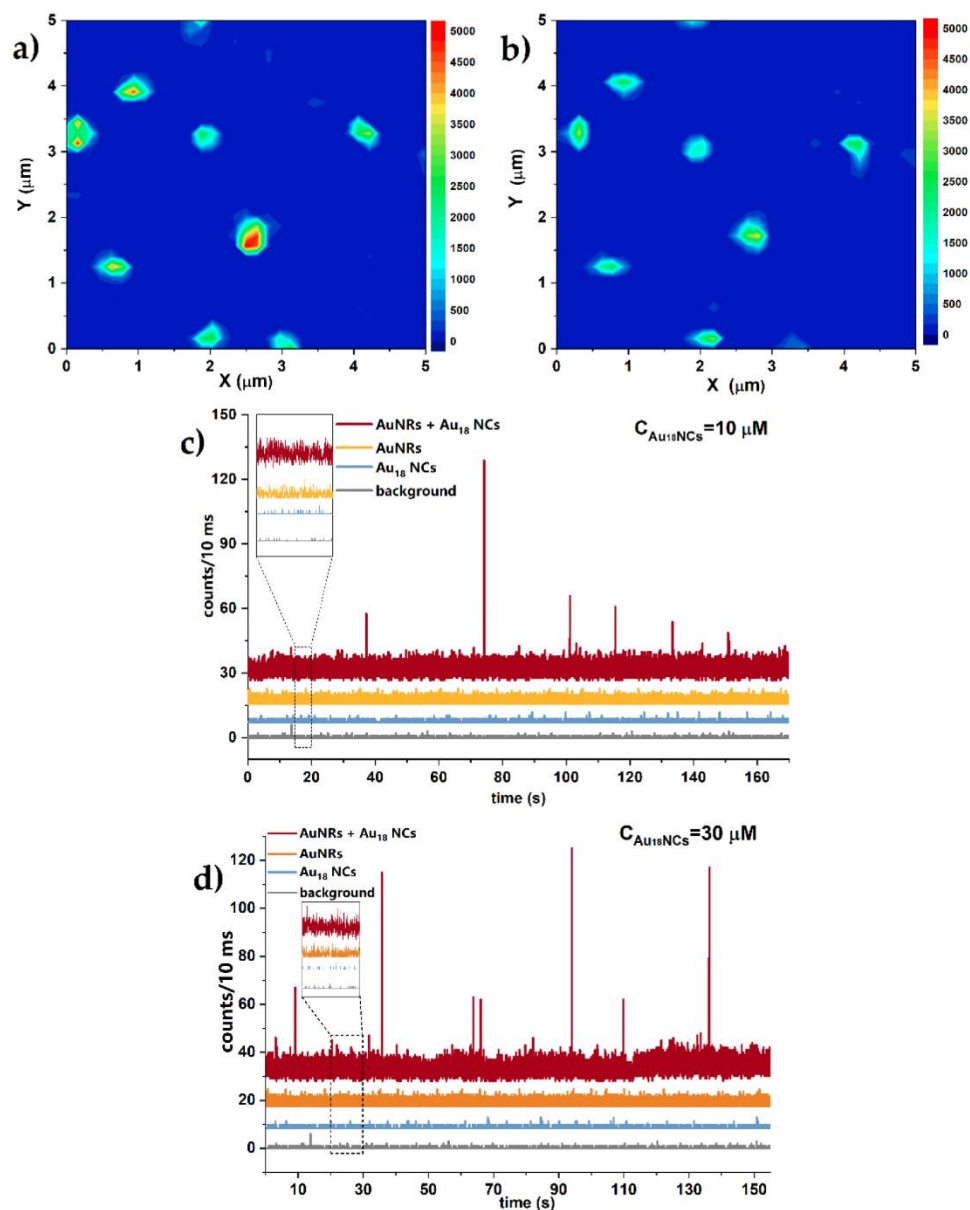


Figure 3. (a,b) TPL intensity map of well-separated AuNRs before (a) and after (b) covering with glycerine solution of AuNCs. (c,d) luminescence time traces of samples: AuNRs with local emission enhancement of floating AuNCs (red), solutions of AuNRs only (orange), AuNCs only (blue), and background noise (grey), monitored under prolonged irradiation of $70 \mu\text{W}$ in 10 ms photon counting window. AuNCs emission enhancement was determined in two concentration dependent conditions: (c) $10 \mu\text{M}$ and (d) $30 \mu\text{M}$.

Gold nanorods immobilised on a glass plate were further covered by $\text{Au}_{18}(\text{SG})_{14}$ solution droplet (1:1, H_2O :glycerine). TPEL intensity scan repeated in exactly the same location of the sample shows unchanged nanorods distribution, indicating good adhesion of bare nanorods to the glass coverslip (Figure 3b). Negligibly lower TPEL intensity after addition of nanoclusters glycerol solution was related with the change of dispersion medium and respective refractive index. TPEL time traces from single gold nanorods show constant TPEL signal with frequent enhanced luminescence bursts from floating AuNCs

in the vicinity of plasmonic nanoparticles, that last for 10–30 ms (Figure 3c,d, red line). To distinguish recorded emission enhancement of AuNCs–AuNRs hybrid from reference signals, we conducted TPEL time traces of separate components: single AuNRs, solution of AuNCs, and the background noise in the same conditions. Size limitations of luminescent techniques exclude the detection of a single gold nanocluster without plasmonic-mediator, thus, we determined the lowest detectable concentration of nanoclusters to be 10 μM at the strongest power illumination (limited by melting and reshaping of nanorods). In these conditions, ≈ 6 single nanoclusters were illuminated at the same time. Therefore, we report up to 25-times stronger luminescence of single Au₁₈ NCs in the close proximity of a NR, compared to TPEL of NCs solution with low concentration of NCs, measured without the presence of gold nanorods.

Calculated average number of occurring events addresses the difference between monitored intensity of AuNCs + AuNRs sample vs. AuNRs alone (Figure 4). To confirm that the observed luminescence bursts are associated with the presence of nanocluster molecules in close proximity of nanorods, we conducted additional experiments of emission time traces in identical conditions, exchanging nanocluster molecules with pure water:glycerol solution. As expected, no luminescence enhancement occurred in this circumstance [Supplementary Materials, Figure S6].

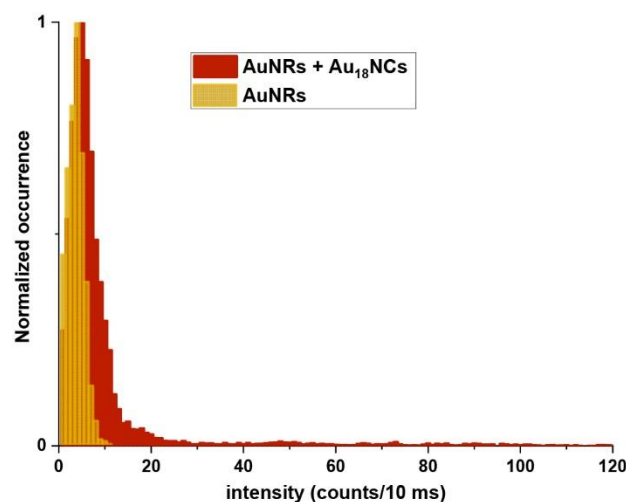


Figure 4. Distribution of number of occurring events of gold nanoclusters TPEL with gold nanorods (red) and gold nanorods itself (yellow).

Establishing the conditions of AuNCs concentration and viscosity are crucial for studies of the photoluminescence intensity enhancement in the vicinity of nanoparticles. We performed two-photon excited luminescence analysis of AuNCs at two concentrations, $C = 10 \mu\text{M}$, $30 \mu\text{M}$, and in different water:glycerine content. The most frequent enhancement events were obtained for $30 \mu\text{M}$ Au₁₈(SG)₁₄ diluted in 1:1 solution of water and glycerine. High viscosity of glycerine slows down the overall movement of single nanoclusters, while pure glycerine generates too high adhesive tensions with the glass surface, which leads to peeling of single nanorods from the support. A 1:1 solution of water and glycerine has the advantage of glycerine usage without causing any dislocation of AuNRs.

3. Discussion

The first requirement of the investigation of the single-molecule two-photon-excited luminescence is appropriate preparation of single nanoparticles sample as an emission enhancement platform for floating fluorophores. Gold nanorods capped with CTAB surfactant stabilize the water suspension, therefore drop-casting the solution of nanoclusters on the top of immobilized nanorods conveyed the nanorods from the surface of glass sample. Removal of CTAB layer resulted in raised surface tension and stronger adhesion of bare nanorods to the surface [34]. Additionally, by decreasing the amount of positively charged

CTAB on the surface of nanoparticle, the overall electric charge of nanoparticles is closer to neutral [35,36]. It creates better conditions for free diffusion of negatively charged AuNCs in a close area of nanorods, without permanent attachment. Removed CTAB layer enabled monitoring of molecule interaction at closest possible distance. Although the literature findings specify the strongest luminescence enhancement at 10–20 nm between metal surface and fluorophore [8], similar to W. Zhang [37] and E. Wientajes [38], we observed more frequent and more intense bursts of luminescence when AuNCs interacted with bare single nanorod at the shorter distance. It finds good agreement with a particular study, where plasmonic assisted two-photon luminescence occurred at shorter distance of interactions than one-photon ones. The closer the excitation was to the surface plasmon resonance band, the stronger the local electric enhancement, and therefore, stronger two-photon excited luminescence was monitored. Moreover, two-photon excitation process involves simultaneous absorption of two photons, and thus, the excitation rate is proportional to the fourth power of local electric field [12].

Monitored 25-fold plasmonic luminescence enhancement of Au₁₈ single molecules might reach higher values, when compared to single Au₁₈ nanoclusters. Nevertheless, monitored enhancements highlight the benefit of single-particle luminescence detection over the average signal of gold nanoclusters bulk solution. However, to study emission enhancement of single molecules, the crucial part is the choice of excitation conditions for monitoring two-photon excited luminescence. The most intensive single molecule luminescence was mainly observed at resonant excitation of plasmonic nanoparticle. Plasmon peak placed between the absorption and emission maximum of fluorophore fulfil the requirements of strongest emission enhancement [39]. In this work, we established conditions for efficient excitation of both longitudinal surface plasmon resonance of AuNRs ($\lambda_{\text{LSPR}} = 770$ nm) and AuNCs in their range of two-photon absorption ($\lambda > 820$ nm). Since chosen resonance excitation wavelengths have major impacts on the final result of luminescence enhancement, shifting of the laser wavelength around 50 nm from the most favourable region of LSPR maximum may lead to more than one order of magnitude in dropped luminescence enhancement [10]. Therefore, we assume that multiphoton luminescence of AuNCs may potentially reach higher values than reported in this work, with 25-fold enhancement at $\lambda_{\text{exc}} = 850$ nm. However, we highlight here the requirements of overlap of LSPR and emission of nanoclusters in NIR region.

Random distribution of enhanced TPEL signal above average 6 counts/10 ms of AuNRs, up to 120 counts/10 ms (Figure 4), was attributed to the AuNCs in close proximity of nanorods and may be initiated by several factors. Different level of enhancement of chromophores were previously explained by random orientation of molecules in the resonance field of nanorods [10]. Au₁₈ NCs presents core-shell elongated structure, as shown on the structure model in Figure S7 [40]. Therefore, we assume that anisotropy of AuNCs structure results in enhancement dependent on the mutual orientation of NCs and a nanorod which may affect final luminescence burst intensities, while freely floating AuNCs near plasmonic particle are in different local position. Moreover, the strongest enhancement of emission signal was monitored at the sharp ends of nanorods, in the strongest local electromagnetic field [4,41]. Thus, free motion of AuNCs around a nanorod allow local interaction, with the tip and lateral side of plasmonic nanoparticle inducing different level emission enhancement proportional to the near-field intensity of a nanorod.

According to W. Zhang [37], when two molecules interact with the same nanorod at the same time, luminescence signal will reach another higher level of enhancement. Although the average <2 nm size of nanoclusters creates space for simultaneous collective action of luminescence enhancement, the experiment was carried with low concentrated AuNCs to prevent multiple circumstances that might disturb single-molecule investigation. Recorded low number of occurrences excludes the possibility of several actions at the same time. Short duration of single bursts in the order of 10 ms confirms the presence of a single nanocluster in the hotspot during local enhancement. Similar duration of emission enhancement of freely diffusing single molecule in the area of a gold nanorod

was previously noted [42]. There were two solutions to preserve molecules for longer in the vicinity of near-field of nanorods: raise the viscosity of solvent, or use additional linkers [37,42]. We examined plasmonic enhancement of nanoclusters in solvents of the range of different densities, however, except of slower diffusion of fluorophores, high glycerine content solvents peel off immobilised nanorods from a glass surface. We report in this work optimised conditions of slow free diffusion for single nanocluster detection.

We highlight the importance of strictly controlled femtosecond laser power in multiphoton studies, since intensive laser source heats up the plasmonic electron gas that induces nanoparticle reshaping, broadening, and/or shift the plasmon resonance [15,16,43], and significantly lower plasmon-mediated enhancement. In this work, we performed multiple experiments on nanorods stability under prolonged fs laser illumination. Chosen average power (70 μ W) did not affect nanoparticles structure, assuring the reproducibility of enhanced luminescence results. Repeatable experiments of two-photon excited luminescence of gold nanoclusters assure future standardization of processes and usability in bio-detection. Technique of plasmon-enhanced luminescence of single molecules already has its first successful bioimaging application in lipid membrane, a model system for studying biological membranes [44]. Application of two-photon excitation ensures strong fluorescence enhancement for single-molecule imaging of cells [12]. Additional benefits of two-photon excitation over one-photon one, e.g., lowered sample photodamage and deeper penetration across the sample are strongly desirable for imaging and sensing applications in near infrared region.

4. Materials and Methods

4.1. Chemical

All the chemicals are commercially available and used without further purification. Gold(III) chloride trihydrate ($\text{HAuCl}_4 \cdot 3\text{H}_2\text{O}$, 99.999%), L-Glutathione reduced (GSH) $\geq 98.0\%$, sodium cyanoborohydride (NaBH_3CN , 95%), sodium borohydride (NaBH_4 , 99.99%), and aqueous suspension of gold nanorods (10 nm diameter, 780 nm SPR absorption maximum) were purchased from Sigma-Aldrich. Aqueous 40% acrylamide and bisacrylamide stock solution (37.5:1), N,N,N',N'-tetramethylethylenediamine (TEMED, 99%), N,N'-methylene bisacrylamide (Bis, $>98\%$), and $10\times$ concentrated SDS-PAGE running buffer (SDS) were supplied from Carl Roth. Ammonium persulfate (APS, 98%), 0.5 M Tris-HCl buffer pH 6.8, and 1.5 M Tris-HCl buffer pH 8.8 were purchased from BIO-RAD. Deionized (milli-Q) water with a resistivity of 18 $\text{M}\Omega \text{ cm}$ was used in this work.

4.2. Synthesis of Gold $\text{Au}_{18}(\text{SG})_{14}$ Nanoclusters

Synthesis of nanoclusters was based on the protocol given by Ghosh [28], with further modifications reported by Manzhou Zhu [30] and Stamplecoskie [29]. Briefly, 0.6 mL of MeOH, 0.6 mL of water, and 150 mg of GSH were gently mixed in 25 mL round flask for 10 min. Then, 0.3 mL aqueous solution of $\text{HAuCl}_4 \cdot 3\text{H}_2\text{O}$ (0.635 M, 75 mg) was added. Colour of stirred solution slowly changed from yellow to almost colourless, indicating the conversion of Au^{3+} to Au^+ . After 10 min, solution was diluted to 15 mL by MeOH, followed by slow dropwise addition of 2.25 mL methanolic solution of NaBH_3CN (220 mM). After 2 h of vigorous stirring, the precipitate was collected and washed with MeOH three times through centrifugal precipitation (10 min, 7000 rcf). Then, solution was dissolved in a small amount of water, centrifuged to remove unreacted thiolate, and finally dried to obtain red powder.

4.3. Synthesis of Gold Au:SG Nanoclusters

Synthesis of gold Au:SG nanoclusters followed the protocol by Tsukuda and co-workers [31]. First, 25 mL of MeOH was carefully stirred with 153 mg of GSH for 10 min in 50 mL round flask. Then, 0.197 mL of aqueous solution of $\text{HAuCl}_4 \cdot 3\text{H}_2\text{O}$ (0.635 M) was added, stirred until mixture became almost colourless, and cooled down in cool bath for 30 min. Next, freshly prepared cold NaBH_4 (6.25 mL, 0.2 M) was rapidly injected into

vigorously stirred mixture. Instant change of colour to dark brown implied fast reduction of gold to Au⁰. After 1 h of vigorous stirring, precipitate was collected and washed repeatedly with MeOH through centrifugal precipitation (10 min, 7000 rcf) to remove the remaining precursors. Then, solution was left to complete evaporation of solvent.

4.4. PAGE Electrophoresis

A separation of the clusters was performed according to the procedure of polyacrylamide gel electrophoresis (PAGE) [45,46]. Detailed volumes are collected in Table S1 (Supplementary Materials). The separating and stacking gels were prepared from acrylamide monomers with the final concentrations of 24.3%T; 3.8%C of high density gel and 20%T; 2.6%C of low density gel, where %T denotes the total monomer (acrylamide and bisacrylamide) concentration and %C is the concentration of the crosslinking. The clusters were dissolved in 5% (v/v) glycerol/water to final concentration of 5 mg/mL. A 1 mm gel thickness was used for preparative separations into cluster fractions. Electrophoresis was carried out for 16 h in a constant voltage mode set to 150 V. Finally, the separating gel was cut into stripes, and the particular fractions were eluted with water.

4.5. Preparation of Gold Nanorods Sample and Imaging of Gold Nanoparticles

Aqueous suspension of gold nanorods purchased from Sigma Aldrich were stabilized by cetyltrimethylammonium bromide (CTAB). To immobilize nanoparticles on the glass coverslip and provide access of floating fluorophores on the surface of bare gold nanorods, an outer layer of CTAB had to be removed. For this purpose, a small amount (50 µL, 30 µg/mL) of the nanoparticles solution was washed with deionized water and centrifuged (300 rcf, 3 min) several times until gold nanorods were still able to suspend in water without permanent aggregation. Such prepared bare gold nanorods in deionized water were deposited by drop casting on purified glass coverslip. After 10 min, the droplet was washed out and air dried. Same procedure was performed for a set of several concentrations (4.2 µg/mL, 0.84 µg/mL, and 0.084 µg/mL). Then, gold nanorods separation and size distribution on glass coverslip were estimated with Atomic Force Microscope (AFM) (Dimensional V scanning probe microscope, Veeco) operating in a tapping mode. Nanoparticles separation was further confirmed with dark field imaging using Nikon Eclipse inverted optical microscope with Nikon Dark Field Condenser. Scattering spectra were recorded using a Shamrock 303i spectrograph from Andor.

The morphological features of the AuNRs and AuNCs were determined using FEI Tecnai G2 20 X-TWIN transmission electron microscopy (TEM).

4.6. Characterization of Linear and Nonlinear Optical Properties of Nanoparticles

Extinction and emission spectra of the synthesized gold nanoclusters and nanorods were obtained using a JASCO V-670 Spectrophotometer and Hitachi F-4500 spectrofluorometer.

Multiphoton experiments of both AuNRs and AuNCs were conducted under custom-made setup. The glass samples were placed on the XYZ piezo-electric scanning stage (TRITOR 102, Piezोजना) and excited using a tuneable, mode-locked Ti:sapphire laser operating at 80 MHz pulse repetition rate (Chameleon, Coherent Inc., Santa Clara, CA, USA). A high numerical aperture Nikon Plan Apo oil immersion objective (100×/1.4 NA) was used for the focusing of a circularly polarized incident laser beam on the sample and for the collection of multiphoton-excited emission in epifluorescence mode. The emitted signal was separated from the incident laser beam on a dichroic mirror and collected by avalanche photodiodes operating in the photon counting regime. The two-photon excited emission spectra were recorded using a Shamrock 303i spectrograph from Andor.

5. Conclusions

In conclusion, our goal was usage of plasmonic nanoparticles to detect gold nanoclusters on the single-molecule level, which is challenging to pursue in conventional techniques. We proved the advantage of single-molecule technique of detection, emphasizing the dif-

ference in the emission intensity of single particles against the average signal of a bulk form of nanoparticles. We conduct, for the first time, the enhancement of weakly emissive atomically-precise nanoclusters on a single plasmonic nanoparticle, under two-photon excitation. Wet-chemically synthesised nanoclusters, $\text{Au}_{18}\text{SG}_{14}$, present 25-times stronger two-photon excited luminescence in close proximity of homogeneous single nanorods by the strong local field of a nanorod under surface plasmon resonance excitation. TPEL enhancement was addressed to well-selected excitation conditions: two-photon excitation of gold nanoclusters at the wavelength between excitation of LSPR of the plasmonic nanoparticle and emission of nanoclusters. Two-photon absorption of nanoclusters was confirmed by quadratic dependence of TPEL of nanoclusters on average power of excitation laser.

Our preliminary study of single nanocluster–single plasmonic nanoparticle interactions provides new opportunities for gold nanoclusters applications in single particle sensing and imaging. We reveal in this work that nanoclusters may find potential application as ultrasmall fluorophores in multiphoton bioimaging and biosensing, with particular interest of luminescence in near-infrared region.

Supplementary Materials: The following supporting information can be downloaded. Figure S1: (a) TEM image and (b) size distribution histogram of $\text{Au}_{18}(\text{SG})_{14}$ nanoclusters.; Table S1: Page electrophoresis; Figure S2: (a) Photograph of electrophoretic polyacrylamide gel with well-separated 2–9 fractions of Au:SG mixture (left) and single fraction of $\text{Au}_{18}(\text{SG})_{14}$ product of synthesis (right), which after electrophoresis separation were cut into pieces and dissolved in water (below). (b) Extinction spectra of 2–9 fractions of Au:SG mixture. (c) Comparison of UV/VIS spectra of as-synthesized $\text{Au}_{18}(\text{SG})_{14}$ NCs and 3rd fraction of Au:SG mixture (identified as Au_{18} NCs) from PAGE separation.; Figure S3: Size distribution of nanorods before and after CTAB layer removal. Average diameter of NRs with CTAB layer is estimated as 42.2 ± 7.64 nm, while NRs without CTAB layer is 31.2 ± 8.22 nm.; Figure S4: (A) Dark field image of gold nanorods well-separated on the glass sample. (B) Extinction spectrum of gold nanorods solution and scattering spectrum (red line) of single gold nanorod.; Figure S5: Log-log plot of the PL intensity of AuNCs as a function of excitation laser power measured at several excitation wavelengths. The slope of the linear fit to each datapoints sets corresponds to the level of multiphoton processes, n (for two-photon absorption $n = 2$).; Figure S6: Luminescence time traces of samples: AuNRs in water: glycerine solution in the absence of AuNCs (red). Samples are compared to AuNRs only (orange) or AuNCs solution only (blue) and background noise (grey), monitored under prolonged irradiation with average power $70 \mu\text{W}$.; Figure S7: 3D model of $\text{Au}_{18}(\text{SG})_{14}$ structure with precise location of gold core (yellow—Au atoms) and staple motifs (yellow—Au atoms, red-S atoms) of nanocluster. Structure was energy-minimized with molecular mechanic MM2 model in Chem3D. References [29,29,47,48] are cited in the supplementary materials.

Author Contributions: Conceptualization, J.O.-B.; methodology, A.P.; investigation, A.P.; writing—original draft preparation, A.P.; writing—review and editing, J.O.-B.; visualization, A.P.; supervision, J.O.-B.; funding acquisition, J.O.-B. All authors have read and agreed to the published version of the manuscript.

Funding: This research was funded by Sonata Bis 9 project (2019/34/E/ST5/00276), financed by National Science Centre in Poland.

Data Availability Statement: Data is contained within the article or Supplementary Materials.

Acknowledgments: We acknowledge Radosław Deska for fruitful discussions regarding the experimental part of two-photon excited luminescence measurements.

Conflicts of Interest: The authors declare no conflict of interest.

Sample Availability: Not available.

References

1. Huang, X.; El-Sayed, M.A. Gold nanoparticles: Optical properties and implementations in cancer diagnosis and photothermal therapy. *J. Adv. Res.* **2010**, *1*, 13–28. [[CrossRef](#)]
2. Gruenke, N.L.; Cardinal, M.F.; McAnally, M.O.; Frontiera, R.R.; Schatz, G.C.; Van Duyne, R.P. Ultrafast and nonlinear surface-enhanced Raman spectroscopy. *Chem. Soc. Rev.* **2016**, *45*, 2263–2290. [[CrossRef](#)] [[PubMed](#)]

3. Geddes, C.D.; Lakowicz, J.R. Editorial: Metal-Enhanced Fluorescence. *J. Fluoresc.* **2002**, *12*, 121–129. [[CrossRef](#)]
4. Khatua, S.; Paulo, P.; Yuan, H.; Gupta, A.; Zijlstra, P.P.; Orrit, M. Resonant Plasmonic Enhancement of Single-Molecule Fluorescence by Individual Gold Nanorods. *ACS Nano* **2014**, *8*, 4440–4449. [[CrossRef](#)]
5. Olesiak-Banska, J.; Waszkielewicz, M.; Obstarczyk, P.; Samoc, M. Two-photon absorption and photoluminescence of colloidal gold nanoparticles and nanoclusters. *Chem. Soc. Rev.* **2019**, *48*, 4087–4117. [[CrossRef](#)]
6. Yuan, H.; Khatua, S.; Zijlstra, P.; Yorulmaz, M.; Orrit, M. Thousand-fold Enhancement of Single-Molecule Fluorescence Near a Single Gold Nanorod. *Angew. Chem. Int. Ed.* **2013**, *52*, 1217–1221. [[CrossRef](#)]
7. Mulpur, P.; Kurdekar, A.; Podila, R.; Rao, A.M.; Kamiseti, V. Surface plasmon coupled emission as a novel analytical platform for the sensitive detection of cysteine. *Nanotechnol. Rev.* **2015**, *4*, 393–400. [[CrossRef](#)]
8. Fu, B.; Flynn, J.D.; Isaacoff, B.P.; Rowland, D.J.; Biteen, J.S. Super-Resolving the Distance-Dependent Plasmon-Enhanced Fluorescence of Single Dye and Fluorescent Protein Molecules. *J. Phys. Chem. C* **2015**, *119*, 19350–19358. [[CrossRef](#)]
9. Tam, F.; Goodrich, G.P.; Johnson, B.R.; Halas, N.J. Plasmonic Enhancement of Molecular Fluorescence. *Nano Lett.* **2007**, *7*, 496–501. [[CrossRef](#)]
10. Zhang, W.; Caldarola, M.; Lu, X.; Orrit, M. Plasmonic Enhancement of Two-Photon-Excited Luminescence of Single Quantum Dots by Individual Gold Nanorods. *ACS Photon* **2018**, *5*, 2960–2968. [[CrossRef](#)]
11. Chen, Y.; Munechika, K.; Ginger, D.S. Dependence of Fluorescence Intensity on the Spectral Overlap between Fluorophores and Plasmon Resonant Single Silver Nanoparticles. *Nano Lett.* **2007**, *7*, 690–696. [[CrossRef](#)] [[PubMed](#)]
12. Zhao, T.; Yu, K.; Li, L.; Zhang, T.; Guan, Z.; Gao, N.; Yuan, P.; Li, S.; Yao, S.Q.; Xu, Q.-H.; et al. Gold Nanorod Enhanced Two-Photon Excitation Fluorescence of Photosensitizers for Two-Photon Imaging and Photodynamic Therapy. *ACS Appl. Mater. Interfaces* **2014**, *6*, 2700–2708. [[CrossRef](#)] [[PubMed](#)]
13. Abadeer, N.S.; Brennan, M.R.; Wilson, W.L.; Murphy, C.J. Distance and Plasmon Wavelength Dependent Fluorescence of Molecules Bound to Silica-Coated Gold Nanorods. *ACS Nano* **2014**, *8*, 8392–8406. [[CrossRef](#)] [[PubMed](#)]
14. Cheng, D.; Xu, Q.-H. Separation distance dependent fluorescence enhancement of fluorescein isothiocyanate by silver nanoparticles. *Chem. Commun.* **2007**, *3*, 248–250. [[CrossRef](#)] [[PubMed](#)]
15. Taylor, A.B.; Siddiquee, A.M.; Chon, J.W.M. Below Melting Point Photothermal Reshaping of Single Gold Nanorods Driven by Surface Diffusion. *ACS Nano* **2014**, *8*, 12071–12079. [[CrossRef](#)] [[PubMed](#)]
16. Gordel, M.; Olesiak-Banska, J.; Matczyszyn, K.; Nogues, C.; Buckle, M.; Samoc, M. Post-synthesis reshaping of gold nanorods using a femtosecond laser. *Phys. Chem. Chem. Phys.* **2014**, *16*, 71–78. [[CrossRef](#)] [[PubMed](#)]
17. Li, X.; Kao, F.-J.; Chuang, C.-C.; He, S. Enhancing fluorescence of quantum dots by silica-coated gold nanorods under one- and two-photon excitation. *Opt. Express* **2010**, *18*, 11335–11346. [[CrossRef](#)]
18. Craciun, A.; Focsan, M.; Gaina, L.; Astilean, S. Enhanced one- and two-photon excited fluorescence of cationic (phenothiazinyl)vinyl-pyridinium chromophore attached to polyelectrolyte-coated gold nanorods. *Dye. Pigment.* **2017**, *136*, 24–30. [[CrossRef](#)]
19. Shokova, M.A.; Bochenkov, V.E. Efficiency of Plasmon-Induced Dual-Mode Fluorescence Enhancement upon Two-Photon Excitation. *Nanomaterials* **2021**, *11*, 3334. [[CrossRef](#)]
20. Sobska, J.; Waszkielewicz, M.; Podleśny-Drabiniok, A.; Olesiak-Banska, J.; Krężel, W.; Matczyszyn, K. Gold Nanoclusters Display Low Immunogenic Effect in Microglia Cells. *Nanomaterials* **2021**, *11*, 1066. [[CrossRef](#)]
21. Zheng, Y.; Lai, L.; Liu, W.; Jiang, H.; Wang, X. Recent advances in biomedical applications of fluorescent gold nanoclusters. *Adv. Colloid Interface Sci.* **2017**, *242*, 1–16. [[CrossRef](#)] [[PubMed](#)]
22. Chen, L.-Y.; Wang, C.-W.; Yuan, Z.; Chang, H.-T. Fluorescent Gold Nanoclusters: Recent Advances in Sensing and Imaging. *Anal. Chem.* **2015**, *87*, 216–229. [[CrossRef](#)] [[PubMed](#)]
23. Yousefalizadeh, G.; Ahmadi, S.; Mosey, N.J.; Stamplecoskie, K.G. Exciting clusters, what does off-resonance actually mean? *Nanoscale* **2020**, *13*, 242–252. [[CrossRef](#)] [[PubMed](#)]
24. Brach, K.; Waszkielewicz, M.; Olesiak-Banska, J.; Samoc, M.; Matczyszyn, K. Two-Photon Imaging of 3D Organization of Bimetallic AuAg Nanoclusters in DNA Matrix. *Langmuir* **2017**, *33*, 8993–8999. [[CrossRef](#)] [[PubMed](#)]
25. Waszkielewicz, M.; Olesiak-Banska, J.; Grzelczak, M.; Sánchez-Iglesias, A.; Pniakowska, A.; Samoc, M. Enhanced one-photon and two-photon excited luminescence of polymer-stabilized AuAg nanoclusters aggregates. *J. Lumin.* **2020**, *221*, 116994. [[CrossRef](#)]
26. Olesiak-Banska, J.; Waszkielewicz, M.; Matczyszyn, K.; Samoc, M. A closer look at two-photon absorption, absorption saturation and nonlinear refraction in gold nanoclusters. *RSC Adv.* **2016**, *6*, 98748–98752. [[CrossRef](#)]
27. Antoine, R.; Bonačić-Koutecký, V. *Liganded Silver and Gold Quantum Clusters. Towards a New Class of Nonlinear Optical Nanomaterials*; Springer: Singapore, 2018.
28. Ghosh, A.; Udayabhaskararao, T.; Pradeep, T. One-Step Route to Luminescent Au₁₈SG₁₄ in the Condensed Phase and Its Closed Shell Molecular Ions in the Gas Phase. *J. Phys. Chem. Lett.* **2012**, *3*, 1997–2002. [[CrossRef](#)]
29. Stamplecoskie, K.G.; Chen, Y.-S.; Kamat, P.V. Excited-State Behavior of Luminescent Glutathione-Protected Gold Clusters. *J. Phys. Chem. C* **2014**, *118*, 1370–1376. [[CrossRef](#)]
30. Yang, Y.; Wang, S.; Chen, S.; Shen, Y.; Zhu, M. Switching the subcellular organelle targeting of atomically precise gold nanoclusters by modifying the capping ligand. *Chem. Commun.* **2018**, *54*, 9222–9225. [[CrossRef](#)]
31. Negishi, Y.; Nobusada, K.; Tsukuda, T. Glutathione-Protected Gold Clusters Revisited: Bridging the Gap between Gold(I)–Thiolate Complexes and Thiolate-Protected Gold Nanocrystals. *J. Am. Chem. Soc.* **2005**, *127*, 5261–5270. [[CrossRef](#)]

32. Sreepasad, T.S.; Samal, A.K.; Pradeep, T. Body- or Tip-Controlled Reactivity of Gold Nanorods and Their Conversion to Particles through Other Anisotropic Structures. *Langmuir* **2007**, *23*, 9463–9471. [[CrossRef](#)] [[PubMed](#)]
33. Meena, S.K.; Celiksoy, S.; Schäfer, P.; Henkel, A.; Sönnichsen, C.; Sulpizi, M. The role of halide ions in the anisotropic growth of gold nanoparticles: A microscopic, atomistic perspective. *Phys. Chem. Chem. Phys.* **2016**, *18*, 13246–13254. [[CrossRef](#)] [[PubMed](#)]
34. Khosharay, S.; Talebi, M.; Saeed, T.A.; Talaghani, S.S. Experimental and modeling study of the surface tension and interface of aqueous solutions of alcohols, cetyltrimethylammonium bromide (CTAB) and their mixtures. *J. Mol. Liq.* **2018**, *249*, 245–253. [[CrossRef](#)]
35. Chen, H.; Shao, L.; Li, Q.; Wang, J. Gold nanorods and their plasmonic properties. *Chem. Soc. Rev.* **2013**, *42*, 2679–2724. [[CrossRef](#)]
36. He, J.; Unser, S.; Bruzas, I.; Cary, R.; Shi, Z.; Mehra, R.; Aron, K.; Sagle, L. The facile removal of CTAB from the surface of gold nanorods. *Colloids Surfaces B Biointerfaces* **2018**, *163*, 140–145. [[CrossRef](#)]
37. Zhang, W.; Caldarola, M.; Lu, X.; Pradhan, B.; Orrit, M. Single-molecule fluorescence enhancement of a near-infrared dye by gold nanorods using DNA transient binding. *Phys. Chem. Chem. Phys.* **2018**, *20*, 20468–20475. [[CrossRef](#)]
38. Wientjes, E.; Renger, J.; Curto, A.; Cogdell, R.; Van Hulst, N.F. Strong antenna-enhanced fluorescence of a single light-harvesting complex shows photon antibunching. *Nat. Commun.* **2014**, *5*, 4236. [[CrossRef](#)]
39. Ming, T.; Chen, H.; Jiang, R.; Li, Q.; Wang, J. Plasmon-Controlled Fluorescence: Beyond the Intensity Enhancement. *J. Phys. Chem. Lett.* **2012**, *3*, 191–202. [[CrossRef](#)]
40. Jin, R.; Zeng, C.; Zhou, M.; Chen, Y. Atomically Precise Colloidal Metal Nanoclusters and Nanoparticles: Fundamentals and Opportunities. *Chem. Rev.* **2016**, *116*, 10346–10413. [[CrossRef](#)]
41. Donehue, J.E.; Wertz, E.; Talicska, C.N.; Biteen, J. Plasmon-Enhanced Brightness and Photostability from Single Fluorescent Proteins Coupled to Gold Nanorods. *J. Phys. Chem. C* **2014**, *118*, 15027–15035. [[CrossRef](#)]
42. Lu, X.; Ye, G.; Punj, D.; Chiechi, R.; Orrit, M. Quantum Yield Limits for the Detection of Single-Molecule Fluorescence Enhanced by a Gold Nanorod. *ACS Photon* **2020**, *7*, 2498–2505. [[CrossRef](#)]
43. Mahoney, C.; Park, K.; Jawaid, A.; Kowalski, B.; Gillman, A.; Tondiglia, V.; Treml, B.; White, T.; Vaia, R.A. Low-energy, nanoparticle reshaping for large-area, patterned, plasmonic nanocomposites. *J. Mater. Chem. C* **2018**, *6*, 7157–7169. [[CrossRef](#)]
44. Pradhan, B.; Khatua, S.; Gupta, A.; Aartsma, T.; Canters, G.; Orrit, M.J. Gold-nanorod-enhanced fluorescence correlation spectroscopy of fluorophores with high quantum yield in lipid bilayers. *Phys. Chem. C* **2016**, *120*, 25996–26003. [[CrossRef](#)]
45. Schaaff, T.G.; Whetten, R.L. Giant Gold–Glutathione Cluster Compounds: Intense Optical Activity in Metal-Based Transitions. *J. Phys. Chem. B* **2000**, *104*, 2630–2641. [[CrossRef](#)]
46. Waszkielewicz, M.; Olesiak-Banska, J.; Comby-Zerbino, C.; Bertorelle, F.; Dagany, X.; Bansal, A.K.; Sajjad, M.T.; Samuel, I.D.W.; Sanader, Z.; Rozycka, M.; et al. pH-Induced transformation of ligated Au₂₅ to brighter Au₂₃ nanoclusters. *Nanoscale* **2018**, *10*, 11335–11341. [[CrossRef](#)]
47. Jin, R. Atomically precise metal nanoclusters: Stable sizes and optical properties. *Nanoscale* **2015**, *7*, 1549–1565. [[CrossRef](#)]
48. Yu, Y.; Yao, Q.; Chen, T.; Lim, G.X.; Xie, J. The Innermost Three Gold Atoms Are Indispensable To Maintain the Structure of the Au₁₈(SR)₁₄ Cluster. *J. Phys. Chem. C* **2016**, *120*, 22096–22102. [[CrossRef](#)]

Plasmonic Enhancement of Two-Photon Excited Luminescence of Gold Nanoclusters

Anna Pniakowska, Joanna Olesiak-Banska

SUPPLEMENTARY MATERIALS

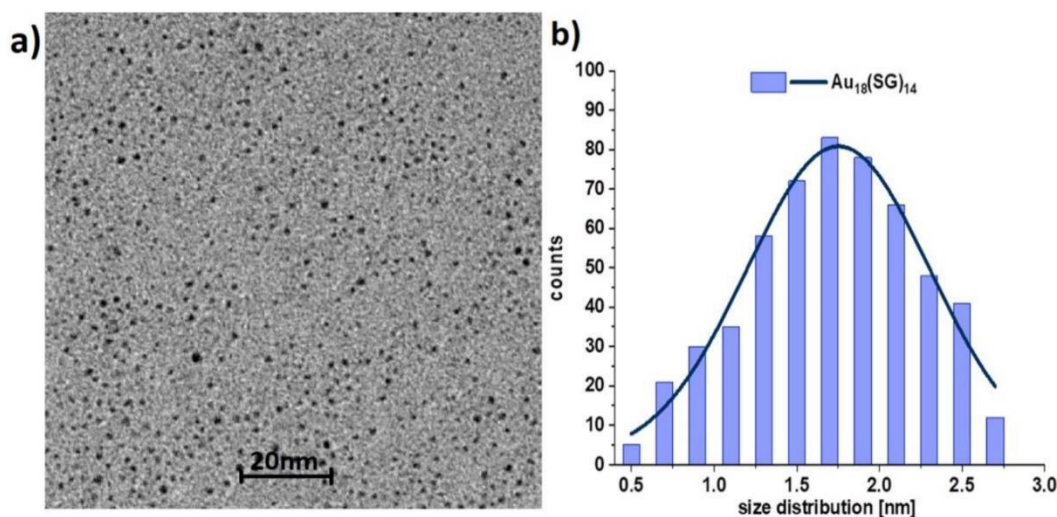


Figure S1. a) TEM image and b) size distribution histogram of $Au_{18}(SG)_{14}$ nanoclusters.

Table S1. Page electrophoresis

Reagent	Low density (LD) 20%T, 2.6%C	High density (HD) 24.3%T; 3.8%C
Monomer	25mL	72mL
N,N'-methylene bisacrylamide	-	18mL
Distilled water	12.5mL	18mL
1.5M Tris-HCl	12.5mL	30mL
10% APS	250 μ L	300 μ L
TEMED	25 μ L	30 μ L

^a40% total monomer (acrylamide+bis-acrylamide) stock solution (37.5:1)

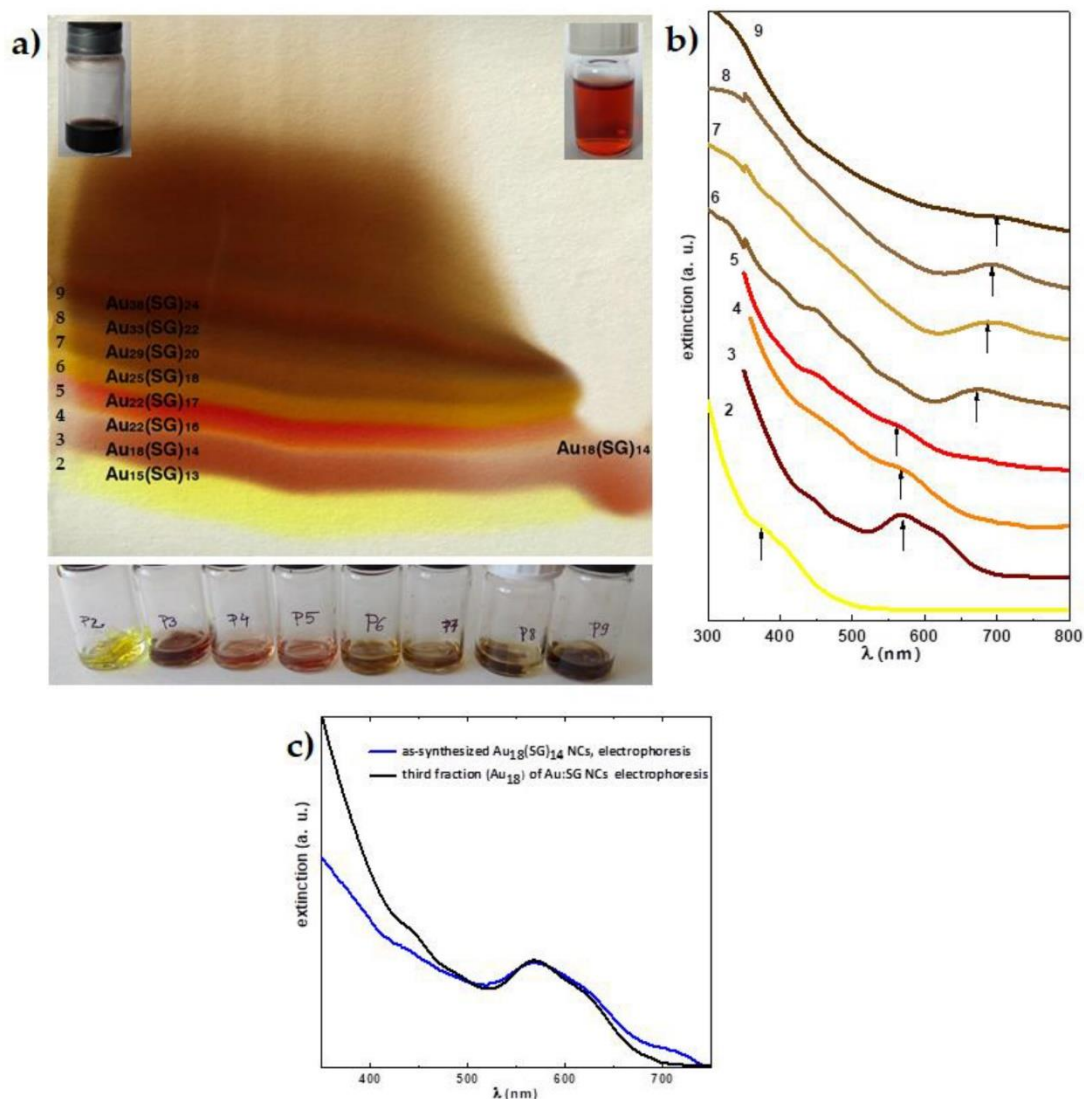


Figure S2. a) Photograph of electrophoretic polyacrylamide gel with well-separated 2-9 fractions of Au:SG mixture (left) and single fraction of Au₁₈(SG)₁₄ product of synthesis (right), which after electrophoresis separation were cut into pieces and dissolved in water (below). b) Extinction spectra of 2-9 fractions of Au:SG mixture. c) Comparison of UV/VIS spectra of as-synthesized Au₁₈(SG)₁₄ NCs and 3rd fraction of Au:SG mixture (identified as Au₁₈ NCs) from PAGE separation.

Off note: electrophoresis induce changes in the structure of nanoclusters, therefore the spectra of nanoclusters after separation are shifted around 110 nm with respect to spectra of initial AuNCs. Yet, both absorption spectra of as-synthesized Au₁₈(SG)₁₄ and shifted third fraction of Au:Ag (fig. S2c) are identified as Au₁₈ NCs in other sources.¹⁻⁴

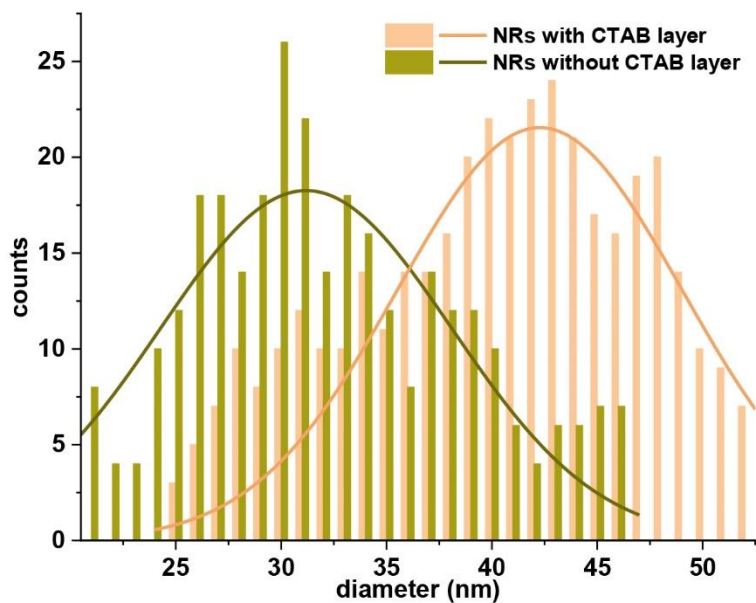


Figure S3. Size distribution of nanorods before and after CTAB layer removal. Average diameter of NRs with CTAB layer is estimated as 42.2 ± 7.64 nm, while NRs without CTAB layer is 31.2 ± 8.22 nm.

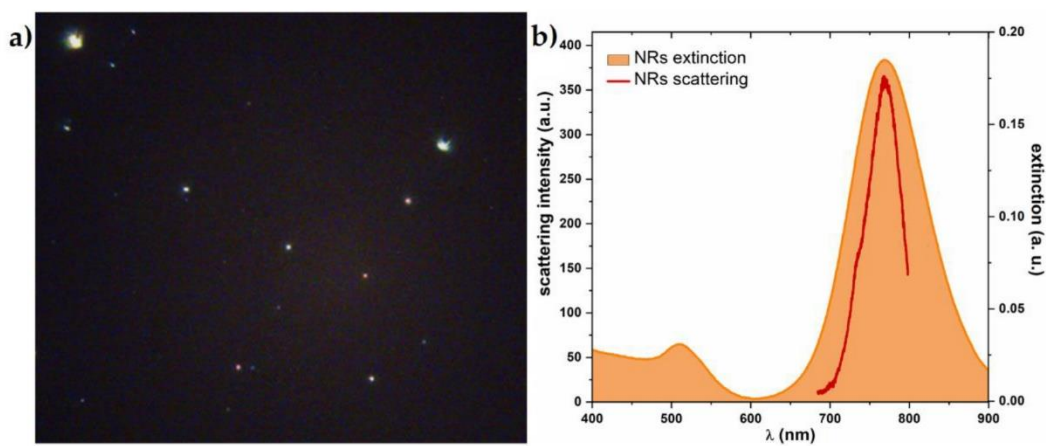


Figure S4. A) Dark field image of gold nanorods well-separated on the glass sample. B) Extinction spectrum of gold nanorods solution and scattering spectrum (red line) of single gold nanorod.

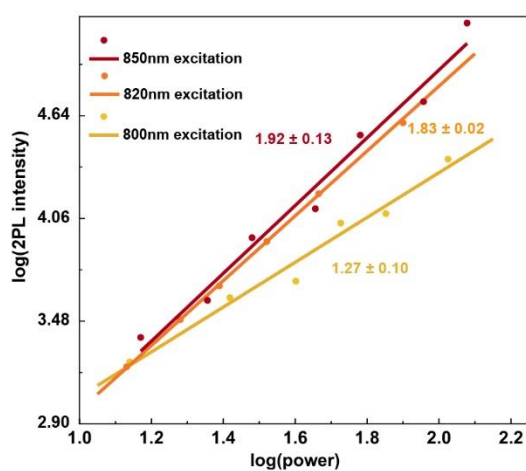


Figure S5. Log-log plot of the PL intensity of AuNCs as a function of excitation laser power measured at several excitation wavelengths. The slope of the linear fit to each datapoints sets corresponds to the level of multiphoton processes, n (for two-photon absorption $n = 2$).

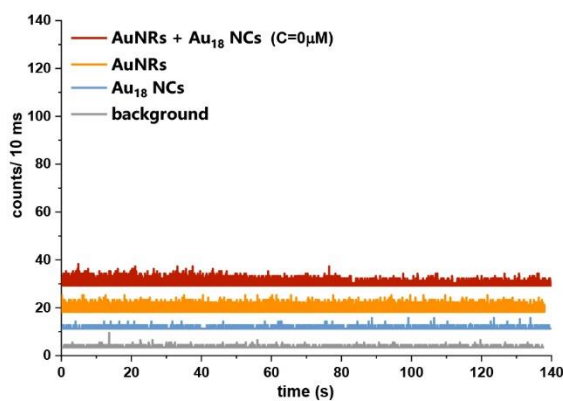


Figure S6. Luminescence time traces of samples: AuNRs in water: glycerine solution in the absence of AuNCs (red). Samples are compared to AuNRs only (orange) or AuNCs solution only (blue) and background noise (grey), monitored under prolonged irradiation with average power 70 μ W.

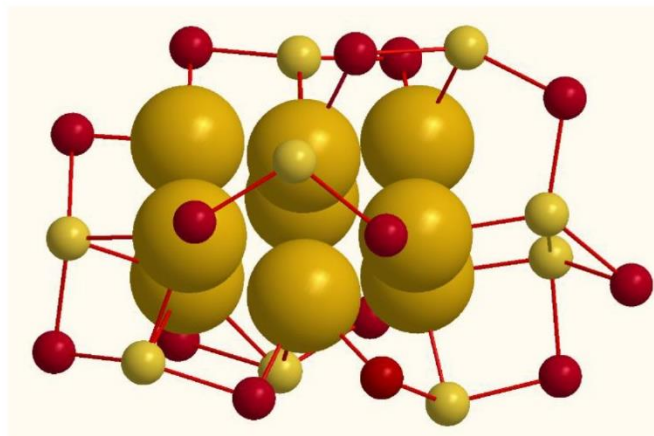


Figure S7. 3D model of $\text{Au}_{18}(\text{SG})_{14}$ structure with precise location of gold core (yellow – Au atoms) and staple motifs (yellow – Au atoms, red-S atoms) of nanocluster. Structure was energy-minimized with molecular mechanic MM2 model in Chem3D.

1. A. Ghosh, T. Udayabhaskararao, T. Pradeep, One-Step Route to Luminescent $\text{Au}_{18}\text{SG}_{14}$ in the Condensed Phase and Its Closed Shell Molecular Ions in the Gas Phase. *J. Phys. Chem. Lett.* **2012**, *3*, 1997–2002.
2. Stamplecoskie, K. G.; Chen, Y.-S.; Kamat, P. V., Excited-State Behavior of Luminescent Glutathione-Protected Gold Clusters. *The Journal of Physical Chemistry C* **2014**, *118* (2), 1370-1376.
3. Jin, R., Atomically precise metal nanoclusters: stable sizes and optical properties. *Nanoscale* **2015**, *7* (5), 1549-1565.
4. Yu, Y.; Yao, Q.; Chen, T.; Lim, G. X.; Xie, J., The Innermost Three Gold Atoms Are Indispensable To Maintain the Structure of the $\text{Au}_{18}(\text{SR})_{14}$ Cluster. *The Journal of Physical Chemistry C* **2016**, *120* (38), 22096-22102.

3.2 ARTICLE 2: GOLD-DOPING EFFECT ON TWO-PHOTON ABSORPTION AND LUMINESCENCE OF ATOMICALLY PRECISE SILVER LIGATED NANOCCLUSERS

3.2.1 Short description of research work and results

INTRODUCTION

Gold and silver nanoclusters bring strong interest since they offer the possibility to accurately tailor the properties of atomically-precise nanoclusters on the route of synthesis, functionalization, doping or other structural modifications. The relation between structure of nanoclusters and physicochemical properties of gold, silver and gold-silver atomically-precise nanoclusters is currently strongly investigated, in both, one- and two-photon regime of excitation. To discuss systematic changes of nanoclusters' atomic composition and related with them optical properties, we worked on nanoclusters built from 25 metal atoms. This type of nanoclusters serve as a model to study structure – properties relations and mechanisms due to good chemical stability, well-defined crystallographic structure and well-developed protocol of synthesis.²⁰ In addition, among atomically-precise silver nanoclusters Ag₂₅ is one of the great significance, because it has a gold analogue - Au₂₅, in terms of super-atom electronic configuration and atomic arrangement. The article 2 presents the detailed insight to the gold atoms doping impact on linear and nonlinear optical properties of atomically-precise ligated silver nanoclusters Ag₂₅. Systematic Au doping effect on Ag₂₅ is then compared to well-known properties of the parent Ag₂₅ cluster.

Current study present advanced control over replacement at the single atom scale, which can offer: enhanced photoluminescence quantum yield (PL QY), longer PL lifetime or improved photo- and chemical stability.¹³⁰ In spite of a growing progress in understanding the role of structure in nanocluster's optical properties,^{98, 99} the impact of hetero-atom doping is still poorly described, especially in nonlinear optical regime. Meanwhile NLO properties of nanoclusters are beneficial for multiphoton applications e.g. imaging, detection, theranostics. Multiphoton studies in a broad wavelengths range are scarcely reported in the literature on nanoclusters. Therefore, quantitative description of two-photon absorption cross-section (σ_2) and two-photon brightness ($\sigma_{2,eff}$) of NCs in a broad near-infrared range of wavelengths (1180-1600 nm) is definitely a valuable contribution to the current knowledge. Comparison of one- and two-photon experimental studies with time-dependent density functional theory (TD-DFT) simulations allows for a deep understanding of single metal doping mechanisms and structure-properties relations.

METHODOLOGY

Here I determined nonlinear optical properties: σ_2 and $\sigma_{2,eff}$ on the route of two-photon excited luminescence (TPEL) measurements, performed with the home-made set-up, which is

in fact a modified set-up presented in chapter 3.1.1. TPEL was collected from nanoclusters solutions in epi-fluorescence mode, through dichroic mirror and shortpass filter. The cuvettes with sample solutions (placed on the top of the objective) were excited with femtosecond Ti:Sapphire laser with an optical parametric oscillator (OPO) tunable in NIR range ($\lambda=1000-1600$ nm). Long-pass filter introduced before samples excluded any possible higher energetic excitation. TPEL spectra were collected at spectrofluorometer from the broad range of excitation: 1180-1600nm, each every 50nm.

Chapter 2.3.3 present the details regarding the two-photon absorption measurements. I have calculated TPA of nanoclusters through indirect, comparative technique, with respect to the reference sample, fluorescent dye - Styryl 9M, according to the formula (5). Here, I have chosen reference specifically to match emission of nanoclusters at the similar spectral range. Styryl 9M and gold-doped nanoclusters were illuminated at the same excitation conditions, set specifically for those samples, avoiding photobleaching and aiming to achieve strong signal for number of repetitive measurements. To determine TPA I have measured quantum yield and concentration of each nanoclusters sample and reference. Precision of determination of those parameters can strongly affect the final values, therefore QY of nanoclusters was established through two methods: using integrating sphere and via comparative method with reference dye, calculated according to the formula:

$$\Phi_f^i = \Phi_f^s \frac{f_R(\lambda_{ex}) \int_{\lambda_{em}} F_s(\lambda_{em}) n_s^2}{f_s(\lambda_{ex}) \int_{\lambda_{em}} F_R(\lambda_{em}) n_R^2}$$

$$f_x(\lambda_{ex}) = 1 - 10^{-A_x(\lambda_{ex})} \quad (6)$$

where Φ_f^s is known QY of reference sample, $\int_{\lambda_{em}} F(\lambda_{em})$ is fluorescence integral, n is refractive index of sample (s) and reference (r). $f_x(\lambda_{ex})$ refers to corresponding absorption factor at excitation wavelength.

Then, I found two-photon brightness from calculated two-photon absorption cross-section multiplied by QY, following the equation:

$$\sigma_{2,eff} = \sigma_{2,s} \varphi_s(\lambda_{reg}) = \frac{F_{2,s}(\lambda_{reg}) C_r \varphi_r(\lambda_{reg})}{F_{2,r}(\lambda_{reg}) C_s} \sigma_{2,r} \quad (7)$$

where $F_{2}(\lambda_{reg})$ is integrated two-photon fluorescence intensity at particular excitation wavelength, C is concentration, and φ is quantum yield of sample (s) and reference (r). $\sigma_{2,r}$ is two-photon absorption cross-section of reference.

I have calculated the error bars of σ_2 and $\sigma_{2,eff}$ from the partial derivatives of each parameters.

RESULTS AND DISCUSSION

Presented work covers the complementary experimental and theoretical studies on ligated nanoclusters: $Ag_{24}Au_1(DMBT)_{18}$, $Ag_{25-x}Au_x(DMBT)_{18}$ and $Ag_{25}(DMBT)_{18}$, in which DMBT refer to

2,4-dimethylbenzenethiol ligand. Listed silver and gold-silver alloys preserves structural integrity upon metal atoms doping, i. e. keeping the same number of building metal atoms and ligands. Therefore I have precisely monitored optical properties: absorption, luminescence, PL QY and PL lifetime properties at the single atom-doping level. In collaboration with the group of prof. Rodolphe Antoine the electrospray ionization mass spectrometry (ESI MS) was applied for all synthesized nanoclusters to confirm homogeneity and purity of atomically precise nanoclusters: $\text{Ag}_{24}\text{Au}_1$ and Ag_{25} , while $\text{Ag}_{25-x}\text{Au}_x$ were found as nanoclusters from the range of $x = 5-10$ of gold atoms. I have further confirmed the identity of nanoclusters through the comparison of UV-Vis, excitation and emission measurements with those reported previously in the literature.¹³¹⁻¹³³ Gold atom doping causes structural changes, therefore monitored shifting of absorption bands (OPA) is substantial in terms of lowest energy bands, which are assigned to core electronic states. Less significant shifting at higher energy bands, related with ligand states, suggests less profound changes from the rearrangements of ligands (Figure 13a). Time-dependent density functional theory (TD-DFT) simulations of absorption bands, performed by group of prof. Vlasta Bonačić-Koutecký, are in agreement with my experimental studies, showing the same shifting of OPA bands (Figure 13b-d).

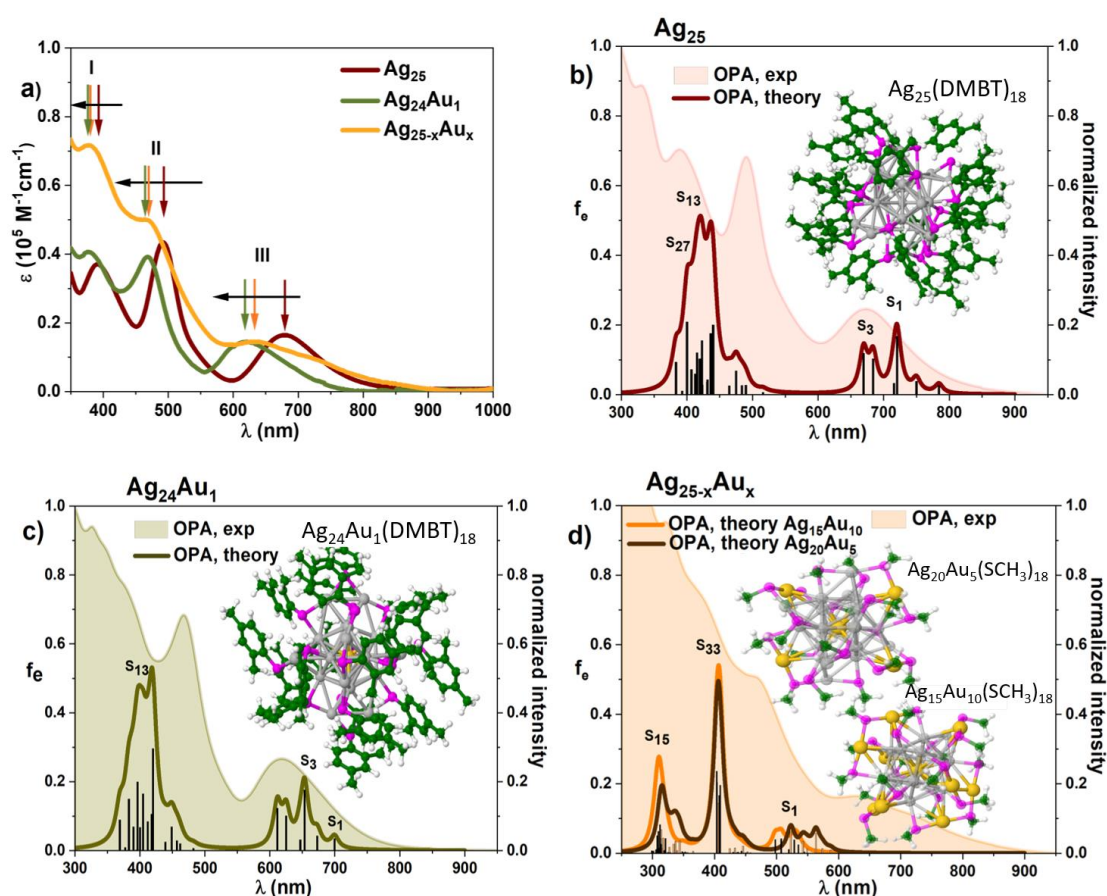


Figure 13. a) Comparison of absorption bands shifting of $\text{Ag}_{25}(\text{DMBT})_{18}$ (red), $\text{Ag}_{24}\text{Au}_1(\text{DMBT})_{18}$ (green) and $\text{Ag}_{25-x}\text{Au}_x(\text{DMBT})_{18}$ (orange). Comparison of experimental absorption (OPA, exp) and simulated one-photon absorption (OPA, theory) spectra of b) Ag_{25} c) $\text{Ag}_{24}\text{Au}_1$ and d) $\text{Ag}_{25-x}\text{Au}_x$ nanoclusters. Optimized structures of nanoclusters is presented in the inset of respective spectra.

Alloying of nanoclusters induces enhancements of one- and two-photon luminescent properties. I have found that $\text{Ag}_{24}\text{Au}_1(\text{DMBT})_{18}$ is an efficient fluorophore, determining 10-times improved QY (from $\phi = 3.08\%$ to 29.91%) and enhanced PL lifetime (from $\tau = 1.1 \mu\text{s}$ to $1.8 \mu\text{s}$) with respect to undoped Ag_{25} nanoclusters. Here I have measured a series of two-photon excited fluorescence spectra to quantitatively determine two-photon absorption (TPA) cross-sections of nanoclusters in a non-resonant range of excitation wavelengths ($\lambda_{\text{exc}} = 1180 - 1600 \text{ nm}$). I have determined strong two-photon absorption cross-sections of nanoclusters, at the level of $\sigma_2 = 50 - 863 \text{ GM}$. Then, owing to the high QY of $\text{Ag}_{24}\text{Au}_1$ I have found significantly enhanced two-photon brightness (from $\sigma_{2,\text{eff}} = 1.5 \text{ GM}$ to 20 GM) for single-doped $\text{Ag}_{24}\text{Au}_1$ NCs with respect to undoped Ag_{25} NCs. This work emphasizes the importance of atomically-precise gold atom doping, since multiply doped nanoclusters do not follow the changes in optical properties observed for $\text{Ag}_{24}\text{Au}_1(\text{DMBT})_{18}$ (Figure 14). I have found 6 times smaller QY (from $\phi = 3.08\%$ to 0.49%) and shorter PL lifetime (from $\tau = 1.1 \mu\text{s}$ to $0.5 \mu\text{s}$) for multiply doped $\text{Ag}_{25-x}\text{Au}_x$ NCs, compared to undoped Ag_{25} NCs. Despite diminished optical properties I have found 3 times enhanced two-photon brightness (from $\sigma_{2,\text{eff}} = 1.5 \text{ GM}$ to 4.25 GM)

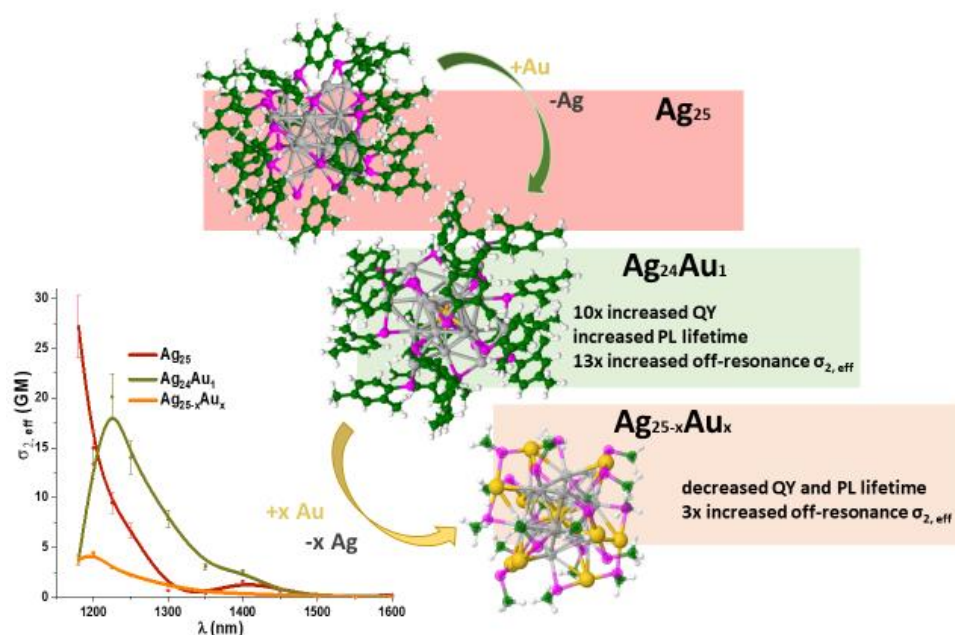


Figure 14. Schematic representation of gold doping effect of Ag_{25} nanoclusters on absorption and luminescent properties for single gold atom doped nanoclusters $\text{Ag}_{24}\text{Au}_1$ and multiply doped $\text{Ag}_{25-x}\text{Au}_x$.

Theoretical simulations of TPA, performed by prof. Vlasta Bonačić-Koutecký are in agreement with my experimental TPA data in terms of the band positions. The off-resonance TPA (i.e. at $\lambda > 1000\text{nm}$), both – experimental and simulated ones, remains small compared to the simulated TPA values obtained under resonance excitation (i.e. at $\lambda < 1000\text{nm}$) (Figure 15). This indicate the importance of detailed characterization of multiphoton optical properties on a broad excitation range, especially when best conditions for effective one- and two-photon excitation can substantially differ. Characterization of TPA solely at single wavelength is currently a common practice in published work, however our investigation in wide excitation

range prove how selection of particular conditions of measurements can provide vastly different values, stressing the urge to perform characterizations on possibly widest spectral range.

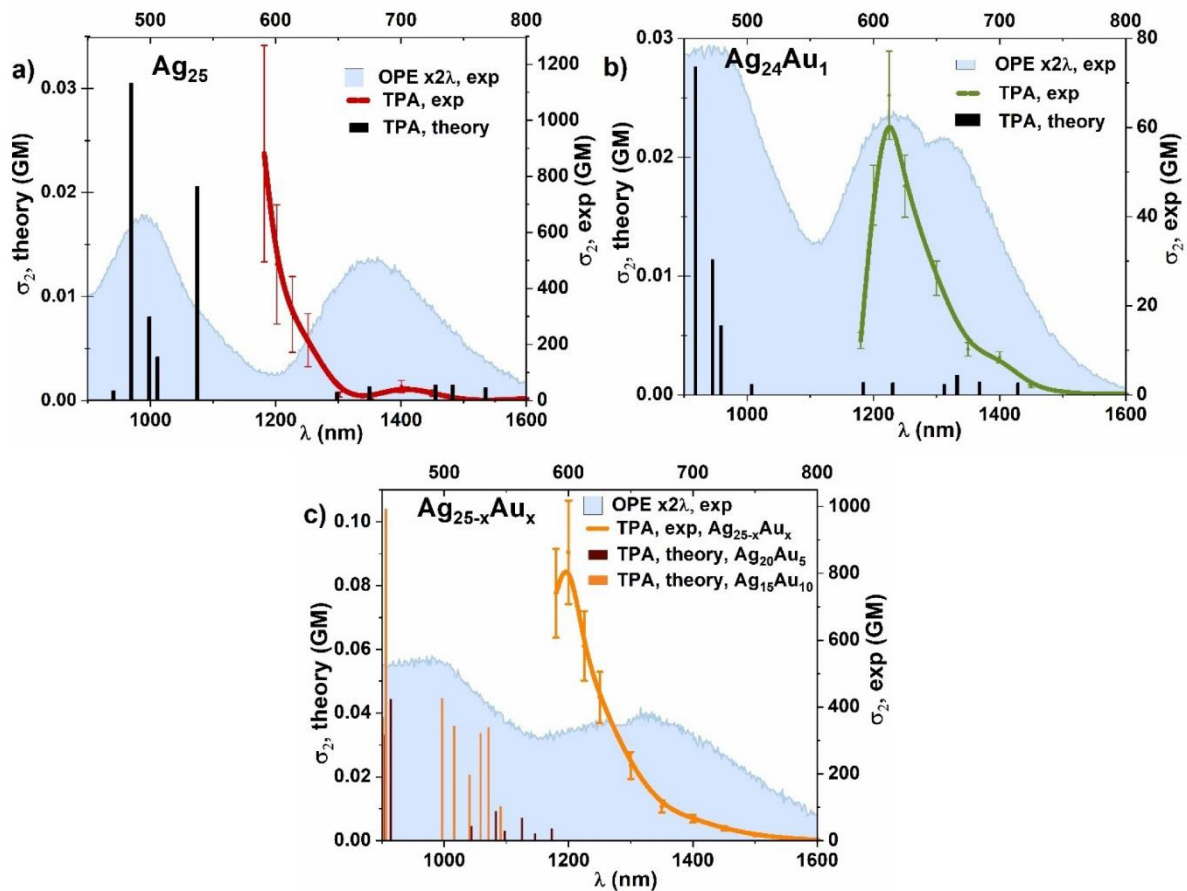


Figure 15. Off-resonance TPA spectra (solid lines) and simulated TPA spectra (columns) (lower wavelength axis) of (a) Ag_{25} , (b) $Ag_{24}Au_1$ and (c) $Ag_{25-x}Au_x$ nanoclusters presented with respective normalized one-photon excitation (OPE) (blue area, upper wavelength axis).

The opposite effect of single and multiply doped nanoclusters on their optical properties is explained by the structural modifications in the core of nanoclusters upon doping of gold atoms. The most probable structure of $Ag_{24}Au_1$ assume incorporation of a gold atom at the icosahedral center of the nanocluster. Further doping locates gold atoms in icosahedron sites or staple motifs. Replacement of the center Ag atom to Au induces strong electron charge in the icosahedral center of nanoclusters, formation of strong Ag-Au bonds and rigidification of the structure. However, addition of more gold atoms deteriorates optical properties due to spread electron distribution in staple motifs.

The article 2 provides comprehensive description of the relation between the composition and structure of gold-doped silver nanoclusters and their linear and nonlinear optical properties. Extensive investigation of improved nonlinear optical properties in near-infrared region hold promise of meaningful applications in second biological window, since presented results are competitive for common organic dyes or proteins used as fluorescent markers. It brings new perspectives in the topic of precise control of nanoparticles properties and design of materials for applications, in particular for imaging and luminescent sensing. Regarding the

scope of the thesis discussed alloying of nanoclusters appeared as another, effective strategy to enhance luminescent properties of nanoclusters. This study supplements the previous work on the discussion of nonlinear optical properties of nanoclusters, considering here the impact of structural composition of clusters on their two-photon absorption.

3.2.2 Research contribution of PhD candidate

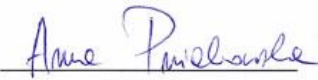
Anna Pniakowska
Institute of Advanced Materials
Wrocław University of Science and Technology

ul. Gdańska 7/9
50-344 Wrocław

Author contribution statement

I, Anna Pniakowska hereby declare that in the article: *A. Pniakowska, K. Ramankutty, P. Obstarczyk, M. Perić, Z. S. Maršić, V. Bonačić-Koutecký, T. Bürgi, J. Olesiak-Bańska "Gold-doping effect on two-photon absorption and luminescence of atomically precise silver ligated nanoclusters" Angewandte Chemie, 2022, 61, 43, s. 1-9*, I was responsible for:

- Methodology
- Investigation:
 - one photon measurements:
 - absorption, excitation, emission,
 - photoluminescence quantum yield,
 - photoluminescence lifetime;
 - two-photon measurements:
 - two-photon excited luminescence,
 - power dependent luminescence measurements,
 - photostability measurements;
 - two-photon absorption and two-photon brightness
- Data analysis
- Writing – original draft
- Visualization


(signature)

3.2.3 Contribution statements of co-authors

Dr. Krishnadas Kumaranchira Ramankutty
Department of Physical Chemistry
Université de Genève
30 Quai Ernest Ansermet
CH-1211 Genève 4

Author contribution statement

I, Krishnadas Kumaranchira Ramankutty hereby declare that in the article:
A. Pniakowska, K. Ramankutty, P. Obstarczyk, M. Perić, Z. S. Maršić, V. Bonačić-Koutecký, T. Bürgi, J. Olesiak-Bańska "Gold-doping effect on two-photon absorption and luminescence of atomically precise silver ligated nanoclusters" Angewandte Chemie, 2022, 61, 43, s. 1-9, I was responsible for:

- Synthesis and mass spectrometric characterization of the metal clusters



(signature)

Dr inż. Patryk Obstarczyk
Institute of Advanced Materials
Wroclaw University of Science and Technology
ul. Gdańska 7/9
50-344 Wroclaw

Autor contribution statement

I, Patryk Obstarczyk hereby declare that in the article: *A. Pniakowska, K. Ramankutty, P. Obstarczyk, M. Perić, Z. S. Maršić, V. Bonačić-Koutecký, T. Bürgi, J. Olesiak-Bańska "Gold-doping effect on two-photon absorption and luminescence of atomically precise silver ligated nanoclusters" Angewandte Chemie, 2022, 61, 43, s. 1-9*, I was responsible for:

-Synthesis and purification of the metal clusters



(signature)

Dr. Martina Perić Bakulić

Faculty of Chemistry and Technology, Physics Department,
Ruđera Boškovića 35, 21000 Split

Autor contribution statement

I, Martina Perić Bakulić hereby declare that in the article: *A. Pniakowska, K. Ramankutty, P. Obstarczyk, M. Perić, Z. S. Maršić, V. Bonačić-Koutecký, T. Bürgi, J. Olesiak-Bańska "Gold-doping effect on two-photon absorption and luminescence of atomically precise silver ligated nanoclusters" Angewandte Chemie, 2022, 61, 43, s. 1-9*, I was responsible for:

- DFT and TDDFT calculations of structural and optical properties (OPA and TPA) of ligated nanoclusters
- Analyzing and interpreting the DFT/TDDFT calculations results.



Dr. Željka Sanader Maršić

Faculty of Science
University of Split
Ruđera Boškovića 33, 21000 Split

Center of Excellence for Science and Technology - Integration of Mediterranean
region (STIM)
University of Split
Mestrovićevo Šetalište 45, 21000 Split

Autor contribution statement

I, Željka Sanader Maršić hereby declare that in the article: *A. Pniakowska, K. Ramankutty, P. Obstarczyk, M. Perić, Z. S. Maršić, V. Bonačić-Koutecký, T. Bürgi, J. Olesiak-Bańska "Gold-doping effect on two-photon absorption and luminescence of atomically precise silver ligated nanoclusters"* *Angewandte Chemie*, 2022, 61, 43, s. 1-9, I was responsible for:

- DFT and TDDFT methodology for calculation of linear and nonlinear optical properties
- writing of the computational part of the results, and for review and editing of the draft

Željka Sanader Maršić

(signature)

Vlasta Bonačić-Koutecký, Prof. Dr. Dr. h.c.
Interdisciplinary Center for Advanced Science and Technology (ICAST)
University of Split
Center of Excellence for Science and Technology - Integration of Mediterranean region (STIM)
University of Split
Mestrovćevo Šetalište 45, 21000 Split

Autor contribution statement

I, Vlasta Bonačić-Koutecký hereby declare that in the article: *A. Pniakowska, K. Ramankutty, P. Obstarczyk, M. Perić, Z. S. Maršić, V. Bonačić-Koutecký, T. Bürgi, J. Olesiak-Bańska "Gold-doping effect on two-photon absorption and luminescence of atomically precise silver ligated nanoclusters" Angewandte Chemie, 2022, 61, 43, s. 1-9,*

I was responsible for:

- writing the theoretical part of the paper.



(signature)



UNIVERSITÉ
DE GENÈVE

FACULTÉ DES SCIENCES

Thomas Bürgi
Professor
Department of Physical Chemistry
University of Geneva
30 Quai Ernest-Ansermet
1211 Geneva
Switzerland

Direct line +41 (0)22 379 65 52
thomas.buerqi@unige.ch

Geneva, 17/06/2024

Author contribution statement

I, Thomas Bürgi hereby declare that in the article: A. Pniakowska, K. Ramankutty, P. Obstarczyk, M. Perić, Z. S. Maršić, V. Bonačić-Koutecký, T. Bürgi, J. Olesiak-Bańska "Gold-doping effect on two-photon absorption and luminescence of atomically precise silver ligated nanoclusters" *Angewandte Chemie*, 2022, 61, 43, s. 1-9, I supervised the preparation of the nanoclusters. I contributed to the writing of the manuscript.

Prof. Thomas Bürgi

Joanna Olesiak-Bańska
PhD, DSc
Institute of Advanced Materials
Wroclaw University of Science and Technology

ul. Gdańska 7/9
50-344 Wroclaw

Autor contribution statement

I, Joanna Olesiak-Bańska hereby declare that in the article: *A. Pniakowska, K. Ramankutty, P. Obstarczyk, M. Perić, Z. S. Maršić, V. Bonačić-Koutecký, T. Bürgi, J. Olesiak-Bańska "Gold-doping effect on two-photon absorption and luminescence of atomically precise silver ligated nanoclusters" Angewandte Chemie, 2022, 61, 43, s. 1-9*, I was responsible for:

- Conceptualization
- Writing : review and editing
- Supervision
- Funding acquisition


(signature)

3.2.4 Article and Supplementary Materials



Gold-Doping Effect on Two-Photon Absorption and Luminescence of Atomically Precise Silver Ligated Nanoclusters

Anna Pniakowska, Krishnadas Kumaranchira Ramankutty, Patryk Obstarczyk, Martina Perić Bakulić, Željka Sanader Maršić, Vlasta Bonačić-Koutecký, Thomas Bürgi, and Joanna Olesiak-Bańska*

Abstract: Noble metal nanoclusters allow for the atomically-precise control of their composition. However, to create nanoclusters with pre-defined optical properties, comprehensive description of their structure-property relation is required. Here, we report the gold atom doping impact on one-photon and two-photon absorption (TPA) and luminescence properties of ligated silver nanoclusters via combined experimental studies and time-dependent density functional theory simulations (TD-DFT). We synthesized a series of $\text{Ag}_{25-x}\text{Au}_x$ - $(\text{DMBT})_{18}$ nanoclusters where $x=0, 1$ and $5-10$. For $\text{Ag}_{24}\text{Au}_1(\text{DMBT})_{18}$ we demonstrate that the presence of the central Au dopant strongly influences linear and non-linear optical properties, increasing photoluminescence quantum yield and two-photon brightness, with respect to undoped silver nanoclusters. With improved TPA and luminescence, atomically-precise AuAg alloys presented in our work can serve as robust luminescent probes e.g. for bioimaging in the second biological window.

Introduction

Noble metal nanoclusters (NCs), in the size regime where each atom counts, exhibit extraordinary optical properties, significantly influenced by the number and type of metal core atoms or protecting ligands.^[1] Their molecule-like behavior and discrete electronic structure can be controlled with chemical synthesis methods. However, the correlation between their optical properties and atomically-precise structures is still not fully understood, especially in the nonlinear optics regime. In order to take full advantage of single atom precision in the design of nanoclusters and create nanoclusters with predefined optical properties, comprehensive description of the structure-property relation is required.

Better understanding of third-order NLO properties with respect to the ligand or atomic composition of NCs is crucial for their potential applications where pulsed laser illumination is needed (e.g., in multiphoton bioimaging or photonics). Various NCs have been proven to manifest noteworthy optical nonlinearities,^[1d,2] which should be examined, understood, and classified in the same terms as for commonly used dyes. The reported two-photon absorption cross-sections of NCs vary from 10^2 to 10^6 GM, however they are usually examined under single wavelength excitation, which reveals only partial information on the NLO spectral characteristics.^[2b]

Recent studies have focused on effective methods for the improvement of NCs optical properties, e.g. the photoluminescence quantum yield (PL QY)^[3] and PL lifetime,^[4] where one of the strategies is doping of NCs with metallic heteroatoms.^[5] Among the investigated clusters, alloys of Ag_{25} are one of the widely studied, and exclusively the only silver nanoclusters possessing direct structural and electronic analogue in gold.^[6] Thus, they are a perfect model to investigate impact of systematic atom doping on linear and nonlinear optical properties. Regarding the structure-dependent stability of Au-doped silver clusters, it was already proven that $\text{Ag}_{24}\text{Au}_1(\text{SR})_{18}$ alloy is the most thermodynamically stable nanocluster among Au-doped Ag_{25} nanoclusters.^[7] Interestingly, it was found that doping of silver nanoclusters with gold atoms results in more rigid structure in comparison to silver-doped gold nanoclusters, which tends to enhance luminescence properties.^[7b,8]

Here, we present systematic investigation of linear and nonlinear optical properties of gold-doped silver nano-

[*] A. Pniakowska, P. Obstarczyk, J. Olesiak-Bańska
Institute of Advanced Materials,
Wrocław University of Science and Technology
Wybrzeże Wyspiańskiego 27, 50-370 Wrocław (Poland)
E-mail: Joanna.olesiak-banska@pwr.edu.pl

K. Kumaranchira Ramankutty, T. Bürgi
Département de Chimie Physique,
Université de Genève
30 Quai Ernest-Ansermet, 1211 Geneva 4 (Switzerland)

M. Perić Bakulić, Ž. Sanader Maršić, V. Bonačić-Koutecký
Center of Excellence for Science and Technology-Integration of
Mediterranean Region (STIM) at Interdisciplinary Center for
Advanced Sciences and Technology (ICAST),
University of Split
Poljička cesta 35, 21000 Split (Croatia)

Ž. Sanader Maršić
Faculty of Science,
University of Split
Ruđera Boškovića 33, 21000 Split (Croatia)

clusters $\text{Ag}_{24}\text{Au}_1(\text{DMBT})_{18}$ (DMBT = 2,4-dimethylbenzenethiolate) and $\text{Ag}_{25-x}\text{Au}_x(\text{DMBT})_{18}$ with respect to the undoped nanocluster, $\text{Ag}_{25}(\text{DMBT})_{18}$ (further called $\text{Ag}_{24}\text{Au}_1$, $\text{Ag}_{25-x}\text{Au}_x$ and Ag_{25} NCs, respectively). We adapted a recent approach and doped the metal core of Ag_{25} with gold in a strictly controlled manner.^[7a,9] We emphasize that the silver clusters analysed in this work preserved their structural integrity upon doping with gold atoms, i.e. 25 metal atoms and 18 DMBT ligands. Challenging maintenance of the same number of building atoms as in the original nanoclusters is the only valid approach of comparison of nanoclusters' properties. Uniformity and purity of the synthesized nanoclusters were proved with electrospray ionization mass spectrometry (ESI MS) and ultraviolet/visible (UV/Vis) absorption spectroscopy, which showed systematic changes of electronic transition bands dependent on the number of dopant Au atoms. Photoluminescence analysis presents a significant enhancement of luminescence intensity and quantum yield, and increase of luminescence lifetime of $\text{Ag}_{24}\text{Au}_1$ in comparison to other AuAg alloys and pure Ag_{25} . We present for the first time the quantitative description of two-photon absorption (TPA) cross-section (σ_2) and two-photon brightness ($\sigma_{2,\text{eff}}$) of NCs determined with the two-photon excited luminescence (TPEL) technique in a broad near-infrared range of wavelengths (1180–1600 nm). Our pioneering off-resonance investigation of nonlinear optical properties clearly shows differences between $\text{Ag}_{24}\text{Au}_1$ with respect to Ag_{25} and $\text{Ag}_{25-x}\text{Au}_x$ clusters. Comparing one- and two-photon experimental studies with time-dependent density functional theory (TD-DFT) simulations brings a detailed insight into Au doping impact on the structure and optical properties of atomically precise silver NCs.

Results and Discussion

Synthesis and characterization of atomically precise nanoclusters

We synthesized 25-atom silver and doped silver nanoclusters stabilized with the same ligand (DMBT), in the presence of triphenylphosphine counterion, PPh_4^+ . $[\text{Ag}_{24}\text{Au}_1(\text{DMBT})_{18}][\text{PPh}_4]$ was synthesized by a diffusion metal exchange of $\text{Ag}_{25}\text{Au}_x(\text{DMBT})_{18}$ with AuPPh_3Cl , and further metal exchange of $[\text{Ag}_{24}\text{Au}_1(\text{DMBT})_{18}][\text{PPh}_4]$ led to $[\text{Ag}_{25-x}\text{Au}_x(\text{DMBT})_{18}][\text{PPh}_4]$. Detailed process of gold atom doping is described in the Experimental Section. Gold atoms were incorporated by post-synthetic galvanic exchange of single silver atoms, described in detail by the mechanism of dynamic heterometallic diffusion.^[7c]

We conducted the negative ion mode ESI MS measurements (Figure S1) to determine the identity and purity of $[\text{Ag}_{25}(\text{DMBT})_{18}][\text{PPh}_4]$, $[\text{Ag}_{24}\text{Au}_1(\text{DMBT})_{18}][\text{PPh}_4]$ and $[\text{Ag}_{25-x}\text{Au}_x(\text{DMBT})_{18}][\text{PPh}_4]$. Expected peaks at m/z 5167 and m/z 5253 suggest identity and purity of those clusters. Nanoclusters doped with more gold atoms, $[\text{Ag}_{25-x}\text{Au}_x(\text{DMBT})_{18}][\text{PPh}_4]$ are mixtures of nanoclusters with gold atoms content in the range of $x = 5$ –10.

One-photon optical properties

The homogeneity of nanoclusters was further confirmed while monitoring the expected narrow bands of absorption, excitation and emission. UV/Vis measurements provided one-photon absorption (OPA) spectra characteristic for Ag_{25} nanoclusters with systematic changes of bands upon gold atom doping (Figure 1). Pure Ag_{25} NCs exhibit absorption spectra which are in agreement with the ones reported previously for $\text{Ag}_{25}(\text{SR})_{18}$, where SR stands for a thiol molecule.^[5a,c,6,10] The distinct absorption bands of these clusters are marked with coloured arrows in Figure 1a as *I*, *II* and *III*. Each of these absorption bands in $\text{Ag}_{24}\text{Au}_1$ and $\text{Ag}_{25-x}\text{Au}_x$ were considerably blue-shifted with respect to Ag_{25} NCs, as indicated with black arrows (Figure 1a). We report increasing blue shift of $\text{Ag}_{24}\text{Au}_1$ compared to Ag_{25} NCs: 21 nm, 24 nm and 55 nm for *I*, *II* and *III* bands, respectively. Blue shift of $\text{Ag}_{25-x}\text{Au}_x$ compared to Ag_{25} is smaller: 21 nm, 22 nm and 43 nm for *I*, *II* and *III* bands, respectively. Metal core doping induces substantial changes at the lowest energy bands, since these bands originate from the core electronic states. Significant blue shift of OPA is directly related with metal core alloying as a consequence of tuning the geometric and electronic structure, as confirmed previously with differential pulse voltammetry (DPV), X-ray crystallography and HOMO–LUMO calculations.^[11] The contribution of the ligand states at higher energy bands shows only slight shifting, meaning less pronounced changes in the arrangement of the ligands in these nanoclusters.

We performed UV/Vis OPA spectra simulations for the optimized structures of nanoclusters complementary to our experimental studies. Simulations of Ag_{25} NCs with DMBT and replaced with simplified SCH_3 ligand do not present noticeable difference, therefore further simulations were conducted for NCs with SCH_3 ligand. TD-DFT spectra are in good agreement with experimental ones, as shown in Figure 1c–e. Since $\text{Ag}_{25-x}\text{Au}_x$ NCs contain 5 to 10 gold atoms, structures of these nanoclusters were optimized for two boundary variants: $\text{Ag}_{20}\text{Au}_5(\text{SCH}_3)_{18}$ and $\text{Ag}_{15}\text{Au}_{10}(\text{SCH}_3)_{18}$, however differences between their simulated bands are negligible. The theoretical spectra show the same tendency of the blue-shift of the spectral bands between $\text{Ag}_{25}(\text{DMBT})_{18}$ and $\text{Ag}_{24}\text{Au}_1(\text{DMBT})_{18}$ clusters, which is a consequence of the presence of Au atom with many d-electron excitations. We note that simulated and experimental results present well matching transition bands, with similar high intensity peaks within respective energy ranges. Notable mismatch of experimental and simulated spectra is located at 400–500 nm, the region of ligand states contribution. Impact of organic ligands on the absorption spectra is notably emphasized in the particular case of charged silver nanoclusters.^[12] Detailed analysis of influence of choice of functionals on structure and absorption spectra $\text{Ag}_{24}\text{Au}_1$ has been presented in ref. [13].^[13]

We measured one-photon luminescence spectra and luminescence lifetimes and determined PL QY of the samples. One-photon luminescence excitation (OPE) spectra of Ag_{25} , $\text{Ag}_{24}\text{Au}_1$ and $\text{Ag}_{25-x}\text{Au}_x$ nanoclusters shown in Figure S2 resemble their OPA transition bands. All of these

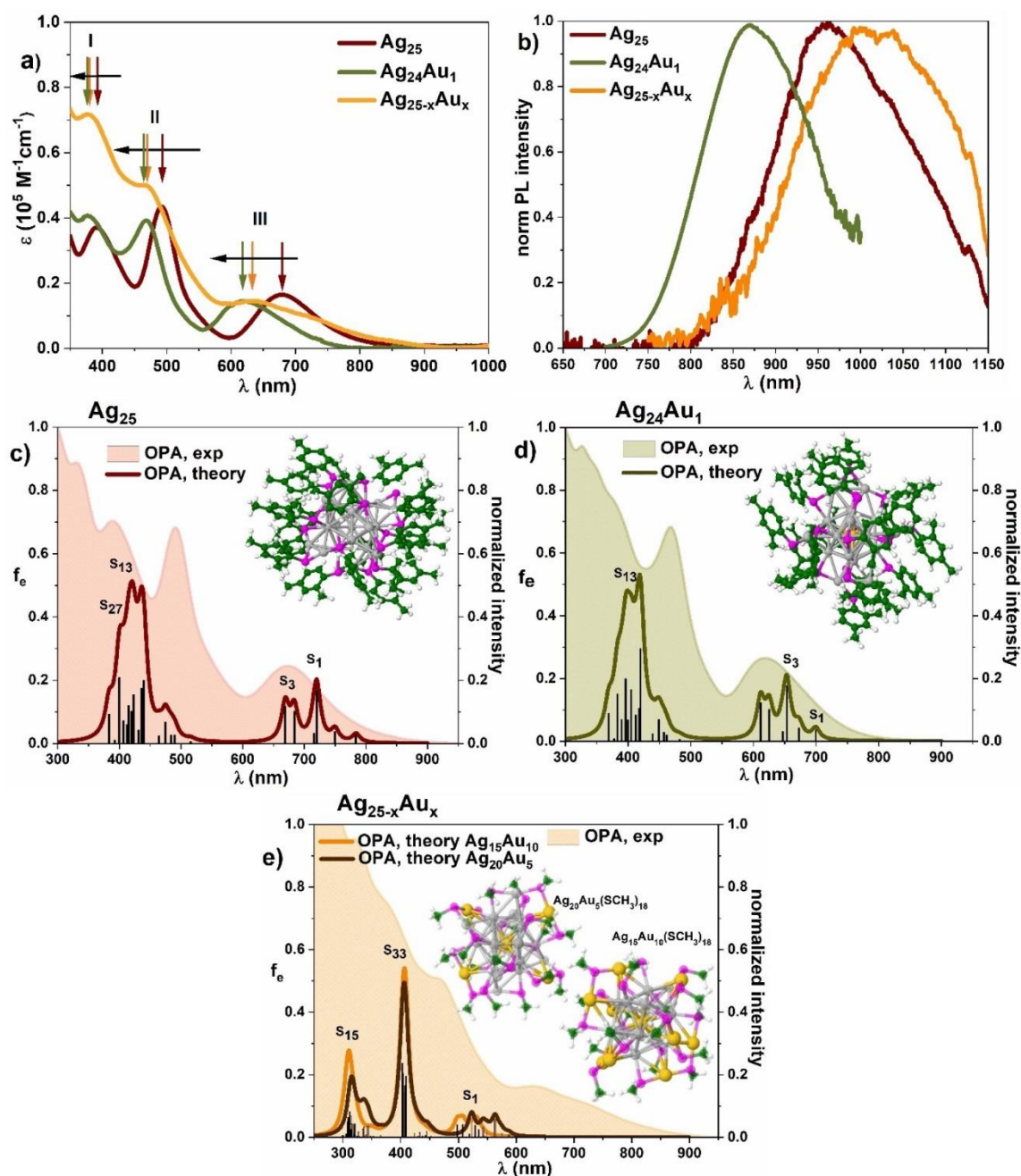


Figure 1. a) absorption and b) luminescence spectra of $\text{Ag}_{25}(\text{DMBT})_{18}$ (red), $\text{Ag}_{24}\text{Au}_1(\text{DMBT})_{18}$ (green) and $\text{Ag}_{25-x}\text{Au}_x(\text{DMBT})_{18}$ (orange). Comparison of experimental absorption (OPA, exp) and simulated one-photon absorption (OPA, theory) spectra of c) Ag_{25} d) $\text{Ag}_{24}\text{Au}_1$ and e) $\text{Ag}_{25-x}\text{Au}_x$ nanoclusters. Upper inset in c, d, e presents optimised structures of nanoclusters, where silver atoms are labelled by grey colour, gold atoms by yellow. DMBT/SCH₃ ligand tail groups are marked: sulfur atoms in purple, carbon atoms in green and hydrogen atoms in white.

clusters exhibit PL in the near infrared (NIR) region. Single Au doped nanoclusters, with emission maximum at 870 nm present 4-times stronger luminescence intensity with respect to the parent nanocluster Ag_{25} . Similar to the absorbance, we found that PL of $\text{Ag}_{24}\text{Au}_1$ undergoes notable blue-shift (see Figure 1b) with respect to Ag_{25} nanoclusters, which correlates well with luminescence blue-shift presented in other works in the case of both, single metal Au-doped Ag_{25} nanoclusters and Ag-doped Au_{25} nanoclusters.^[7a,14] Interest-

ingly, doping with more gold atoms does not improve luminescence intensity, however the luminescence of $\text{Ag}_{25-x}\text{Au}_x$ nanoclusters red-shifts to 1015 nm.

Improved PL QY is one of the advantages arising from metal alloying of nanoclusters.^[5b,5b,15] Using an integrating sphere, we recorded 10-times higher PL QY after doping with single gold atom, from $\Phi=3.08\%$ for Ag_{25} to $\Phi=29.91\%$ for $\text{Ag}_{24}\text{Au}_1$ (Table 1), which is the highest QY reached for doped silver nanoclusters reported so far.^[5b,d,15,16]

Table 1: Quantum yield of Ag₂₅, Ag₂₄Au₁ and Ag_{25-x}Au_x nanoclusters.

Sample	Φ [%]
Ag ₂₅ (DMBT) ₁₈ [PPh ₃]	3.08 ± 2.00 ^a
Ag ₂₄ Au ₁ (DMBT) ₁₈ [PPh ₃]	29.91 ± 2.00 ^a
Ag _{25-x} Au _x (DMBT) ₁₈ [PPh ₃]	0.49 ± 0.05 ^b

QY determined using [a] integrating sphere [b] comparative method using styryl 9M in CHCl₃ as a reference.

Strong QY improvement was confirmed in separate comparative QY experiment using Styryl 9M ($\Phi = 27.2 \pm 2.0\%$, integrating sphere) as a reference (see Figure S3 and Table S1).

On the contrary, incorporation of more than one Au atom into Ag₂₅ nanoclusters decreases PL QY. Since QY of Ag_{25-x}Au_x was detected at the level of measurement error in the integrating sphere, the precise value of QY was limited to indirect QY measurements.

To get deeper insight into PL mechanism, we performed luminescence lifetime measurements with excitation at 450 nm. The PL lifetime components, τ_1 and τ_2 , of NCs recorded with TCSPC system are presented in Figure S4 and Table S2. Since PL decays are biexponential, with two characteristic decay times and respective amplitudes, the intensity-weighted average lifetime τ_{int} was calculated with Eq. 4 (see Experimental Section). Comparing average PL lifetimes of investigated NCs, Ag₂₄Au₁ differs considerably, with the longest luminescence decay $\tau_{\text{int}} = 1.797 \mu\text{s}$, compared to shorter decay of Ag₂₅ with $\tau_{\text{int}} = 1.162 \mu\text{s}$. The presented results are in good agreement with luminescence lifetimes reported for similar gold-doped silver nanoclusters.^[7a] Elongation of luminescence lifetime upon single atom Au doping together with the increase of PL QY suggest that the rate of nonradiative decay is reduced in Ag₂₄Au₁, which corresponds well with observed rigidification of the structure of nanoclusters with single Au dopant, as discussed in following paragraphs. In contrast, Ag_{25-x}Au_x NCs demonstrate shortening of the excited-state lifetime ($\tau_{\text{int}} = 0.543 \mu\text{s}$), which may originate from increased rate of non-radiative decays. Interpretation of the individual lifetimes is not trivial, as a number of factors may affect the rate of luminescence decay, e.g. structure of the cluster, ligands and environmental factors.^[5d] In this work we compare nanoclusters stabilized with the same ligand in the same solvent, thus all observed changes come from the differences in electronic structure of individual nanoclusters. In our results bi-exponential functions of Ag₂₄Au₁(DMBT)₁₈ have dominant contribution of τ_2 ($\approx 95\%$), which equals 1.876 μs , while in Ag_{25-x}Au_x NCs $\tau_2 \approx 0.660 \mu\text{s}$ and its contribution is significantly lower (70%).

NLO properties

We present what we believe are the first results on nonlinear optical properties of silver and gold-doped silver nanoclusters based on the same structural framework of atomically precise clusters containing 25 atoms. The nonlinear optical response of the nanoclusters and a reference sample

of Styryl 9M was monitored by the two-photon excited luminescence technique using femtosecond pulsed laser excitation in the near infrared region from 1180 to 1600 nm. Two-photon absorption (TPA) cross sections σ_2 shown in Figure 2 were determined from TPEL spectra (see Figure S5) according to the Eq. 5 (see Experimental Section). The absence of significant one-photon absorption of nanoclusters at the multiphoton excitation range above 1000 nm confirms off-resonance excitation of the multiphoton processes. Validation of two-photon character of the excitation of observed PL was performed with laser power-dependent photoluminescence intensity measurements. The slope of linear fit in log-log plots of luminescence intensity as a function of the excitation laser power indicates the quadratic dependence and confirms the two-photon absorption as the origin of observed processes (Figure S6).

Due to the fact that the measurements of TPA were carried out via TPEL, only transitions leading to PL will be probed, thus we present obtained TPA results together with one-photon excitation (OPE) spectra plotted at double the wavelength (Figure 2). The TPA spectra in the lowest energy transition range of Ag₂₅ and Ag₂₄Au₁ are closely matched with corresponding OPE at twice the excitation wavelength. They present moderate values of σ_2 ($\sigma_2 = 50.1 \pm 22.0 \text{ GM}$ at 1400 nm and $\sigma_2 = 67.2 \pm 9.9 \text{ GM}$ at 1225 nm) of Ag₂₅ and Ag₂₄Au₁, respectively. In turn, Ag_{25-x}Au_x NCs, similarly as parent Ag₂₅ NCs present the highest nonlinear response in shorter NIR region, with the maximum σ_2 at $\lambda = 1180 \text{ nm}$ and $\lambda = 1200 \text{ nm}$ ($\sigma_2 = 881.3 \pm 386.6 \text{ GM}$ and $\sigma_2 = 894.4 \pm 154.9 \text{ GM}$, for Ag₂₅ and Ag_{25-x}Au_x, respectively). These large σ_2 values are attributed to the excitation of higher energy states (OPE $\approx 475\text{--}500 \text{ nm}$). Since the one-photon absorption spectrum of Ag_{25-x}Au_x is significantly blue-shifted with respect to that of Ag₂₅, the two-photon absorption is shifted as well, causing overlap of two lowest transition bands and flattening of TPA spectra, with σ_2 from 105 to 68 GM in 1350–1400 nm range (see Figure 2c). When comparing TPA cross-sections of corresponding states, σ_2 values increase slightly upon gold atom doping and equal $\approx 50 \text{ GM}$, $\approx 67 \text{ GM}$ and $\approx 68 \text{ GM}$ for the lowest energy transition band of Ag₂₅, Ag₂₄Au₁ and Ag_{25-x}Au_x, respectively.

We performed simulations of TPA spectra for the optimized structures of Ag₂₅(SCH₃)₁₈, Ag₂₄Au₁(SCH₃)₁₈ and two multiply doped Ag_{25-x}Au_x(SCH₃)₁₈ NCs, where $x = 5\text{--}10$ Au atoms: Ag₂₀Au₅(SCH₃)₁₈ and Ag₁₅Au₁₀(SCH₃)₁₈ (see Figure S7 and Computational section for details) in a broad range of wavelengths, including both, resonant and off-resonance range. Note that we modelled DMBT ligand with SCH₃ groups due to the computationally demanding TPA simulations. Simulated TPA spectra show strong nonlinear response in the resonance region, with $\sigma_2 = 4 \cdot 10^7 \text{ GM}$, $1.7 \cdot 10^6 \text{ GM}$ and 200 GM for Ag₂₅(SCH₃)₁₈, Ag₂₄Au₁(SCH₃)₁₈ and Ag_{25-x}Au_x(SCH₃)₁₈ NCs, respectively (see Figure S7). The order of magnitude of simulated values correlates with the literature findings regarding double resonance theory of two-photon absorption in silver nanoclusters.^[17] Large TPA signal at $< 1000 \text{ nm}$ is assigned to double-resonance effect, which occurs when excitation energy of an OPA state is

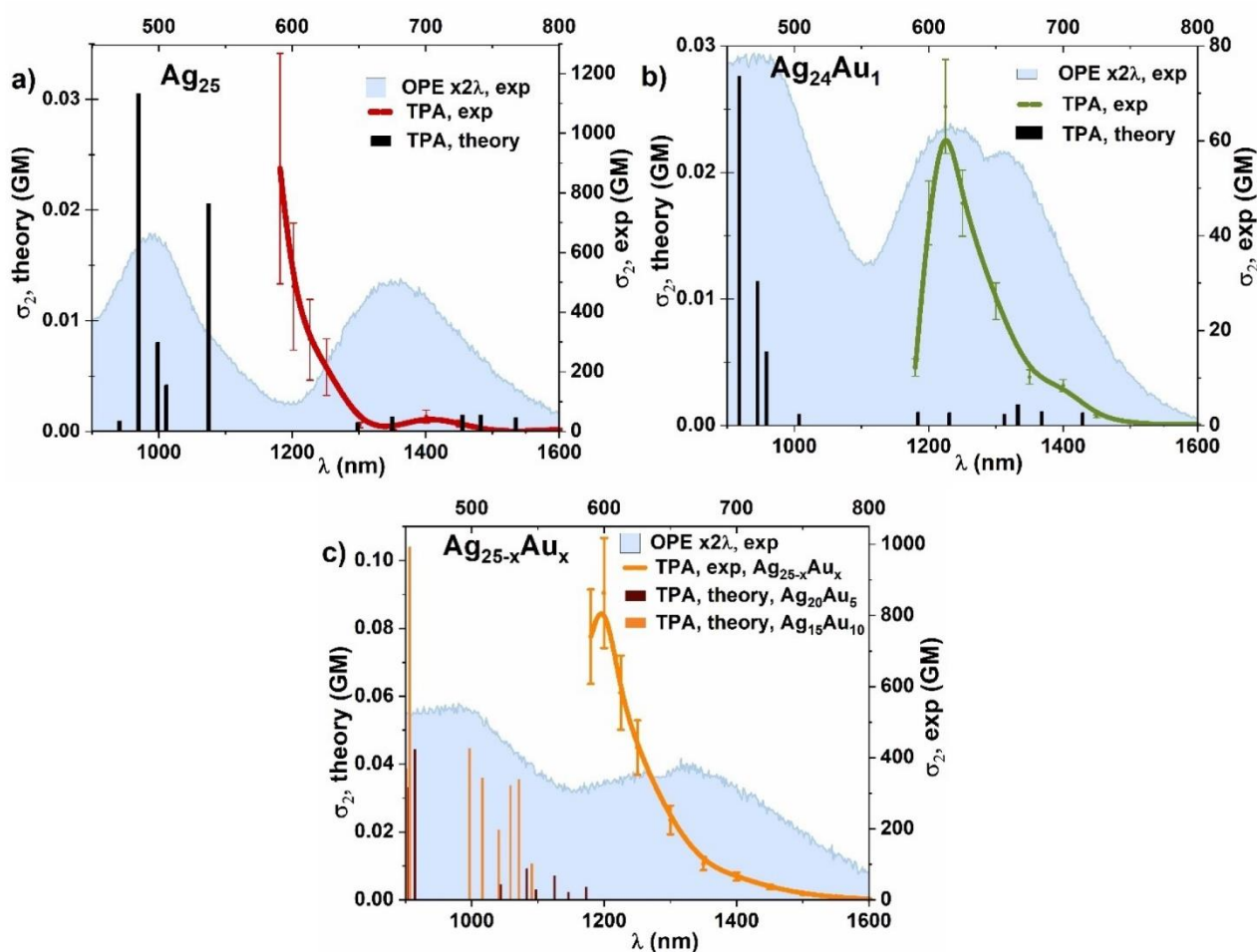


Figure 2. Off-resonance TPA spectra (solid lines, wavelength dependence of two-photon absorption cross-sections in GM units) and simulated TPA spectra (black, brown and orange columns) of a) Ag_{25} , b) $\text{Ag}_{24}\text{Au}_1$ and c) $\text{Ag}_{25-x}\text{Au}_x$ nanoclusters presented with respective normalized one-photon excitation (OPE) at twice the wavelength (blue area).

close to a half of the energy of a TPA state.^[1d] On the contrary, the off-resonance TPA in NIR region remains small.^[18] We present off-resonance simulated values together with experimental TPA spectra in Figure 2. Although the values from simulations are incomparably small with respect to the experimental ones, we found similar relative relation between them. We observe similar ratio of decreasing σ_2 values upon shift from $\approx 900\text{--}1200\text{ nm}$ to $\approx 1200\text{--}1400\text{ nm}$ between simulated and experimental spectra. In both cases we determine one order of magnitude lower TPA values between these two wavelength ranges (e.g. $\text{Ag}_{20}\text{Au}_5(\text{SCH}_3)_{18}$ shows theoretical values of $\approx 0.04\text{ GM}$ at 900 nm and 0.003 GM at $\approx 1200\text{ nm}$, while corresponding $\text{Ag}_{20}\text{Au}_5\text{-(DMBT)}_{18}$ experimental results equal $\approx 832\text{ GM}$ at 1200 nm and $\approx 68\text{ GM}$ at 1400 nm). The same trend was observed for Ag_{25} NCs and $\text{Ag}_{24}\text{Au}_1$.

In order to evaluate the potential of application of nanoclusters in two-photon luminescence imaging and sensing two-photon brightness, $\sigma_{2,\text{eff}}$ (in other sources called also an effective cross-section or action cross-section) was calculated. $\sigma_{2,\text{eff}}$ is defined as the product of TPA cross-section and PL quantum yield ($\sigma_{2,\text{eff}} = \sigma_2 \Phi$) (Eq. 6, Exper-

imental Section).^[1d] Owing to several times stronger PL quantum yield, $\text{Ag}_{24}\text{Au}_1$ presents the highest $\sigma_{2,\text{eff}} = 20\text{ GM}$ (at $\lambda = 1225\text{ nm}$), comparing the lowest transition bands of Ag_{25} , $\text{Ag}_{24}\text{Au}_1$ and $\text{Ag}_{25-x}\text{Au}_x$ (Figure 3).

To discuss potential of nanoclusters for multiphoton applications we verified photostability of nanoclusters under prolonged laser illumination. $\text{Ag}_{24}\text{Au}_1$ NCs in contrary to Ag_{25} NCs ensure improved laser power strength in 100 mW and 300 mW , while Ag_{25} most likely decompose under 100 mW of sustained irradiation (Figure S8).

Discussion on the influence of gold atom doping of silver nanoclusters on linear and nonlinear optical properties

In order to understand the influence of single Au atom doping on optical properties of silver nanoclusters, characterization of absorption and luminescence properties should be analysed regarding modified geometries of nanoclusters at the single atom-doping level. Structures of $\text{Ag}_{25}(\text{DMBT})_{18}$, $\text{Ag}_{24}\text{Au}_1(\text{DMBT})_{18}$, $\text{Ag}_{15}\text{Au}_{10}(\text{SCH}_3)_{18}$ and $\text{Ag}_{20}\text{Au}_5(\text{SCH}_3)_{18}$ nanoclusters are shown in Figure 1c–e. Three possible atom

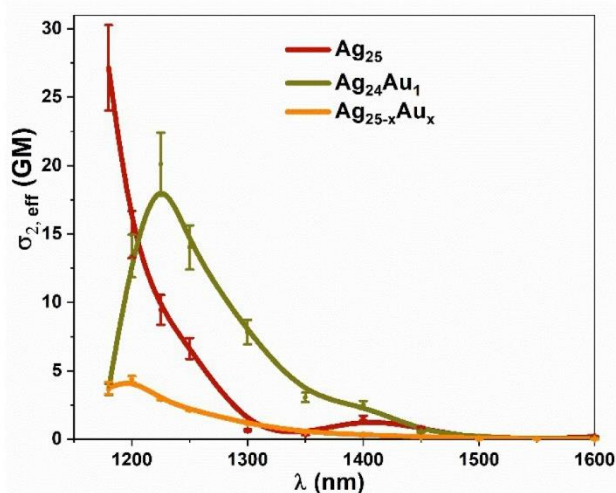


Figure 3. Comparative juxtaposition of two-photon brightness $\sigma_{2,\text{eff}}$ spectra of Ag_{25} , $\text{Ag}_{24}\text{Au}_1$ and $\text{Ag}_{25-x}\text{Au}_x$ (calculated regarding the molar mass at the boundary Au content, knowing that $x=5-10$), determined using Eq. 6 (Experimental Section).

positions include the centre of icosahedron, surface of icosahedron and staple motifs. Single Au atom doping occurs at the icosahedral centre of the nanocluster, preserving the initial framework of $\text{Ag}_{25}(\text{SR})_{18}$ structure, in a form of icosahedral $\text{M}@\text{Ag}_{12}$ kernel protected with $\text{Ag}_2(\text{SR})_3$ dimeric staples. $\text{Ag}_{24}\text{Au}_1$ nanocluster structure is characterized by strong bonds with central Au atom. Further incorporation of gold atoms may occur at two other positions: icosahedron sites or staple motifs.^[7a,b,11] Our study reveals that next preferable location is in staple motifs. It is in good agreement with recent simulations^[7c,9,19] and X-ray crystallography studies.^[20]

Trying to establish the origin of luminescence, several experimental studies already proposed ligand-to-metal charge transfer mechanism of luminescence for gold, silver and gold-doped silver nanoclusters with 25-atom framework.^[5a,11,21] However, some of theoretical calculations predict that core-based transitions between P-D superatomic orbitals are involved in luminescence processes rather than charge-transfer states.^[5c,22] Our experimental study shows long photoluminescence lifetimes ($>1 \mu\text{s}$) implying charge-transfer type transitions. Qualitative theoretical prediction of energies and characters of higher excited states indicate that the charge transfer is involved.

Gold atoms possess higher electron affinity than silver ones. Therefore, the central silver atom replacement with Au atom leads to localization of electron charge in the icosahedral centre inducing changes in electronic structure of $\text{Ag}_{24}\text{Au}_1$. Considering the lowest-energy transition, one and two-photon luminescence properties (luminescence intensity, QY, PL lifetime and $\sigma_{2,\text{eff}}$) of nanoclusters follow the order: $\text{Ag}_{25-x}\text{Au}_x < \text{Ag}_{25} < \text{Ag}_{24}\text{Au}_1$. Since OPA and TPA of AuAg nanoclusters are blue-shifted with respect to Ag_{25} nanoclusters, TPA of Ag_{25} has higher values in comparison with other NCs at the same wavelength. TPA of higher energy bands ($\lambda < 1200 \text{ nm}$) shows enhanced σ_2 due to

proximity of resonant conditions of excitation. Although the presented quantitative TPA results suggest minor two-photon absorption cross-section changes upon gold-atom doping, nevertheless, they strongly support enhancement of two-photon excited luminescence properties of $\text{Ag}_{24}\text{Au}_1$ clusters, making them a robust material for one-photon and two-photon luminescence applications.

Our observation suggests that gradual incorporation of gold atoms into Ag_{25} does not gradually enhance optical properties of nanoclusters, similarly like in the latest results of Zhu et al., for Au doped $\text{Ag}_{25}(\text{SPhMe}_2)_{18}$.^[26] The opposite observation was reported in the case of doping $\text{Ag}_{29}(\text{SR})_{12}(\text{PPh}_3)_4$ NCs.^[27] We note that optical properties of nanoclusters are strictly dependent on the number of building atoms as well as number and type of metallic dopants or stabilizing ligands, therefore comparison of our and literature results may not be trivial when σ_2 was examined in different spectral ranges, using different techniques or nanoparticles with various ligands, and in different environmental conditions.^[14,17a,28] In this work, we omit these problems by comparing NCs stabilized with the same ligand, in the same solvent, using the same technique. However, we admit the difficulties in discussion of $\text{Ag}_{25-x}\text{Au}_x$ optical properties, which may be affected by particular NCs among $\text{Ag}_{20}\text{Au}_5$ to $\text{Ag}_{15}\text{Au}_{10}$ NCs.

Although literature is already full of extensive studies of NLO properties of gold nanoclusters we note that silver and gold-silver alloys findings are incomplete in this field. In Table 2 we collected exclusive σ_2 and $\sigma_{2,\text{eff}}$ values of silver nanoclusters and its gold alloys available in the literature, established for particular wavelengths. As shown there, TPA of $\text{Ag}_{25}(\text{DMBT})_{18}$ determined by G. Yousefzadeh and our results report similar values: 1300 GM at 1028 nm^[17a] and 881 GM at 1180 nm (this report). We observe a similar tendency comparing our TPA results of $\text{Ag}_{25-x}\text{Au}_x$ nanoclusters and 50:50 Ag:Au alloys.^[17a] Good agreement between these two works confirms credibility of using TPEL as well as femtosecond pump/probe transient absorption spectroscopy to establish σ_2 of nanomaterials. Our results in Table 2 present most essential values of σ_2 and $\sigma_{2,\text{eff}}$ determined at selected wavelengths, however full spectra in a broad wavelength range ($\lambda = 1180-1600 \text{ nm}$) are presented in Figure 2 and 3, contrary to the most reports from the literature, which present nonlinear properties solely at a single/few wavelengths in the range $< 1000 \text{ nm}$ of resonant conditions.

Conclusion

In summary, we presented here a systematic investigation of linear and nonlinear optical properties supported by complementary TD-DFT simulations to determine the influence of gold atom doping of atomically precise silver nanoclusters on absorption and luminescence properties. We observed that incorporating a single heteroatom into atomically-precise nanocluster has the strongest influence on the structure, resulting in strong enhancement of luminescence quantum yield (10-times), increase of luminescence lifetime

Table 2: Complete summary of NLO properties of Ag and Au-doped silver nanoclusters.

Sample	α_z [GM]	$\alpha_{z,eff}$ [GM]	λ [nm]	Technique	source
Ag ₂₉ (DHIA) ₁₂	12930 GM/	0.48 GM	790 nm/	TPEL	I. Russier-Antoine ^[23]
	873 GM/	0.065 GM	860 nm/		
	N/A	0.031 GM	950 nm (in-resonance)		
Ag ₃₁ (SG) ₁₉ Ag ₁₅ (SG) ₁₁	668 GM	60 000 GM	(2.62 eV)	TD-DFT calculation	P. N. Day ^[24]
	60 000 GM		(off-resonance) (1.85 eV) (in-resonance)		
Ag ₁₁ (SG) ₇ Ag ₁₅ (SG) ₁₁ Ag ₃₁ (SG) ₁₉	6.6 GM	0.00033 GM	800 nm	TPEL	I. Russier-Antoine ^[17b]
	63.5 GM	0.00169 GM	(in-resonance)		
	950 GM	0.066 GM			
Ag ₂₅ (DMBT) ₁₈	Ag ₂₅ (DMBT)		1028 nm (off-resonance)	fsTAS (femtosecond pump/probe transient absorption spectroscopy)	G. Yousefalizadeh ^[17a]
Au ₁₅ @Ag Au ₁₈ @Ag Au ₂₅ @Ag	1900 GM		800 nm	TPEL	T. Goodson ^[25]
	3900 GM		(in-resonance)		
	888 000 GM				
50:50 Ag:Au alloy	2260 GM		1028 nm (off-resonance)	fsTAS (femtosecond pump/probe transient absorption spectroscopy)	G. Yousefalizadeh ^[17a]
Ag ₂₅ (DMBT) ₁₈	881.3 GM/	27.1 GM/	1180 nm/	TPEL	This work
	50.1 GM	1.5 GM	1400 nm		
	67.2 GM	20.1 GM	1225 nm		
	893.3 GM	4.25 GM	1200 nm (off-resonance)		
Ag ₂₄ Au ₁ (DMBT) ₁₈ Ag _{25-x} Au _x (DMBT) ₁₈					

(from 1.1 to 1.8 μs), and two-photon brightness (from 1.5 GM to 20 GM) of $\text{Ag}_{24}\text{Au}_1$ with respect to Ag_{25} parent nanoclusters. Interestingly, further doping of Au atoms to $\text{Ag}_{24}\text{Au}_1$ NCs leads to weaker luminescence properties, and we show that the opposite consequences of single and multiple atom doping result from different geometries and electron charge localization. A single Au in the centre of $\text{Ag}_{24}\text{Au}_1$ NCs causes high stability and enhanced luminescence properties due to stronger electron affinity of gold compared to silver atoms. Conversely, Au atoms in multiply doped NCs appear in staple motifs inducing lower quantum yield, shorter PL lifetimes and lower values of two-photon brightness $\sigma_{2,\text{eff}}$ of $\text{Ag}_{25-x}\text{Au}_x$ in comparison with Ag_{25} .

To this date, nonlinear optical properties of silver and gold-doped silver nanoclusters have been scarcely studied, especially in a wide wavelength, off-resonance range. We extend current knowledge in this field by a broad two-photon excited luminescence analysis in 1180–1600 nm range. We also propose $\text{Ag}_{24}\text{Au}_1$ nanocluster as a robust emitter of improved photostability. Comparison of two-photon brightness of gold-doped silver NCs and commonly used fluorescent organic dyes^[29] or fluorescent proteins^[30] shows that gold-doped silver nanoclusters can easily compete with red-emissive fluorophores. Taking into consideration the fact that NCs both, absorb and emit in the NIR range of wavelengths, NCs prevail organic dyes, as there are only few commercial fluorophores with emission wavelength > 900 nm. Moreover, both two-photon excitation and luminescence of these nanoparticles is located in the second biological window (1000–1700 nm), which is favourable for deep-tissue bioimaging and *in vivo* biosensing applications.

Acknowledgements

This work was supported by the First Team program of the Foundation for Polish Science (First TEAM/2017-3/27) co-financed by the European Union (P.O.) as well as Sonata Bis project from National Science Centre (2019/34/E/ST5/00276) (A.P.). This research was partially supported under the project STIM–REI, Contract Number: KK.01.1.1.01.0003, a project funded by the European Union through the European Regional Development Fund—the Operational Programme Competitiveness and Cohesion 2014–2020 (KK.01.1.1.01) (V.B.K. and M.P.B.). We acknowledge the financial support from the Swiss National Science Foundation (grant 200020_192232) and the University of Geneva (T. B.).

Conflict of Interest

The authors declare no conflict of interest.

Data Availability Statement

The data that support the findings of this study are available from the corresponding author upon reasonable request.

Keywords: Alloy Clusters • Metallic Doping • Nonlinear Optics • Silver Nanoclusters • Two-Photon Absorption

- [1] a) S. Takano, T. Tsukuda, *J. Am. Chem. Soc.* **2021**, *143*, 1683–1698; b) K. Weerawardene, H. Häkkinen, C. M. Aikens, *Annu. Rev. Phys. Chem.* **2018**, *69*, 205–229; c) R. Jin, *Nanoscale* **2015**, *7*, 1549–1565; d) V. Bonačić-Koutecký, R. Antoine, *Nanoscale* **2019**, *11*, 12436–12448.
- [2] a) R. Antoine, V. Bonačić-Koutecký, in *Ligated silver and gold quantum clusters. Towards a new class of nonlinear optical nanomaterials*, Springer International Publishing, Cham, **2018**, pp. 5–20; b) J. Olesiak-Banska, M. Waszkielewicz, P. Obstarczyk, M. Samoc, *Chem. Soc. Rev.* **2019**, *48*, 4087–4117.
- [3] a) M. Waszkielewicz, J. Olesiak-Banska, M. Grzelczak, A. Sánchez-Iglesias, A. Pniakowska, M. Samoc, *J. Lumin.* **2020**, *221*, 116994; b) S. Wang, X. Meng, A. Das, T. Li, Y. Song, T. Cao, X. Zhu, M. Zhu, R. Jin, *Angew. Chem. Int. Ed.* **2014**, *53*, 2376–2380; *Angew. Chem.* **2014**, *126*, 2408–2412.
- [4] X. Le Guével, V. Trouillet, C. Spies, K. Li, T. Laaksonen, D. Auerbach, G. Jung, M. Schneider, *Nanoscale* **2012**, *4*, 7624–7631.
- [5] a) A. Ghosh, O. F. Mohammed, O. M. Bakr, *Acc. Chem. Res.* **2018**, *51*, 3094–3103; b) G. Soldan, M. A. Aljuhani, M. S. Bootharaju, L. G. AbdulHalim, M. R. Parida, A. H. Emwas, O. F. Mohammed, O. M. Bakr, *Angew. Chem. Int. Ed.* **2016**, *55*, 5749–5753; *Angew. Chem.* **2016**, *128*, 5843–5847; c) K. L. D. M. Weerawardene, C. M. Aikens, *J. Phys. Chem. C* **2018**, *122*, 2440–2447; d) M. van der Linden, A. J. van Bunningen, L. Amidani, M. Bransen, H. Elnaggar, P. Glatzel, A. Meijerink, F. M. F. de Groot, *ACS Nano* **2018**, *12*, 12751–12760.
- [6] C. P. Joshi, M. S. Bootharaju, M. J. Alhilaly, O. M. Bakr, *J. Am. Chem. Soc.* **2015**, *137*, 11578–11581.
- [7] a) M. S. Bootharaju, C. P. Joshi, M. R. Parida, O. F. Mohammed, O. M. Bakr, *Angew. Chem. Int. Ed.* **2016**, *55*, 922–926; *Angew. Chem.* **2016**, *128*, 934–938; b) K. R. Krishnadas, D. Ghosh, A. Ghosh, G. Natarajan, T. Pradeep, *J. Phys. Chem. C* **2017**, *121*, 23224–23232; c) K. Zheng, V. Fung, X. Yuan, D.-E. Jiang, J. Xie, *J. Am. Chem. Soc.* **2019**, *141*, 18977–18983.
- [8] a) K. Pyo, V. D. Thanthirige, K. Kwak, P. Pandurangan, G. Ramakrishna, D. Lee, *J. Am. Chem. Soc.* **2015**, *137*, 8244–8250; b) C. Yao, C.-Q. Xu, I.-H. Park, M. Zhao, Z. Zhu, J. Li, X. Hai, H. Fang, Y. Zhang, G. Macam, J. Teng, L. Li, Q.-H. Xu, F.-C. Chuang, J. Lu, C. Su, J. Li, J. Lu, *Angew. Chem. Int. Ed.* **2020**, *59*, 8270–8276; *Angew. Chem.* **2020**, *132*, 8347–8353.
- [9] K. R. Krishnadas, A. Bakshi, A. Ghosh, G. Natarajan, T. Pradeep, *Nat. Commun.* **2016**, *7*, 13447.
- [10] O. M. Bakr, V. Amendola, C. M. Aikens, W. Wenseleers, R. Li, L. Dal Negro, G. C. Schatz, F. Stellacci, *Angew. Chem. Int. Ed.* **2009**, *48*, 5921–5926; *Angew. Chem.* **2009**, *121*, 6035–6040.
- [11] X. Liu, J. Yuan, C. Yao, J. Chen, L. Li, X. Bao, J. Yang, Z. Wu, *J. Phys. Chem. C* **2017**, *121*, 13848–13853.
- [12] F. Muniz-Miranda, *Nanomaterials* **2021**, *11*, 2409.
- [13] M. Medves, L. Sementa, D. Toffoli, G. Fronzoni, K. R. Krishnadas, T. Bürgi, S. Bonacchi, T. Dainese, F. Maran, A. Fortunelli, M. Stener, *J. Chem. Phys.* **2021**, *155*, 084103.
- [14] Y. Negishi, T. Iwai, M. Ide, *Chem. Commun.* **2010**, *46*, 4713–4715.
- [15] D. Mishra, V. Lobodin, C. Zhang, F. Aldeek, E. Lochner, H. Mattoussi, *Phys. Chem. Chem. Phys.* **2018**, *20*, 12992–13007.
- [16] X. Dou, X. Yuan, Y. Yu, Z. Luo, Q. Yao, D. T. Leong, J. Xie, *Nanoscale* **2014**, *6*, 157–161.
- [17] a) G. Yousefalizadeh, S. Ahmadi, N. J. Mosey, K. G. Stamplecoskie, *Nanoscale* **2021**, *13*, 242–252; b) I. Russier-Antoine, F. Bertorelle, N. Calin, Ž. Sanader, M. Krstić, C. Comby-Zerbino,

- P. Dugourd, P.-F. Brevet, V. Bonačić-Koutecký, R. Antoine, *Nanoscale* **2017**, *9*, 1221–1228.
- [18] a) P. N. Day, K. A. Nguyen, R. Pachter, *J. Chem. Theory Comput.* **2010**, *6*, 2809–2821; b) H. H. Mai, V. E. Kaydashev, V. K. Tikhomirov, E. Janssens, M. V. Shestakov, M. Meledina, S. Turner, G. Van Tendeloo, V. V. Moshchalkov, P. Lievens, *J. Phys. Chem. C* **2014**, *118*, 15995–16002.
- [19] M. Neumaier, A. Baksi, P. Weis, E. K. Schneider, P. Chakraborty, H. Hahn, T. Pradeep, M. M. Kappes, *J. Am. Chem. Soc.* **2021**, *143*, 6969–6980.
- [20] C. Kumara, C. M. Aikens, A. Dass, *J. Phys. Chem. Lett.* **2014**, *5*, 461–466.
- [21] K. G. Stamplecoskie, Y.-S. Chen, P. V. Kamat, *J. Phys. Chem. C* **2014**, *118*, 1370–1376.
- [22] K. L. D. M. Weerawardene, C. M. Aikens, *J. Am. Chem. Soc.* **2016**, *138*, 11202–11210.
- [23] I. Russier-Antoine, F. Bertorelle, R. Hamouda, D. Rayane, P. Dugourd, Ž. Sanader, V. Bonačić-Koutecký, P.-F. Brevet, R. Antoine, *Nanoscale* **2016**, *8*, 2892–2898.
- [24] P. N. Day, R. Pachter, K. A. Nguyen, T. P. Bigioni, *J. Phys. Chem. A* **2016**, *120*, 507–518.
- [25] R. Ho-Wu, P. K. Sahu, N. Wu, T. K. Chen, C. Yu, J. Xie, T. Goodson, *J. Phys. Chem. C* **2018**, *122*, 24368–24379.
- [26] Q. Yuan, X. Kang, D. Hu, C. Qin, S. Wang, M. Zhu, *Dalton Trans.* **2019**, *48*, 13190–13196.
- [27] X.-Y. Xie, P. Xiao, X. Cao, W.-H. Fang, G. Cui, M. Dolg, *Angew. Chem. Int. Ed.* **2018**, *57*, 9965–9969; *Angew. Chem.* **2018**, *130*, 10114–10119.
- [28] H. A. Kindi, A. Mohamed, S. Kajimoto, N. Zhanpeisov, H. Horino, Y. Shibata, I. I. Rzeznicka, H. Fukumura, *J. Photochem. Photobiol. A* **2018**, *357*, 168–174.
- [29] J. Mütze, V. Iyer, J. J. Macklin, J. Colonell, B. Karsh, Z. Petrášek, P. Schwille, L. L. Looger, L. D. Lavis, T. D. Harris, *Biophys. J.* **2012**, *102*, 934–944.
- [30] M. Drobizhev, S. Tillo, N. S. Makarov, T. E. Hughes, A. Rebane, *J. Phys. Chem. B* **2009**, *113*, 855–859.

Manuscript received: July 1, 2022

Accepted manuscript online: August 25, 2022

Version of record online: September 14, 2022

Supporting Information

**Gold-Doping Effect on Two-Photon Absorption and Luminescence
of Atomically Precise Silver Ligated Nanoclusters**

*A. Pniakowska, K. Kumaranchira Ramankutty, P. Obstarczyk, M. Perić Bakulić,
Ž. Sanader Maršić, V. Bonačić-Koutecký, T. Bürgi, J. Olesiak-Bañska**

SUPPORTING INFORMATION

TABLE OF CONTENTS

Table of Contents	2
Experimental Procedures	2
Materials.....	2
Synthesis of $[Ag_{25}(DMBT)_{18}][PPh_4]$	2
Synthesis of $[Ag_{24}Au_1(DMBT)_{18}][PPh_4]$	3
Synthesis of $[Ag_{25-x}Au_x(DMBT)_{18}][PPh_4]$	3
ESI MS spectrometry	3
DFT calculations.....	3
UV-Vis and fluorescence measurements	4
Fluorescence decay characterization	4
Nonlinear optical properties characterization	4
Supplementary figures.....	5
Figure S1	6
Figure S2	7
Figure S3	8
Figure S4	8
Table S1	9
Figure S5	9
Figure S6	10
Figure S7	11
Figure S8	12
References.....	12

EXPERIMENTAL PROCEDURES

MATERIALS

Silver nitrate ($AgNO_3$), 2,4-dimethylbenzene thiol (DMBT), tetraphenylphosphonium bromide (PPh_4Br), and sodium borohydride ($NaBH_4$) were purchased from Sigma-Aldrich. Chloro-(triphenylphosphine)gold(I) ($AuClPPh_3$) was purchased from Acros Chemicals. All solvents used, dichloromethane (DCM), methanol, etc., were of analytical grade and used without further purification. Bio Beads SX-1 (Bio-Rad) for column size-exclusion chromatography was purchased from Bio-Rad Companies, USA.

SYNTHESIS OF $[Ag_{25}(DMBT)_{18}][PPh_4]$

It was synthesized by adopting a reported procedure with slight modifications. 76 mg of $AgNO_3$ were dissolved in 4 mL of methanol by ultrasonication. This $AgNO_3$ solution was then transferred into a round bottom flask and moderately stirred at $0^\circ C$ (ice bath). 190 μL of pure 2,4-dimethylbenzenethiol were then poured into the $AgNO_3$ solution in one quick addition which resulted in the formation of yellow-coloured Ag-DMBT thiolates. Following, 34 mL of DCM were added and the reaction mixture was stirred at about 1400 rpm for about 20 minutes. Then, a freshly prepared solution of PPh_4Br (15 mg) in 1 mL methanol was added in one shot into the reaction mixture. Then a freshly prepared solution of $NaBH_4$ (30 mg in 1 mL ice cold water) was added to the mixture dropwise. The reaction mixture was then stirred at the same speed for about 6 hours in the ice bath. After 6h, the solution was kept overnight at $4^\circ C$ in the refrigerator.

SUPPORTING INFORMATION

After this period, the organic fraction (the DCM part) of the solution was carefully transferred to a centrifuge tube leaving the insoluble material in the aqueous layer at the bottom of the flask. The collected organic fraction was then centrifuged at around 10000 rpm for about 10 minutes. After the first centrifugation, the solution is carefully transferred to a round bottom flask and rotary evaporated till the solution becomes a paste-like material; the solution was not dried completely at this stage. Afterward, about 15 mL of methanol is added to the round bottom flask in order to precipitate the clusters from the impurities. Centrifugation at around 10000 rpm for about 10 minutes was used to collect more easily the precipitate, meanwhile the supernatant (methanol solution) was discarded. This washing procedure was repeated 2-3 more times, in order to remove most of the free DMBT ligands and the residues formed from the reducing agents. The collected precipitate was then dissolved in 15 mL of DCM in the centrifuge tube, the dissolved clusters were centrifuged at around 10000 rpm for about 10 minutes. The solution was carefully transferred to a round bottom flask, leaving any insoluble material at the bottom of the centrifuge tube, and dried using a rotary evaporator. The dried material was then purified with size exclusion chromatography (BioBeads S-X1) using DCM as eluting solvent to obtain pure $[\text{Ag}_{25}(\text{DMBT})_{18}][\text{TOA}]$ clusters.

SYNTHESIS OF $[\text{Ag}_{24}\text{Au}_1(\text{DMBT})_{18}][\text{PPH}_4]$

$[\text{Ag}_{24}\text{Au}_1(\text{DMBT})_{18}][\text{PPH}_4]$ was synthesized by the reaction of $[\text{Ag}_{25}(\text{DMBT})_{18}][\text{PPH}_4]$ with $\text{AuCl}(\text{PPh}_3)_2$ by adopting a reported procedure with slight modifications. 16 mg of $[\text{Ag}_{25}(\text{DMBT})_{18}][\text{PPH}_4]$ were dissolved in 5 mL of DCM. 200 μL of $\text{AuCl}(\text{PPh}_3)_2$ solution (4.2 mg in 500 μL DCM) was then added to it. The reaction mixture was gently shaken with hand for some minutes to allow the mixing of the reagents and then kept unmoved for about 2 hours. The colour of the solution changed from dark brown to dark green during this time interval, indicating the formation of $[\text{Ag}_{24}\text{Au}_1(\text{DMBT})_{18}][\text{PPH}_4]$. Formation of the alloy cluster was confirmed using UV-Vis spectroscopy as well. Then the reaction mixture is then centrifuged to remove AgCl , Ag -thiolates and any other insoluble materials formed in this reaction. The clear DCM part was rotary evaporated and then purified using size-exclusion chromatography.

SYNTHESIS OF $[\text{Ag}_{25-x}\text{Au}_x(\text{DMBT})_{18}][\text{PPH}_4]$

$[\text{Ag}_{25-x}\text{Au}_x(\text{DMBT})_{18}][\text{PPH}_4]$ was synthesized by reaction of $[\text{Ag}_{24}\text{Au}_1(\text{DMBT})_{18}][\text{PPH}_4]$ with Au-DMBT thiolates. The latter was prepared by mixing 150 μL of neat DMBT into $\text{HAuCl}_4 \cdot 3\text{H}_2\text{O}$ solution (50 mM, 5 mL). The precipitates formed are collected by centrifugation and washed 3-4 times by methanol to remove free thiols. 20 mg of this dried Au-DMBT thiolates is added to a solution of $[\text{Ag}_{24}\text{Au}_1(\text{DMBT})_{18}][\text{PPH}_4]$ (12 mg in 3 mL DCM) and stirred for 4 hours. After this period, the mixture is centrifuged to get rid of the insoluble thiolates and the DCM solution part is collected separately and dried using rotary evaporation. This dried product contains $[\text{Ag}_{25-x}\text{Au}_x(\text{DMBT})_{18}][\text{PPH}_4]$ clusters which is purified by size exclusion chromatography.

ESI MS SPECTROMETRY

Electrospray ionization mass spectra were measured on a QSTAR pulsar i (AB Sciex) using a quadrupole and time-of-flight analysers. The spectra were measured in the mass range of m/z 500–12,000 in the negative ion mode. Further details of the instrumental parameters used for the measurements are provided below.

The sample solubilized in dichloromethane was analysed by nano-electrospray high resolution mass spectrometry (nano-ESI-HRMS) with the following settings:

- QSTAR Pulsar (AB Sciex)
- nano-ESI voltage = -2600 kV and -2200 kV (negative),
- Curtain gas (N_2) = 25 psi
- Declustering and focusing lenses: DP = -50 V, DP2 = -15 V, FP = -120 V
- Mass range: m/z 100 – 12'000 (accumulation time = 1s) with external TOF calibration (Agilent) - Bin = 1 (automatic signal smoothing)
- Data processing software: PeakView 2.2 (AB Sciex)

DFT CALCULATIONS

Density functional theory (DFT) and time-dependent density functional theory (TD-DFT) have been used to investigate the structural and optical properties of gold doped liganded silver NCs. Since the focus was on comparison between $\text{Ag}_{25}(\text{DMBT})_{18}$ and doped $\text{Ag}_{24}\text{Au}_1(\text{DMBT})_{18}$, the ligands corresponding to experimental choice have been used, while for the other systems $\text{Ag}_{25-x}\text{Au}_x$ DMBT ligand has been replaced by SCH_3 . All the TPA spectra were obtained with SCH_3 ligand due to computational demand. For the optimization of the structures SVP atomic orbital (AO) basis set^[1] was used for all atoms, together with relativistic effective core potential (RECP) of the Stuttgart group^[2] for silver and gold atoms. PBE functional^{[3] [4]} as implemented in Gaussian computational chemistry software^[5] was employed for the structural optimizations. The initial structure for $\text{Ag}_{25}(\text{DMBT})_{18}$ was taken from crystal structure $\text{Ag}_{25}(\text{SPhMe}_2)_{18}$ ^[6] and the crystal structure of $\text{Ag}_{24}\text{Au}_1(\text{DMBT})_{18}$ ^[7] was reoptimized with above described methodology to ensure comparability. Extensive search for the selected doped structures $\text{Ag}_{20}\text{Au}_5(\text{SCH}_3)_{18}$ and $\text{Ag}_{15}\text{Au}_{10}(\text{SCH}_3)_{18}$ was performed with Turbomole computational chemistry software (TURBOMOLE V7.4.1 2019, a development of University of Karlsruhe and Forschungszentrum Karlsruhe GmbH, 1989-2007, TURBOMOLE GmbH, since 2007) using the same level of theory (SVP basis set and PBE functional). The structures of the $\text{Au}_{25}(\text{SCH}_2\text{CH}_2\text{Ph})_{18}$ ^[8] and $\text{Ag}_{24}\text{Au}_1(\text{DMBT})_{18}$ ^[7] served as starting points for further doping

SUPPORTING INFORMATION

by silver or gold respectively, while ligands were modeled by (SCH₃). In the first step, only the core atoms were doped with Au/Ag, while the staples remained unchanged. In the second step, the staple was doped by one of the Au/Ag atoms, while the core was doped with the remaining Au/Ag atoms. In the each consecutive step number of Au/Ag atoms doped within staples increased until all of them were included and simultaneously number of Au/Ag atoms doped in the core decreases. The lowest energy isomers were found which have one Au atom doped into central position of the Ag₁₃ icosahedral core forming Ag₁₂Au₁ core, and the rest of the Au atoms were in the staples (4 Au atom in the Ag₂₀Au₅(SCH₃)₁₈ and 9 Au atoms in the structure of Ag₁₅Au₁₀(SCH₃)₁₈).

One-photon absorption (OPA) spectra were calculated for all the structures using the TD-DFT as implemented in Gaussian: Coulomb-attenuated version of Becke's three-parameter non-local exchange functional together with the Lee–Yang–Parr gradient-corrected correlation functional (CAM-B3LYP)^[9] and SVP AO basis set^[11] for silver, gold and sulfur atoms. Relativistic effective core potential (RECP) of the Stuttgart group^[2] was employed for silver and gold atoms. For ligands 3-21G split-valence basis set^[10] was used.

Two-photon absorption (TPA) spectra were obtained with Dalton package program^[11] for: Ag₂₅(SCH₃)₁₈, Ag₂₄Au₁(SCH₃)₁₈, Ag₂₀Au₅(SCH₃)₁₈ and Ag₁₅Au₁₀(SCH₃)₁₈. TD-DFT for TPA spectra were calculated at the same level of theory as OPA spectra: CAM-B3LYP and two AO basis sets SVP and 3-21G split-valence basis set for ligands. TPA cross sections (σ_2) were obtained using single residue quadratic response theory.^[12]

UV-VIS AND FLUORESCENCE MEASUREMENTS

Optical measurements were carried out in solutions, then all synthesized nanoclusters were freshly dissolved in DCM before analysis. Absorption spectra was recorded using a Jasco V-670 spectrophotometer, while excitation and fluorescence spectra using an FS5 Spectrofluorometer (Edinburgh Instruments) equipped with a Xenon lamp.

Fluorescence quantum yield was determined using an integrating sphere (module SC-30, FS5 Spectrofluorometer) and by comparative method. with the equation^[13]:

$$\Phi_f^i = \Phi_f^s \frac{f_s(\lambda_{ex}) \int_{\lambda_{em}} F^i(\lambda_{em}) n_i^2}{f_i(\lambda_{ex}) \int_{\lambda_{em}} F^s(\lambda_{em}) n_s^2} \quad (1)$$

$$f_x(\lambda_{ex}) = 1 - 10^{A_x(\lambda_{ex})} \quad (2)$$

where Φ is fluorescence quantum yield of reference sample, $F(\lambda_{em})$ and $F^s(\lambda_{em})$ corresponds to fluorescence integral of sample and reference, respectively, n_i and n_r corresponds to refractive index of sample and reference, respectively, and $f_x(\lambda_{ex})$ refers to corresponding absorption factor at excitation wavelength. Since different solvents were used (CHCl₃ and DCM), the appropriate refractive indices were considered.

FLUORESCENCE DECAY CHARACTERIZATION

Time-correlated single photon counting (TCSPC) was employed to collect fluorescence lifetime spectra using an FS5 Edinburgh Instruments spectrofluorometer, equipped with a 450 nm ps pulsed diode laser source: LED EPLED-450 (Edinburgh Instruments) and time-correlated single photon counting module covering the range from a few ns to a few microseconds. Emission wavelength was set at 870 nm, 960 nm and 1015 nm for Ag₂₄Au₁, Ag₂₅ and Ag_{25-x}Au_x, respectively. Instrument response functions was determined from colloidal silica.

Biexponential model decay was applied in dedicated *Fluoracle* software as follows:

$$I = A + B_1 e^{-\frac{t}{\tau_1}} + B_2 e^{-\frac{t}{\tau_2}} \quad (3)$$

Calculated average lifetime of decay processes follows the formula:

$$\langle \tau \rangle = \frac{B_1 \tau_1^2 + B_2 \tau_2^2}{B_1 \tau_1 + B_2 \tau_2} \quad (4)$$

where B_1 and B_2 is the contribution of particular lifetime.

NONLINEAR OPTICAL PROPERTIES CHARACTERIZATION

Two-photon excited luminescence were measured using a custom-built multiphoton microscope consisting of a femtosecond mode-locked Ti:Sapphire laser (~100 fs, 80 MHz, Chameleon, Coherent Inc.) with incident wavelength range tunable within $\lambda = 690$ -1080 nm and an optical parametric oscillator Chameleon OPO (Coherent Inc.) with an output signal tunable at $\lambda = 1000$ -1600 nm. Luminescence was collected in epi-fluorescence mode through a dichroic mirror (cutoff wavelength 1150 nm) and shortpass filter (cutoff wavelength

SUPPORTING INFORMATION

1000 nm). In order to exclude the potential excitation at lower wavelength range a 1000 nm long-pass filters were applied. The two-photon excited emission spectra were measured with a spectrograph (Shamrock 303i Andor). Measurement conditions were set the same for each nanoclusters sample and reference sample. Solutions in the same cuvettes were illuminated with output power set to 150 mW for each wavelength in the range of 1180-1600 nm. The experimental conditions were chosen to prevent photobleaching and achieve a high signal to noise ratio. Two-photon absorption cross sections were calculated with the equation:

$$\sigma_{2,s} = \frac{F_{2,s}(\lambda_{reg})C_r\varphi_r(\lambda_{reg})}{F_{2,r}(\lambda_{reg})C_s\varphi_s(\lambda_{reg})}\sigma_{2,r} \quad (5)$$

where $F_{2,s}(\lambda_{reg})$ and $F_{2,r}(\lambda_{reg})$ is integrated two-photon fluorescence intensity at particular excitation wavelength, C_s and C_r is concentration, and φ_s and φ_r is quantum yield of sample and reference, respectively. $\sigma_{2,r}$ is two-photon absorption cross-section of reference.

Two-photon brightness was calculated with equation:

$$\sigma_{2,s,eff} = \sigma_{2,s}\varphi_s(\lambda_{reg}) = \frac{F_{2,s}(\lambda_{reg})C_r\varphi_r(\lambda_{reg})}{F_{2,r}(\lambda_{reg})C_s}\sigma_{2,r} \quad (6)$$

Sample concentration in Eq. 5 and 6 was determined applying known molar mass from gold and silver atom content of nanoclusters: Ag₂₅, Ag₂₄Au₁. Molar mass of Ag_{25-x}Au_x NCs was averaged, knowing that x=5-10.

SUPPLEMENTARY FIGURES

SUPPORTING INFORMATION

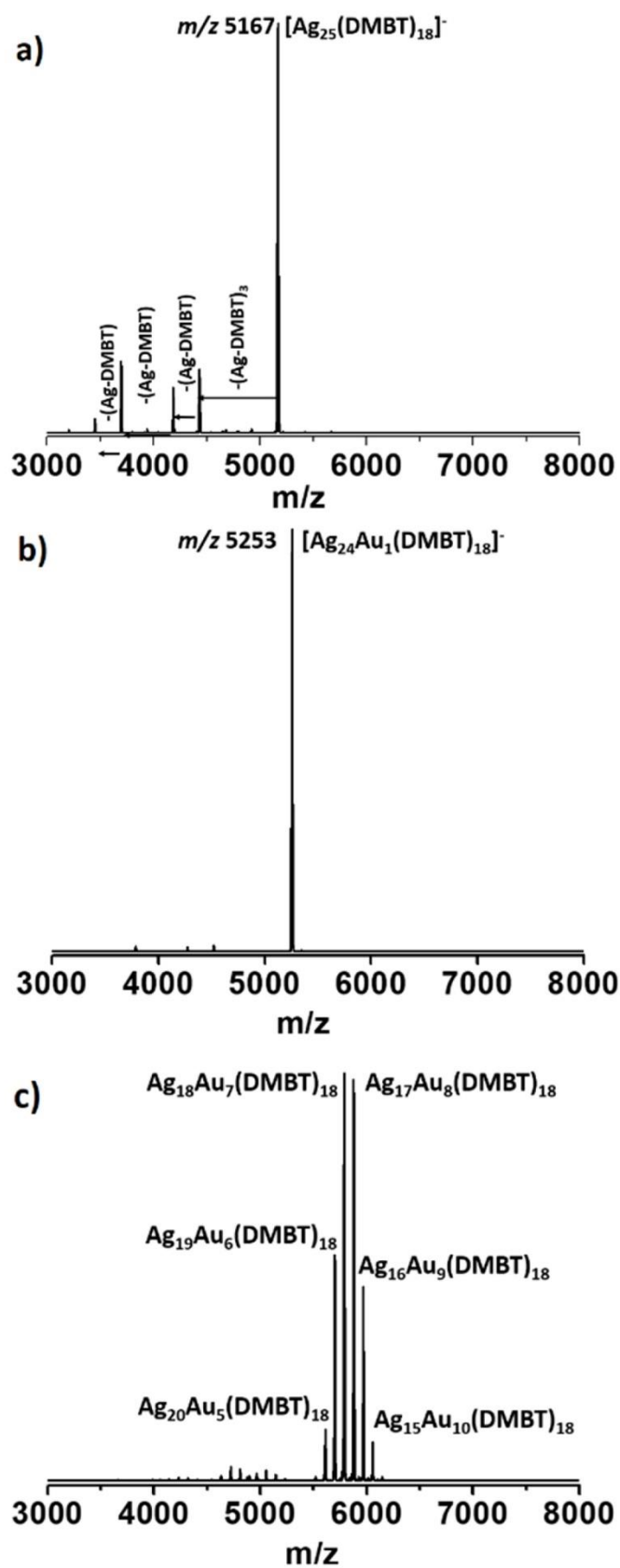


Figure S1. The negative ion mode ESI mass spectrum of (a) $[\text{Ag}_{25}(\text{DMBT})_{18}][\text{PPh}_4]$, (b) $[\text{Ag}_{24}\text{Au}_1(\text{DMBT})_{18}][\text{PPh}_4]$ and (c) $[\text{Ag}_{25-x}\text{Au}_x(\text{DMBT})_{18}][\text{PPh}_4]$ with $x = 5-10$.

SUPPORTING INFORMATION

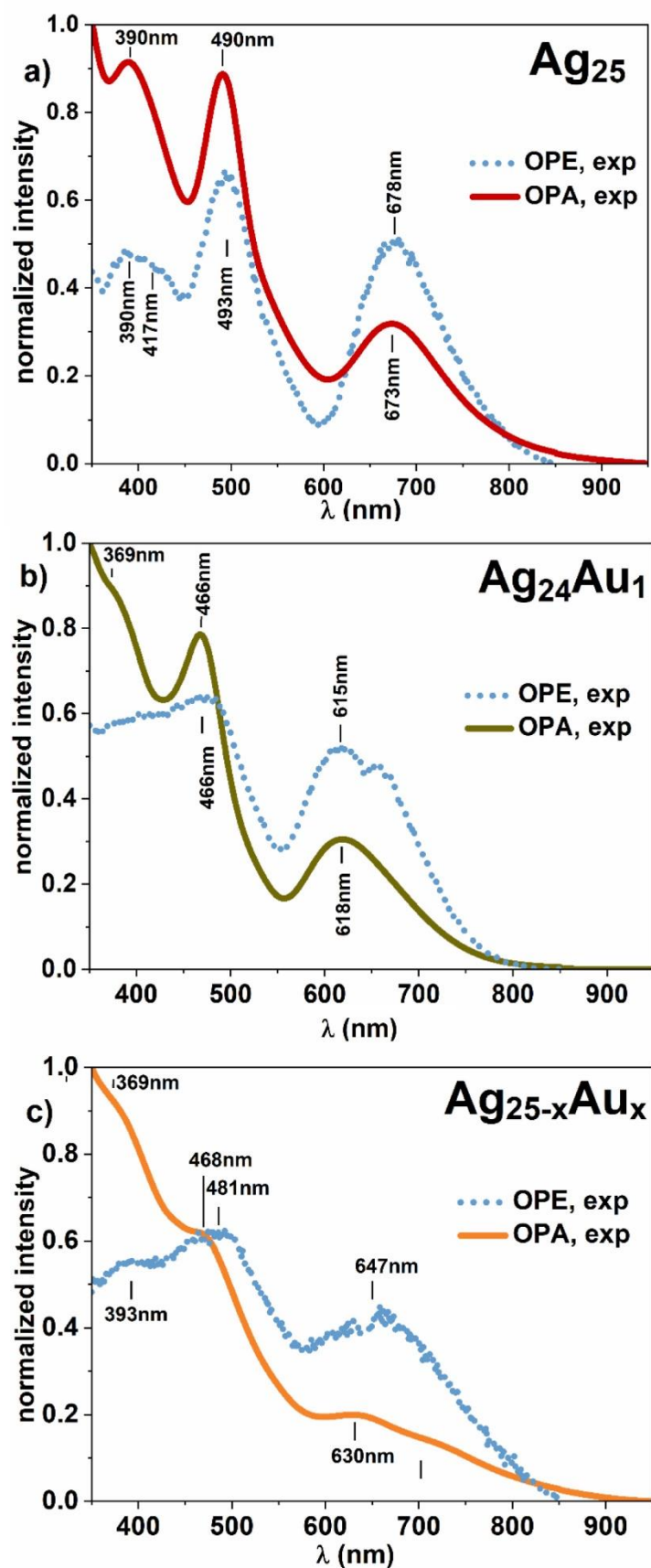


Figure S2. UV/Vis absorption and excitation spectra of a) Ag₂₅, b) Ag₂₄Au₁ and c) Ag_{25-x}Au_x NCs.

SUPPORTING INFORMATION

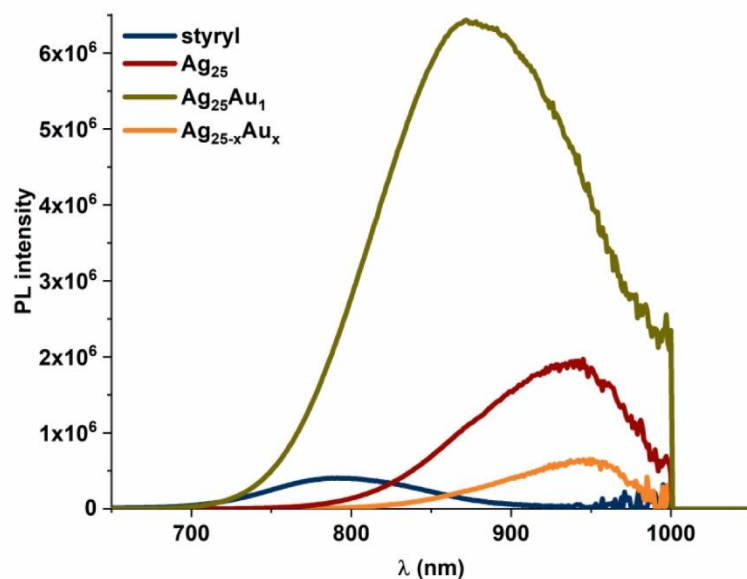


Figure S3. Photoluminescence spectra of Ag_{25} , $\text{Ag}_{24}\text{Au}_1$ and $\text{Ag}_{25-x}\text{Au}_x$ nanoclusters and Styryl 9M dye recorded for determination of QY in indirect, comparative method.

Table S1. QY of Ag_{25} , $\text{Ag}_{24}\text{Au}_1$ and $\text{Ag}_{25-x}\text{Au}_x$ nanoclusters determined in indirect, comparative method.

Sample	Φ [%] indirect, comparative method (QY of Styryl 9M = $27.2 \pm 2.0\%$, integrating sphere)
$\text{Ag}_{25}(\text{DMBT})_{18}[\text{PPh}_3]$	2.51 ± 0.32
$\text{Ag}_{24}\text{Au}_1(\text{DMBT})_{18}[\text{PPh}_3]$	34.81 ± 5.48
$\text{Ag}_{25-x}\text{Au}_x(\text{DMBT})_{18}[\text{PPh}_3]$	0.49 ± 0.05

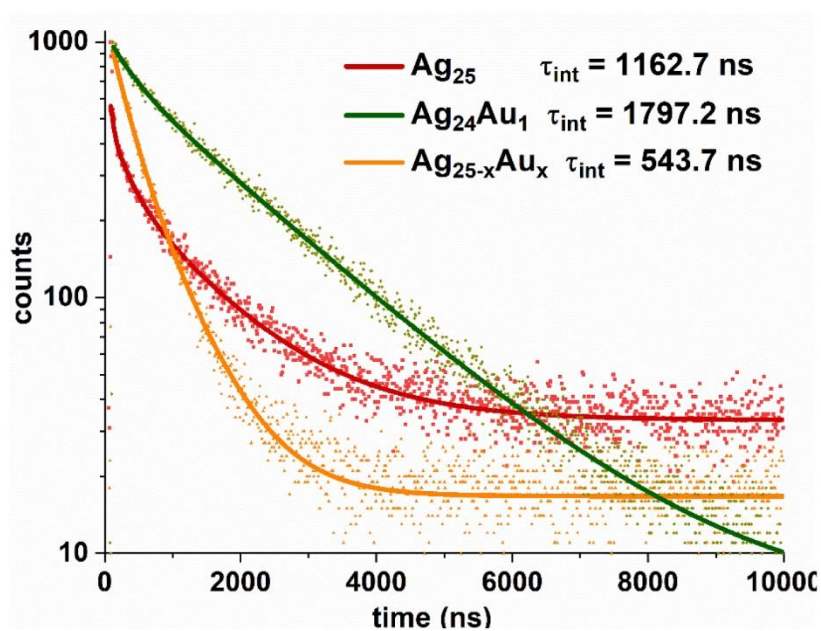
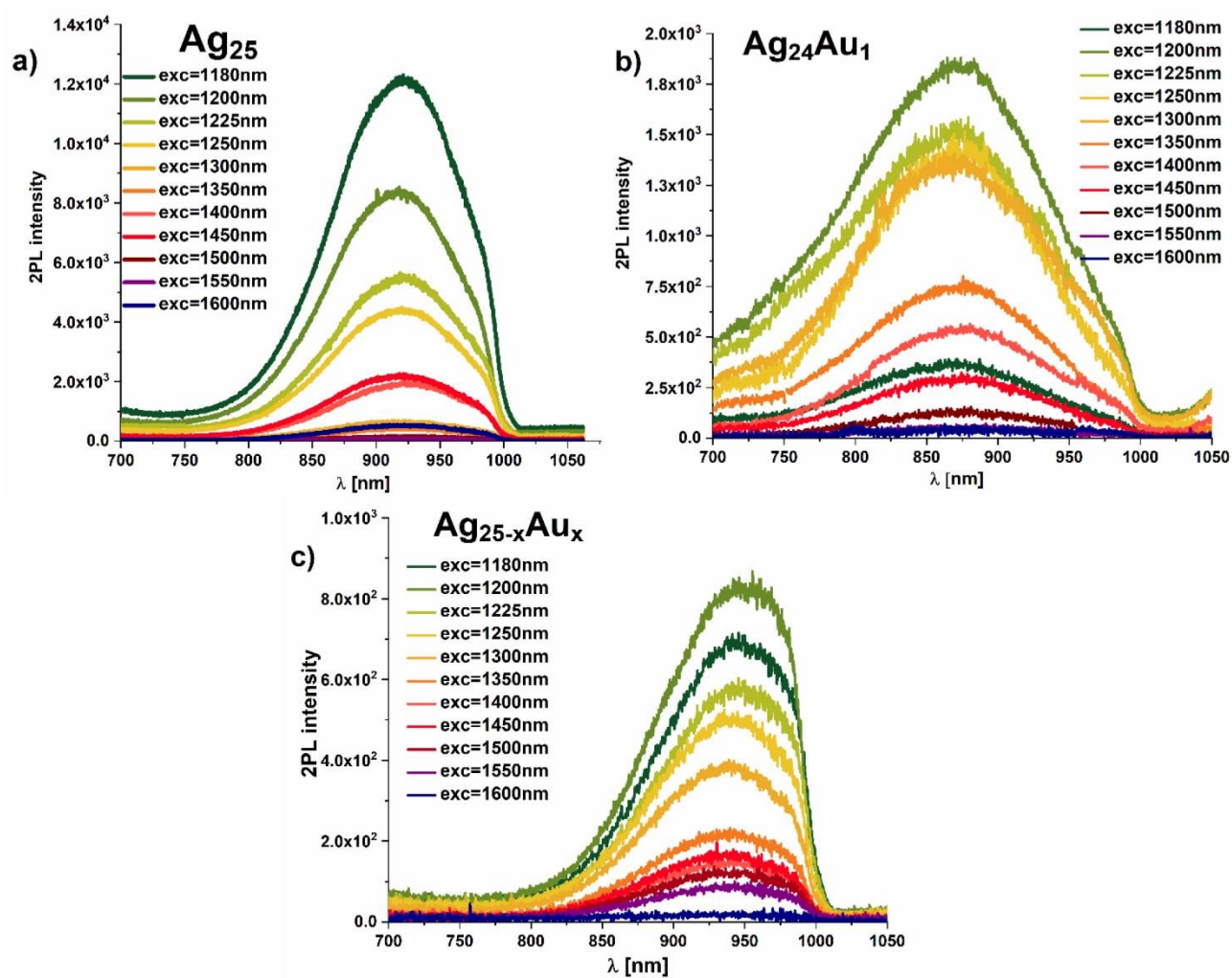


Figure S4. Fluorescence decay curves of silver Ag_{25} nanoclusters (red) and gold-doped silver nanoclusters: $\text{Ag}_{24}\text{Au}_1$ (green) and $\text{Ag}_{25-x}\text{Au}_x$ (orange).

SUPPORTING INFORMATION

Table S1. Fluorescence lifetimes τ_1 and τ_2 and their relative contributions for Ag_{25} , $\text{Ag}_{24}\text{Au}_1$ and $\text{Ag}_{25-x}\text{Au}_x$ nanoclusters.

	Ag_{25}	$\text{Ag}_{24}\text{Au}_1$	$\text{Ag}_{25-x}\text{Au}_x$
τ_1 [ns]	253 ± 29 (10.9%)	362 ± 36 (5.3%)	277 ± 24 (30.1%)
τ_2 [ns]	1274 ± 31 (89.1%)	1876 ± 17 (94.7%)	659 ± 26 (69.9%)
τ_{int} [ns]	1163 ± 32	1797 ± 18	544 ± 24
χ^2	1.01	0.96	1.15

**Figure S5.** Two-photon luminescence (2PL) spectra of a) Ag_{25} , b) $\text{Ag}_{24}\text{Au}_1$ and c) $\text{Ag}_{25-x}\text{Au}_x$ nanoclusters recorded at 1180nm-1600nm excitation wavelengths range.

SUPPORTING INFORMATION

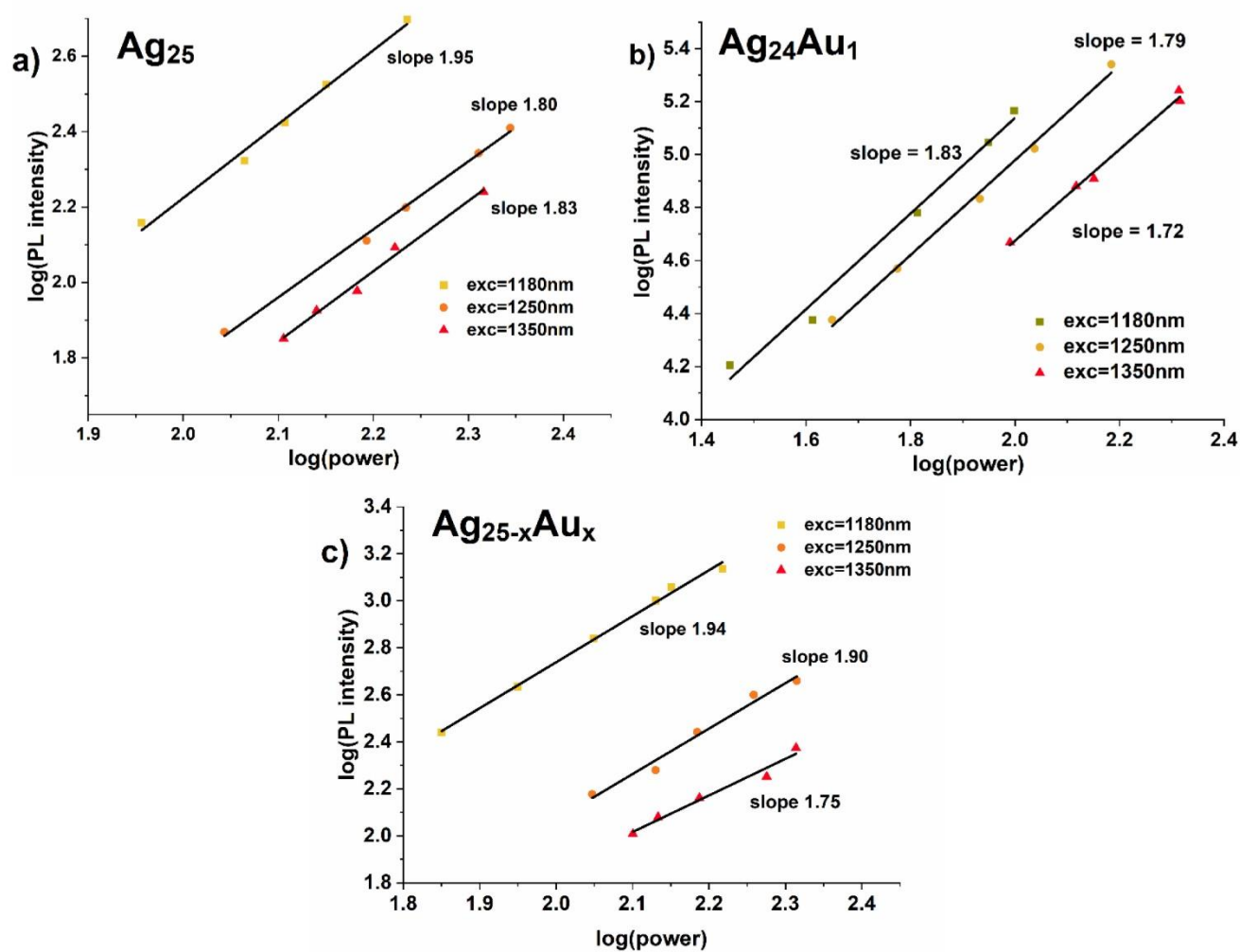


Figure S6. Log-log plot of the PL intensity of a) Ag_{25} , b) $\text{Ag}_{24}\text{Au}_1$ and c) $\text{Ag}_{25-x}\text{Au}_x$ nanoclusters as a function of average incident laser power measured at several excitation wavelengths. The slope of the linear fit corresponds to the order of multiphoton processes.

SUPPORTING INFORMATION

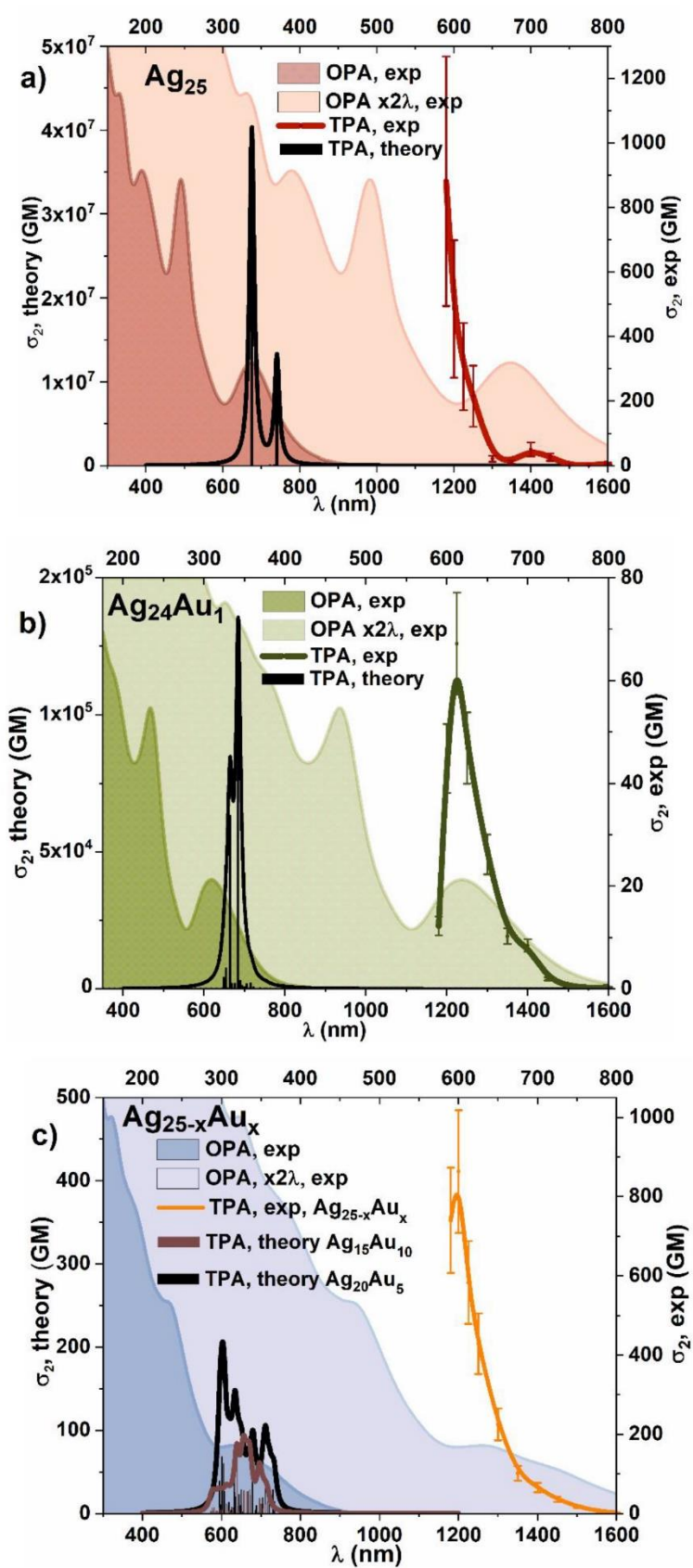


Figure S7. Experimental and TD-DFT TPA spectra (in GM unit) of (a) Ag₂₅, (b) Ag₂₄Au₁ and (c) Ag_{25-x}Au_x nanoclusters together with normalized one-photon absorption (OPA) at double the wavelength and simulated TPA spectra.

SUPPORTING INFORMATION

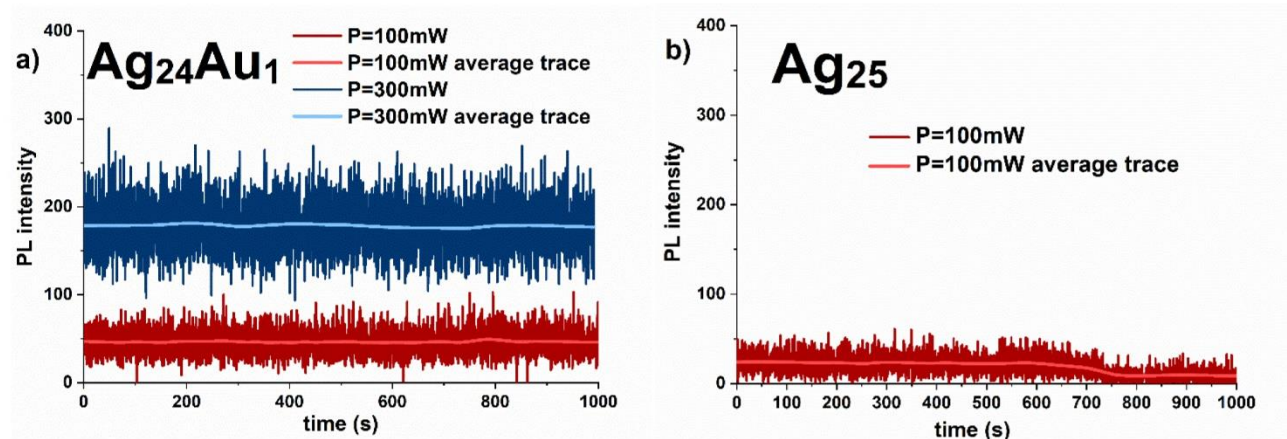


Figure S8. Two-photon luminescence time traces of a) $\text{Ag}_{24}\text{Au}_1$ and b) Ag_{25} monitored for 1000s under $P=100\text{mW}$ and $P=300\text{mW}$ illumination of femtosecond Ti:Sapphire laser at 1250 nm excitation.

REFERENCES

- [1] F. Weigend, R. Ahlrichs, *Physical Chemistry Chemical Physics* 2005, 7, 3297-3305.
- [2] M. Dolg, H. Stoll, H. Preuss, *Journal of Chemical Physics* 1989, 90, 1730-1734.
- [3] J. P. Perdew, Y. Wang, *Physical Review B* 1992, 45, 13244-13249.
- [4] J. P. Perdew, K. Burke, M. Ernzerhof, *Physical Review Letters* 1996, 77, 3865-3868.
- [5] M. J. Frisch, G. W. Trucks, H. B. Schlegel, G. E. Scuseria, M. A. Robb, J. R. Cheeseman, G. Scalmani, V. Barone, G. A. Petersson, H. Nakatsuji, X. Li, M. Caricato, A. V. Marenich, J. Bloino, B. G. Janesko, R. Gomperts, B. Mennucci, H. P. Hratchian, J. V. Ortiz, A. F. Izmaylov, J. L. Sonnenberg, Williams, F. Ding, F. Lipparini, F. Egidi, J. Goings, B. Peng, A. Petrone, T. Henderson, D. Ranasinghe, V. G. Zakrzewski, J. Gao, N. Rega, G. Zheng, W. Liang, M. Hada, M. Ehara, K. Toyota, R. Fukuda, J. Hasegawa, M. Ishida, T. Nakajima, Y. Honda, O. Kitao, H. Nakai, T. Vreven, K. Throssell, J. A. Montgomery Jr., J. E. Peralta, F. Ogliaro, M. J. Bearpark, J. J. Heyd, E. N. Brothers, K. N. Kudin, V. N. Staroverov, T. A. Keith, R. Kobayashi, J. Normand, K. Raghavachari, A. P. Rendell, J. C. Burant, S. S. Iyengar, J. Tomasi, M. Cossi, J. M. Millam, M. Klene, C. Adamo, R. Cammi, J. W. Ochterski, R. L. Martin, K. Morokuma, O. Farkas, J. B. Foresman, D. J. Fox, Wallingford, CT, 2016.
- [6] C. P. Joshi, M. S. Bootharaju, M. J. Alhilaly, O. M. Bakr, *Journal of the American Chemical Society* 2015, 137, 11578-11581.
- [7] K. R. Krishnadas, L. Sementa, M. Medves, A. Fortunelli, M. Stener, A. Fürstenberg, G. Longhi, T. Bürgi, *ACS Nano* 2020, 14, 9687-9700.
- [8] M. Zhu, C. M. Aikens, F. J. Hollander, G. C. Schatz, R. Jin, *Journal of the American Chemical Society* 2008, 130, 5883-5885.
- [9] T. Yanai, D. P. Tew, N. C. Handy, *Chemical Physics Letters* 2004, 393, 51-57.
- [10] a) K. D. Dobbs, W. J. Hehre, *Journal of Computational Chemistry* 1987, 8, 880-893; b) S. Binkley, J. A. Pople, W. J. Hehre, *Journal of the American Chemical Society* 1980, 102, 939-947.
- [11] K. Aidas, C. Angeli, K. L. Bak, V. Bakken, R. Bast, L. Boman, O. Christiansen, R. Cimraglia, S. Coriani, P. Dahle, E. K. Dalskov, U. Ekström, T. Enevoldsen, J. J. Eriksen, P. Ettenhuber, B. Fernández, L. Ferrighi, H. Fliegl, L. Frediani, K. Hald, A. Halkier, C. Hättig, H. Heiberg, T. Helgaker, A. C. Hennen, H. Hettema, E. Hjertenæs, S. Høst, I.-M. Høyvik, M. F. Iozzi, B. Jansik, H. J. A. Jensen, D. Jonsson, P. Jørgensen, J. Kauczor, S. Kirpekar, T. Kjærgaard, W. Klopper, S. Knecht, R. Kobayashi, H. Koch, J. Kongsted, A. Krapp, K. Kristensen, A. Ligabue, O. B. Lutnæs, J. I. Melo, K. V. Mikkelsen, R. H. Myhre, C. Neiss, C. B. Nielsen, P. Norman, J. Olsen, J. M. H. Olsen, A. Osted, M. J. Packer, F. Pawłowski, T. B. Pedersen, P. F. Provasi, S. Reine, Z. Rinkevicius, T. A. Ruden, K. Ruud, V. V. Rybkin, P. Salek, C. C. M. Samson, A. S. de Merás, T. Saue, S. P. A. Sauer, B. Schimmelpennig, K. Sneskov, A. H. Steindal, K. O. Sylvester-Hvid, P. R. Taylor, A. M. Teale, E. I. Tellgren, D. P. Tew, A. J. Thorvaldsen, L. Thøgersen, O. Vahtras, M. A. Watson, D. J. D. Wilson, M. Ziolkowski, H. Ågren, *WIREs Computational Molecular Science* 2014, 4, 269-284.
- [12] P. Norman, *Physical Chemistry Chemical Physics* 2011, 13, 20519-20535.
- [13] K. Rurack, M. Spieles, *Analytical Chemistry* 2011, 83, 1232-1242.

3.3 ARTICLE 3: STRONG FLUORESCENCE-DETECTED TWO-PHOTON CIRCULAR DICHROISM OF CHIRAL GOLD NANOCCLUSERS

3.3.1 Short descriptions of research work and results

INTRODUCTION

Recent interest in chiral nanoclusters is observed by raised number of published protocols of syntheses,¹³⁴ investigations of the origin of chirality¹³⁵ and appearance of the first applications of chiral nanoclusters in enantioselective catalysis⁷², detection,¹³⁶ imaging,¹³⁷ or antimicrobial¹³⁸ applications. Attractive robust chirality of nanoclusters is commonly analyzed in one-photon, UV-Vis region. However, NLO chiroptical studies, particularly in NIR range of wavelengths can find great interest in terms of in vivo imaging and sensing applications, most favorably performed in low-energetic region. Therefore, the aim of the study is to present deep insight into nonlinear chiroptical properties of gold nanoclusters. First, and the only reports on multiphoton chiroptical effects of nanoclusters were published in our group, providing extremely promising two orders of magnitude greater two-photon circular dichroism of Au₂₅Capt₁₈, than one-photon one.⁹¹ Encouraged by this preliminary study we investigated the one- and two-photon chiroptical potential of gold nanoclusters stabilized with two ligands: 6-aza-2-thiotymine and L – and D- arginine (L/D-Arg/ATT AuNCs), however applying here new, fluorescent based technique of circular dichroism detection.

Our work emphasizes the significance of chiroptical characterization of Arg/ATT AuNCs in their both enantiomeric forms, which are scarcely studied in the literature, even in one-photon region. Presented results are pioneering in terms of used technique for determination of two-photon chiroptical effects. Meanwhile, presented results are comparable to the only work on nonlinear chiroptical properties of nanoclusters, performed with the other technique.⁹¹ Strong similarities between those two results have raised an urgent question about how general the enhancement of two-photon chiroptical effects is in nanoscale structures. The article 3 brings new perspectives in the topics of chirality-based research techniques and the utility of chiral materials for future applications, especially for chirality-based imaging and sensing.

METODOLOGY

The novelty of these studies is addressed in the innovative technique of quantitative determination of two-photon circular dichroism, monitored via fluorescent methods of detection. Proposed approach for determination of nonlinear chiroptical effects have never been used for nanoclusters, and only rarely explored for other chiral materials. The nonlinear circular dichroism is mainly explored theoretically, while experimental studies are limited solely to several organic compounds.¹³⁹⁻¹⁴² The reason for scarcely studied technique can be related with limitations from the samples, which needs to fulfil the requirements of certain chirality and fluorescence to be suitable for fluorescence detected circular dichroism (FDCCD). However, new materials, such as nanoclusters, can quite easily meet the demands of FDCCD measurements, since they can be specifically design as fluorescent and chiral. It is claimed in

the literature sources that FDCD offer better sensitivity and selectivity than common absorption-based techniques of circular dichroism, due to abilities to perform measurements at lower concentrations.^{143, 144} However, even low-concentration samples require reasonable luminescence properties. Here in this work strong quantum yield of studied samples assured measurements in micro- and nanomolar scale.

Chapter 2.2.2. discusses in details the FDCD measurements basis and possible artifacts generated upon FDCD measurements. In this work the FDCD technique was adapted into two-photon range of excitation. Two-photon FDCD (TP-FDCD) measurements were performed on home-built set up, which I construct as presented in scheme 16. Two photon excitation was generated by pulsed Ti:Sapphire laser. Long-pass filters are placed before sample to eliminate contribution of lower wavelength excitation. Short-pass filters placed at the emission path cut-off the incident beam from detection. Circularly polarized excitation was generated via Babinet-Soleil compensator, which eliminated any potential residual linear polarization. To ensure the best quality of polarization entering the compensator, a Glan-Thompson polarizer was used. Ellipticity of incident beam was verified before measurements by polarizer, placed directly in the sample optical path position. The luminescence was collected at so-called *magic angle* of 54.7°, which is set between the propagation vector of the laser and the polarizer axis^{145, 146} as shown in Figure 16a.

It is assumed that the fluorescence of axially symmetric systems provides equivalent response in every direction of luminescence polarization. The ellipticity of an incident beam can be already estimated from TPEL spectra of non-chiral samples, recorded from left- (LP) and right- (RP) handed circularly polarized two-photon excitation. As shown in Figure 16d, fully overlapped spectra of LP and RP TPEL from achiral fluorescein indicate the exact same intensity of recorded circularly excited luminescence. Since the ellipticity of the circularly polarized incident beam was verified before the measurements with polarimeter and achiral sample present, it can be assured that any residual linear polarization of the incident laser beam was eliminated on Babinet-Soleil compensator.

Due to opposite chirality of L- and D-Arg/ATT-AuNCs, nanoclusters emit stronger upon two-photon excitation of certain, left- or right-handed circularly polarized laser beam (Figure 16 b, c). The two-photon circular dichroism (TP-CD, Θ_{TPCD}) can be calculated from the difference in left- and right-handed two-photon absorption cross-section, as follows:

$$\Theta_{TPCD} = 2 \frac{\sigma_{2,L} - \sigma_{2,R}}{\sigma_{2,L} + \sigma_{2,R}}, \quad (8)$$

where $\sigma_{2,L}$ and $\sigma_{2,R}$ corresponds to two-photon absorption cross-sections determined at particular left- and right handed circularly polarized excitation, respectively. $\sigma_{2,L}$ and $\sigma_{2,R}$ are determined with respective formulas:

$$\sigma_{2,L} = \frac{F_{2,L,S}(\lambda_{exc}) C_r \varphi_r}{F_{2,L,R}(\lambda_{exc}) C_s \varphi_s} \sigma_{2,r}, \quad (9)$$

$$\sigma_{2,R} = \frac{F_{2,R,S}(\lambda_{exc}) C_r \varphi_r}{F_{2,R,R}(\lambda_{exc}) C_s \varphi_s} \sigma_{2,r}, \quad (10)$$

where ($F_{2,L}$) and ($F_{2,R}$) is left- and right handed circularly polarized two-photon excited luminescence, respectively; (φ) is a quantum yield and (C) denotes concentration of sample (s) and reference (r).

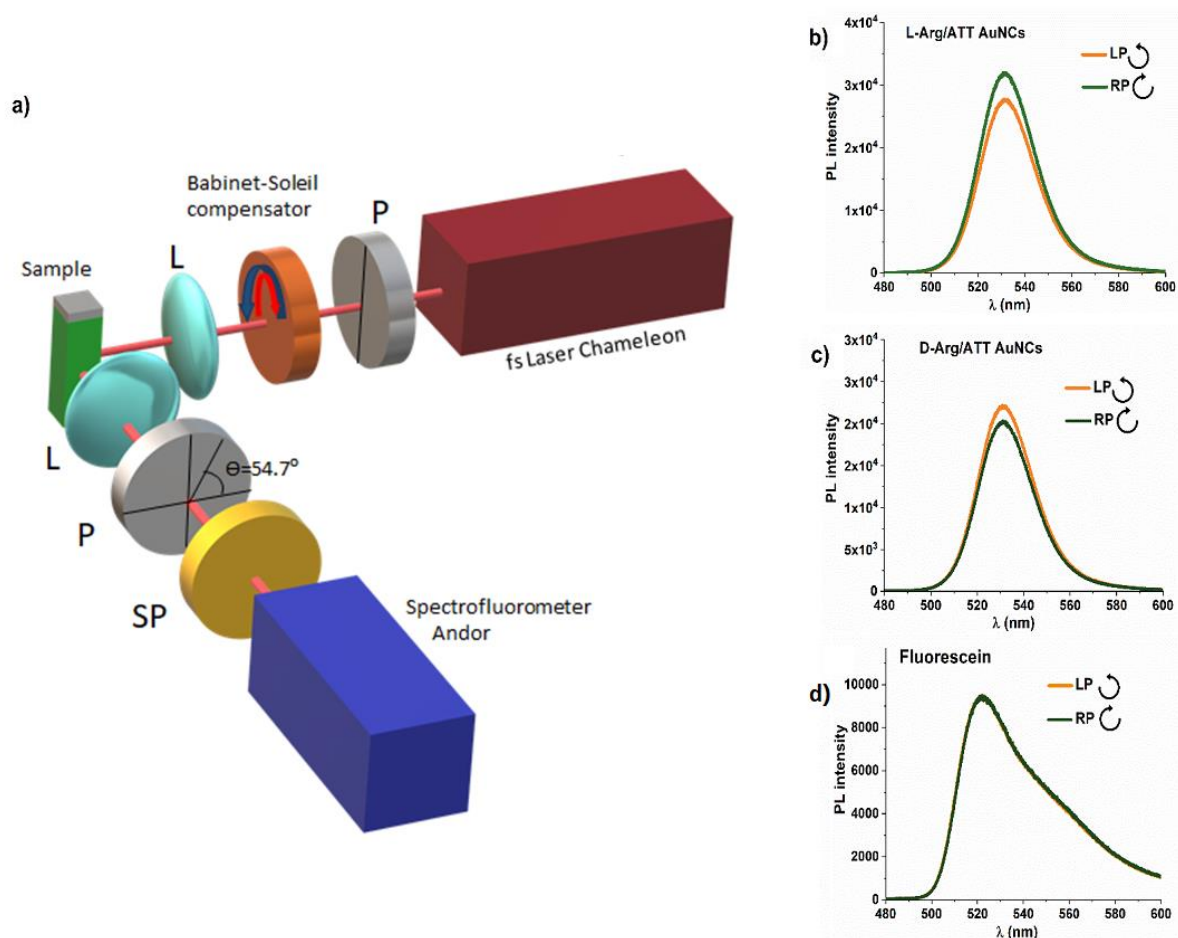


Figure 16. a) scheme of FDCD optical path (P- polarizer, L-lens, SP- shortpass filter used for measurements of two-photon excited luminescence of b) L-Arg/ATT-AuNCs c) D-Arg/ATT-AuNCs and d) fluorescein, as non-chiral reference sample.

RESULTS AND DISCUSSION

ATT-AuNCs were synthesized with additional capping ligand - arginine for two reasons: (I) to rigidify structure of nanoclusters and improve luminescent properties, and (II) to induce chiral properties of nanoclusters.

Luminescent properties of ATT-AuNCs were tremendously enhanced as a result of supramolecular interaction of 6-aza-2-thiopyrimidine (ATT) with L- and D-arginine (L-Arg and D-Arg, respectively) ligands. Strong hydrogen bonds in host-guest interaction from ATT and Arg molecules lead to rigidification of nanoclusters' structure by blocking the rotation and vibration movements of ligands. Rigid structure promotes radiative processes over non-radiative relaxations, what was observed in 45- and 43- times stronger PL for L-Arg/ATT-AuNCs and D-Arg/ATT-AuNCs, respectively compared to uncoated ATT-AuNCs (Figure 17a). Similarly, quantum yields were multiply enhanced, from $1.4 \pm 0.3\%$ to $63.2 \pm 2.0\%$ and $58.4 \pm 2.0\%$ for L-Arg/ATT-AuNCs and D-Arg/ATT-AuNCs, respectively, while PL lifetimes 6-times elongated, from 7 ns to 42 ns, for both nanoclusters (Figure 17b).

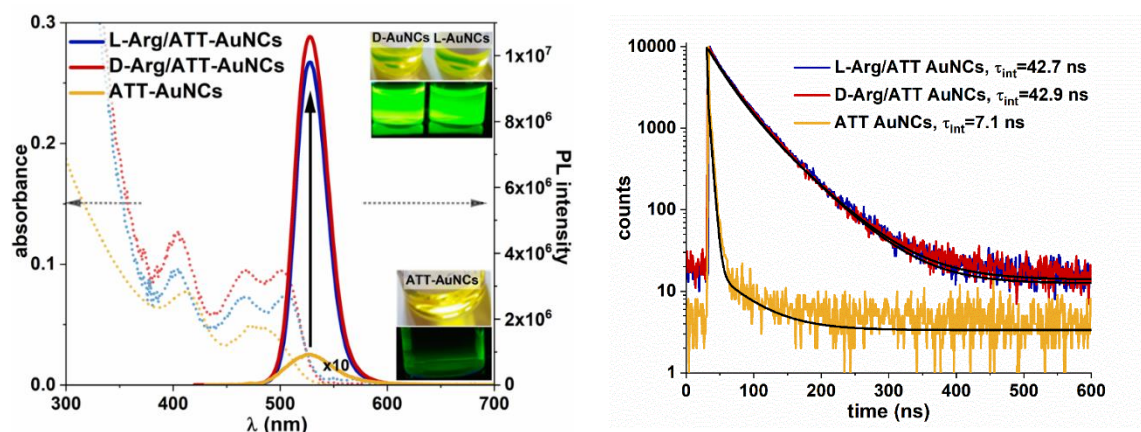


Figure 17. a) absorption and emission spectrum of low-luminescent ATT-AuNCs and strongly luminescent L- and D-Arg/ATT-AuNCs. b) Fluorescence lifetime with biexponential decay fitting of L-Arg/ATT-AuNCs (blue), D-Arg/ATT-AuNCs (red) and of ATT-AuNCs (blue) (orange).

Chiral properties of nanoclusters were induced by arginine ligand, however CD spectra of L- and D-Arg is not transferred directly on the chiral activity of L- and D-Arg/ATT-AuNCs (Figure 18). Despite the chirality of the ligands itself, nanoclusters present unique chiroptical effects due to arrangement of ligands within the structure of nanoclusters. It is in agreement with proposed structure of ATT-AuNCs and Arg/ ATT-AuNCs.¹⁴⁷

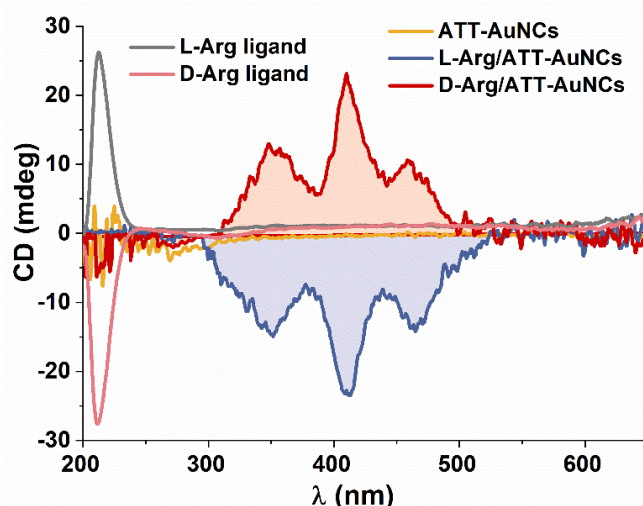


Figure 18. Circular dichroism of achiral nanoclusters ATT-AuNCs and chiral nanoclusters of L- and D-Arg-ATT-AuNCs, compared with CD of chiral ligands: L- arginine and D-arginine.

Owing to the strong circular dichroism and luminescence of nanoclusters, the two-photon chiroptical properties were measured on custom-built TP-FDCD setup. Two-photon anisotropy factor (Θ_{TPCD}) follows the mirror-image of one-photon anisotropy factor (g_{abs}) (Figure 19), confirming that one- and two-photon processes involve the same ground and excited states. Recorded nonlinear chiroptical response is two orders of magnitude stronger than one-photon one at the corresponding wavelength. Multiphoton studies were provided here in a broad range of near infrared excitation wavelengths ($\lambda_{\text{exc}}=700\text{-}930\text{ nm}$), being a milestone progress to common literature investigations achieved solely at a particular wavelength.

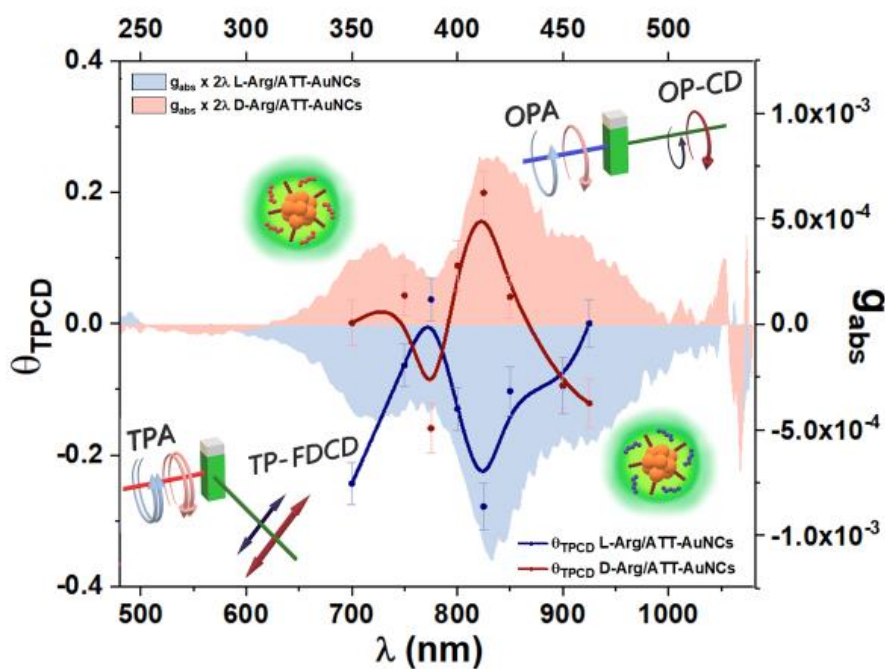


Figure 19. Two-photon circular dichroism (blue and red dots and lines, left and bottom axes) correlated with one-photon dissymmetry factor (blue and red areas, right and upper axes). Schemes of one-photon circular dichroism and two-photon fluorescence detected circular dichroism effects are presented in the corners.

Nanoclusters present strong two-photon absorption and luminescent properties, reaching remarkable values of σ_2 and $\sigma_{2,eff}$ (two-photon brightness): $\sigma_2 = 1743$ GM and 1453 GM for L- and D-Arg/ATT-AuNCs, respectively, with corresponding $\sigma_{2,eff} = 1102$ GM and 848 GM, respectively. Strong values, especially $\sigma_{2,eff}$, were found several times higher than for other nanoclusters in the literature,^{148, 149} and significantly larger than for commonly used fluorophores, e.g. dyes¹⁵⁰ and fluorescent proteins.¹⁵¹ Strong two-photon absorption and two-photon brightness, in combination with high quantum yield and long luminescence lifetime gives an opportunity for nanoclusters to serve as efficient fluorophores for imaging or sensing in near infrared region (NIR). Furthermore, strong chiroptical properties of nanoclusters in both, one- and two-photon region open new possibilities for multifunctional applications.

3.3.2 Research contribution of PhD candidate

Anna Pniakowska
Institute of Advanced Materials
Wroclaw University of Science and Technology

ul. Gdańska 7/9
50-344 Wroclaw

Author contribution statement

I, Anna Pniakowska hereby declare that in the article: *A. Pniakowska, M. Samoć, J. Olesiak-Bańska "Strong fluorescence-detected two-photon circular dichroism of chiral gold nanoclusters", Nanoscale, 2023, 15, 19, s. 8597-8602*, I was responsible for:

- Methodology
- Investigation
 - synthesis of nanoclusters
 - determination of size of nanoclusters via TEM measurements
 - one photon measurements: absorption, emission, circular dichroism, quantum yield and PL lifetime
 - building the optical set-up for two-photon circular dichroism measurements, determination of two-photon circular dichroism
 - two-photon measurements: two-photon excited luminescence, two-photon circular dichroism, power dependent luminescence measurement; two-photon absorption and two-photon brightness
- Visualization
- Data analysis
- Writing – original draft,


(signature)

3.3.3 Contribution statements of co-authors

Joanna Olesiak-Bańska
Institute of Advanced Materials
Wroclaw University of Science and Technology

ul. Gdańska 7/9
50-344 Wroclaw

Author contribution statement

I, Joanna Olesiak-Bańska hereby declare that in the article: *A. Pniakowska, M. Samoć, J. Olesiak-Bańska "Strong fluorescence-detected two-photon circular dichroism of chiral gold nanoclusters", Nanoscale, 2023, 15, 19, s. 8597-8602*, I was responsible for:

- Conceptualization
- Writing : review and editing
- Supervision
- Funding acquisition


(signature)

Prof. Marek Samoć, DSc, PhD, Eng
Institute of Advanced Materials
Wrocław University of Science and Technology

building A-2, room 405
Wybrzeże Wyspiańskiego 29,
50-371 Wrocław

Autor contribution statement

I, Marek Samoć hereby declare that in the article: A. Pniakowska, M. Samoć, J. Olesiak-Bańska "Strong fluorescence-detected two-photon circular dichroism of chiral gold nanoclusters", *Nanoscale*, 2023, 15, 19, s. 8597-8602, I was responsible for:

- Conceptualization
- Writing: review and editing



(signature)

3.3.4 Article and Supplementary Materials

COMMUNICATION

Strong fluorescence-detected two-photon circular dichroism of chiral gold nanoclustersAnna Pniakowska^a, Marek Samoć^a, Joanna Olesiak-Bańska^{a*}Received 00th January 20xx,
Accepted 00th January 20xx

DOI: 10.1039/x0xx00000x

Progress in syntheses and understanding of the intriguing properties of chiral noble metal nanoclusters sparks interest to extend investigations of their chiroptical response to the nonlinear optics regime. We present a quantitative determination of two-photon circular dichroism of chiral gold nanoclusters with ATT and L- or D-Arg ligands (ATT=6-aza-2-thiopyrimidine and Arg=arginine). Introduction of arginine ligands enables the formation of two enantiomers of the nanoclusters, with strong chiroptical effects in both linear and nonlinear regime. We present two-photon absorption and luminescent properties measured in a wide range of wavelengths, with the two-photon absorption cross section reaching 1743 GM and two-photon brightness ~1102 GM at 825 nm. We report strong, 245-fold enhancement of the two-photon circular dichroism of nanoclusters with respect to the one-photon absorption counterpart – the dissymmetry factor. The presence of multiple advantages of nanoclusters: high fluorescence quantum yield, strong nonlinear optical properties and well-controlled chirality is a powerful combination for applications of such clusters in multiphoton microscopy.

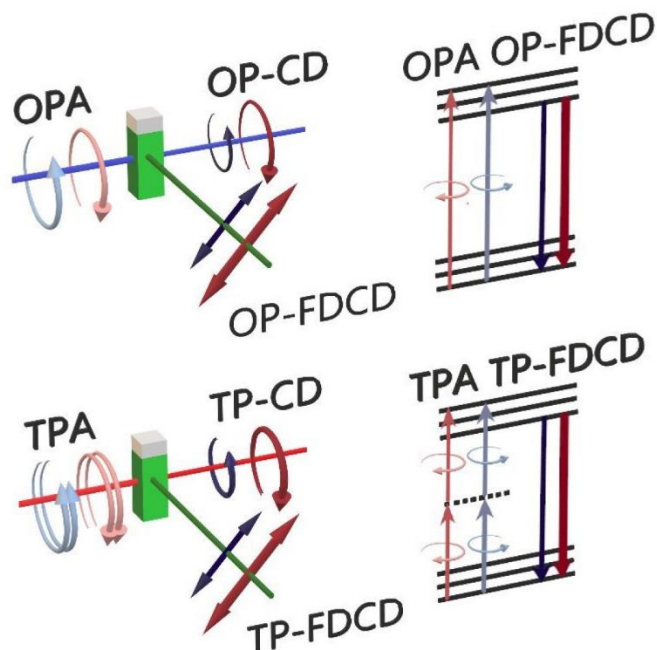
Chirality is a common natural attribute, which refers to the objects with non-superimposable mirror image¹ and, since it is exhibited by biomolecules such as amino acids, proteins, sugars and nucleic acids, there is much interest in both exploiting the properties arising from the chirality in bio-applications and in mimicking the natural chirality in new functional nanomaterials and nanostructures. Recent raise of the interest in chirality at nanoscale is motivated by the needs of chirality-based applications, e.g. enantioselective separation,² catalysis,³ bioimaging,⁴ sensing,⁵ and theranostics.⁶

Inspired by this significant interest in fundamental studies and emerging applications of chiral nanomaterials, we have decided

to explore in detail the chiroptical properties of gold nanoclusters (AuNCs) taking advantage of their luminescent properties. Nanoclusters are defined as ultra-small, 1-2 nm sized nanoobjects. They consist of a few to a few hundred noble metal atoms, stabilized by a precise number of ligands. Due to discrete character of their electronic energy levels and the absence of localized surface plasmon excitations, the gold nanoclusters differ from the bigger metal nanoparticles and demonstrate unusual optical properties in both linear and nonlinear regime.⁷ Features like high luminescence yield and several orders of magnitude stronger two-photon absorption cross sections of nanoclusters⁸ against other, well-known nonlinear absorbers⁹ initiated the development of strategies for fabrication of nanoclusters with the desired enhanced optical properties.

Chiroptical activity of AuNCs was observed for the first time by Shaaff and Whetten.¹⁰ Up to date a significant progress has been made concerning introduction and investigation of chiroptical properties of such clusters.^{11, 12} A common strategy for inducing chirality of nanoclusters is protection of their metal core with optically active ligands, e.g. L-glutathione (L-GSH),¹⁰ L-captopril,¹³ D-/L-penicillamine (Pen),¹⁴ 2,2'-bis(diphenylphosphino)-1,1'-binaphthyl (BINAP)¹⁵ and bidentate 1,1'-binaphthyl-2,2'-dithiol (BINAS).¹⁶ However, the chiral properties of NCs (the circular dichroism) are predominantly established in the UV/Vis range, while various applications, e. g. *in vivo* bioimaging, biosensing, and theranostics favour near-infrared (NIR) excitation. Therefore, one is tempted to consider the multiphoton excitation, which provides low phototoxicity, deeper penetration into samples and higher axial resolution: the features that are strongly beneficial for those applications. AuNCs present a combination of characteristics favourable for multiphoton microscopy: large two-photon absorption cross-sections^{7, 8} and bright luminescence, together with ultra-small sizes and good biocompatibility.^{17, 18} Owing to the listed features, gold nanoclusters have already proved to be robust biosensors and

^a Institute of Advanced Materials, Wrocław University of Science and Technology, Wybrzeże Wyspiańskiego 27, 50-370 Wrocław, Poland
Electronic Supplementary Information (ESI) available: [details of any supplementary information available should be included here]. See DOI: 10.1039/x0xx00000x



Scheme 1. Scheme of one-photon (OP) and two-photon (TP) circular dichroism (CD) and fluorescence detected circular dichroism (FDCD) effects. Left and right circularly polarized OP and TP excitation can be formed by periodically modulating polarization of the beam (e.g. using a photoelastic modulator, PEM) or created separately (e.g. using a quarter-wave plate or a Babinet-Soleil compensator). The linear polarization of the photoluminescence indicated by the arrows in the picture does not implicate that it has this polarization as emitted, but that it is detected after passing through a polarizer positioned at a magic angle.

biomarkers for multiphoton applications.^{19, 20}

Arg/ATT-AuNCs, *i.e.* clusters stabilized with two ligands: 6-aza-2-thiopyrimidine (ATT) and arginine (Arg) are water soluble nanoclusters with particularly high photoluminescent quantum yield, which has recently been successfully applied in imaging^{21, 22} and detection of arginase activity.²³ Large nonlinear optical (NLO) potential of proposed nanoclusters was recently found in multiphoton *in vivo* bioimaging of living cells with Arg/ATT-AuNCs²⁴ and silver doped ATT-AuNCs.²⁵ Despite impressive multiphoton investigations, chiroptical properties of these clusters have not been investigated, neither in linear nor nonlinear regime. In fact, NLO chirality of nanoclusters have been yet poorly investigated, although one-photon chirality of nanoclusters already gained a lot of interests.

Our previous studies on two-photon circular dichroism of Au₂₅(Capt)₁₈ NCs was first and currently the only work on NLO chirality of nanoclusters. It have shown a significantly higher anisotropy factor in the regime of two-photon vs one-photon absorption, which inspired us to further investigation of two-photon circular dichroism in gold nanoclusters.¹³ Two-photon circular dichroism (TP-CD) denoted here as Θ_{TPCD} , can be defined as the difference in the two-photon absorption cross-section (σ_2) for left-handed and right-handed circularly polarized

incident light, normalized with the average two-photon absorption cross-section:

$$\Theta_{TPCD} = 2 \frac{\sigma_{2,L} - \sigma_{2,R}}{\sigma_{2,L} + \sigma_{2,R}} \quad (1)$$

More generally, the nonlinear circular dichroism can be defined to include other types of nonlinear absorption, like multiphoton absorption or absorption saturation. The nonlinear circular dichroism has been discussed in theoretical works,^{26, 27} but the experimental studies of the phenomenon have been scarce and concerned a limited group of materials, e.g. lanthanides,²⁸ naphthols,²⁹ helicene derivatives,³⁰ and ruthenium salts,³¹ which not include nanoclusters.

In this work we propose for the first time the use of fluorescence-detected circular dichroism (FDCD) for examination of nonlinear chiroptical properties of nanoclusters. In general, one-photon FDCD can serve as a complementary technique to absorption based measurements of the circular dichroism (Scheme 1). Fluorescence intensity is directly proportional to the rate of absorption of photons, where the proportionality constant involves the quantum yield of emission. When the quantum yield is assumed to be independent on the polarization of light, the circular dichroism strength can be derived from a difference of fluorescence intensity for left and right-handed circularly polarized light illumination.³² Introducing higher order processes of circular excitation presumably affects the magnitude of processes observed in linear regime.

While the technique of FDCD is applicable solely to optically active fluorescent samples, it is attractive since it assures better sensitivity and selectivity than absorption-based CD measurements.^{33, 34} Many sources claim that fluorescence-based techniques provide superior sensitivity since the measurements can be performed at lower concentrations.^{33, 35} Moreover, FDCD eliminates scattering artifacts generated in absorption detected CD and provides stronger CD response as soon as the samples exhibit quantum yield (QY) >0.1-0.2.^{32, 34} Despite the appealing potential of this technique, application of FDCD is limited by complex conditions of measurements in order to obtain explicit results. One must be aware that major artifacts may be generated in FDCD by the presence of residual linear polarization in incident circularly polarized light.^{36, 37} Yet, FDCD already appeared as a useful tool for determination of conformational and structural changes of the samples, unmeasurable using common CD spectroscopy.^{34, 37}

Here, we introduce the fluorescence-based technique of chirality measurements to nonlinear optical spectroscopy. We established a protocol of TP-FDCD measurements on a modified two-photon excited luminescence (TPEL) optical set-up. We present an expanded characterization of TP-FDCD of specifically chosen - strongly luminescent and chiral gold nanoclusters of L- and D-Arg/ATT-AuNCs, which optical properties have not been yet considered in two enantiomeric forms of ligands, neither in linear and nonlinear regime. Multiphoton studies have been provided in broad NIR range instead of common characterization at single excitation wavelength. We also compare TP-FDCD to one-photon CD characterization of gold

nanoclusters. Our study shows more than 245–times enhanced two-photon luminescence-detected circular dichroism (Θ_{TPCD}) compared to the one-photon dissymmetry factor (g_{abs}).

Results and discussion

Chiral gold nanoclusters Arg/ATT-AuNCs, stabilized with 6-aza-2-thiopyrimidine and arginine, were synthesized according to the previously reported procedure³⁸ with minor modifications (see supporting information). We established their average diameter to be equal to 1.89 ± 0.28 nm and 1.94 ± 0.29 nm for ATT-AuNCs and L-Arg/ATT-AuNCs, respectively, using Transmission Electron Microscopy (TEM) (Fig. S1). Thus, no significant change in the diameters of nanoclusters before and after addition of Arg was observed.

One-photon absorption spectrum of ATT-protected nanoclusters presents two absorption bands, at 415 nm and 480 nm. Addition of Arg causes sharpening and shifting of the former band to 405 nm and splitting of the latter band into well resolved peaks around 466 nm and 505 nm for L/D-Arg/ATT-AuNCs (Fig. 1), which is in good agreement with recent reports.^{38, 39} Fig. S2 present differences in band-gap energies. Excitation spectra shown in Fig. S3 resemble the same well separated transition bands.

Addition of Arg does not shift the emission maximum ($\lambda_{\text{max}}=528$ nm), however, it strongly influences the photoluminescence (PL) intensity: 45- and 43-fold enhancement of PL for L-Arg/ATT-AuNCs and D-Arg/ATT-AuNCs, respectively, is observed, with respect to ATT-Au NCs. The strong green fluorescence observed under UV light irradiation is shown in the inset of Fig. 1. Dramatically enhanced PL properties of NCs stabilized with Arg can be explained by rigidification of their structure via host-guest assemblies, formed by hydrogen bonds between ATT ligand and guanidine

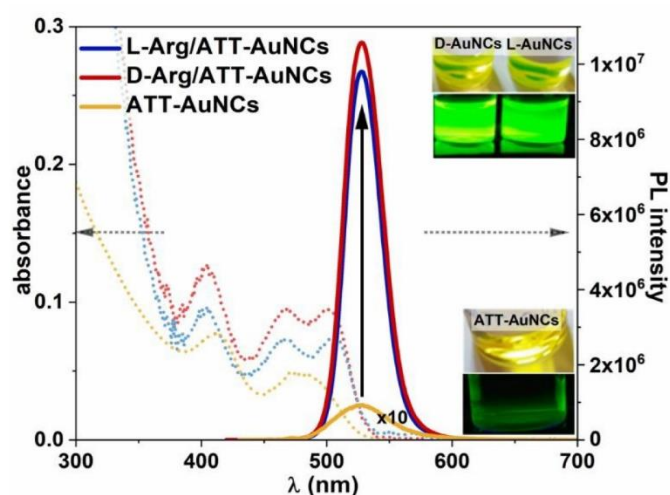


Figure 1. Absorption and emission spectra of ATT-AuNCs and two enantiomeric forms of Arg/ATT-AuNCs. Solid black arrow indicates PL enhancement of nanoclusters after addition of Arg to ATT-AuNCs. Photographs in the inset present eye-visible green luminescence.

group of Arg.³⁸ Supramolecular interaction of Arg and ATT-AuNCs hinders the intramolecular vibration and rotation of ATT and reduces the non-radiative relaxation of excited states, resulting in enhanced photoluminescence. Strong improvement of luminescent properties is also observed in PL lifetime characterization: 7 ns PL decay time of AuATT NCs is elongated to 42 ns after functionalization with Arginine. The PL decay curves of the NCs are well fitted with biexponential model (Eqs. 7,8, Supporting Information) as shown in Fig. S4 and Table S1. We also examined the QY in a direct QY measurement using an

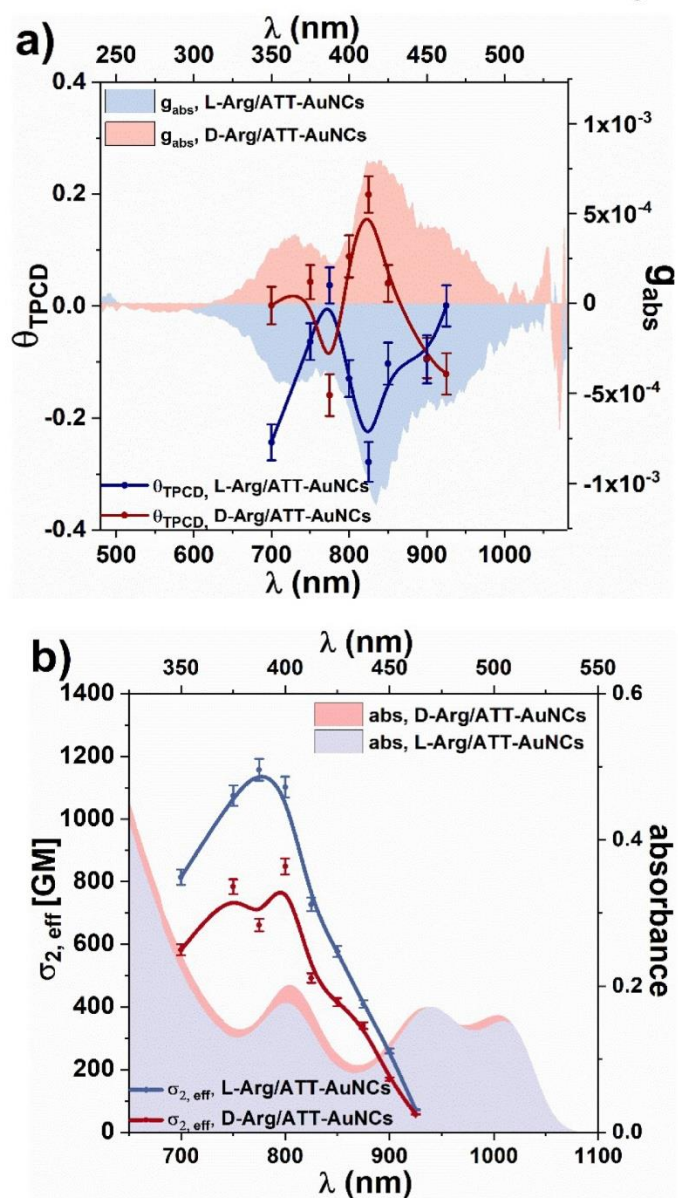


Figure 2. a) Two-photon circular dichroism (blue and red dots and lines, left and bottom axes) correlated with one-photon dissymmetry factor (blue and red areas, right and upper axes). b) Two-photon brightness spectra of L-Arg/ATT-AuNCs and D-Arg/ATT-AuNCs (blue and red dots and lines, left and bottom axes) correlated with absorbance of those nanoclusters (blue and red areas, right and upper axes).

COMMUNICATION

Table 1. One-photon and two-photon optical and chiroptical characterization of L/D-Arg/ATT-AuNCs.

Sample	One-photon		Two-photon		
	integrating sphere QY [%]	g_{abs} (415nm)	σ_2 [GM] (800nm)	$\sigma_{2,eff}$ [GM] (800nm)	Φ_{TPCD} [GM] (825nm)
L-Arg/ATT-AuNCs	63.2 ± 2.0%	-1.1·10 ⁻³	1743 ± 52	1102 ± 33	-0.27 ± 0.04
D-Arg/ATT-AuNCs	58.4 ± 2.0%	7.8·10 ⁻⁴	1453 ± 44	848 ± 25	0.19 ± 0.03

integrating sphere. The values determined for L-Arg/ATT-AuNCs and D-Arg/ATT-AuNCs were $\Phi = 63.2 \pm 2.0\%$ and $\Phi = 58.4 \pm 2.0\%$, respectively. The QY of AuATT NCs was below the integrating sphere sensitivity, therefore the QY of uncoated AuNCs was determined using a comparative method with respect to fluorescein, obtaining $\Phi = 1.4 \pm 0.3\%$. Our values of QY and PL lifetime of both enantiomers correspond well with the values determined for L-Arg/ATT-AuNCs reported previously.³⁹ Analysis of radiative and nonradiative rate constants (k_r and k_{nr}) from QY and PL lifetime confirm enhanced radiative or reduced nonradiative processes after functionalization with Arg (Table S1).

Fig. S5 shows CD spectra of Arg/ATT-AuNCs, which present distinct mirror images for L- and D- form of Arg/ATT-AuNCs with strongest CD peaks around 350 nm, 415 nm and 470 nm, which differ from the CD response of pure L-Arg and D-Arg ligands themselves. ATT-AuNCs are nonchiral nanoclusters therefore they do not generate any CD signal. The one-photon anisotropy factor g_{abs} (Fig. 2a) was determined according to Eq. 1 in Experimental Section, SI. The chiroptical properties of any enantiomeric forms of Arg/ATT-AuNCs have not been reported in the literature, but the magnitude of g_{abs} is comparable with the values common for other gold nanoclusters stabilized with chiral ligands.^{40, 41} Zhong et al. proposed most probable structure of ATT-AuNCs and Arg/ATT-AuNCs⁴², which shows unique structure organisation, that may suggest the origin of chirality being in chiral arrangement of ligands.

Fluorescence detected circular dichroism was measured on a custom-built TP-FDCD system presented in Fig. S6. We optimized the procedure of TP-FDCD measurements in order to compensate for any depolarization and artefacts, as described in detail in the SI. Briefly, left- and right- circularly polarized laser beam was formed using a Babinet-Soleil compensator to eliminate any linear polarization contribution. To ensure the best quality of polarization, a Glan-Thompson polarizer was introduced at the entrance of the optical path. Following the principles given by Tinoco³⁵ and Bain³⁶, during one-photon and two-photon FDCD measurements the luminescence was collected at so-called *magic angle* of 54.7°, which is positioned between the

propagation vector of the laser and the polarizer axis,^{32, 36} as shown in Fig. S6. It is assumed that the fluorescence of axially symmetric systems provides equivalent response in every direction of luminescence polarization.

Examples of two-photon excited luminescence spectra of the chiral nanoclusters and achiral fluorescein are collected in Fig. S7 to indicate the impact of left- and right-circularly polarized excitation. Owing to the opposite chirality of two enantiomeric nanoclusters, different PL intensities are detected depending on the direction of circularly polarized excitation (Fig. S7a,b). We used fluorescein solution as a reference sample, which, in a properly calibrated FDCD set-up, provides identical two-photon luminescence intensity for left- and right-handed circular polarization (Fig. S7c). To validate two-photon character of luminescence we performed laser power-dependent photoluminescence intensity measurements, which results in quadratic dependence of log-log plots (Figure S8).

To evaluate the potential of nanoclusters in two-photon chiroptical sensing and imaging via luminescence we determined the left- and right- handed two-photon brightness ($\sigma_{2,eff}$), as the product of two-photon absorption cross-section (σ_2) and PL quantum yield, according to Eq.2:

$$\sigma_{2,eff,s} = \sigma_2 \varphi_s = \frac{F_{2,s}(\lambda_{exc})C_r\varphi_r}{F_{2,r}(\lambda_{exc})C_s}\sigma_{2,r}, \quad (2)$$

where φ is the quantum yield, C is the concentration and F is the integrated fluorescence at a particular excitation wavelength for s –sample and r - reference solution. TPA cross-sections are usually quoted in the units of Göppert-Mayer, where 1 GM refers to $10^{-50} \text{ cm}^4 \text{ s photon}^{-1}$. We determined the two-photon absorption properties in a wide range of 700-930 nm excitation wavelengths. Both enantiomeric forms of nanoclusters present strong two-photon absorption around 750-800 nm that corresponds to respective (one-photon) absorption bands plotted at doubled wavelength (Fig. S9). The highest values are $\sigma_{2,s} = 1743 \text{ GM}$ and 1453 GM for L- and D-Arg/ATT-AuNCs, respectively, they compare favorably with σ_2 reported for other gold nanoclusters examined with the same method of TPEL.⁸ Due to strong QY of the fluorescent nanoclusters described here,

Journal Name

also their $\sigma_{2,\text{eff}}$ values are very respectable: 1102 GM and 848 GM (Fig. 2b) for L- and D- Arg/ATT-AuNCs samples, respectively, which are several times higher than $\sigma_{2,\text{eff}}$ of other nanoclusters reported in the literature.^{43, 44} Furthermore, the reported $\sigma_{2,\text{eff}}$ are significantly larger than those for commonly used fluorophores, e.g. dyes⁴⁵ and fluorescent proteins,⁴⁶ suggesting that Arg/ATT-AuNCs are outstanding candidates for multiphoton imaging applications.

Having the left- and right-handed circularly polarized two-photon absorption cross-sections, we could calculate the two-photon circular dichroism Θ_{TPCD} according to Equation 1 and contrast it with the one-photon anisotropy factor g_{abs} (Fig. 2a). Θ_{TPCD} follows the mirror-image of respective negative and positive bands of g_{abs} L/D-Arg/ATT-AuNCs. It is expected for non-centrosymmetric systems of chiral nanoclusters since OPA and TPA involve the same excited states. The strongest $\Theta_{\text{TPCD}} = -0.27$ is obtained at 825 nm. It presents ~ 245 -times increased chiroptical response in comparison to the one-photon anisotropy factor at a corresponding wavelength (Table 1). To the best of our knowledge Θ_{TPCD} of nanoclusters was studied only once previously, by the Z-scan technique. For Au₂₅ gold nanoclusters, two orders of magnitude enhancement of the two-photon anisotropy factor was found, as compared to one-photon chiral response.¹³ It corresponds well with our findings of Θ_{TPCD} , determined with the TP-FDCD technique. The deeper discussion on the nonlinear chiroptical properties would require extensive theoretical study, going beyond the usual point dipoles approximation. Already the first theoretical descriptions of two-photon CD by Power²⁶ and Bain³⁶ involved multipolar and magnetic transitions, and further investigations were performed by Rizzo⁴⁷. However, as there are no theoretical and computational studies of circular dichroism of Arg/ATT-AuNCs nanoclusters and no two-photon circular dichroism simulations of any of atomically-precise nanoclusters, a question whether universal theories provide satisfactory explanation for nonlinear chiroptical effects in complex systems of chiral nanoclusters cannot be currently answered.

One-photon FDCD of various types of materials proved to follow the CD response with the same quantitative features.^{35, 48} Determination if two-photon CD enhancement presents a more general trend among nanoclusters and other materials will require in-depth analysis of the chirality of ground and excited electronic energy levels in one-photon and two-photon absorption. As two-photon FDCD is yet poorly examined in the literature, comparison between experimental CD and FDCD studies is lacking, especially for nanomaterials. Thus, our contribution gives a valuable input to the description of chiroptical properties of nanoclusters and we hope it will stimulate further research in this area.

Conclusions

In this work we presented the quantitative description of two-photon circular dichroism of gold nanoclusters established via luminescence in a wide range of wavelengths. We evaluated linear and nonlinear optical properties of chiral L-Arg/ATT-AuNCs and D-Arg/ATT-AuNCs. Large two-photon absorption cross-sections (~ 1743 GM) and two-photon brightness (~ 1102 GM) confirm excellent NLO properties of these AuNCs. Subsequently, we determined TP-FDCD spectra of these clusters, obtaining maximum values of $\Theta_{\text{TPCD}} = -0.27$ and 0.19 for L-Arg/ATT-AuNCs and D-Arg/ATT-AuNCs, respectively. Our two-photon FDCD findings revealed over two orders of magnitude enhanced circular dichroism vs one-photon characteristics of L/D-Arg/ATT-AuNCs. Similarity of this finding to the enhancement factor reported for Au₂₅ nanoclusters¹³ rises a question about how general such boosting of the chiroptical response in two-photon regime is in nanoscale structures. Comparing results of CD and FDCD, the fluorescent technique is indeed found to present stronger sensitivity than the absorption-based one, offering prospective applications in enantioselective imaging, catalysis, sensing or biomedicine.

Author Contributions

The manuscript was written through contributions of all authors. AP : Methodology, Investigation, Writing - original draft, Visualization; JOB: Conceptualization, Writing - review & editing, Supervision, Funding acquisition. MS: Conceptualization, Writing - review & editing.

Conflicts of interest

There are no conflicts to declare

References

1. L. D. Barron, *Molecular Light Scattering and Optical Activity*, Cambridge University Press, Cambridge, 2 edn., 2004.
2. N. Shukla, M. A. Bartel and A. J. Gellman, *Journal of the American Chemical Society*, 2010, **132**, 8575-8580.
3. S. Jiang, M. Chekini, Z.-B. Qu, Y. Wang, A. Yeltik, Y. Liu, A. Kotlyar, T. Zhang, B. Li, H. V. Demir and N. A. Kotov, *Journal of the American Chemical Society*, 2017, **139**, 13701-13712.
4. C. Hao, X. Wu, M. Sun, H. Zhang, A. Yuan, L. Xu, C. Xu and H. Kuang, *Journal of the American Chemical Society*, 2019, **141**, 19373-19378.
5. M. Matuschek, D. P. Singh, H.-H. Jeong, M. Nesterov, T. Weiss, P. Fischer, F. Neubrech and N. Liu, *Small*, 2018, **14**, 1702990.

COMMUNICATION

6. Z. Peng, L. Yuan, J. XuHong, H. Tian, Y. Zhang, J. Deng and X. Qi, *Journal of Nanobiotechnology*, 2021, **19**, 220.
7. J. Olesiak-Banska, M. Waszkielewicz, P. Obstarczyk and M. Samoc, *Chemical Society Reviews*, 2019, **48**, 4087-4117.
8. V. Bonačić-Koutecký and R. Antoine, *Nanoscale*, 2019, **11**, 12436-12448.
9. P. A. Shaw, E. Forsyth, F. Haseeb, S. Yang, M. Bradley and M. Klausen, *Frontiers in chemistry*, 2022, **10**, 921354.
10. T. G. Schaaff, G. Knight, M. N. Shafigullin, R. F. Borkman and R. L. Whetten, *The Journal of Physical Chemistry B*, 1998, **102**, 10643-10646.
11. Y. Li, T. Higaki, X. Du and R. Jin, *Advanced Materials*, 2020, **32**, 1905488.
12. Y. Zhu, J. Guo, X. Qiu, S. Zhao and Z. Tang, *Accounts of Materials Research*, 2021, **2**, 21-35.
13. J. Olesiak-Banska, M. Waszkielewicz and M. Samoc, *Physical Chemistry Chemical Physics*, 2018, **20**, 24523-24526.
14. H. Yao, T. Fukui and K. Kimura, *The Journal of Physical Chemistry C*, 2008, **112**, 16281-16285.
15. S. Takano and T. Tsukuda, *The Journal of Physical Chemistry Letters*, 2016, **7**, 4509-4513.
16. S. Knoppe, A. Dass and T. Bürgi, *Nanoscale*, 2012, **4**, 4211-4216.
17. J. Sobska, M. Waszkielewicz, A. Podleśny-Drabiniok, J. Olesiak-Banska, W. Krężel and K. Matczyszyn, *Nanomaterials*, 2021, **11**, 1066.
18. A. Cantelli, G. Battistelli, G. Guidetti, J. Manzi, M. Di Giosia and M. Montalti, *Dyes and Pigments*, 2016, **135**, 64-79.
19. R. Han, M. Zhao, Z. Wang, H. Liu, S. Zhu, L. Huang, Y. Wang, L. Wang, Y. Hong, Y. Sha and Y. Jiang, *ACS Nano*, 2020, **14**, 9532-9544.
20. L. Polavarapu, M. Manna and Q.-H. Xu, *Nanoscale*, 2011, **3**, 429-434.
21. H. Yang, Y. Wu, H. Ruan, F. Guo, Y. Liang, G. Qin, X. Liu, Z. Zhang, J. Yuan and X. Fang, *Analytical Chemistry*, 2022, **94**, 3056-3064.
22. S. Bhunia, K. Gangopadhyay, A. Ghosh, S. K. Seth, R. Das and P. Purkayastha, *ACS Applied Nano Materials*, 2021, **4**, 305-312.
23. H.-H. Deng, X.-Q. Shi, H.-P. Peng, Q.-Q. Zhuang, Y. Yang, A.-L. Liu, X.-H. Xia and W. Chen, *ACS Applied Materials & Interfaces*, 2018, **10**, 5358-5364.
24. Z. Wei, Y. Pan, G. Hou, X. Ran, Z. Chi, Y. He, Y. Kuang, X. Wang, R. Liu and L. Guo, *ACS Applied Materials & Interfaces*, 2022, **14**, 2452-2463.
25. Y. Peng, X. Huang and F. Wang, *Chemical Communications*, 2021, **57**, 13012-13015.
26. E. A. Power, *The Journal of Chemical Physics*, 1975, **63**, 1348-1350.
27. F. Hache, H. Mesnil and M. C. Schanne-Klein, *Physical Review B*, 1999, **60**, 6405-6411.
28. K. E. Gunde and F. S. Richardson, *Chemical Physics*, 1995, **194**, 195-206.
29. C. Toro, L. De Boni, N. Lin, F. Santoro, A. Rizzo and F. E. Hernandez, *Chemistry – A European Journal*, 2010, **16**, 3504-3509.
30. Y. Vesga, C. Diaz, J. Crassous and F. E. Hernandez, *The Journal of Physical Chemistry A*, 2018, **122**, 3365-3373.
31. H. Mesnil, M. C. Schanne-Klein, F. Hache, M. Alexandre, G. Lemerrier and C. Andraud, *Physical Review A*, 2002, **66**, 013802.
32. I. Tinoco, in *Optical Activity and Chiral Discrimination: Proceedings of the NATO Advanced Study Institute held at the University of Sussex, Falmer, England, September 10–22, 1978*, ed. S. F. Mason, Springer Netherlands, Dordrecht, 1979, DOI: 10.1007/978-94-015-7644-4_4, pp. 57-85.
33. M. Thomas, G. Patonay and I. Warner, *Review of Scientific Instruments*, 1986, **57**, 1308-1313.
34. T. Nehira, K. Ishihara, K. Matsuo, S. Izumi, T. Yamazaki and A. Ishida, *Analytical Biochemistry*, 2012, **430**, 179-184.
35. D. H. Turner, I. Tinoco and M. Maestre, *Journal of the American Chemical Society*, 1974, **96**, 4340-4342.
36. A. J. Bain and A. J. McCaffery, *The Journal of Chemical Physics*, 1985, **83**, 2632-2640.
37. E. W. Lobenstine and D. H. Turner, *Journal of the American Chemical Society*, 1980, **102**, 7786-7787.
38. H.-H. Deng, X.-Q. Shi, F.-F. Wang, H.-P. Peng, A.-L. Liu, X.-H. Xia and W. Chen, *Chemistry of Materials*, 2017, **29**, 1362-1369.
39. L. Yang, B. Zhang, L. Fu, K. Fu and G. Zou, *Angewandte Chemie (International ed. in English)*, 2019, **58**, 6901-6905.
40. Y. Yanagimoto, Y. Negishi, H. Fujihara and T. Tsukuda, *The Journal of Physical Chemistry B*, 2006, **110**, 11611-11614.
41. S. Si, C. Gautier, J. Boudon, R. Taras, G. Serafino and T. Bürgi, *J. Phys. Chem. C*, 2009, **113**, 12966-12969.
42. Y. Zhong, J. Zhang, T. Li, W. Xu, Q. Yao, M. Lu, X. Bai, Z. Wu, J. Xie and Y. Zhang, *Nature Communications*, 2023, **14**, 658.
43. A. Pniakowska, K. Kumaranchira Ramankutty, P. Obstarczyk, M. Perić Bakulić, Ž. Sanader Maršić, V. Bonačić-Koutecký, T. Bürgi and J. Olesiak-Banska, *Angewandte Chemie International Edition*, 2022, **61**, e202209645.
44. C.-L. Liu, M.-L. Ho, Y.-C. Chen, C.-C. Hsieh, Y.-C. Lin, Y.-H. Wang, M.-J. Yang, H.-S. Duan, B.-S. Chen, J.-F. Lee, J.-K. Hsiao and P.-T. Chou, *The Journal of Physical Chemistry C*, 2009, **113**, 21082-21089.
45. M. A. Albota, C. Xu and W. W. Webb, *Appl. Opt.*, 1998, **37**, 7352-7356.
46. M. Drobizhev, N. S. Makarov, S. E. Tillo, T. E. Hughes and A. Rebane, *Nature methods*, 2011, **8**, 393-399.
47. D. H. Friese, C. Hättig and A. Rizzo, *Physical Chemistry Chemical Physics*, 2016, **18**, 13683-13692.
48. A. Ben Moshe, D. Szwarcman and G. Markovich, *ACS Nano*, 2011, **5**, 9034-9043.

SUPPORTING INFORMATION

Strong fluorescence-detected two-photon circular dichroism of chiral gold nanoclusters

Anna Pniakowska^a, Marek Samoć^a, Joanna Olesiak-Bańska^{a*}

Institute of Advanced Materials, Wrocław University of Science and Technology, Wybrzeże Wyspiańskiego 27, 50-370 Wrocław, Poland

Experimental

Materials and methods

6-Aza-2-thiothymine (ATT) was purchased from Alfa Aesar Chemicals. H₂AuCl₄·3H₂O, L-arginine, D-arginine, NaOH, fluoresceine were purchased from Sigma Aldrich. All materials were used without additional purification. Aqueous solutions were prepared using milli-Q water. All glassware was cleaned with aqua regia and rinsed with water prior to use.

Synthesis of AuATT NCs

ATT (5 mL, 80 mM) was dissolved with 0.2 M NaOH. H₂AuCl₄·3H₂O water solution (5 mL, 10 mg/mL) was added and continuously stirred at room temperature for 1h. Solution colour was changing from dark brown, red, orange to light yellow. The as-synthesized ATT-Au NCs were purified by ultrafiltration (Millipore, 50 kDa) at 7 000 rpm for 10min. Purified nanoclusters were dissolved in 10mL Milli-Q water and stored at 4 °C in the dark prior to use.

Synthesis of AuATT-L/D-Arg NCs

2mL of purified ATT-AuNCs diluted in Milli-Q water (pH=10) was mixed with 230μL, 40 mM L- and D-Arg solutions (pH=10) in two separate vials. Both solutions were allowed to react at 37 °C for 24 h. The Arg/ATT-AuNCs solution could be stored at 4 °C in the dark for one year with negligible changes in its optical properties.

Characterization of AuNCs

The sizes and morphologies of AuNCs were determined using a FEI Tecnai G2 20 X-TWIN transmission electron microscope (TEM). UV/VIS spectra were measured in solutions, therefore all synthesized nanoclusters were freshly dissolved in ultra-pure milli-Q water before analysis. Absorption and circular dichroism were recorded using a Jasco V-670 spectrophotometer and a JASCO J-815 CD spectropolarimeter, respectively in 10-mm quartz cells. One-photon anisotropy factor, denoted as g_{CD} or g_{abs} was calculated with the equation:

$$g_{abs} = \frac{\Delta\varepsilon}{\varepsilon} = \frac{\Delta A}{A} = \frac{\theta}{32\,980 \cdot A} \quad (1)$$

Photoluminescence (PL) and photoluminescence excitation (PLE) were determined using a HORIBA FluoroMax 4 and FS5 Spectrofluorometer (Edinburgh Instruments) equipped with a Xenon lamp. Fluorescence quantum yield was determined using integrating sphere in the FS5 Spectrofluorometer (Edinburgh Instruments) and by comparative method with the following equation:

$$\Phi_f^s = \Phi_f^r \frac{f_r(\lambda_{ex}) \int_{\lambda_{em}} F^s(\lambda_{em}) d\lambda_{em} n_s^2}{f_s(\lambda_{ex}) \int_{\lambda_{em}} F^r(\lambda_{em}) d\lambda_{em} n_r^2} \quad (2)$$

$$f_x(\lambda_{ex}) = 1 - 10^{-A_x(\lambda_{ex})} \quad (3)$$

where Φ_f^r is fluorescence quantum yield of reference sample, $\int_{\lambda_{em}} F^s(\lambda_{em}) d\lambda_{em}$ and $\int_{\lambda_{em}} F^r(\lambda_{em}) d\lambda_{em}$ correspond to integrated areas of fluorescence intensity of sample and reference, respectively and n_s and n_r correspond to refractive index of sample and

reference, respectively. $f_x(\lambda_{ex})$ refers to the corresponding absorption correction factor and $A_x(\lambda_{ex})$ to the absorbance of sample ($x=s$) or reference ($x=r$) at excitation wavelength.

Time-correlated single-photon counting (TCSPC) method was applied to determine PL lifetime using the FS5 Spectrofluorometer (Edinburgh Instruments) equipped with a 475nm diode laser as excitation source. Fluoracle software was used to determine the decay curve fitting with biexponential function:

$$I = A + B_1 e^{-\frac{t}{\tau_1}} + B_2 e^{-\frac{t}{\tau_2}} \quad (4)$$

The average lifetime was calculated with the formula:

$$\langle \tau_{int} \rangle = \frac{B_1 \tau_1^2 + B_2 \tau_2^2}{B_1 \tau_1 + B_2 \tau_2} \quad (5)$$

where B_1 and B_2 are the contributions of particular lifetime. The χ^2 value determined the quality of fit.

The radiative (k_r) and nonradiative (k_{nr}) rate constants were calculated from the determined fluorescence quantum yield (Φ) and average fluorescence lifetime (τ_{int}) using the following equations:

$$K_r = \frac{\Phi}{\tau_{int}} \quad (6)$$

$$K_{nr} = \frac{1}{\tau_{int}} - k_r \quad (7)$$

Two-photon optical characterization of AuNCs

Two-photon excited luminescence was measured using a custom-built set-up consisting of a femtosecond mode-locked Ti:Sapphire laser (~140 fs, 80 MHz, Chameleon, Coherent Inc.) with incident wavelength range tuneable within $\lambda = 680$ -1080 nm. Luminescence was collected in parallel shortpass filter (cut-off wavelength 650 nm). In order to exclude the potential excitation at lower wavelength range 700 nm long-pass filters were applied. The two-photon excited emission spectra were measured with a spectrograph (Shamrock 303i Andor). Measurement conditions were set the same for each nanoclusters sample and reference sample. Solutions in the same cuvettes were illuminated in the range of $\lambda=700$ -930nm excitation. Since the Babinet-Soleil compensator is wavelength dependent, taking a set of measurements at a particular excitation wavelength required a new calibration. The exciting laser power was set in the range 22-30 mW in such a manner as to obtain exactly the same luminescence intensity signal from the nonchiral, reference sample at each wavelength. The experimental conditions were chosen to prevent photobleaching and achieve a high signal to noise ratio. Two-photon absorption cross sections were calculated with the equation:

$$\sigma_{2,s} = \frac{F_{2,s}(\lambda_{exc}) C_r \phi_r}{F_{2,r}(\lambda_{exc}) C_s \phi_s} \sigma_{2,r} \quad (8)$$

Fluorescein dye was used in this work as an optically inactive (non-chiral), fluorescent reference sample. The reference dye was carefully chosen to have a similar range of emission as the cluster samples examined in this work to exclude possible FDCD shifting.¹

The Θ_{TPCD} , defined according to Eq. 1 is consistent with the Θ_{TPCD} definitions adopted in other Z-scan² and polarization modulated Z-scan techniques of measuring two-photon circular dichroism.³

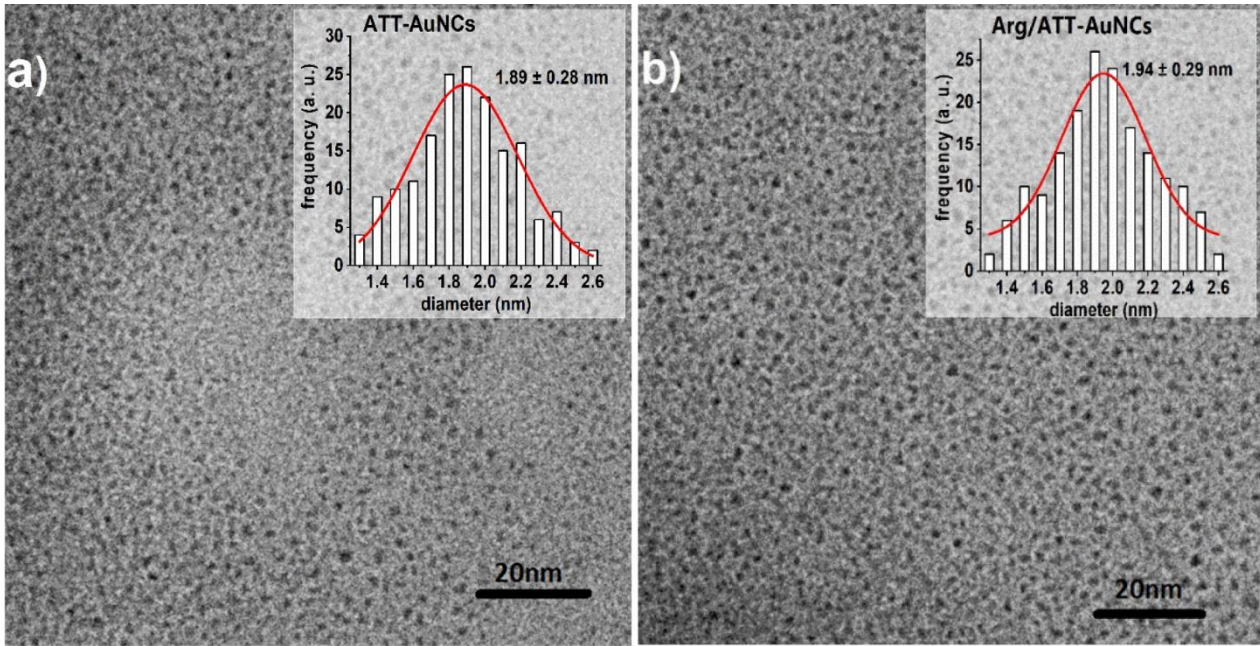


Figure S1. TEM images of and a) ATT-AuNCs and b) L-Arg/ATT-AuNCs. The inset of each figure presents corresponding size distribution histogram of NCs. FWHM of given curves of fitted size distribution are equal to 0.57 nm and 0.55 nm, giving 1.61-2.18 nm and 1.67-2.22 nm for ATT-AuNCs and Arg/ATT-AuNCs.

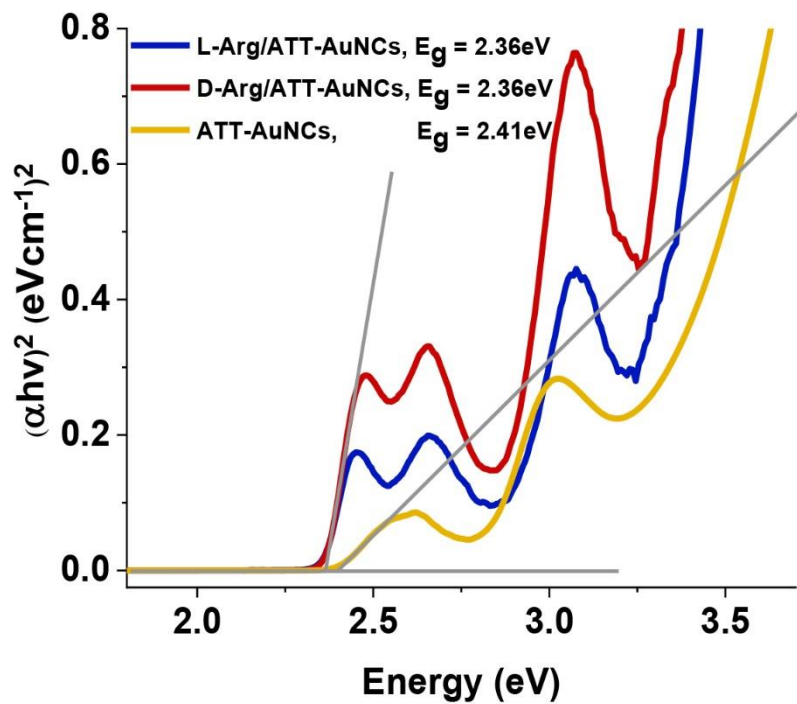


Figure S2. Determination of bandgap energies of ATT-AuNCs, Arg-L/ATT-AuNCs, Arg-D/ATT-AuNCs.

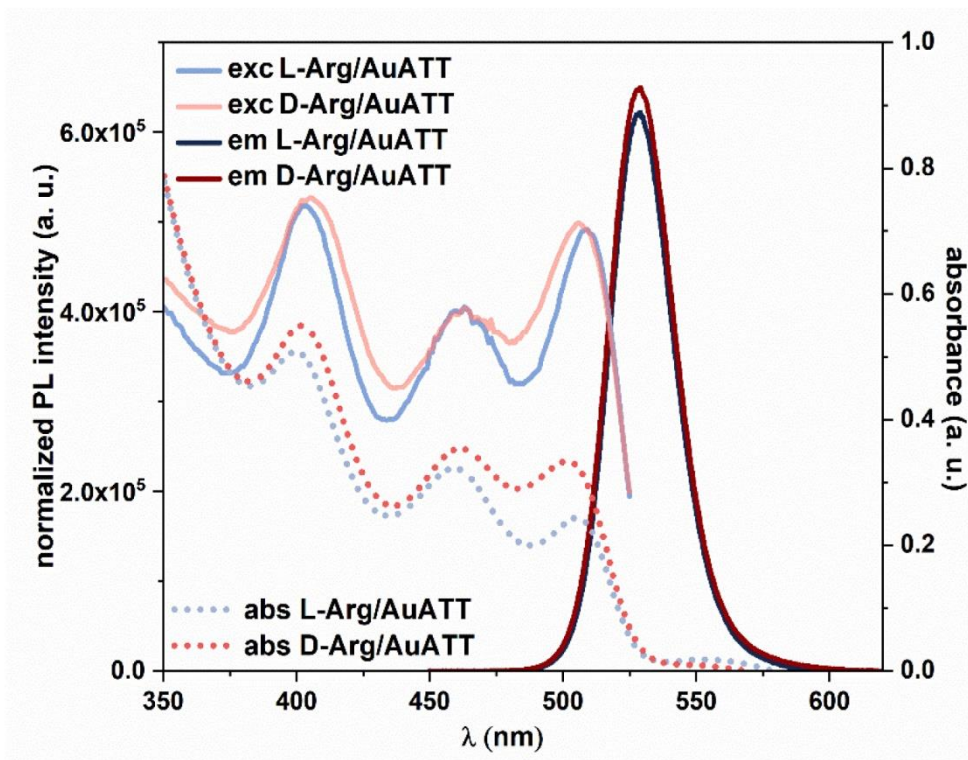


Figure S3. Absorption, excitation and emission spectra of L-Arg/ATT-AuNCs (blue) and D-Arg/ATT-AuNCs (red).

Table S1. Quantum yield (Φ), fluorescence lifetimes (τ_1 , τ_2) and their relative contributions, average lifetime (τ_{int}), radiative (k_r) and nonradiative rate (k_{nr}) constants determined for ATT-AuNCs, L-Arg/ATT-AuNCs and D-Arg/ATT-AuNCs.

	Φ [%]	τ_1 [ns]	τ_2 [ns]	τ_{int} [ns]	k_r [10^7 s $^{-1}$]	k_{nr} [10^7 s $^{-1}$]
ATT-AuNCs	1.4 ± 0.3	3.9 ± 0.1 (99.4%)	50.0 ± 5.4 (0.6%)	7.1 ± 0.8 ($\chi^2=1.2$)	0.20	13.9
L-Arg/ATT-AuNCs	63.2 ± 2.0	24.2 ± 0.5 (58.9%)	54.5 ± 0.6 (41.1%)	42.7 ± 0.5 ($\chi^2=1.26$)	1.48	0.86
D-Arg/ATT-AuNCs	58.4 ± 2.0	27.5 ± 0.5 (67.5%)	58.0 ± 0.8 (32.5%)	42.9 ± 0.7 ($\chi^2=1.37$)	1.36	0.97

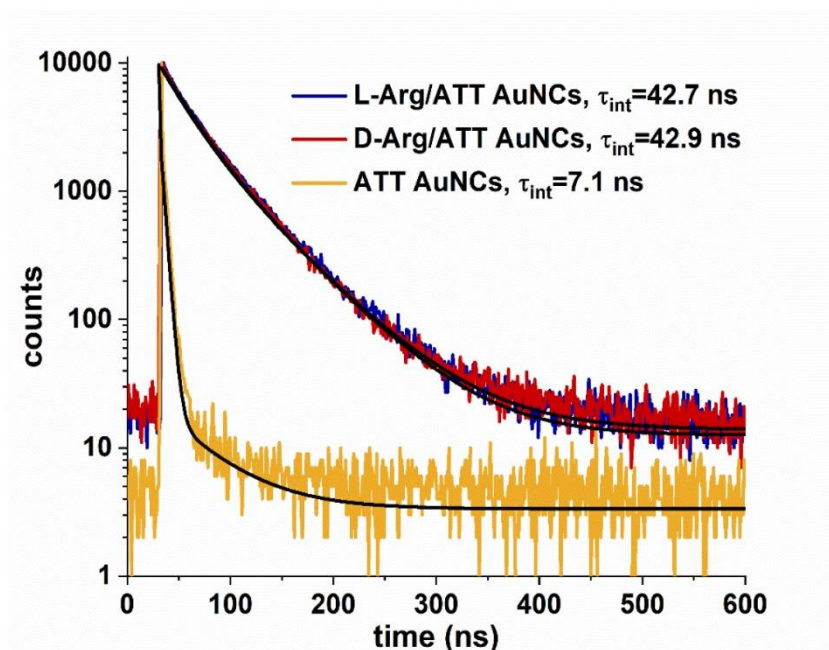


Figure S4. Fluorescence decay curves of L-Arg/ATT-AuNCs (blue) and D-Arg/ATT-AuNCs (red) compared to ATT-AuNCs (orange).

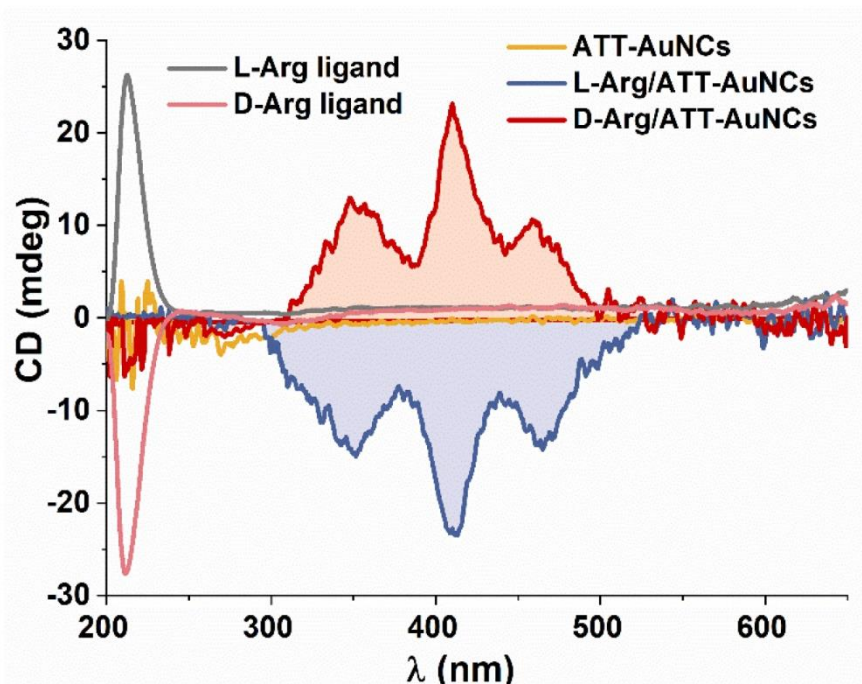


Figure S5. A comparison of CD spectra of L- and D- Arg/ATT-AuNCs with CD spectra of respective chiral ligands L-Arg and D-Arg, as well as nonchiral nanoclusters without arginine coating: ATT-AuNCs.

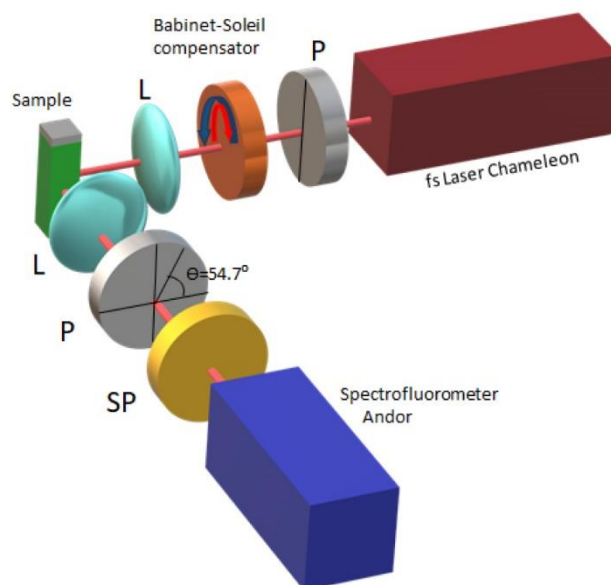


Figure S6. A scheme of the FDCD optical set-up (P=polarizer, L=lens, SP=shortpass filter).

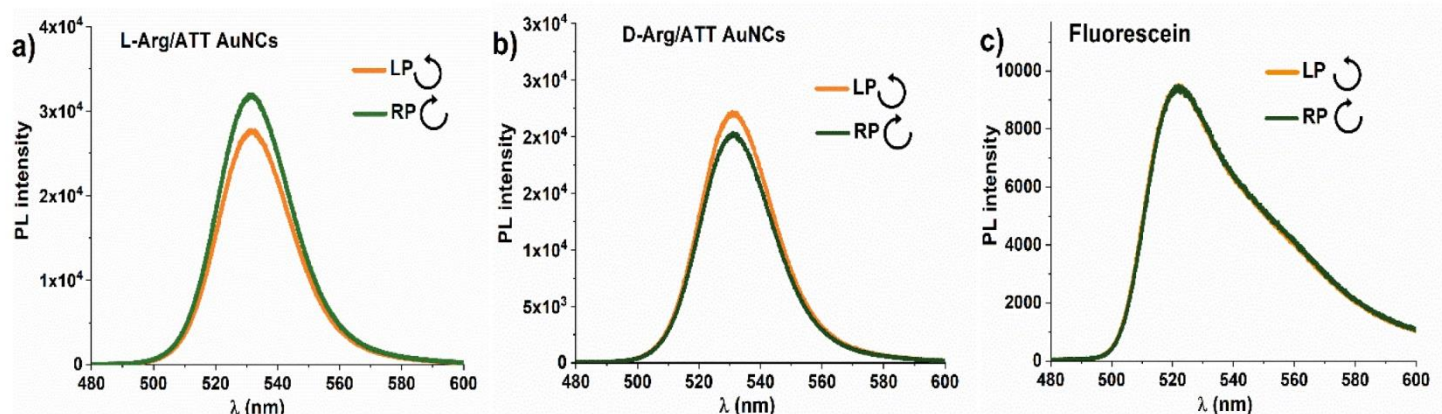


Figure S7. Two-photon excited luminescence of a) L-Arg/ATT-AuNCs, b) D-Arg/ATT-AuNCs and c) fluorescein, recorded at magic angle polarization of emission. Arrows in labels indicate direction of circularly polarized excitation, LP=left-handed polarization, RP= right-handed polarization.

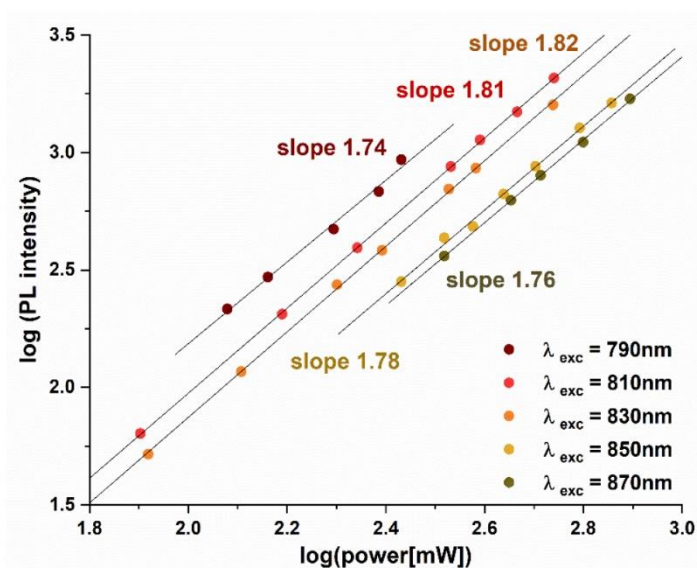


Figure S8. Log-log plot of the PL intensity of L-Arg/ATT-AuNCs as a function of average incident laser power measured at several excitation wavelengths. The slope of the linear fit corresponds roughly to the expected order of multiphoton processes.

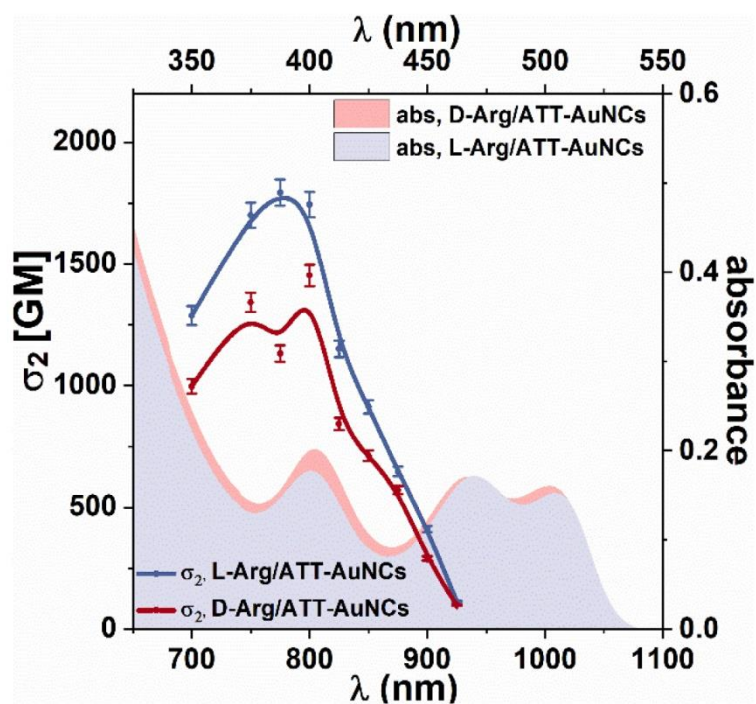


Figure S9. Two-photon absorption of L-Arg/ATT-AuNCs and D-Arg/ATT-AuNCs (blue and red dots and lines, left and bottom axes) correlated with absorption of those nanoclusters (blue and red areas, right and upper axes).

1. Turner, D. H.; Tinoco, I.; Maestre, M., Fluorescence detected circular dichroism. *Journal of the American Chemical Society* **1974**, *96* (13), 4340-4342.
2. Olesiak-Banska, J.; Waszkielewicz, M.; Samoc, M., Two-photon chiro-optical properties of gold Au25 nanoclusters. *Physical Chemistry Chemical Physics* **2018**, *20* (38), 24523-24526.
3. Samoc, M.; Samoc, A.; Miniewicz, A.; Markowicz, P.; Prasad, P.; Grote, J., *Cubic nonlinear optical effects in deoxyribonucleic acid (DNA) based materials containing chromophores*. SPIE: 2007; Vol. 6646.

4 SUMMARY AND PERSPECTIVES

This PhD dissertation describes the potential of unique, fluorescent and chiroptical properties of noble metal nanoclusters for multiphoton microscopy. Luminescence is a powerful tool, which in the frame of this thesis was utilized for determination of other optical properties, such as two-photon absorption or circular dichroism. Herein, referring to the formulated hypotheses, I will summarize the collected research results. After that, I will discuss future challenges and perspectives of my findings.

First hypothesis states that photoluminescence of nanoclusters can be significantly improved by specifically adapted chemical and physical treatments, e.g. structure modification, functionalization. Here in this work I have verified three strategies of luminescence enhancements: single metal atom doping, rigidification of structure of nanoclusters through functionalization with additional ligands and the usability of plasmonic nanoparticles for enhancement of luminescence. Structural composition modifications induced by gold doping resulted in enhancement of luminescent properties: quantum yield from $\phi = 3.08 \pm 2.0\%$ to $29.91 \pm 2.0\%$ and PL lifetime from $\tau = 1.1 \mu\text{s}$ to $1.8 \mu\text{s}$ for $\text{Ag}_{24}\text{Au}_1(\text{DMBT})_{18}$ nanoclusters, compared to undoped $\text{Ag}_{25}(\text{DMBT})_{18}$. Due to luminescence enhancement of $\text{Ag}_{24}\text{Au}_1(\text{DMBT})_{18}$, two-photon brightness raised from $\sigma_{2,\text{eff}} = 1.5 \text{ GM}$ to 20 GM . Another strategy of luminescence enhancement by functionalization of arginine ligands on the outer layer of AuATT NCs resulted in improved QY from $\phi = 1.4 \pm 0.3\%$ to $\phi = 63.2 \pm 2.0\%$ and $\phi = 58.4 \pm 2.0\%$ for L-Arg/ATT-AuNCs and D-Arg/ATT-AuNCs, respectively. Host-guest interactions between arginine and 6-aza-2-thiopyrimidine resulted also in 6-times elongated PL lifetimes, from 7 ns to 42 ns, for both arginine-ligated nanoclusters. Here again, the adapted strategy of luminescence enhancement found applicability in two-photon regime of excitation, revealing strong two-photon brightness $\sigma_{2,\text{eff}} = 1102 \text{ GM}$ and 848 GM for L- and D-Arg/ATT-AuNCs. Finally, the last strategy of improvement of luminescent properties was dedicated to plasmonic enhancement in close proximity of nanoclusters to gold nanorods. This study was performed solely under multiphoton excitation. Here individual gold nanoclusters are detected at the single-particle level with 25-times enhanced two-photon signal through plasmonic nanoparticle as nanoantenna. Nanoclusters obtained through wet-chemical syntheses demonstrated good chemical stability and photostability upon strong laser irradiation, therefore supplementing robust optical one-photon properties they could serve as an excellent material for multiphoton investigations.

Second hypothesis states that gold-atom doping influence two-photon optical properties of silver nanoclusters. Number of gold-atom dopant affects strongly multiphoton optical response. The Article 2 provides the detailed analysis of changes in one- and two-photon properties after single Au atom doping of silver nanoclusters Ag_{25} and after multiple Au doping of the same structure of Ag_{25} nanoclusters. The opposite result of improved and suppressed optical properties upon single and multiple atom doping indicates the importance of investigation of atomically precise nanoclusters' structure. The doping effect was discussed in one- and two-photon regime and confirmed experimentally and theoretically. It was proved that single gold atom introduced to icosahedral structure of Ag_{25} nanoclusters predominantly occupies the center of the kernel.

Third hypothesis states that luminescence can be used as a tool to determine two-photon circular dichroism of nanoclusters. The Article 3 provide the detailed discussion on the luminescent properties of nanoclusters, e. g. quantum yield, luminescence lifetime or two-photon brightness. These luminescent properties were further utilized to determine chiroptical properties. Excellent chiroptical response of L/D-Arg/AuATT NCs resulted in over two orders of magnitude stronger two-photon circular dichroism vs one-photon one.

The findings presented within this thesis solve numerous problems of new probes for multiphoton study, such as low luminescence or challenging detection of low concentrated solutions. However, below I have listed an additional challenges, which would be beneficial to address in the future:

- Future work on two-photon study of single gold nanoclusters in the vicinity of plasmonic nanoparticles should consider the improvement of excitation conditions to benefit the potential stronger luminescence enhancement (e. g. referring to up to 1000-fold strong plasmon enhanced luminescence of a crystal violet dye⁵²).The general rule of strongest plasmonic assisted enhancement assume occurrence of excitation in plasmon resonance wavelengths. In the case of the study presented in Article 1 – the excitation conditions were limited by the optics of used set-up.
- Further study of plasmonic enhanced single gold nanoclusters should be performed in a simple one-photon experiment, possibly in better distance-controlled interaction between nanoclusters and nanoparticles. Conjugation of nanoclusters to precisely known diameter joint, e.g. DNA strand could help to control better the nanocluster-nanoparticle system and predict possible interactions.
- Since alloying of nanoclusters results in enhanced and reduced luminescent properties depending on the number of gold-doped nanoclusters, future study could determine the boundaries of number of exchanged Ag atoms, in which Au@Ag alloys present enhanced properties.
- Despite remarkable repetition of synthesis and optical properties of L-/D-Arg/AuTT NCs, the proposed protocol of synthesis could be improved to obtain atomically-precise structures. Future research could optimize synthesis to different size-selective procedures or propose advanced separation techniques.
- Fluorescence detected circular dichroism have been proposed in this work in two-photon region of excitation, however the potential of nanoclusters in one-photon study of FDCD also have never been determined. Supplementation of my findings in one-photon region would open the discussion how two-photon excitation impact the magnitude of circular dichroism.
- Finally, potential of all synthesized and characterized nanoclusters in this thesis could be verified *in vitro* or *in vivo* in a biological sample under multiphoton microscope. Taking the advantage of strong absorption, enhanced luminescence or unique chiroptical activity nanoclusters could serve as a prominent probe for imaging and detection either in one- or two-photon studies.

5 PUBLISHED WORKS

1. **A. Pniakowska**, M. Samoć, J. Olesiak-Bańska "Strong fluorescence-detected two-photon circular dichroism of chiral gold nanoclusters", **Nanoscale**, 2023, 15, 19, p. 8597-8602.
2. **A. Pniakowska**, K. Ramankutty, P. Obstarczyk, M. Perić, Z. S. Maršić, V. Bonačić-Koutecký, T. Bürgi, J. Olesiak-Bańska "Gold-doping effect on two-photon absorption and luminescence of atomically precise silver ligated nanoclusters" **Angewandte Chemie International Edition**, 2022, 61, 43, p. 1-9, e202209645, **Angewandte Chemie**, 134, e202209645
3. **A. Pniakowska**, J. Olesiak-Bańska "Plasmonic Enhancement of Two-Photon Excited Luminescence of Gold Nanoclusters" **Molecules**, 2022, 27(3), 807, p. 1-12
4. D. Bain, H. Yuan, **A. Pniakowska**, A. Hajda, C. Bouanchaud, F. Chirot, C. Comby-Zerbino, V. Gueguen-Chaignon, V. Bonačić-Koutecký, J. Olesiak-Bańska, Z. Sanader Marsic, R. Antoine, "One- and Two-Photon Brightness of Proteins Interacting with Gold. A Closer Look at Gold-Insulin Conjugates" **Nanoscale**, 2024, 16(31), p. 14953-14958
5. P. D. Obstarczyk, **A. Pniakowska**, Nonappa, M. Grzelczak, J. Olesiak-Bańska "Crown ether-capped gold nanoclusters as a multimodal platform for bioimaging", **ACS Omega**, 2023, 8, 12, p. 11503-11511
6. O. Kaczmarczyk, **A. Pniakowska**, Andrzej Żak „Comparison of differential phase Contrast, Lorentz and non-Lorentz transmission electron microscopy for microstructural and magnetic imaging of alnico magnet" **Materials Letters**, 2024, 366, 136513
7. D. Bain, I. Russier-Antoine, H. Yuan, S. Kolay, S. Maclot, C. Moulin, E. Salmon, P.-Francois Brevet, **A. Pniakowska**, J. Olesiak-Bańska, R. Antoine "Solvent-induced aggregation of self-assembled copper–cysteine nanoparticles reacted with glutathione: enhancing linear and nonlinear optical properties", **Langmuir**, 2023, 39, 46, p. 16554-16561.
8. N. A. Saleh, D. Kundu, N. Vanthuyne, J. Olesiak-Bańska, **A. Pniakowska**, K. Matczyszyn, V. Y. Chang, G. Muller, J. A. G. Williams, M. Srebro-Hooper, J. Autschbach, J. Crassous "Dinuclear rhenium complexes with a bridging helicene-bis-bipyridine ligand: synthesis, structure, and photophysical and chiroptical properties", **ChemPlusChem**, 2020, 85, p. 1-10
9. M. Waszkielewicz, J. Olesiak-Bańska, M. Grzelczak, A. Sánchez-Iglesias, **A. Pniakowska**, M. Samoć "Enhanced one-photon and two-photon excited luminescence of polymer-stabilized AuAg nanoclusters aggregates". **Journal of Luminescence**, 2020, 221, 116994, p. 1-6.

6 BIBLIOGRAPHY

1. R. Jin and T. Higaki, *Communications Chemistry*, 2021, **4**, 28.
2. J. Zheng, C. Zhou, M. Yu and J. Liu, *Nanoscale*, 2012, **4**, 4073-4083.
3. R. Jin, C. Zeng, M. Zhou and Y. Chen, *Chemical Reviews*, 2016, **116**, 10346-10413.
4. W. W. Xu, E. Wang and X. C. Zeng, *Accounts of Materials Research*, 2024, **5**, 1134-1145.
5. H. Qian, M. Zhu, Z. Wu and R. Jin, *Accounts of Chemical Research*, 2012, **45**, 1470-1479.
6. M. Zhu, C. M. Aikens, F. J. Hollander, G. C. Schatz and R. Jin, *Journal of the American Chemical Society*, 2008, **130**, 5883-5885.
7. S. Chen, S. Wang, J. Zhong, Y. Song, J. Zhang, H. Sheng, Y. Pei and M. Zhu, *Angewandte Chemie (International ed. in English)*, 2015, **54**, 3145-3149.
8. S. Basu, A. Paul and R. Antoine, *Nanomaterials*, 2022, **12**, 62.
9. L. He and T. Dong, *CrystEngComm*, 2024, **26**, 3998-4016.
10. M. Brust, M. Walker, D. Bethell, D. J. Schiffrin and R. Whyman, *Journal of the Chemical Society, Chemical Communications*, 1994, DOI: 10.1039/C39940000801, 801-802.
11. Q. Yan, Z. Yuan, Y. Wu, C. Zhou, Y. Dai, X. Wan, D. Yang, X. Liu, N. Xue, Y. Zhu and Y. Yang, *Precision Chemistry*, 2023, **1**, 468-479.
12. X.-D. Zhang, D. Wu, X. Shen, P.-X. Liu, F.-Y. Fan and S.-J. Fan, *Biomaterials*, 2012, **33**, 4628-4638.
13. X. D. Zhang, J. Chen, Z. Luo, D. Wu, X. Shen, S. S. Song, Y. M. Sun, P. X. Liu, J. Zhao, S. Huo, S. Fan, F. Fan, X. J. Liang and J. Xie, *Advanced healthcare materials*, 2014, **3**, 133-141.
14. X. Le Guével, V. Trouillet, C. Spies, K. Li, T. Laaksonen, D. Auerbach, G. Jung and M. Schneider, *Nanoscale*, 2012, **4**, 7624-7631.
15. W. Ma, L. Xu, A. F. de Moura, X. Wu, H. Kuang, C. Xu and N. A. Kotov, *Chemical Reviews*, 2017, **117**, 8041-8093.
16. Y. Li, T. Zhai, J. Chen, J. Shi, L. Wang, J. Shen and X. Liu, *Chemistry – A European Journal*, 2022, **28**, e202103736.
17. Y. Zhao, S. Zhuang, L. Liao, C. Wang, N. Xia, Z. Gan, W. Gu, J. Li, H. Deng and Z. Wu, *Journal of the American Chemical Society*, 2020, **142**, 973-977.
18. C.-A. J. Lin, T.-Y. Yang, C.-H. Lee, S. H. Huang, R. A. Sperling, M. Zanella, J. K. Li, J.-L. Shen, H.-H. Wang, H.-I. Yeh, W. J. Parak and W. H. Chang, *ACS Nano*, 2009, **3**, 395-401.
19. Y. Li, O. Zaluzhna, B. Xu, Y. Gao, J. M. Modest and Y. J. Tong, *Journal of the American Chemical Society*, 2011, **133**, 2092-2095.
20. M. S. Bootharaju, C. P. Joshi, M. R. Parida, O. F. Mohammed and O. M. Bakr, *Angewandte Chemie International Edition*, 2016, **55**, 922-926.
21. Y. Du, H. Sheng, D. Astruc and M. Zhu, *Chemical Reviews*, 2020, **120**, 526-622.
22. N. Alam, A. K. Das, P. Chandrashekar, P. Baidya and S. Mandal, *Nanoscale*, 2024, **16**, 10087-10107.
23. M. B. Mohamed, V. Volkov, S. Link and M. A. El-Sayed, *Chemical Physics Letters*, 2000, **317**, 517-523.
24. J. M. Forward, D. Bohmann, J. P. Fackler Jr and R. J. Staples, *Inorganic chemistry*, 1995, **34**, 6330-6336.
25. S.-H. Cha, J.-U. Kim, K.-H. Kim and J.-C. Lee, *Chemistry of Materials*, 2007, **19**, 6297-6303.
26. J. Zheng, C. Zhang and R. M. Dickson, *Phys Rev Lett*, 2004, **93**, 077402.
27. Z. Wu and R. Jin, *Nano Letters*, 2010, **10**, 2568-2573.
28. S. Wang, X. Zhu, T. Cao and M. Zhu, *Nanoscale*, 2014, **6**, 5777-5781.
29. Y. Negishi, K. Nobusada and T. Tsukuda, *Journal of the American Chemical Society*, 2005, **127**, 5261-5270.
30. X. Kang and M. Zhu, *Chemical Society Reviews*, 2019, **48**, 2422-2457.
31. H.-H. Deng, X.-Q. Shi, F.-F. Wang, H.-P. Peng, A.-L. Liu, X.-H. Xia and W. Chen, *Chemistry of Materials*, 2017, **29**, 1362-1369.
32. K. Pyo, V. D. Thanthirige, K. Kwak, P. Pandurangan, G. Ramakrishna and D. Lee, *Journal of the American Chemical Society*, 2015, **137**, 8244-8250.

33. M. R. Narouz, S. Takano, P. A. Lummis, T. I. Levchenko, A. Nazemi, S. Kaappa, S. Malola, G. Yousefalizadeh, L. A. Calhoun, K. G. Stamplecoskie, H. Häkkinen, T. Tsukuda and C. M. Crudden, *Journal of the American Chemical Society*, 2019, **141**, 14997-15002.
34. X. Kang, S. Wang, Y. Song, S. Jin, G. Sun, H. Yu and M. Zhu, *Angewandte Chemie International Edition*, 2016, **55**, 3611-3614.
35. Z. Luo, X. Yuan, Y. Yu, Q. Zhang, D. T. Leong, J. Y. Lee and J. Xie, *Journal of the American Chemical Society*, 2012, **134**, 16662-16670.
36. S. Chakraborty, D. Bain, S. Maity, S. Kolay and A. Patra, *The Journal of Physical Chemistry C*, 2022, **126**, 2896-2904.
37. D. Bain, I. Russier-Antoine, H. Yuan, S. Kolay, S. Maclot, C. Moulin, E. Salmon, P.-F. Brevet, A. Pniakowska, J. Olesiak-Bańska and R. Antoine, *Langmuir*, 2023, **39**, 16554-16561.
38. J. Wang, X. Lin, T. Shu, L. Su, F. Liang and X. Zhang, *International journal of molecular sciences*, 2019, **20**.
39. F. Chang, M. Zhang, W. Chen, J. Lin, Y. Wang and L. Yang, *ACS Applied Materials & Interfaces*, 2024, **16**, 39847-39856.
40. J. Wang, N. Goswami, T. Shu, L. Su and X. Zhang, *Materials Chemistry Frontiers*, 2018, **2**, 923-928.
41. B. Musnier, K. D. Wegner, C. Comby-Zerbino, V. Trouillet, M. Jourdan, I. Häusler, R. Antoine, J.-L. Coll, U. Resch-Genger and X. Le Guével, *Nanoscale*, 2019, **11**, 12092-12096.
42. A. Ghosh, O. F. Mohammed and O. M. Bakr, *Accounts of Chemical Research*, 2018, **51**, 3094-3103.
43. Y. Negishi, W. Kurashige, Y. Niihori, T. Iwasa and K. Nobusada, *Physical Chemistry Chemical Physics*, 2010, **12**, 6219-6225.
44. J. Yan, H. Su, H. Yang, C. Hu, S. Malola, S. Lin, B. K. Teo, H. Häkkinen and N. Zheng, *Journal of the American Chemical Society*, 2016, **138**, 12751-12754.
45. M. A. Tofanelli, T. W. Ni, B. D. Phillips and C. J. Ackerson, *Inorganic Chemistry*, 2016, **55**, 999-1001.
46. M. Zhou, C. Yao, M. Y. Sfeir, T. Higaki, Z. Wu and R. Jin, *The Journal of Physical Chemistry C*, 2018, **122**, 13435-13442.
47. C. Yao, Y.-j. Lin, J. Yuan, L. Liao, M. Zhu, L.-h. Weng, J. Yang and Z. Wu, *Journal of the American Chemical Society*, 2015, **137**, 15350-15353.
48. X. Liu, J. Yuan, C. Yao, J. Chen, L. Li, X. Bao, J. Yang and Z. Wu, *The Journal of Physical Chemistry C*, 2017, **121**, 13848-13853.
49. S. Wang, X. Meng, A. Das, T. Li, Y. Song, T. Cao, X. Zhu, M. Zhu and R. Jin, *Angewandte Chemie International Edition*, 2014, **53**, 2376-2380.
50. G. Soldan, M. A. Aljuhani, M. S. Bootharaju, L. G. AbdulHalim, M. R. Parida, A. H. Emwas, O. F. Mohammed and O. M. Bakr, *Angewandte Chemie (International ed. in English)*, 2016, **55**, 5749-5753.
51. M. J. Levene, J. Kurlach, S. W. Turner, M. Foquet, H. G. Craighead and W. W. Webb, *Science*, 2003, **299**, 682-686.
52. S. Khatua, P. M. R. Paulo, H. Yuan, A. Gupta, P. Zijlstra and M. Orrit, *ACS Nano*, 2014, **8**, 4440-4449.
53. J. Wenger, D. Gérard, J. Dintinger, O. Mahboub, N. Bonod, E. Popov, T. W. Ebbesen and H. Rigneault, *Opt. Express*, 2008, **16**, 3008-3020.
54. M. Baibakov, S. Patra, J.-B. Claude, A. Moreau, J. Lumeau and J. Wenger, *ACS Nano*, 2019, **13**, 8469-8480.
55. M. Kayyil Veedu, J. Osmólska, A. Hajda, J. Olesiak-Bańska and J. Wenger, *Nanoscale Advances*, 2024, **6**, 570-577.
56. T. Zhao, K. Yu, L. Li, T. Zhang, Z. Guan, N. Gao, P. Yuan, S. Li, S. Q. Yao, Q.-H. Xu and G. Q. Xu, *ACS Applied Materials & Interfaces*, 2014, **6**, 2700-2708.
57. H. Yuan, S. Khatua, P. Zijlstra, M. Yorulmaz and M. Orrit, *Angew. Chem., Int. Ed*, 2013, **52**, 1217-1221.
58. M. A. Shokova and V. E. Bochenkov, *Nanomaterials*, 2021, **11**, 3334.
59. W. Zhang, M. Caldarola, X. Lu and M. Orrit, *ACS Photonics*, 2018, **5**, 2960-2968.
60. L. Shang, N. Azadfar, F. Stockmar, W. Send, V. Trouillet, M. Bruns, D. Gerthsen and G. U. Nienhaus, *Small*, 2011, **7**, 2614-2620.
61. S. Huang, C. Li, W. Wang, H. Li, Z. Sun, C. Song, B. Li, S. Duan and Y. Hu, *International journal of nanomedicine*, 2017, **12**, 5163-5176.
62. T.-K. Chang, T.-M. Cheng, H.-L. Chu, S.-H. Tan, J.-C. Kuo, P.-H. Hsu, C.-Y. Su, H.-M. Chen, C.-M. Lee and T.-R. Kuo, *ACS Sustainable Chemistry & Engineering*, 2019, **7**, 15479-15486.
63. H.-Y. Huang, K.-B. Cai, P.-W. Chen, C.-A. J. Lin, S.-H. Chang and C.-T. Yuan, *The Journal of Physical Chemistry C*, 2018, **122**, 20019-20026.

64. T. G. Schaaff and R. L. Whetten, *The Journal of Physical Chemistry B*, 2000, **104**, 2630-2641.
65. S. Kumar and R. Jin, *Nanoscale*, 2012, **4**, 4222-4227.
66. S. Knoppe, A. C. Dharmaratne, E. Schreiner, A. Dass and T. Bürgi, *Journal of the American Chemical Society*, 2010, **132**, 16783-16789.
67. I. Dolamic, S. Knoppe, A. Dass and T. Bürgi, *Nature Communications*, 2012, **3**, 798.
68. Y. Zhu, J. Guo, X. Qiu, S. Zhao and Z. Tang, *Accounts of Materials Research*, 2021, **2**, 21-35.
69. S. M. Kelly, T. J. Jess and N. C. Price, *Biochimica et biophysica acta*, 2005, **1751**, 119-139.
70. H. Yao, T. Fukui and K. Kimura, *The Journal of Physical Chemistry C*, 2007, **111**, 14968-14976.
71. M. Monti, M. F. Matus, S. Malola, A. Fortunelli, M. Aschi, M. Stener and H. Häkkinen, *ACS Nano*, 2023, **17**, 11481-11491.
72. M. Farrag, M. Tschurl and U. Heiz, *Chemistry of Materials*, 2013, **25**, 862-870.
73. H. Yao, *Progress in Natural Science: Materials International*, 2016, **26**, 428-439.
74. P. D. Jadzinsky, G. Calero, C. J. Ackerson, D. A. Bushnell and R. D. Kornberg, *Science*, 2007, **318**, 430-433.
75. K. Hou, J. Zhao, H. Wang, B. Li, K. Li, X. Shi, K. Wan, J. Ai, J. Lv, D. Wang, Q. Huang, H. Wang, Q. Cao, S. Liu and Z. Tang, *Nat Commun*, 2020, **11**, 4790.
76. H. Qian, M. Zhu, C. Gayathri, R. R. Gil and R. Jin, *ACS Nano*, 2011, **5**, 8935-8942.
77. H. Yao, N. Nishida and K. Kimura, *Chemical Physics*, 2010, **368**, 28-37.
78. H. Tanaka, Y. Inoue and T. Mori, *ChemPhotoChem*, 2018, **2**, 386-402.
79. K. Tanaka, G. Pescitelli, K. Nakanishi and N. Berova, *Monatshefte für Chemie / Chemical Monthly*, 2005, **136**, 367-395.
80. D. H. Turner, I. Tinoco, Jr. and M. Maestre, *Journal of the American Chemical Society*, 1974, **96**, 4340-4342.
81. A. Prabodh, Y. Wang, S. Sinn, P. Albertini, C. Spies, E. Spuling, L. P. Yang, W. Jiang, S. Bräse and F. Biedermann, *Chemical science*, 2021, **12**, 9420-9431.
82. E. M. Sánchez-Carnerero, A. R. Agarrabeitia, F. Moreno, B. L. Maroto, G. Muller, M. J. Ortiz and S. de la Moya, *Chemistry – A European Journal*, 2015, **21**, 13488-13500.
83. I. Tinoco, Jr., B. Ehrenberg and I. Z. Steinberg, *The Journal of Chemical Physics*, 1977, **66**, 916-920.
84. M. L. Lamos and D. H. Turner, *Biochemistry*, 1985, **24**, 2819-2822.
85. Z. Dai, G. Proni, D. Mancheno, S. Karimi, N. Berova and J. W. Canary, *Journal of the American Chemical Society*, 2004, **126**, 11760-11761.
86. K. Wu, L. Geng, M. J. Joseph and L. B. McGown, *Analytical Chemistry*, 1993, **65**, 2339-2345.
87. R. Hofsäß, S. Sinn, F. Biedermann and H.-A. Wagenknecht, *Chemistry – A European Journal*, 2018, **24**, 16257-16261.
88. A. Ben Moshe, D. Szwarcman and G. Markovich, *ACS Nano*, 2011, **5**, 9034-9043.
89. L. Cui, X. Yang, B. Reynier, C. Schwob, S. Bidault, B. Gallas and M. Mivelle, *ACS Photonics*, 2023, **10**, 3850-3857.
90. J. W. Jarrett, T. Zhao, J. S. Johnson, X. Liu, P. F. Nealey, R. A. Vaia and K. L. Knappenberger, Jr., *The Journal of Physical Chemistry Letters*, 2016, **7**, 765-770.
91. J. Olesiak-Banska, M. Waszkielewicz and M. Samoc, *Physical Chemistry Chemical Physics*, 2018, **20**, 24523-24526.
92. Y.-x. Zhang and Y.-h. Wang, *RSC Advances*, 2017, **7**, 45129-45144.
93. A. J. Bain, in *Photonics*, 2015, DOI: <https://doi.org/10.1002/9781119009719.ch9>, pp. 279-320.
94. F. Dell'Anno, S. De Siena and F. Illuminati, *Physics Reports*, 2006, **428**, 53-168.
95. D. Smirnova and Y. S. Kivshar, *Optica*, 2016, **3**, 1241-1255.
96. K. Zhang, F.-R. Chen, L. Wang and J. Hu, *Small*, 2023, **19**, 2206044.
97. P. T. So, C. Y. Dong, B. R. Masters and K. M. Berland, *Annual review of biomedical engineering*, 2000, **2**, 399-429.
98. J. Olesiak-Banska, M. Waszkielewicz, P. Obstarczyk and M. Samoc, *Chemical Society Reviews*, 2019, **48**, 4087-4117.
99. G. Ramakrishna, O. Varnavski, J. Kim, D. Lee and T. Goodson, *Journal of the American Chemical Society*, 2008, **130**, 5032-5033.
100. A. Hajda, R. Guha, S. M. Copp and J. Olesiak-Bańska, *Chemical science*, 2024, DOI: 10.1039/d4sc05853d.
101. H. C. Ishikawa-Ankerhold, R. Ankerhold and G. P. C. Drummen, *Molecules*, 2012, **17**, 4047-4132.
102. W. R. Zipfel, R. M. Williams and W. W. Webb, *Nature Biotechnology*, 2003, **21**, 1369-1377.

103. R. Antoine and V. Bonačić-Koutecký, *Liganded silver and gold quantum clusters. Towards a new class of nonlinear optical nanomaterials*, Springer, Cham, 2018.
104. F. Bertorelle, C. Moulin, A. Soleilhac, C. Comby-Zerbino, P. Dugourd, I. Russier-Antoine, P.-F. Brevet and R. Antoine, *ChemPhysChem*, 2018, **19**, 165-168.
105. M. Waszkielewicz, J. Olesiak-Banska, M. Grzelczak, A. Sánchez-Iglesias, A. Pniakowska and M. Samoc, *Journal of Luminescence*, 2020, **221**, 116994.
106. L. Polavarapu, M. Manna and Q.-H. Xu, *Nanoscale*, 2011, **3**, 429-434.
107. Y. Peng, X. Huang and F. Wang, *Chemical Communications*, 2021, **57**, 13012-13015.
108. M. Rumi and J. W. Perry, *Adv. Opt. Photon.*, 2010, **2**, 451-518.
109. E. Van Stryland and M. Sheik-Bahae, *Z-scan technique for nonlinear materials characterization*, SPIE, 1997.
110. G. Yousefalizadeh, S. Ahmadi, N. J. Mosey and K. G. Stamplecoskie, *Nanoscale*, 2021, **13**, 242-252.
111. I. Russier-Antoine, F. Bertorelle, R. Hamouda, D. Rayane, P. Dugourd, Ž. Sanader, V. Bonačić-Koutecký, P.-F. Brevet and R. Antoine, *Nanoscale*, 2016, **8**, 2892-2898.
112. P. N. Day, R. Pachter, K. A. Nguyen and T. P. Bigioni, *The Journal of Physical Chemistry A*, 2016, **120**, 507-518.
113. I. Russier-Antoine, F. Bertorelle, N. Calin, Ž. Sanader, M. Krstić, C. Comby-Zerbino, P. Dugourd, P.-F. Brevet, V. Bonačić-Koutecký and R. Antoine, *Nanoscale*, 2017, **9**, 1221-1228.
114. R. Ho-Wu, P. K. Sahu, N. Wu, T. K. Chen, C. Yu, J. Xie and T. Goodson, *The Journal of Physical Chemistry C*, 2018, **122**, 24368-24379.
115. G. Ramakrishna, O. Varnavski, J. Kim, D. Lee and T. Goodson, *J Am Chem Soc*, 2008, **130**, 5032-5033.
116. J. Olesiak-Banska, M. Waszkielewicz, K. Matczyszyn and M. Samoc, *RSC Advances*, 2016, **6**, 98748-98752.
117. P. N. Day, K. A. Nguyen and R. Pachter, *Journal of Chemical Theory and Computation*, 2010, **6**, 2809-2821.
118. K. Brach, M. Waszkielewicz, J. Olesiak-Banska, M. Samoc and K. Matczyszyn, *Langmuir*, 2017, **33**, 8993-8999.
119. L. Shang, R. M. Dörlich, S. Brandholt, R. Schneider, V. Trouillet, M. Bruns, D. Gerthsen and G. U. Nienhaus, *Nanoscale*, 2011, **3**, 2009-2014.
120. V. P. Nguyen, W. Qian, Y. Li, B. Liu, M. Aaberg, J. Henry, W. Zhang, X. Wang and Y. M. Paulus, *Nature Communications*, 2021, **12**, 34.
121. J. H. Lee, H. Y. Cho, H. K. Choi, J. Y. Lee and J. W. Choi, *International journal of molecular sciences*, 2018, **19**.
122. D. Semeniak, D. F. Cruz, A. Chilkoti and M. H. Mikkelsen, *Advanced Materials*, 2023, **35**, 2107986.
123. C. Song, M. G. Blaber, G. Zhao, P. Zhang, H. C. Fry, G. C. Schatz and N. L. Rosi, *Nano letters*, 2013, **13**, 3256-3261.
124. V. Amendola, R. Pilot, M. Frasconi, O. M. Maragò and M. A. Iatì, *Journal of Physics: Condensed Matter*, 2017, **29**, 203002.
125. A. Ghosh, T. Udayabhaskararao and T. Pradeep, *The Journal of Physical Chemistry Letters*, 2012, **3**, 1997-2002.
126. Y. Yang, A. Dev, I. Sychugov, C. Häggglund and S.-L. Zhang, *The Journal of Physical Chemistry Letters*, 2023, **14**, 2339-2346.
127. F. D. Stefani, K. Vasilev, N. Bocchio, N. Stoyanova and M. Kreiter, *Physical Review Letters*, 2005, **94**, 023005.
128. G. J. Nusz, S. M. Marinakos, A. C. Curry, A. Dahlin, F. Höök, A. Wax and A. Chilkoti, *Analytical Chemistry*, 2008, **80**, 984-989.
129. M. Jankowska, K. Sulowska, K. Wiwatowski, J. Niedziółka-Jönsson and S. Mackowski, *Chemosensors*, 2022, **10**, 149.
130. K. R. Krishnadas, L. Sementa, M. Medves, A. Fortunelli, M. Stener, A. Fürstenberg, G. Longhi and T. Bürgi, *ACS Nano*, 2020, **14**, 9687-9700.
131. C. P. Joshi, M. S. Bootharaju, M. J. Alhilaly and O. M. Bakr, *Journal of the American Chemical Society*, 2015, **137**, 11578-11581.
132. O. M. Bakr, V. Amendola, C. M. Aikens, W. Wenseleers, R. Li, L. Dal Negro, G. C. Schatz and F. Stellacci, *Angewandte Chemie International Edition*, 2009, **48**, 5921-5926.
133. K. L. D. M. Weerawardene and C. M. Aikens, *The Journal of Physical Chemistry C*, 2018, **122**, 2440-2447.
134. Q. Xu, S. Kumar, S. Jin, H. Qian, M. Zhu and R. Jin, *Small*, 2014, **10**, 1008-1014.
135. C. Zeng and R. Jin, *Chemistry – An Asian Journal*, 2017, **12**, 1839-1850.

136. W.-M. He, J. Zha, Z. Zhou, Y.-J. Cui, P. Luo, L. Ma, C. Tan and S.-Q. Zang, *Angewandte Chemie International Edition*, 2024, **63**, e202407887.
137. M. Lipok, P. Obstarczyk, S. Parzyszek, Y. Wang, M. Bagiński, T. Buergi, W. Lewandowski and J. Olesiak-Bańska, *Advanced Optical Materials*, 2023, **11**, 2201984.
138. Z. Wang, Y. Tian, J. Hao, Y. Liu, J. Tang, Z. Xu, Y. Liu, B. Tang, X. Huang, N. Zhu, Z. Li, L. Hu, L. Li, Y. Wang and G. Jiang, *ACS Nano*, 2024, **18**, 7253-7266.
139. K. E. Gunde and F. S. Richardson, *Chemical Physics*, 1995, **194**, 195-206.
140. C. Toro, L. De Boni, N. Lin, F. Santoro, A. Rizzo and F. E. Hernandez, *Chemistry – A European Journal*, 2010, **16**, 3504-3509.
141. Y. Vesga, C. Diaz, J. Crassous and F. E. Hernandez, *The Journal of Physical Chemistry A*, 2018, **122**, 3365-3373.
142. H. Mesnil, M. C. Schanne-Klein, F. Hache, M. Alexandre, G. Lemerrier and C. Andraud, *Physical Review A*, 2002, **66**, 013802.
143. M. Thomas, G. Patonay and I. Warner, *Review of Scientific Instruments*, 1986, **57**, 1308-1313.
144. T. Nehira, K. Ishihara, K. Matsuo, S. Izumi, T. Yamazaki and A. Ishida, *Analytical Biochemistry*, 2012, **430**, 179-184.
145. A. J. Bain and A. J. McCaffery, *The Journal of Chemical Physics*, 1985, **83**, 2632-2640.
146. I. Tinoco, in *Optical Activity and Chiral Discrimination: Proceedings of the NATO Advanced Study Institute held at the University of Sussex, Falmer, England, September 10–22, 1978*, ed. S. F. Mason, Springer Netherlands, Dordrecht, 1979, DOI: 10.1007/978-94-015-7644-4_4, pp. 57-85.
147. Y. Zhong, J. Zhang, T. Li, W. Xu, Q. Yao, M. Lu, X. Bai, Z. Wu, J. Xie and Y. Zhang, *Nature Communications*, 2023, **14**, 658.
148. A. Pniakowska, K. Kumaranchira Ramankutty, P. Obstarczyk, M. Perić Bakulić, Ž. Sanader Maršić, V. Bonačić-Koutecký, T. Bürgi and J. Olesiak-Bańska, *Angewandte Chemie International Edition*, 2022, **61**, e202209645.
149. C.-L. Liu, M.-L. Ho, Y.-C. Chen, C.-C. Hsieh, Y.-C. Lin, Y.-H. Wang, M.-J. Yang, H.-S. Duan, B.-S. Chen, J.-F. Lee, J.-K. Hsiao and P.-T. Chou, *The Journal of Physical Chemistry C*, 2009, **113**, 21082-21089.
150. M. A. Albota, C. Xu and W. W. Webb, *Appl. Opt.*, 1998, **37**, 7352-7356.
151. M. Drobizhev, N. S. Makarov, S. E. Tillo, T. E. Hughes and A. Rebane, *Nature methods*, 2011, **8**, 393-399.